

ÉCOLE DOCTORALE DES SCIENCES CHIMIQUES
Laboratoire de Chimie des Matériaux Moléculaires-UMR7509

THÈSE

présentée par :

Haifa BEN AZIZA

soutenue le : 28 septembre 2015

pour obtenir le grade de : **Docteur de l'université de Strasbourg**

Discipline/ Spécialité : Chimie

**Le pillar[5]arène comme cœur polyfonctionnel
pour l'élaboration de matériaux moléculaires**

THÈSE dirigée par :

Jean-François NIERENGARTEN
Rym ABIDI

Dr., Université de Strasbourg
Prof., Université de Carthage

RAPPORTEURS :

Remi CHAUVIN
Hatem MADJOUR

Pr., Université Paul Sabatier de Toulouse
Dr., Université de Monastir

MEMBRES DU JURY :

Vincent RITLENG
Moufida YOUNES-ROMDHANE

Dr., Université de Strasbourg
Pr., Université de Carthage



UNIVERSITÉ DE CARTHAGE



Faculté des Sciences de Bizerte

**Laboratoire d'Applications de la Chimie aux Ressources et
Substances Naturelles et 0 l'Environnement**

THÈSE

présentée par :

Haifa BEN AZIZA

soutenue le : 28 septembre 2015

pour obtenir le grade de : **Docteur de l'université de Carthage**

Discipline/ Spécialité : Chimie

**Le pillar[5]arène comme cœur polyfonctionnel
pour l'élaboration de matériaux moléculaires**

THÈSE dirigée par :

Rym ABIDI

Jean-François NIERENGARTEN

Prof., Université de Carthage

Dr., Université de Strasbourg

RAPPORTEURS :

Remi CHAUVIN

Hatem MADJOUR

Pr., Université Paul Sabatier de Toulouse

Dr., Université de Monastir

MEMBRES DU JURY :

Vincent RITLÉNG

Moufida YOUNES-ROMDHANE

Dr., Université de Strasbourg

Pr., Université de Carthage

A ma mère, mon père

A mon frère et ma sœur

Remerciements

Avant d'exposer les résultats de ce travail, je tiens à exprimer ma gratitude envers toutes les personnes qui ont contribué de près ou de loin dans l'aboutissement de ce travail.

Ce travail a été effectué sous la direction du Dr, J.F NIERENGARTEN de l'université de Strasbourg et du Pr. Rym ABIDI de l'université de Carthage.

Je tiens à remercier Jean-François de m'avoir offert l'opportunité de faire mes premiers pas dans le monde de la synthèse organique au sein de son groupe. Ses conseils, son soutien scientifique et surtout sa patience, dont il m'a fait bénéficier, ont contribué à approfondir mes capacités théoriques et scientifiques. Merci d'avoir partagé sa passion pour la chimie, travailler sous sa direction est un véritable apprentissage au quotidien. Pour tout cela, je lui adresse mes sincères remerciements.

Je tiens aussi exprimer ma reconnaissance à Madame Rym Abidi, son implication dans ma formation remonte au master et se poursuit encore aujourd'hui. Ses conseils précieux et son soutien indéfectible tout au long de ces années m'ont permis d'avancer afin d'atteindre mes objectifs. Pour sa disponibilité, son suivi, ses qualités scientifiques et humaines je lui adresse ma gratitude.

Je remercie énormément le Dr Michel Holler, pour son aide, sa patience et ses conseils. Merci « Mimiche » pour m'avoir assisté pendant les expériences dangereuses et moins dangereuses et d'avoir consacré du temps pour répondre à toutes mes questions. « Ben machin, ne te remerciera jamais assez !! »

J'adresse mes sincères remerciements aux membres du jury qui ont accepté de juger ce travail :
Pr. Rémy Chauvin, Dr. Hatem Madjoub, Pr. Moufida Younes Romdhani et
Dr. Vincent Ritleng.

Je remercie l'université de Carthage de m'avoir octroyé un financement pour rendre possible mon séjour en France ce qui m'a permis de mener à termes ma thèse dans de bonnes conditions.

Je tiens à remercier également Dr. Iwona Nierengarten de m'avoir accueilli sous sa paillasse à mon arrivée et de m'avoir initié à la chimie des pillararenes mais aussi pour son aide tout au long de ce projet et ses conseils.

Un grand merci au Dr. Uwe Hahn, qui n'a jamais hésité à mettre à ma disposition son expérience de laboratoire et partager les petits « astuces de la paillasse ». Merci pour tous les cours d'anglais gratuits « you are a great Teacher, Thank you !! ».

Ce travail a été le fruit de plusieurs collaborations fructueuses. Dans ce contexte, je remercie vivement Pr. Robert Deschenaux et son équipe (Université de Neuchâtel, Suisse) pour les analyses par DSC et POM, Dr. Béatrice DELAVAUX-NICOT (LCC-CNRS, Toulouse) pour les mesures d'électrochimie et Dr. Joaquin Barbera (Université de ZARAGOZA, Espagne) pour les mesures RX.

Des collaborations au sein même du laboratoire ont vu le jour. Un grand merci à Sebastiano GUERRA et Minh NUGHET TRINH d'avoir contribué à enrichir ce travail pendant leur passage au laboratoire en tant que post-doc.

Je tiens aussi à remercier Michel Schmidt pour toutes les mesures RMN, Jean Marc Strub pour les mesures de spectrométrie de masse, Lydia Brelot pour les analyses RX et Matthieu Chessé pour les mesures spectrophotométriques.

Je remercie les membres de l'équipe de Chimie des Matériaux Moléculaires actuelle et passée : Eric, Franck, Yassine, Alberto, Samir, Mr Billmaneee, Lucie, Radian, Mathilde, David ... Mon stagiaire préféré Xavier, Selma, Thomas...

Je remercie aussi les membres de l'équipe Lacresne : Najah, Amel, Mouna, Imene...

Je remercie Meera pour m'avoir aidé à m'installer dès mon arrivée à Strasbourg et pour son amitié, Adela pour toutes les pauses café et papotage qu'on a pu partager.

Je remercie tous les amis de Strasbourg qui ont su être une vraie famille pour moi tout au long de ces années de thèse : Marwa, Walid, Assil, Asma, Ines, Mehdi, Sarra, Lobna, Ferdaous, Ahmed, Jihed, Wafa, Olfa, Nour, Olfa et Aymen, Hakam....

Et de l'autre côté de la méditerranée, je remercie chaleureusement mes amis pour leur présence et leur soutien moral malgré la distance : Amira et Raouf, Manel, Rymmoucha, Anas, Mriwa...

Enfin, je ne remercierai jamais assez mes parents, mon frère et ma soeur dont l'amour et le soutien moral et financier étaient inconditionnels. J'espère les rendre fier de moi.

Haifa BEN AZIZA

Résumé de la thèse

Chapitre I : Introduction

Tout comme les calixarènes et les cyclotrivératrylènes, les pillararènes sont des composés macrocycliques constitués de groupements aromatiques reliés entre eux par des ponts méthylènes (Figure 1). La différence entre ces trois familles de composés macrocycliques est liée à la position relative des deux groupements CH_2 de chacun des cycles aromatiques : *ortho* pour les cyclotrivératrylènes (A), *méta* pour les calixarènes (B) et *para* pour les pillararènes (C).

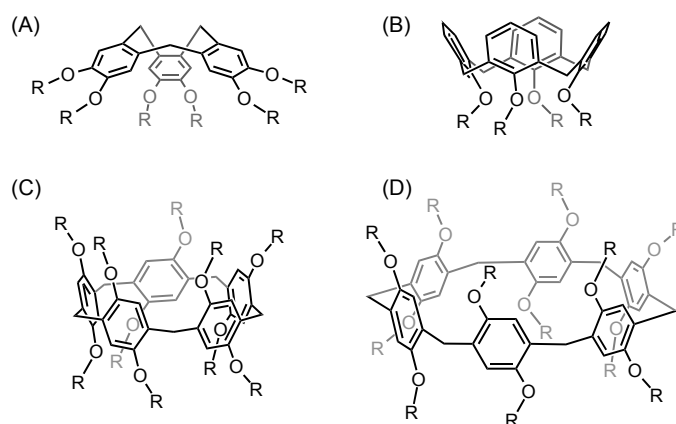


Figure 1. (A) Cyclotrivératrylène; (B) calix[4]arène; (C) pillar[5]arène (D) pillar[6]arène.

Le premier représentant de la famille des pillararènes a été récemment décrit par Ogoshi, Nakamoto et collaborateurs. Un pentamère cyclique a été préparé par réaction du 1,4-diméthoxybenzène avec du paraformaldéhyde en présence d'un acide de Lewis. Les conditions de préparation des pillar[5]arènes à partir de 1,4-dialkyloxybenzène et de paraformaldéhyde ont été optimisées (Figure 2). Les meilleurs résultats ont été obtenus en utilisant du $\text{BF}_3 \cdot \text{Et}_2\text{O}$ comme catalyseur et du 1,2-dichloroéthane comme solvant. Il peut aussi être noté qu'en utilisant du CHCl_3 comme solvant et du FeCl_3 comme acide de Lewis, la formation du cyclohexamère est favorisée (Figure 2). A l'état solide, le pillar[5]arène adopte une conformation en pentagone régulier et en raison de l'analogie de forme avec une colonne (*pillar* en anglais), le nom de *pillar[n]arènes* a été attribué à cette nouvelle famille de

composés macrocycliques, où n représente le nombre d'unités aromatiques constituant le macrocycle.

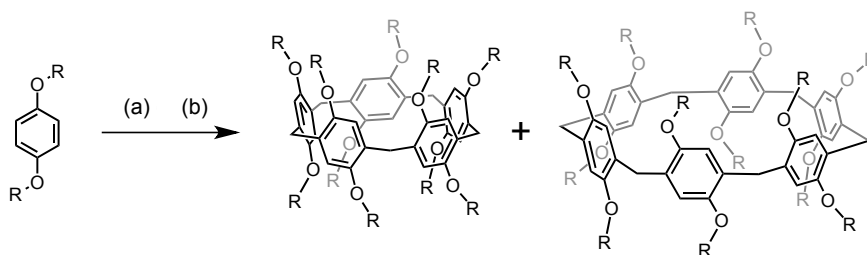


Figure 2. Conditions de synthèse des pillar[5] et pillar[6]arènes. *Conditions et réactifs* : (a) $(\text{CH}_2\text{O})_n$, $\text{BF}_3 \cdot \text{Et}_2\text{O}$, $\text{CH}_2\text{ClCH}_2\text{Cl}$, r.t. (pillar[5]arène: 30-60%, pillar[6]arène: traces); (b) $(\text{CH}_2\text{O})_n$, FeCl_3 , CHCl_3 , 45°C (pillar[5]arène: 10-30%, pillar[6]arène: 20-40%).

La préparation de pillar[5]arène se fait dans les conditions de Friedel-Crafts. Ces conditions sont incompatibles avec de nombreux groupements fonctionnels. Le rendement de la cyclisation est aussi très sensible à l'encombrement stérique. Afin de s'affranchir de ses problèmes, le groupe de Jean-François Nierengarten a développé des pillar[5]arènes post-fonctionnalisables. Les monomères de départ étant simples, les pillar[5]arènes sont obtenus avec de bons rendements. Les groupements périphériques sont alors introduits sur le macrocycle déjà construit. Ceci a été possible en tirant profit de la cycloaddition 1,3-dipolaire entre un alcyne vrai et un azoture catalysée par le cuivre(I) (*chimie click*). Ces conditions étant compatibles avec un grand nombre de groupes fonctionnels, il est maintenant possible de préparer des pillar[5]arènes portant divers groupements périphériques. Dans ce contexte, nous nous sommes proposés d'exploiter ces synthons post-fonctionnalisables pour la construction de nanomatériaux ayant des propriétés mésomorphes (chapitre 2) et de systèmes multiporphyriniques ayant des propriétés photophysiques originales (chapitres 3 et 4).

Chapitre II : Des pillar[5]arènes mésomorphes

Un premier dérivé de pillar[5]arène doté de propriétés mésomorphes a été préparé au sein de notre groupe. Cette nouvelle famille de cristaux-liquides présentait une organisation de type lamellaire. A partir de ces résultats, nous nous sommes intéressés à la possibilité de préparer des pillar[5]arènes s'organisant en phase colonnaire afin d'obtenir une structure tubulaire au sein d'une mésophase. Dans ce but, notre choix s'est porté sur la fonctionnalisation du pillar[5]arène avec des dendrons de type *Percec*. Ces dendrons de types

polybenzyléthers sont effectivement connus pour leur capacité à s'auto-assembler mésophases colonnaires.

Quatre produits finaux ont été obtenus par deux voies de synthèses différentes :

- Par acylation d'un décabromo-pillar[5]arène avec un carboxylate : composés **1** et **2** (Figure 3: A et B).
- Par cycloaddition 1,3-dipolaire catalysée au cuivre(I) d'un décaazido-pillar[5]arène avec un alcyne vrai : composés **3** et **4** (Figure 3: C et D).

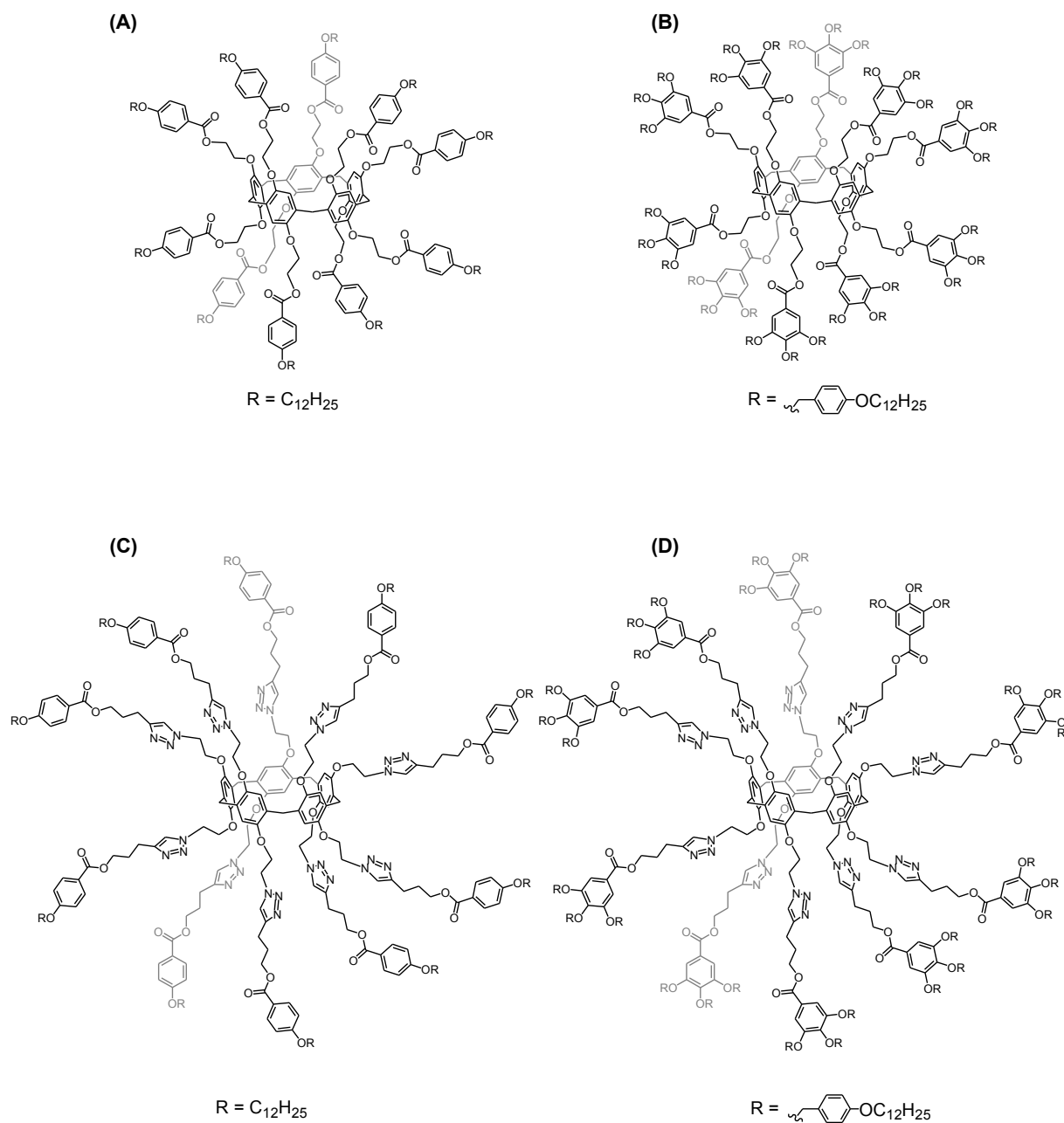


Figure 3. Structures des dérivés : (A) **1**, (B) **2**, (C) **3**, (D) **4**.

En collaboration avec le groupe du Prof. Robert Deschenaux (Université de Neuchâtel), les propriétés liquides-cristallines des différents composés obtenus ont été étudiées par microscopie à lumière polarisée (POM) et par calorimétrie à balayage différentielle (DSC) (Figure 4).

Les températures et les enthalpies de transitions des composés **1**, **2**, **3** et **4** sont présentées dans le tableau suivant :

Composés	Température (°C)	Phase de transition ^(a)	ΔH (KJ/mol)
1	42	Cr \rightarrow I	24.8
2	130	Col _h \rightarrow I	17.7
3	44	T_g	6.3
	95	SmA \rightarrow I	
4	136	Col _h \rightarrow I	9.9

(a) Cr: solide cristallin, Col_h: phase colonnaire hexagonale, I: liquide isotrope, SmA: phase smectique A

Des études par DRX (Diffractions des Rayons X), effectuées en collaboration avec le groupe du Prof. Joaquin Barbera (Université de Saragosse), ont montré que les molécules **2** et **4** s'empilent en colonnes et que le macrocycle est localisé au cœur de ces colonnes. En d'autres termes, le cœur des colonnes est vide et le système s'auto-organise en tube. Nous avons également montré que le cœur des colonnes peut servir de récepteur supramoléculaire et les propriétés mésomorphes sont influencées par la nature du substrat localisé dans la cavité du macrocycle.

Dans ce contexte, des complexes d'inclusion des dérivés **1**, **2**, **3** et **4** en présence de 1,6-dicyano-hexane ont été préparés. A l'état solide, des interactions de type dipôle-dipôle ont souvent été observés entre les groupements nitriles de molécules voisines. Afin de voir l'influence de ces interactions sur l'organisation supramoléculaire de nos composés liquide-cristallins, les propriétés mésomorphes des complexes formés ont été étudiées. A partir des études par POM et DSC, les complexes formés à partir du dérivé **1** et **3** se sont montrés thermiquement instables; une séparation de phase a été observée dès que l'état liquide est atteint. Par contre, les complexes d'inclusion formés à partir des dérivés dendronisés **2** et **4**, se sont montrés thermiquement stables et des textures caractéristiques d'une phase colonnaire ont été observées. Il faut noter aussi que le liquide biréfringent s'est avéré plus visqueux que celui observé pour les dérivés **2** et **4**. Ce dernier résultat pourrait être expliqué par la

contribution des groupements nitriles, présents aux extrémités du dicyanohexane complexé, à rigidifier l'organisation tubulaire par des interactions de types dipôles-dipôles.

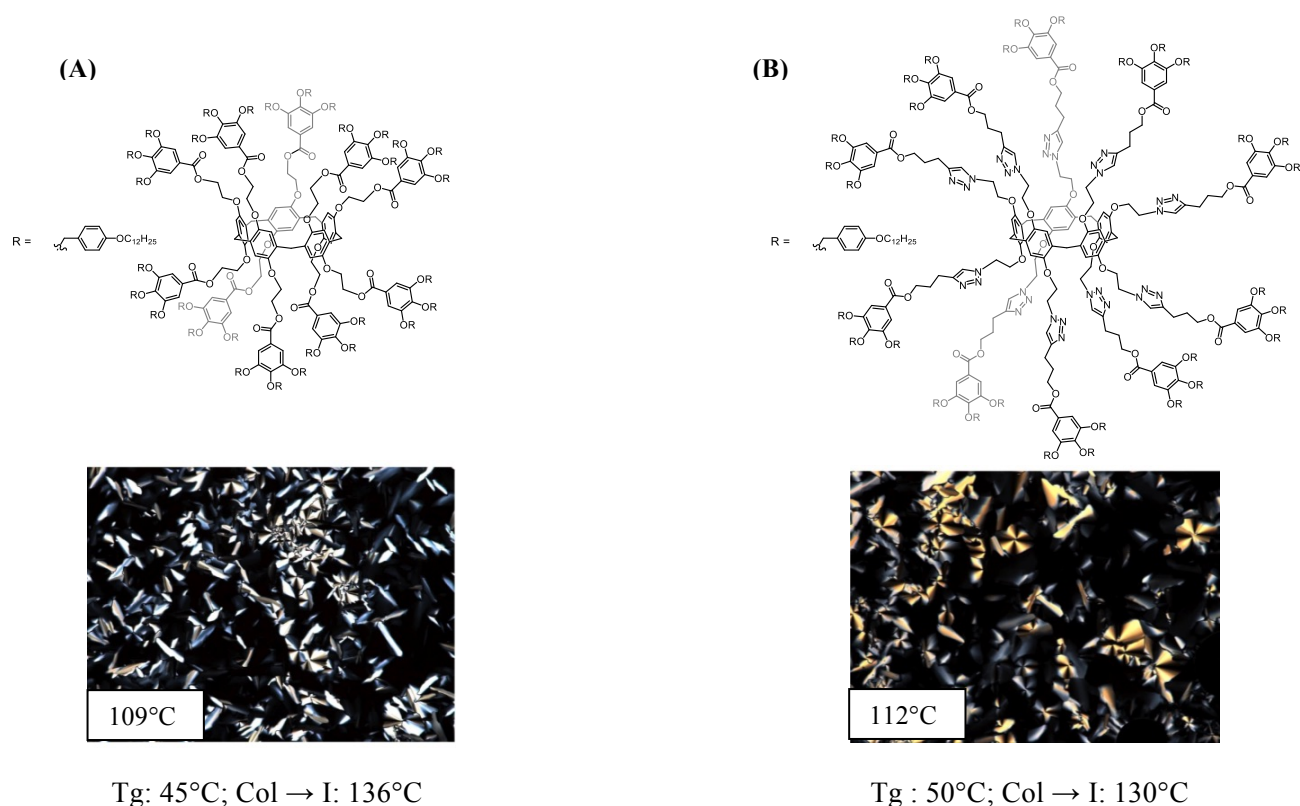


Figure 4. (A) textures caractéristiques de phase colonnaires du dérivé **2**, (B) textures caractéristiques de phase colonnaires du dérivé **4** (Tg : température de transition vitreuse, I: liquide isotrope)

Chapitre III : Systèmes multiporphyriniques à base de pillar[5]arène

Nous avons également cherché à exploiter le potentiel de notre squelette post-fonctionnalisable pour préparer des dérivés du pillar[5]arène ayant des propriétés photophysiques intéressantes. Nous avons ainsi décidé d'introduire des unités de porphyrines. Ces dernières ont été souvent utilisées comme chromophores pour la construction de dispositifs moléculaires photoactifs. De plus, leurs propriétés électroniques peuvent être contrôlées en changeant la nature de leurs substituants ou par métallation.

Les dérivés **5** et **7** du pillar[5]arènes portant dix unités porphyrines périphériques ont été préparés à partir d'un support pillar[5]arène cliquable et de dérivés de porphyrine de Zn(II)

portant une fonction alcyne terminale. Leurs analogues portant dix porphyrines base libre (**6** et **8**) ont été obtenu par démétallation de **5** et **7** (Figure 5).

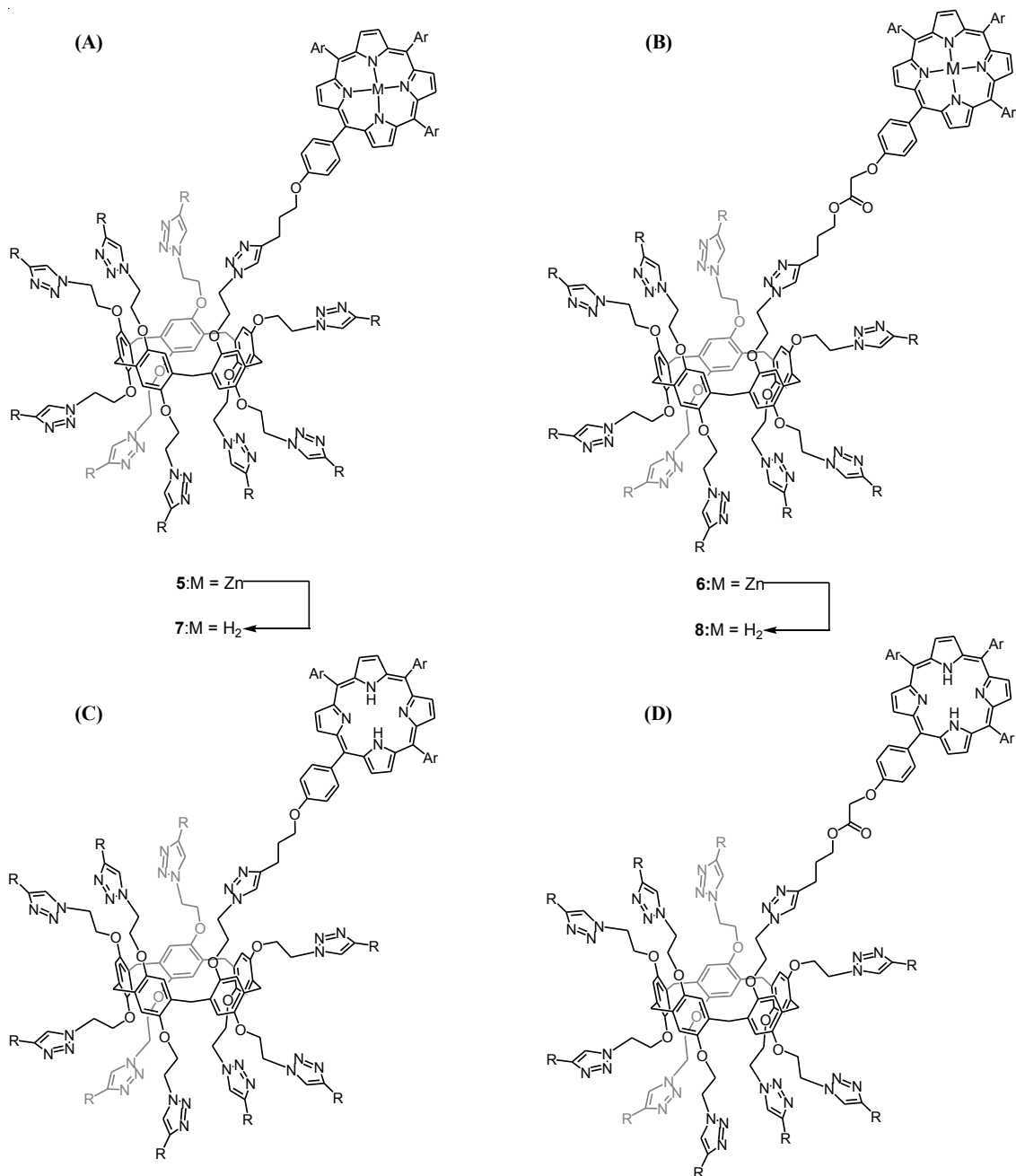


Figure 5. Structures des dérivés : (A) **5**, (B) **6**, (C) **7**, (D) **8**.

Les spectres RMN du proton des dérivés **5** et **7** sont larges à température ambiante alors que ceux des dérivés « base libre » correspondants **6** et **8** sont bien résolus. Ces observations suggèrent que l'élargissement des signaux observés pour **5** et **7** est lié à la présence des du métal. De fait, une complexation intramoléculaire des unités porphyrines de Zn(II) par les groupements 1,2,3-triazole est responsable de ce changement conformationnel.

Cet équilibre conformationnel dynamique a été mis en évidence par des analyses de RMN du proton à températures variables. A haute température, l'équilibre thermodynamique est déplacé vers les espèces non-coordinées et les spectres RMN enregistrés pour les dérivés **5** et **7** sont bien résolus (Figure 6). Ces spectres sont similaires à ceux obtenus dans les mêmes conditions pour les dérivés démétaillés **6** et **8**. Par contre, à basse température l'équilibre est déplacé vers des espèces coordonnées et les spectres subissent des changements très importants (Figure 7).

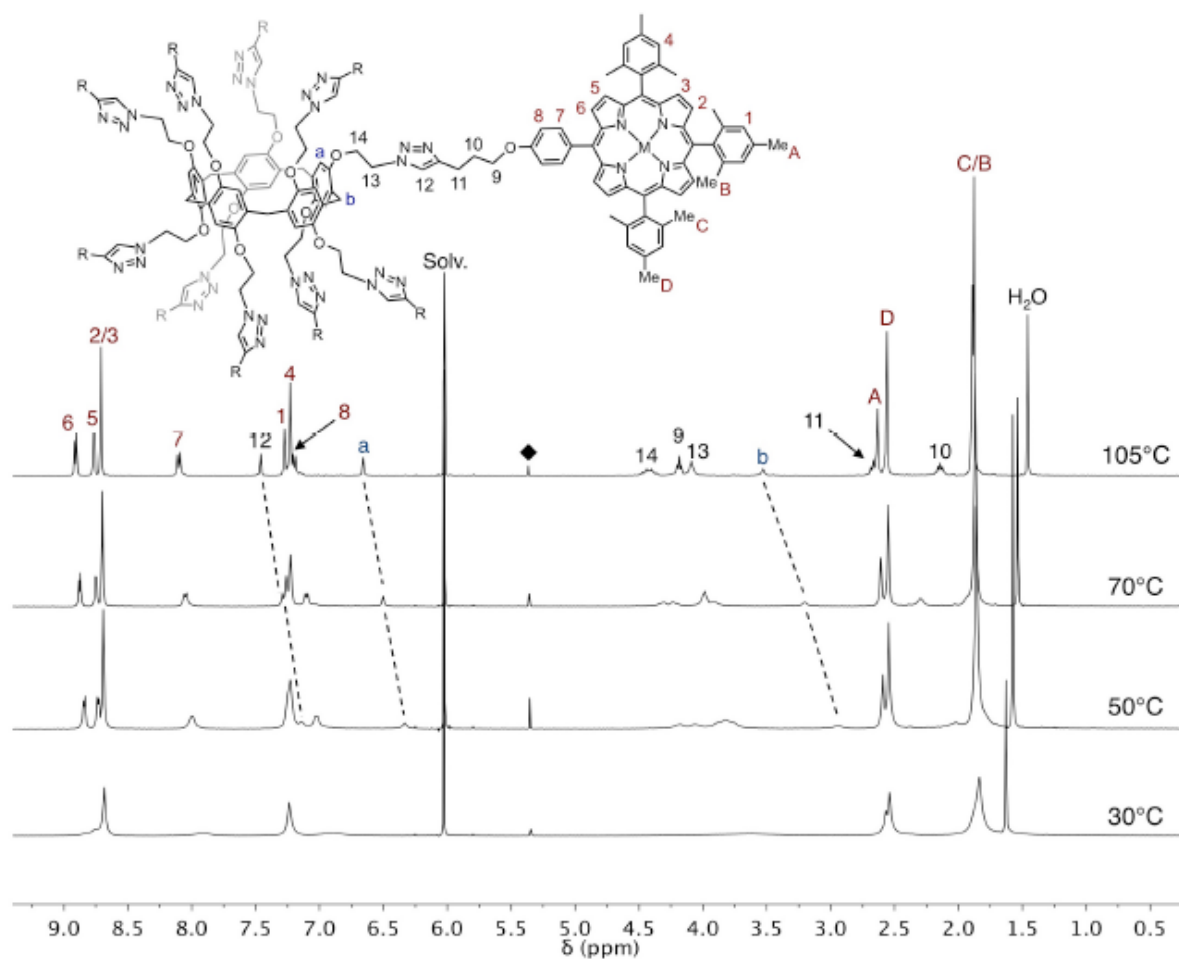


Figure 6. Spectres RMN du proton ($\text{CDCl}_2\text{CDCl}_2$, 400 MHz) à températures variables du dérivé **5**.

Afin de contrôler ce changement conformationnel, un excès de phénylimidazole, réputé plus coordonnant des porphyrines de Zn(II) que le groupement 1,2,3-triazole,¹¹ a été ajouté en solution aux dérivés métallés **5** et **7** et des études spectrophotométriques ont été conduites. Par conséquent, au même titre que l'augmentation de la température, nous avons observé que l'ajout du phénylimidazole empêchait la coordination apicale entre la porphyrine

de Zn(II) et les groupements 1,2,3-triazole et déclençait un mouvement de dépliage de la molécule semblable à l'épanouissement d'une fleur.

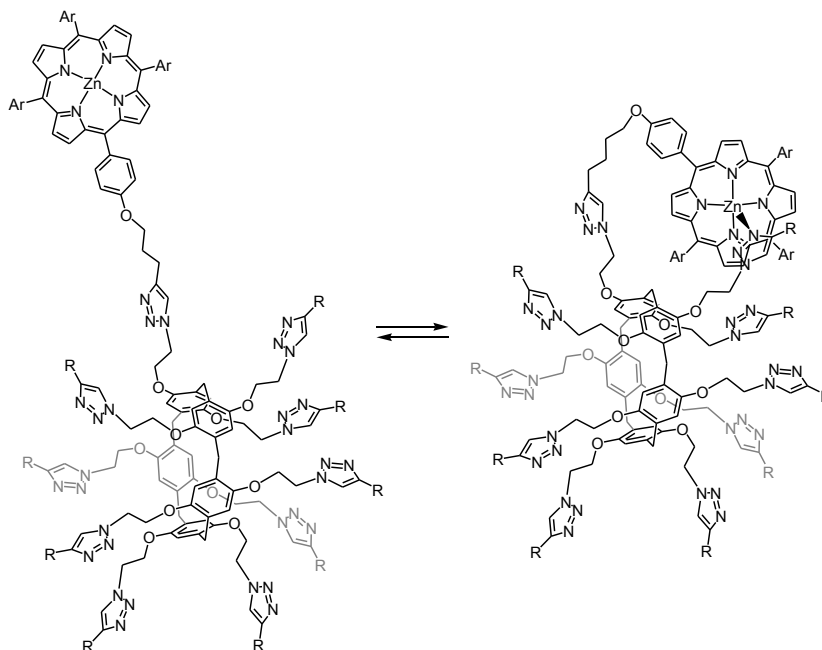


Figure 7. Représentation schématique du changement conformationnel dynamique dû à la coordination intramoléculaire des porphyrines de Zn(II) par les groupements 1,2,3-triazole.

Chapitre IV : Rotaxanes à base de Pillar[5]arène

Cette dernière partie de la thèse a pour but de préparer des systèmes photoactifs à base de pillar[5]arène combinant différentes fonctions afin de mimer les antennes collectrices de lumière du système photosynthétique naturel. Nous nous sommes ainsi proposé de combiner le système multiporphyrine de Zn(II) préparé dans le chapitre précédent avec une entité porphyrine base libre. Dans ce but, nous avons préparé un [2]rotaxane possédant une porphyrine base libre comme bouchon et un pillar[5]arène portant dix fonctions azotures. Les dix porphyrines de Zn(II) ont été greffées sur le cœur macrocyclique, Le [2]rotaxane **9** a été obtenu avec un bon rendement de 60% et a été caractérisé par RMN et MALDI-TOF (Figure 9). Finalement, le rotaxane modèle **10** a aussi été préparé pour servir de référence pour les études photophysiques.

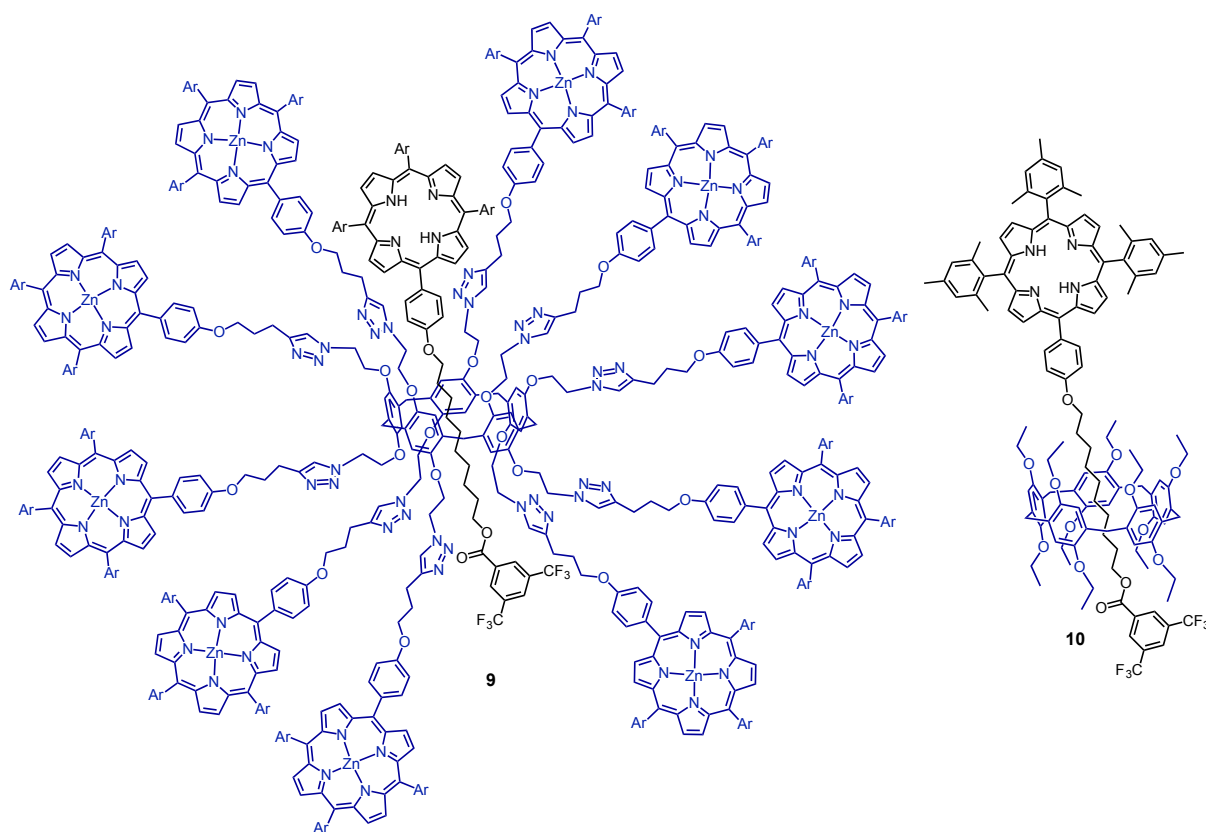


Figure 9. [2]Rotaxanes **9** et **10**.

Des études photophysiques des dérivés **5**, **9** et **10** ont été effectuées dans différents solvants. Dans le toluène, les spectres d'émission du dérivé **5** et du [2]rotaxane **10**, enregistrés à partir de solutions ayant la même densité optique, ont montré un piégeage de la fluorescence des porphyrines de Zn(II), qui a été estimé à 75% (Figure 10A). Nous avons aussi observé, en enregistrant les spectres d'émission dans le même solvant et à partir de solutions ayant la même concentration, une augmentation de 5 fois de l'émission de la porphyrine base libre dans le cas du dérivé **9** comparé à celle du [2]rotaxane modèle **10** (Figure 10B). Ces observations mettent ainsi en évidence un transfert d'énergie de type singulet-singulet des porphyrines de Zn(II) vers la porphyrine base libre. Le spectre d'excitation enregistrés dans la région de 650-750 nm pour le [2]rotaxane **9** était similaire au spectre d'absorption du dérivé **10**, puisque nous avons pu observer les bandes d'émission de la porphyrine base libre après excitation des porphyrines de Zn(II) (Figure 11). Avec ce dernier résultat, nous avons pu confirmer l'existence d'un transfert d'énergie des porphyrines de Zn(II) vers la porphyrine base libre et donc la formation d'un système mimant les antennes collectrices de lumière.

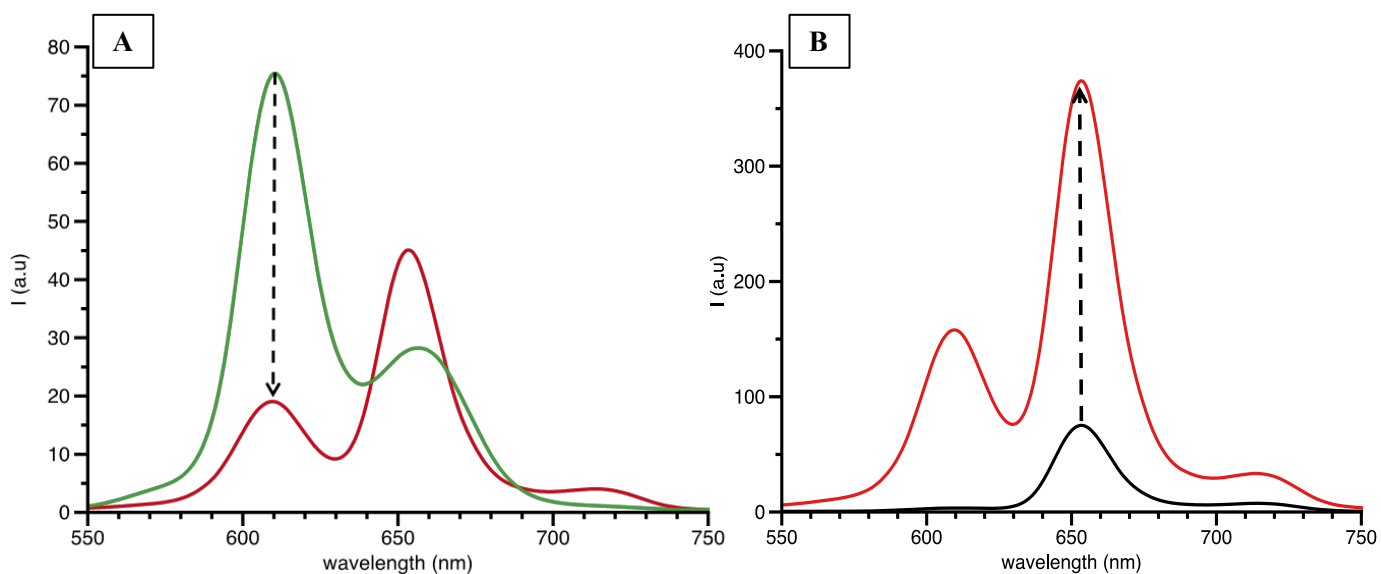


Figure 10. (A) Spectres d'émission dans le toluène de solutions ayant la même densité optique du dérivé **5** (en vert) et du dérivé **9** (en rouge) (25°C , $\lambda_{\text{exc}} = 425 \text{ nm}$). (B) Spectres d'émission dans le toluène de solutions ayant la même concentration du dérivé **10** (en noir) et du dérivé **9** (en rouge) (25°C , $\lambda_{\text{exc}} = 425 \text{ nm}$).

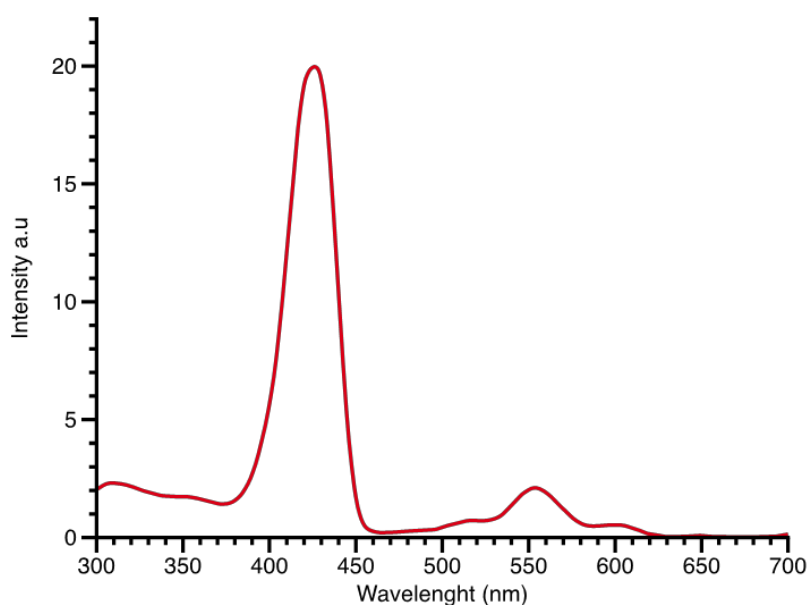


Figure 11. Spectre d'excitation dans le toluène du dérivé **9** (en rouge) (25°C , $\lambda_{\text{em}} = 720 \text{ nm}$).

Conclusion

Dans le cadre du programme de recherche de notre groupe qui consiste à l'utilisation du pillar[5]arène comme support pour la préparation de nanomatériaux, cette thèse a été

dévouée à la préparation de dérivés pillaréniques ayant des propriétés mésomorphes (Chapitre 2) et des dérivés comportant dix porphyrines de Zn(II) (Chapitre 3).

Dans la première partie, nous avons réussi à greffer différents groupes mésogènes sur le cœur macrocyclique du pillar[5]arène. Certains de ces composés ont montré des propriétés mésomorphes et à partir des études thermiques et optiques, nous avons pu conclure que l'organisation supramoléculaire en mésophase dépend fortement du type d'unités périphériques greffées sur le pillar[5]arène.

Dans la deuxième partie, nous avons préparé des systèmes complexes portant dix porphyrines métallées ou base libre à partir d'un dérivé clickable du pillar[5]arène. Des études RMN du proton à températures variables, ont mis en évidence un équilibre conformationnel dynamique qui conduit à une conformation repliée de la molécule.

Dans la dernière partie, des dispositifs moléculaires photoactifs ont été préparés en utilisant un support rotaxane. Plus précisément, un [2]rotaxane à base de pillar[5]arène cliquable comportant un bouchon de porphyrine base libre a été préparé et fonctionnalisé avec dix unités de porphyrines de Zn(II). Les études photophysiques de ce système ont mis en évidence un transfert d'énergie des porphyrines métallées vers le centre porphyrine base libre par un transfert d'énergie de type singulet-singulet.

1. Introduction	1
1.1. Synthesis of pillar[n]arenes	2
1.2. Conformation and chirality of pillar[5]arenes	3
1.3. Nonsymmetrical pillar[5]arenes	4
1.4. Pillar[n]arenes as scaffolds for the preparation of nanomaterials	4
1.5. Pillar[n]arene-containing pseudorotaxanes and rotaxanes	9
1.6. Research plan	12
2. Liquid-crystalline pillar[5]arene derivatives	17
2.1. Introduction	17
2.2. Synthesis	18
2.3. Host-guest complexes	24
2.3.1. NMR binding studies	25
2.3.2. X-ray crystal structure of inclusion complex [13 ⊂ 12]	29
2.4. Liquid-crystalline properties	31
2.4.1. <i>p</i> -Dodecyloxybenzoate derivative	32
2.4.2. Dendronized compounds	34
2.5. Conclusion	38
2.6. Experimental section	40
3. Porphyrin-substituted pillar[5]arenes	49
3.1. Introduction	49
3.2. Synthesis	50
3.2.1. Preparation of the clickable porphyrin building blocks	50
3.2.2. Preparation of porphyrin-substituted pillar[5]arenes	53
3.3. Characterization of the porphyrin-substituted pillar[5]arene derivatives	55
3.4. Conclusion	62
3.5. Experimental section	64

4. Pillar[5]arene-based rotaxanes	78
4.1. Introduction	78
4.2. Synthesis	79
4.3. Electronic properties	88
4.4. Conclusion	91
4.5. Experimental section	93
5. Conclusion	106
S1. Supporting information (Chapter 2)	i
S2. Supporting information (Chapter 3)	xxiii
S3. Supporting information (Chapter 4)	xlix

1. Introduction

Macrocyclic compounds are playing a major role in the field of supramolecular chemistry.¹ Emblematic examples include crown-ethers,² cyclodextrins,³ cucurbiturils,⁴ cyclotrimeratrylenes (CTV)⁵ and calix[*n*]arenes.⁶ Whereas CTVs and calix[*n*]arenes are known from decades, their *para*-cyclophane analogues, namely pillar[*n*]arenes (*n* = 5 or 6), have been only recently discovered (Figure 1).⁷ Pillar[*n*]arenes are composed of 1,4-disubstituted hydroquinone subunits linked by methylene bridges in their 2,5-positions.⁷ In contrast to CTV and calix[*n*]arenes that adopt generally cone-shaped conformations, pillar[*n*]arenes are tubular-shaped compounds.

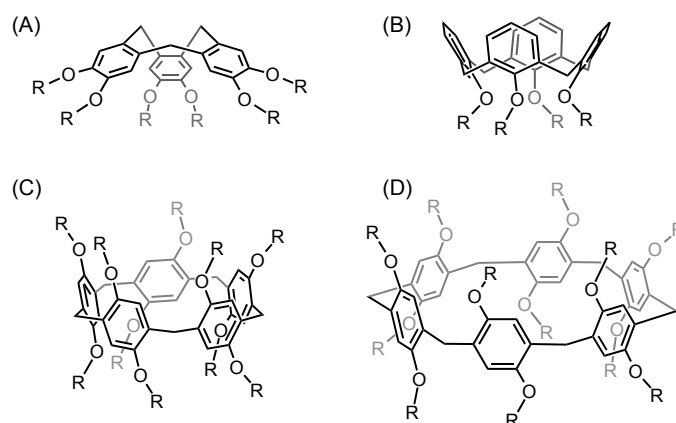


Figure 1. (A) Cyclotrimeratrylene; (B) calix[4]arene; (C) pillar[5]arene; (D) pillar[6]arene.

Following their first synthesis in 2008, pillar[*n*]arenes have generated significant research efforts focused on both the improvements of their synthetic methods and their

incorporation in supramolecular structures.⁸ Despite their recent discovery, pillar[*n*]arenes appear already as an important class of macrocyclic compounds for all kinds of applications in the field of supramolecular chemistry.⁸

1.1. Synthesis of pillar[*n*]arenes

As far as their synthesis is concerned, pillar[*n*]arenes are usually prepared in excellent yields from 1,4-dialkoxybenzene and paraformaldehyde in the presence of $\text{BF}_3 \cdot \text{Et}_2\text{O}$ (Figure 2).⁹ When the reaction is performed in CH_2Cl_2 or 1,2-dichloroethane, the cyclopentamer ($n = 5$) is the only product of cyclisation,⁹ in a few cases however the cyclohexamer ($n = 6$) is also obtained but always as a secondary product and in quite low yields.⁹ In contrast, the preferential preparation of pillar[6]arenes is observed when the reaction between 1,4-dialkoxybenzene and paraformaldehyde is carried out in CHCl_3 with FeCl_3 as the Lewis acid catalyst.¹⁰ The latter observations suggest that the solvent molecules are somehow templating the cyclisation leading to the cyclooligomers. In other words, the outcome of the reaction is related to the affinity of the pillar[*n*]arene derivative for the solvent.¹¹

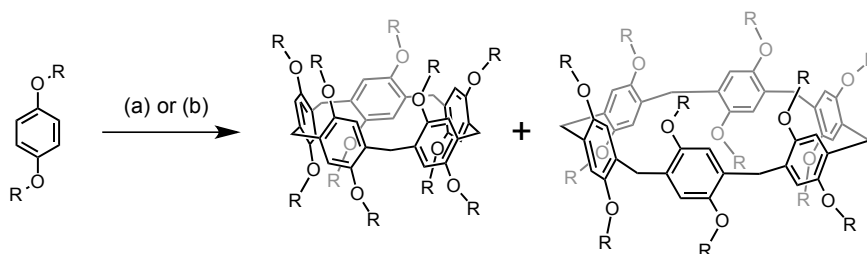


Figure 2. Typical conditions for the synthesis of pillar[5] and pillar[6]arenes. *Reagents and conditions:* (i) $(\text{CH}_2\text{O})_n$, $\text{BF}_3 \cdot \text{Et}_2\text{O}$, $\text{CH}_2\text{ClCH}_2\text{Cl}$, r.t. (pillar[5]arene: 30-60%, pillar[6]arene: traces); (ii) $(\text{CH}_2\text{O})_n$, FeCl_3 , CHCl_3 , 45°C (pillar[5]arene: 10-30%, pillar[6]arene: 20-40%).

Moreover, it has been shown that the cyclooligomerization is thermodynamically driven owing to the reversibility of the Friedel-Crafts reaction, thus explaining the high yielding synthesis of pillar[*n*]arenes.¹² Finally, when the cyclization reaction is performed under kinetic control, it is possible to obtain larger pillar[*n*]arenes ($n = 7-10$).¹³ The largest member of this family of macrocycles remains however exotic species and the main part of the work done in the field of pillar[*n*]arenes involves cyclo-penta and -hexamers.⁸

1.2. Conformation and chirality of pillar[5]arenes

One of the features of pillar[n]arenes that differs from other classical macrocycles is related to their planar chirality resulting from the position of the alkoxy substituents (Figure 3). When the alkyl group is small enough, oxygen-through-the-annulus movements of the hydroquinone units is possible.¹⁴ In the case of the cyclopentamer, there are in principle eight possible conformers (actually four pairs of enantiomers) depending on the relative orientation of the OR subunits. However, for steric reasons, the D_5 -symmetrical conformers (A and *en-A*) are largely favoured. When the alkoxy group is large enough to prevent the rotation of the hydroquinone subunits, the Friedel-Crafts reaction provides almost exclusively pillar[n]arenes with a D_n symmetry. In the particular case of pericyclohexylmethyl-pillar[5]arene, the enantiomers have been separated by chiral HPLC.¹⁵

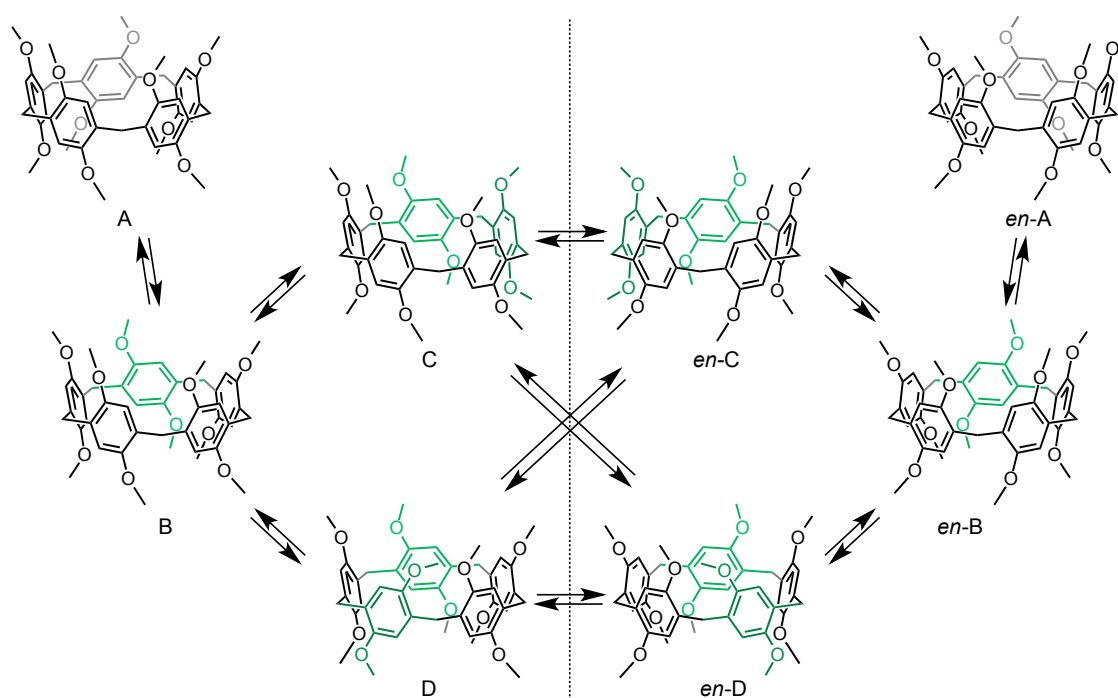


Figure 3. All possible conformers of a pillar[5]arene derivative (four pairs of enantiomers, A: D_5 -symmetric; B, C and D: C_2 -symmetric). For steric reasons, the D_5 -symmetrical conformers (A and *en-A*) are largely favoured but racemization is observed when the alkoxy substituents are small enough to allow oxygen-through-the-annulus movements.

1.3. Nonsymmetrical pillar[5]arenes

As shown in Figure 4, nonsymmetrical pillar[5]arenes have been prepared from non symmetrical 1,4-dialkoxybenzene monomers (i.e. substituted with two different alkoxy units). The cyclopentameric product is obtained as a mixture of four constitutional isomers that have been separated by tedious chromatographic separations in some cases.¹⁶ The co-cyclization from two distinct monomers has been also investigated.¹⁷ In this case, eight possible cyclization products are possible and their relative proportion depends on the relative ratio of the two starting monomers. The preparation of pillar[5]arene derivatives bearing different groups is actually limited due to the formation of mixtures of products and new synthetic methods allowing for the preparation of selected isomers are clearly needed.

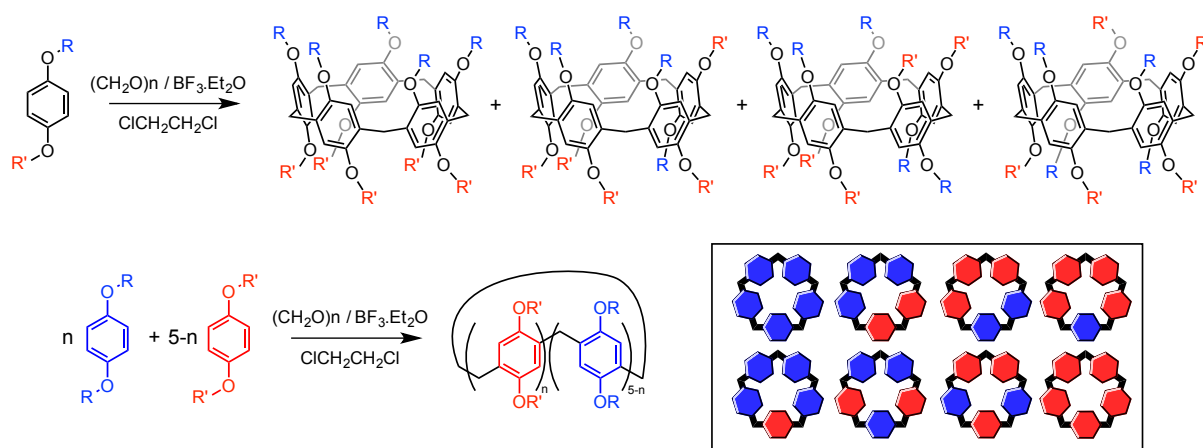


Figure 4. Top: the preparation of pillar[5]arenes from nonsymmetrical monomers leads to four constitutional isomers. Bottom: the co-cyclization from two distinct monomers provides a mixture of 8 cyclization products.

1.4. Pillar[n]arenes as scaffolds for the preparation of nanomaterials

As part of this research, our research team became interested in the use of a pillar[5]arene core as a scaffold for the preparation of nanomaterials with a controlled distribution of functional groups on the macrocyclic framework.¹⁸ As already discussed, pillar[5]arenes are usually prepared from 1,4-dialkoxybenzene derivatives and paraformaldehyde in the presence of a Lewis acid catalyst.⁸ These reaction conditions are

however not compatible with a large variety of functional groups and the direct synthesis of pillar[5]arenes bearing sophisticated substituents is often not possible. The cyclisation reaction is also sensitive to steric effects and the presence of large substituents on the starting 1,4-dialkoxybenzene considerably lowers the yields.⁸ These major problems have been solved by producing readily accessible pillar[5]arene derivatives bearing 10 terminal groups allowing their further functionalization to generate structurally more complicated systems (Figure 5).^{18,19,20}

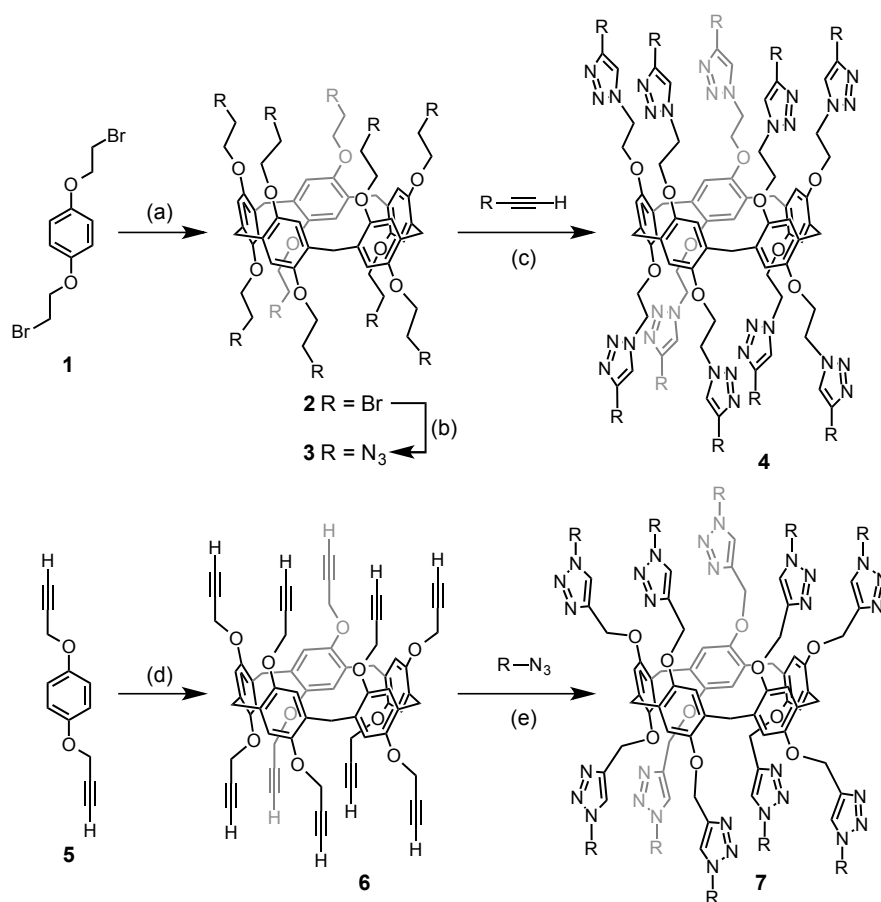


Figure 5. Clickable pillar[5]arene scaffolds developed in our group. *Reagents and conditions:* (a) $\text{BF}_3 \cdot \text{Et}_2\text{O}$, $(\text{CH}_2\text{O})_n$, $\text{ClCH}_2\text{CH}_2\text{Cl}$ (60%); (b) NaN_3 , DMF (98%); (c) $\text{CuSO}_4 \cdot 5\text{H}_2\text{O}$, sodium ascorbate, $\text{CH}_2\text{Cl}_2/\text{H}_2\text{O}$; (d) $\text{BF}_3 \cdot \text{Et}_2\text{O}$, $(\text{CH}_2\text{O})_n$, $\text{ClCH}_2\text{CH}_2\text{Cl}$ (40%); (e) $\text{CuSO}_4 \cdot 5\text{H}_2\text{O}$, sodium ascorbate, $\text{CH}_2\text{Cl}_2/\text{H}_2\text{O}$.

Building block **6** has been already used to produce polycationic derivatives for transfection experiments.²⁰ As shown in Figure 6, dendritic pillar[5]arene derivatives **8** and **9** have been efficiently prepared by grafting dendrons with peripheral Boc-protected amine

subunits onto a preconstructed pillar[5]arene scaffold. Upon cleavage of the Boc-protected groups, water-soluble pillar[5]arene derivatives **10** and **11** with 20 and 40 peripheral ammonium groups, respectively, have been obtained.

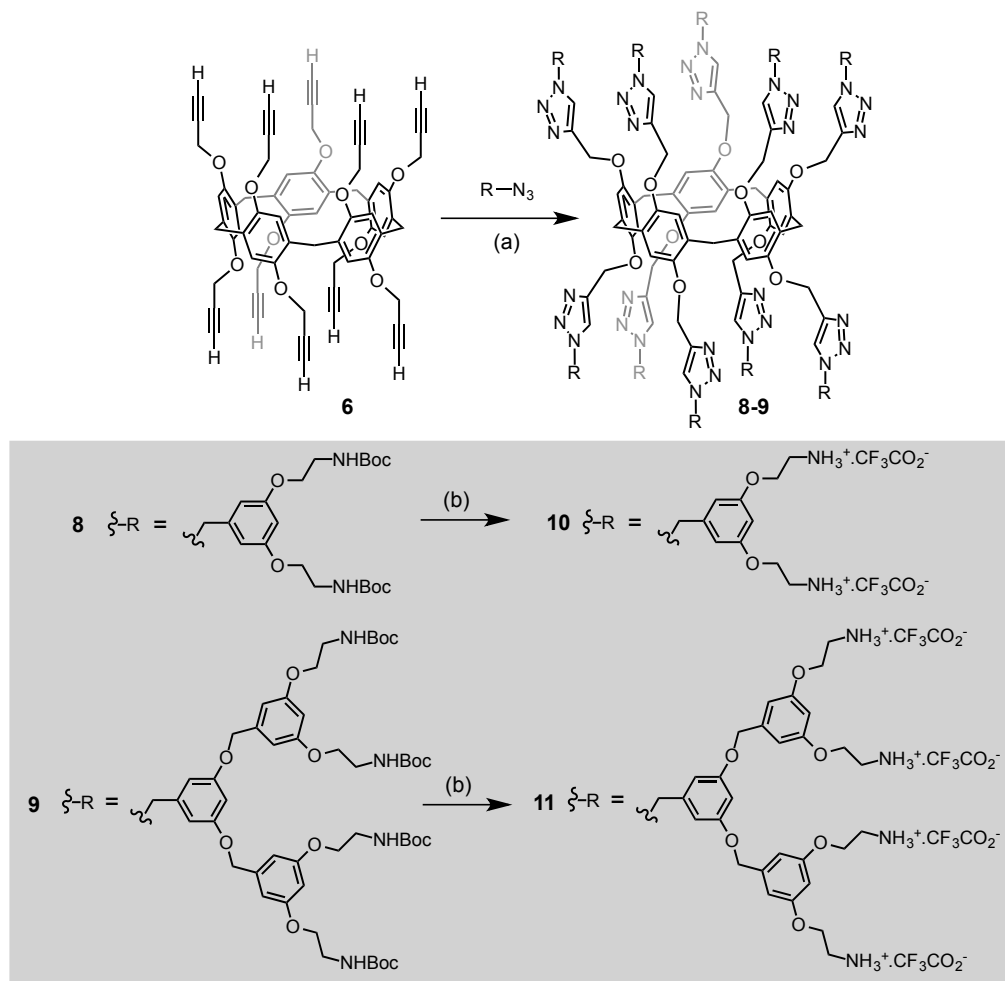


Figure 6. Preparation of polycationic pillar[5]arene derivatives from building block **6**.

Reagents and conditions: (a) $CuSO_4 \cdot 5H_2O$, sodium ascorbate, CH_2Cl_2/H_2O (**8**: 88%, **9**: 81%);

(b) TFA (**10**: quantitative, **11**: quantitative).

The capability of these compounds to form stable nanoparticles with plasmid DNA has been demonstrated by gel electrophoresis, transmission electronic microscopy (TEM) and dynamic light scattering (DLS) investigations. Finally, the capability of both **10** and **11** to efficiently condense plasmid DNA into stable and positively charged polyplexes has been exploited for gene delivery experiments. The transfection efficiencies found for both **10** and **11** are good even if slightly lower than that obtained for the “golden standard” JET-PEITM (commercially available gene delivery system developed by Polyplus-Transfection, Illkirch,

France). What is more, these pillar[5]arene derivatives exhibit good efficiency, while maintaining low toxicity. Both **10** and **11** are by far less toxic than JET-PEI™.

Pillar[5]arene has also been used as a multivalent core unit to prepare glycoconjugates (Figure 7) and mannosylated pillar[5]arene derivative **12** prepared in our group has been assayed as an inhibitor of the adhesion of an uropathogenic *Escherichia coli* strain to red blood cells.²¹ Following this first report on glycopillar[5]arenes, another approach has been reported by Huang and co-workers.²² They have prepared amphiphilic pillar[5]arene **13** containing galactose subunits as the hydrophilic part and alkyl chains as the hydrophobic part.^[10] This compound self-assembles in water to produce nanotubular structures that have been utilized as cell glues to agglutinate *Escherichia coli*.

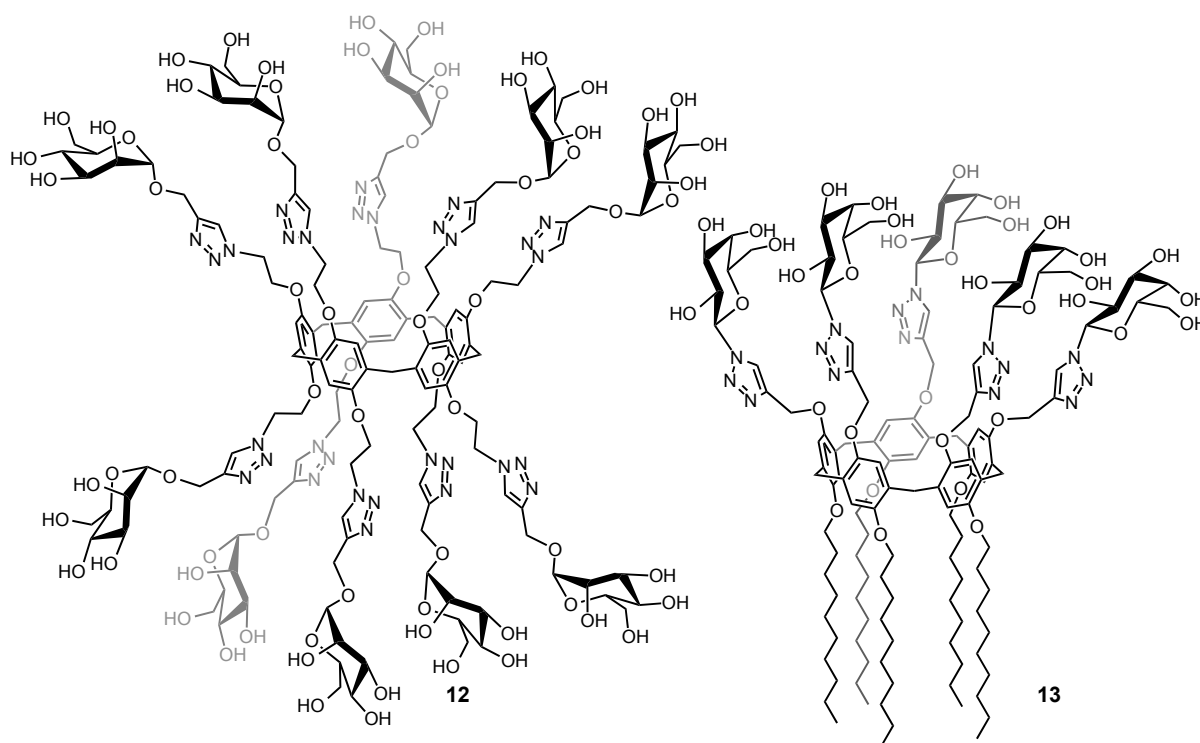


Figure 7. Glycoconjugates **12** and **13**.

Clickable pillar[n]arene ($n = 5$ or 6) building blocks bearing peripheral azide functions have been also decorated with cyanobiphenyl moieties to provide the first examples of liquid-crystalline pillar[n]arene derivatives (compounds **15** and **16**, Figure 8).^{18,23} Importantly, comparison of their mesomorphic properties with those of a model monomer revealed the

dramatic influence of the pillar[*n*]arene core. Indeed, whereas only a monotropic mesophase was observed for the model monomeric compound (**14**: I \rightarrow SmA: 149 °C; SmA \rightarrow Cr: 125 °C), a broad enantiotropic mesophase was evidenced by linking together five (**15**: T_g : 32 °C; SmA \rightarrow I: 201 °C) or six (**16**: T_g : 28 °C; SmA \rightarrow I: 209 °C) linear subunits through the central macrocyclic pillar[*n*]arene core.

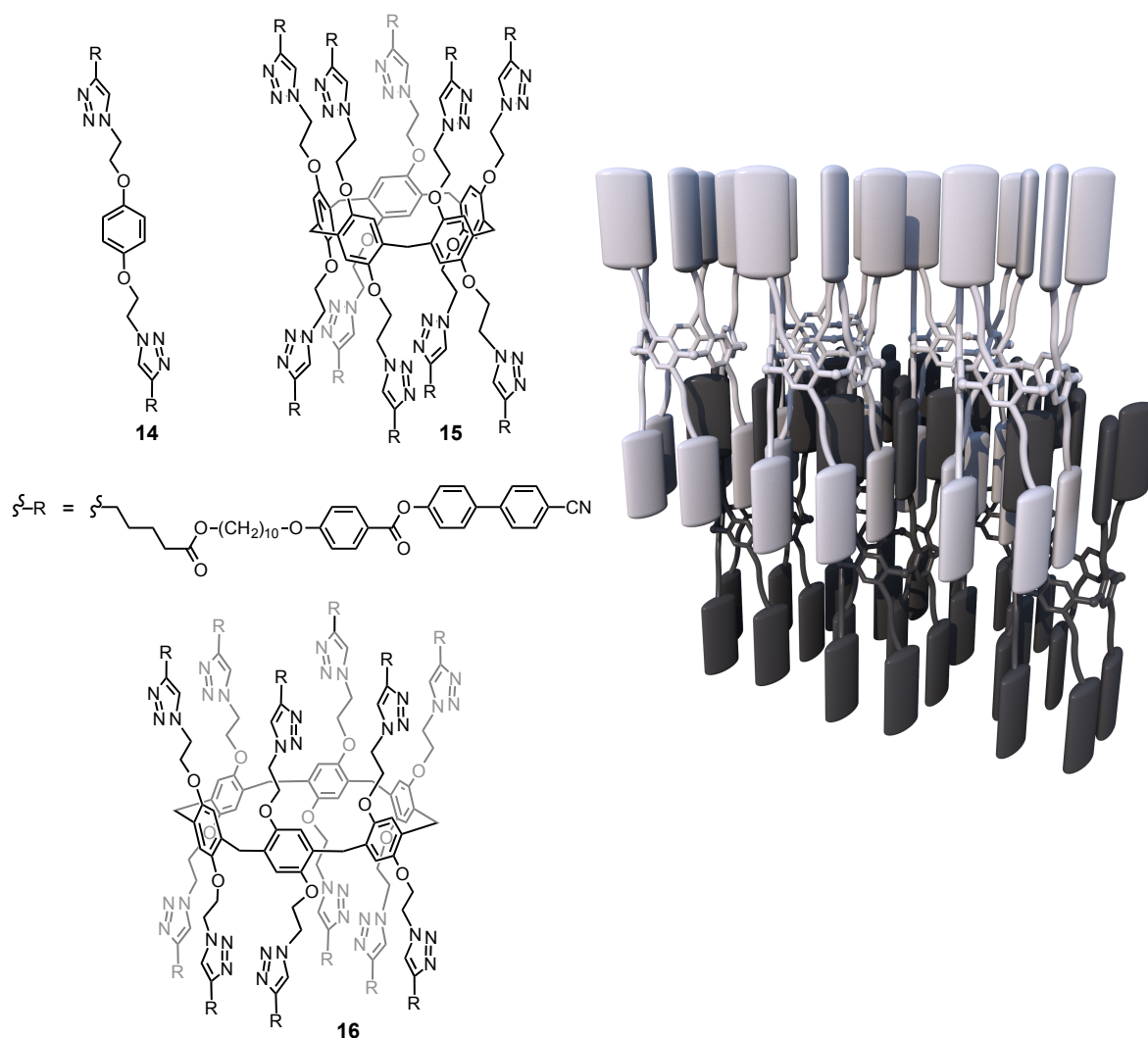


Figure 8. Liquid-crystalline pillar[*n*]arene derivatives **15** and **16** and the corresponding monomeric model compound **14**. Inset: postulated arrangement in the SmA phase for pillar[5]arene derivative **15** deduced from the X-ray diffraction studies.

The specific orientation of the cyanobiphenyl moieties attached on both rims of the macrocyclic core forces the system to adopt a supramolecular organization in which each smectic layer is interdigitated with its two neighboring ones. In this way, the mesophase is

stable over a broad temperature range and this explains the macrocyclic effect observed for pillar[*n*]arene derivatives **15** and **16** when compared to monomeric model compound **14**.

More recently, a similar approach has been used by L. Wang, D. Chen and co-workers to prepare pillar[5]arene liquid crystalline materials incorporating azobenzene subunits (compounds **17** and **18**, Figure 9).²⁴ Both compounds exhibited very wide temperature range smectic A mesophases (**17**: T_g : 48 °C; SmA → I: 189 °C; **18**: T_g : 63 °C; SmA → I: 262 °C). The tubular pillar[5]arene scaffold provides sufficient free volume for the azobenzene moieties to achieve reversible *cis-trans* photoisomerization within the mesophase. Moreover, their thin-films have shown light-triggered modulation of surface free energy and wettability.

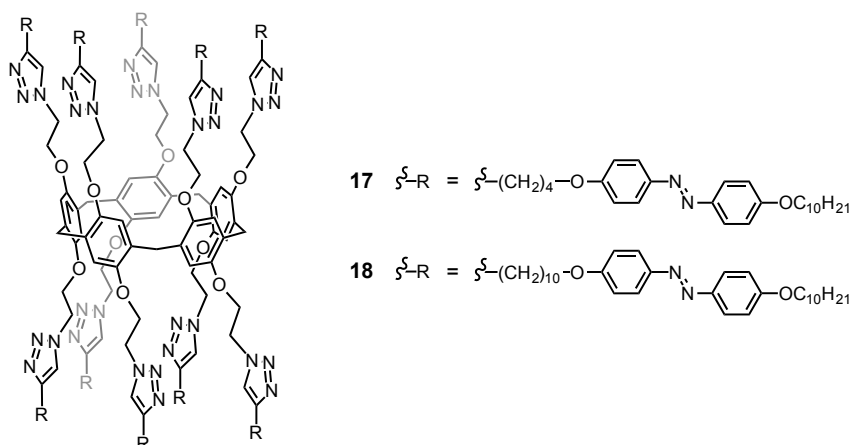


Figure 9. Liquid-crystalline pillar[*n*]arene derivatives **17** and **18**.

1.5. Pillar[*n*]arene-containing pseudorotaxanes and rotaxanes

The host-guest chemistry of pillar[*n*]arene has been intensively investigated.⁸ Owing to the electron-rich nature of their constitutive aromatic subunits, pillar[5]arenes exhibit interesting host-guest properties with electron-accepting molecules such as viologen^{7,25} and imidazolium cations.²⁶ Huang and co-workers have for example shown that the formation of supramolecular complexes between percarboxylated pillar[6]arenes and paraquat is capable of inhibiting the toxicity of paraquat.²⁷ Indeed, the formation of stable host-guest complexes reduces the interaction of paraquat with reducing agents in the cell and the generation of its radical cation is thus more difficult resulting in efficient reduction of paraquat toxicity.

Along with charge-transfer interactions occurring between the electron-rich cavity of pillar[5]arenes and electron-deficient guest molecules, C-H $\cdots\pi$ interaction is also a driving force in the formation of inclusion complexes.⁸ Indeed, simple alkyl-substituted guests are efficiently encapsulated in the cavity of pillar[5]arenes to generate pseudo-rotaxanes.^{16b,27} Such host-guest complexes are indeed perfectly suited for the synthesis of [2]rotaxanes. Stoddart and co-workers have been the first to report the synthesis of a pillar[5]arene-containing [2]rotaxane by treatment of a 1,8-diaminooctane guest with 3,5-di-*tert*-butylbenzaldehyde (Figure 10).²⁸ The yield was however rather low due to the low association constants between the axle and the pillar[5]arene in the solvent system used for the reaction. Following this first example, other [2]rotaxanes have been reported through the installation of bulky stoppers using various reactions. Examples include reactions of acyl chlorides with alcohols³⁰ and copper-catalyzed alkyne-azide cycloadditions.³¹ In the latter cases, the [2]rotaxanes were obtained in fair to good yields.

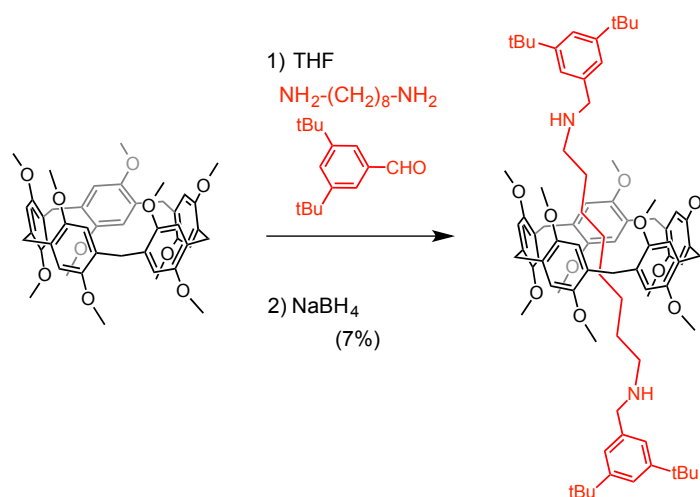


Figure 10. Preparation of the first pillar[5]arene-containing [2]rotaxane.

As part of this research, our group has recently shown that pillar[5]arene-based [2]rotaxanes can be also obtained from the reaction of diacyl chloride reagents with various amine stoppers (Figure 11).³² The yield in [2]rotaxane is actually sensitive to the reaction conditions (solvent, stoichiometry) but also to structural and electronic factors. In particular, the nature of the starting amine reagent has a dramatic influence on the yields of [2]rotaxanes thus showing that the outcome of the reaction is not simply related to the binding constant of the diacyl chloride reagent with the pillar[5]arene. Indeed, the difference in yields must be

related to the difference in affinity for the various mono-acylated intermediates. The yields of [2]rotaxane are also influenced by several structural factors such as the chain length of the bis-acyl chloride reagent or the size of the peripheral substituents of the pillar[5]arene building block.

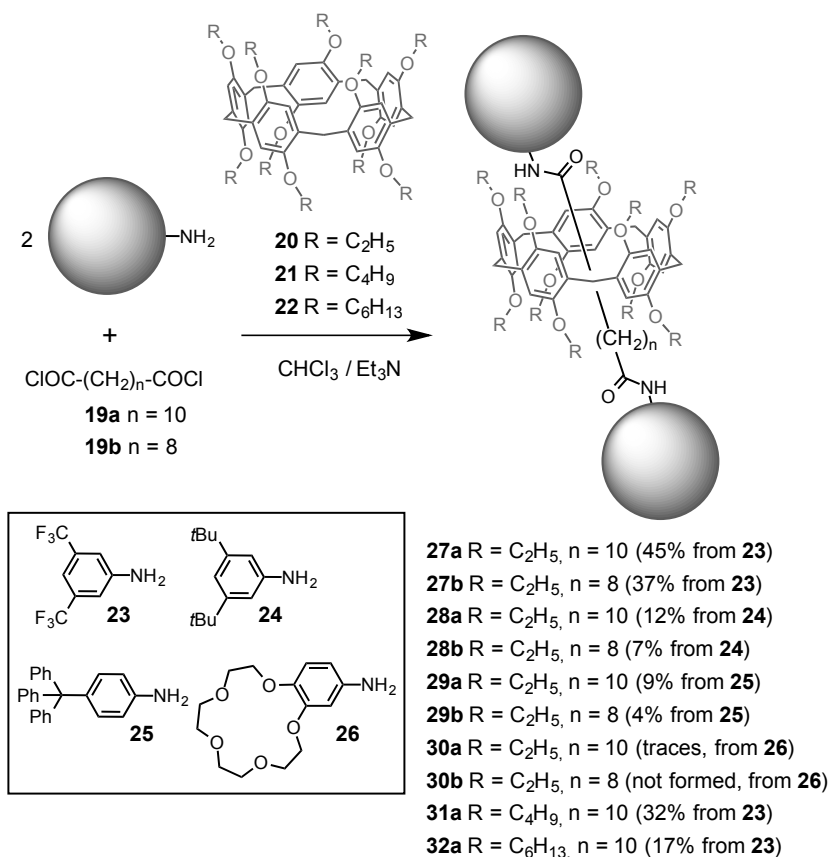


Figure 11. Typical examples of pillar[5]arene-based [2]rotaxanes obtained from the reaction of diacyl chloride reagents with various amine stoppers.

Whereas the synthesis of pillar[5]arene-containing rotaxanes have been at the centre of many studies, the most recent developments are oriented towards their applications.³³ It is also clear that a good understanding of the self-organization capabilities of pillar[*n*]arene-containing rotaxanes is essential for many future applications. As part of this research, our group has recently reported the organization of pillar[5]arene-containing [2]rotaxanes in Langmuir and Langmuir-Blodgett films.³⁴ The amphiphilic compounds are depicted in Figure 12. In the particular case of the [2]rotaxane incorporating a 1,4-diethoxypillar[5]arene subunit, the structure of the compound was confirmed by X-ray crystal structure analysis.

Owing to a good hydrophilic/hydrophobic balance, stable Langmuir films have been obtained for these rotaxanes and the size of the peripheral alkyl chains on the pillar[5]arene subunit has a dramatic influence on the reversibility during compression-decompression cycles. Indeed, when these are small enough, molecular reorganization of the rotaxane by gliding motions are capable of preventing strong π - π interactions between neighbouring macrocycles in the thin film.

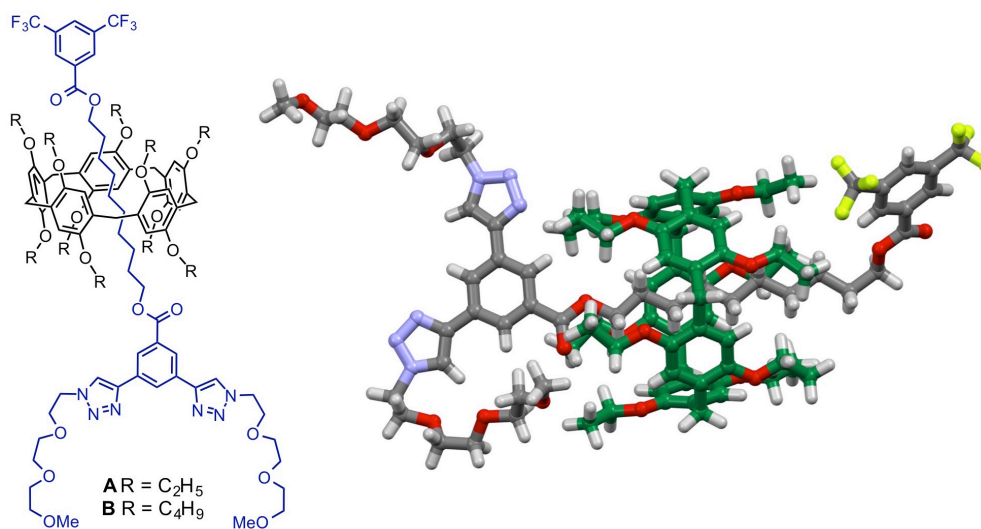


Figure 8. Left: amphiphilic pillar[5]arene-containing [2]rotaxanes **A** and **B** that have been used for the preparation of Langmuir and Langmuir-Blodgett films. Right: X-ray crystal structure of **A** (N: blue, O: red, F: pale green, C: gray for the dumbbell and dark green for the pillar[5]arene subunit).

1.6. Research plan

Pillar[*n*]arenes are a new class of macrocycles that are efficiently prepared from readily available building blocks. They have been already used for the construction of various supramolecular assemblies including [2]rotaxanes. The combination of pillararene chemistry with materials science is appealing as the unique structural features of pillar[*n*]arenes (multivalency, shape and chirality) should afford new materials that may be not produced by using other macrocyclic hosts. To further explore the potential of our clickable pillar[*n*]arene building blocks, the present PhD thesis has been devoted to the preparation of liquid-

crystalline pillar[5]arenes showing columnar mesomorphism (chapter 2) and to the synthesis of electro- and/or photo-active molecular devices (chapters 3 and 4). We have also combined our recent concepts for the preparation of multifunctional nanomolecules (click chemistry on multifunctional scaffolds) with supramolecular chemistry (self-assembly to prepare pseudo-rotaxanes and rotaxanes) to prepare sophisticated supramolecular materials combining two different functional subunits (chapter 4). In particular, multiporphyrinic arrays mimicking the natural light-harvesting antennae of the photosynthetic center have been thus prepared.

References

- 1) F. Diederich, P. Stang, R. R. Tykwinski (Eds.), *Modern Supramolecular Chemistry*, Wiley-VCH, **2008**.
- 2) M. Hiraoka, *Crown Ethers and Analogous Compounds*, Elsevier Science & Technology Books, **1992**.
- 3) H. Dodziuk (Ed.), *Cyclodextrins and their Complexes*, Wiley-VCH, **2006**.
- 4) K. Kim, Y. Ho Ko, N. Selvapalam, *Cucurbiturils: Chemistry, Supramolecular Chemistry and Applications*, World Scientific Publishing Company, **2013**.
- 5) M. J. Hardie, *Chem. Soc. Rev.* **2010**, *39*, 516.
- 6) J. Harrowfield, J. Vicens (Eds.), *Calixarenes in the nanoworld*, Springer, **2007**.
- 7) T. Ogoshi, S. Kanai, S. Fujinami, T. Yamagishi, Y. Nakamoto, *J. Am. Chem. Soc.* **2008**, *130*, 5022.
- 8) For reviews on pillar[n]arenes, see: a) P. J. Cragg, K. Sharma, *Chem. Soc. Rev.* **2012**, *41*, 597; b) M. Xue, Y. Yang, X. Chi, Z. Zhang, F. Huang, *Acc. Chem. Res.* **2012**, *45*, 1294; c) T. Ogoshi, *J. Incl. Phenom. Macrocycl. Chem.* **2012**, *72*, 247; d) T. Ogoshi, T.-a. Yamagishi, *Eur. J. Org. Chem.* **2013**, 2961; e) H. Zhang, Y. Zhao, *Chem. Eur. J.* **2013**, *19*, 16862; f) D. Cao, H. Meier, *Asian J. Org. Chem.* **2014**, 244; g) T. Ogoshi, T. Yamagishi, *Chem. Commun.* **2014**, 4776; h) N. L. Strutt, H. Zhang, S. T. Schneebeli, J. F. Stoddart, *Acc. Chem. Res.* **2014**, *47*, 2631.
- 9) a) T. Ogoshi, T. Aoki, K. Kitajima, S. Fujinami, T.-a. Yamagishi, Y. Nakamoto, *J. Org. Chem.* **2011**, *76*, 328; b) D. Cao, Y. Kou, J. Liang, Z. Chen, L. Wang, H. Meier, *Angew. Chem. Int. Ed.* **2009**, *48*, 9721; c) Y. Kou, H. Tao, D. Cao, Z. Fu, D. Schollmeyer, H. Meier, *Eur. J. Org. Chem.* **2010**, 6464; d) Y. Ma, Z. Zhang, X. Ji, C. Han, J. He, Z. Abliz, W. Chen, F. Huang, *Eur. J. Org. Chem.* **2011**, 5331.
- 10) H. Tao, D. Cao, L. Liu, Y. Kou, L. Wang, H. Meier, *Sci. China Chem.* **2012**, *55*, 223.
- 11) T. Boinski, A. Szumma, *Tetrahedron* **2012**, *68*, 9419-9422.
- 12) M. Holler, N. Allenbach, J. Sonet, J.-F. Nierengarten, *Chem. Commun.* **2012**, 48, 2576
- 13) a) X.-B. Hu, Z. Chen, L. Chen, L. Zhang, J.-L. Hou, Z.-T. Li, *Chem. Commun.* **2012**, 48, 10999; b) C. Han, Z. Zhang, X. Chi, M. Zhang, G. Yu, F. Huang, *Acta Chim. Sinica* **2012**, *70*, 1775; c) Y. Chen, H. Q. Tao, H. Meier, J. L. Fu, D. R. Cao, *Chinese Chem. Lett.* **2012**, *23*, 509.

-
- 14) T. Ogoshi, K. Kitayama, T. Aoki, S. Fujinami, T. Yamagashi, Y. Nakamoto, *J. Org. Chem.* **2010**, *75*, 3268.
- 15) T. Ogoshi, K. Masaki, R. Shiga, K. Kitayama, T.-a. Yamagashi, *Org. Lett.* **2011**, *13*, 1264.
- 16) a) T. Ogoshi, K. Kitayama, T.-a. Yamagashi, Y. Nakamoto, *Org. Lett.* **2010**, *12*, 636; b) Z. Zhang, Y. Luo, B. Xia, C. Han, Y. Yu, X. Chen, F. Huang, *Chem. Commun.* **2011**, *47*, 2417; c) Y. H. Kou, H. Q. Tao, D. R. Cao, Z. Y. Fu, D. Schollmeyer, H. Meier, *Eur. J. Org. Chem.* **2010**, 6464.
- 17) a) Z. Zhang, B. Xia, C. Han, Y. Yu, F. Huang, *Org. Lett.* **2010**, *12*, 3285; b) L. Liu, D. Cao, Y. Jin, H. Tao, Y. Kou, H. Meier, *Org. Biomol. Chem.* **2011**, *9*, 7007.
- 18) I. Nierengarten, S. Guerra, M. Holler, J.-F. Nierengarten, R. Deschenaux, *Chem. Commun.* **2012**, *48*, 8072.
- 19) For other examples of clickable pillar[5]arene derivatives, see: a) H. Zhang, N. L. Strutt, R. S. Stoll, H. Li, Z. Zhu, J. F. Stoddart, *Chem. Commun.* **2011**, *47*, 11420; b) N. L. Strutt, H. Zhang, M. A. Giesener, J. Lei, J. F. Stoddart, *Chem. Commun.* **2012**, *48*, 1647; c) H. Deng, X. Shu, X. Hu, J. Li, X. Jia, C. Li, *Tetrahedron Lett.* **2012**, *53*, 4609; d) G. Yu, Z. Zhang, J. He, Z. Abliz, F. Huang, *Eur. J. Org. Chem.* **2012**, 5902.
- 20) I. Nierengarten, M. Nothisen, D. Sigwalt, T. Biellmann, M. Holler, J.-S. Remy, J.-F. Nierengarten, *Chem. Eur. J.* **2013**, *19*, 17552.
- 21) I. Nierengarten, K. Buffet, M. Holler, S. P. Vincent, J.-F. Nierengarten, *Tetrahedron Lett.* **2013**, *54*, 2398.
- 22) G. Yu, Y. Ma, C. Han, Y. Yao, G. Tang, Z. Mao, C. Gao, F. Huang, *J. Am. Chem. Soc.* **2013**, *135*, 10310.
- 23) I. Nierengarten, S. Guerra, M. Holler, L. Karmazin-Brelot, J. Barbera, R. Deschenaux, J.-F. Nierengarten, *Eur. J. Org. Chem.* **2013**, 3675.
- 24) S. Pan, M. Ni, B. Mu, Q. Li, X.-Y. Hu, C. Lin, D. Chen, L. Wang, *Adv. Funct. Mater.* **2015**, *25*, 3571.
- 25) a) C. Li, Q. Xu, J. Li, Y. Feina, X. Jia, *Org. Biomol. Chem.* **2010**, *8*, 1568; b) T. Ogoshi, D. Yamafuji, T. Aoki, T.-a. Yamagishi, *J. Org. Chem.* **2011**, *76*, 9497.
- 26) a) T. Ogoshi, S. Tanaka, T.-a. Yamagishi, Y. Nakamoto, *Chem. Lett.* **2011**, *40*, 96; b) C. Li, L. Zhao, J. Li, X. Ding, S. Chen, Q. Zhang, Y. Yu, X. Jia, *Chem. Commun.* **2010**, *46*, 11294.

-
- 27) G. Yu, X. Zhou, Z. Zhang, C. Han, Z. Mao, C. Gao, F. Huang, *J. Am. Chem. Soc.* **2012**, *134*, 19489.
- 28) For selected examples, see: a) C. Li, Q. Xu, J. Li, F. Yao, X. Jia, *Org. Biomol. Chem.* **2010**, *8*, 1568; b) C. Li, L. Zhao, J. Li, X. Ding, S. Chen, Q. Zhang, Y. Yu, X. Jia, *Chem. Commun.* **2010**, *46*, 9016; c) T. Ogoshi, Y. Nishida, T.-a. Yamagishi, Y. Nakamoto, *Chem. Commun.* **2010**, *46*, 3708.
- 29) N. L. Strutt, R. S. Forgan, J. M. Spruell, Y. Botros, J. F. Stoddart, *J. Am. Chem. Soc.* **2011**, *133*, 5668.
- 30) a) T. Ogoshi, D. Yamafuji, T. Aoki, K. Kitajima, T.-a. Yamagishi, Y. Hayashi, S. Kawauchi, *Chem. Eur. J.* **2012**, *18*, 7493, b) T. Ogoshi, R. Shiga, T.-a. Yamagishi, *J. Am. Chem. Soc.* **2012**, *134*, 4577.
- 31) a) S. Dong, C. Han, B. Zheng, M. Zhang, F. Huang, *Tetrahedron Lett.* **2012**, *53*, 3668; b) P. Wei, X. Yan, J. Li, Y. Ma, Y. Yao, F. Huang, *Tetrahedron* **2013**, *68*, 9179.
- 32) R. Milev, A. Lopez-Pacheco, I. Nierengarten, T. M. N. Trinh, M. Holler, R. Deschenaux, J.-F. Nierengarten, *Eur. J. Org. Chem.* **2015**, 479.
- 33) a) X.-Y. Hu, X. Wu, Q. Duan, T. Xiao, C. Lin, L. Wang, *Org. Lett.* **2012**, *14*, 4826; b) T. Ogoshi, D. Yamafuji, T.-a. Yamagishi, A. M. Brouwer, *Chem. Commun.* **2013**, *49*, 5468; c) C. Ke, N. L. Strutt, H. Li, X. Hou, K. J. Hartlieb, P. R. McGonigal, Z. Ma, J. Iehl, C. L. Stern, C. Cheng, Z. Zhu, N. A. Vermeulen, T. J. Meade, Y. Y. Botros, J. F. Stoddart, *J. Am. Chem. Soc.* **2013**, *135*, 17019; d) X. Hou, C. Ke, C. Cheng, N. Song, A. K. Blackburn, A. A. Sarjeant, Y. Y. Botros, Y.-W. Yang, J. F. Stoddart, *Chem. Commun.* **2014**, *50*, 6196.
- 34) T. M. N. Trinh, I. Nierengarten, M. Holler, J.-L. Gallani, J.-F. Nierengarten, *Chem. Eur. J.* **2015**, *21*, 8019.

2. *Liquid-crystalline pillar[5]arene derivatives*

2.1. *Introduction*

Following the first example of liquid-crystalline pillar[n]arene derivatives reported in our group,¹ the first part of the present work is aiming to further explore the potential of this new class of macrocyclic compounds in the field of liquid crystals. The self-organization of pillar[n]arene derivatives into tubular nanostructure within columnar phases has not been achieved so far and represents an interesting conceptual challenge. In this respect, we propose to functionalize our clickable pillar[5]arene building blocks with Percec-type poly(benzylether) dendrons in order to achieve such a supramolecular organization. These dendrons have been selected as they are known to promote self-organization into columnar phases.^{2,3} This molecular design is also inspired by a recent work performed in our group.⁴ Dendronized fullerene hexa-adducts have been prepared from a preconstructed fullerene hexa-adduct and appropriate dendritic building blocks under copper-catalyzed alkyne-azide cycloaddition (CuAAC) conditions. Typical examples are shown in Figure 1. Mesomorphic properties have been evidenced for all these compounds. The conformation adopted by the compounds is mainly dominated by the self-assembling capabilities of the peripheral dendrons. Indeed, the twelve dendrons drive the conformational equilibrium towards the formation of disc-shaped structures perfectly suited for the self-organization into columnar liquid-crystalline phases. The C₆₀ cores are located at the center of the columns to generate 1-dimensional C₆₀-nanowires. It can also be noted that the spacer subunits between the dendrons and the core play a role in the hierarchical information transfer. This is effectively the case

when the spacer incorporates a stereogenic centre (compound **B**) leading to the self-organization of chiral columns as evidenced by circular dichroism measurements.

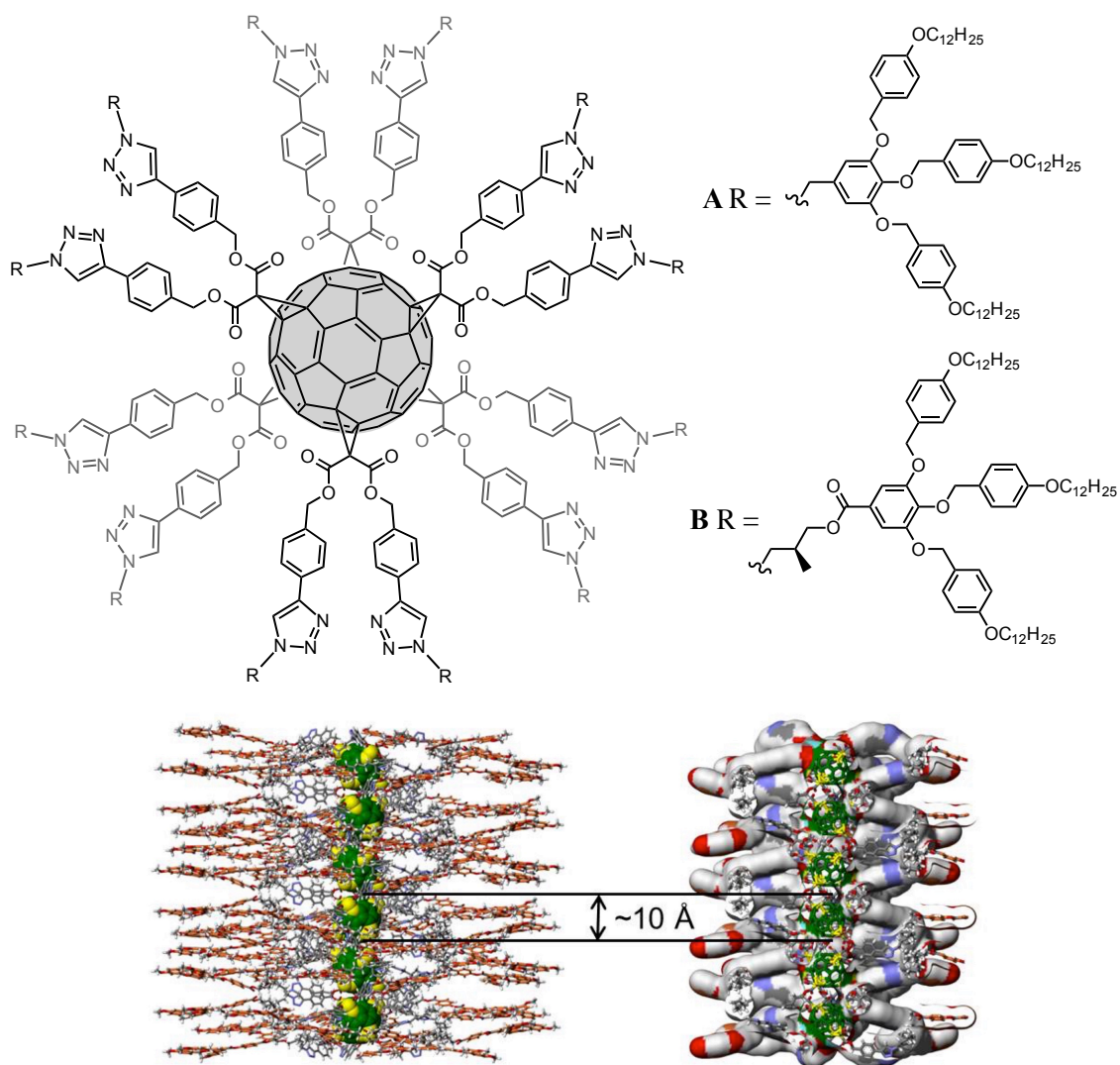
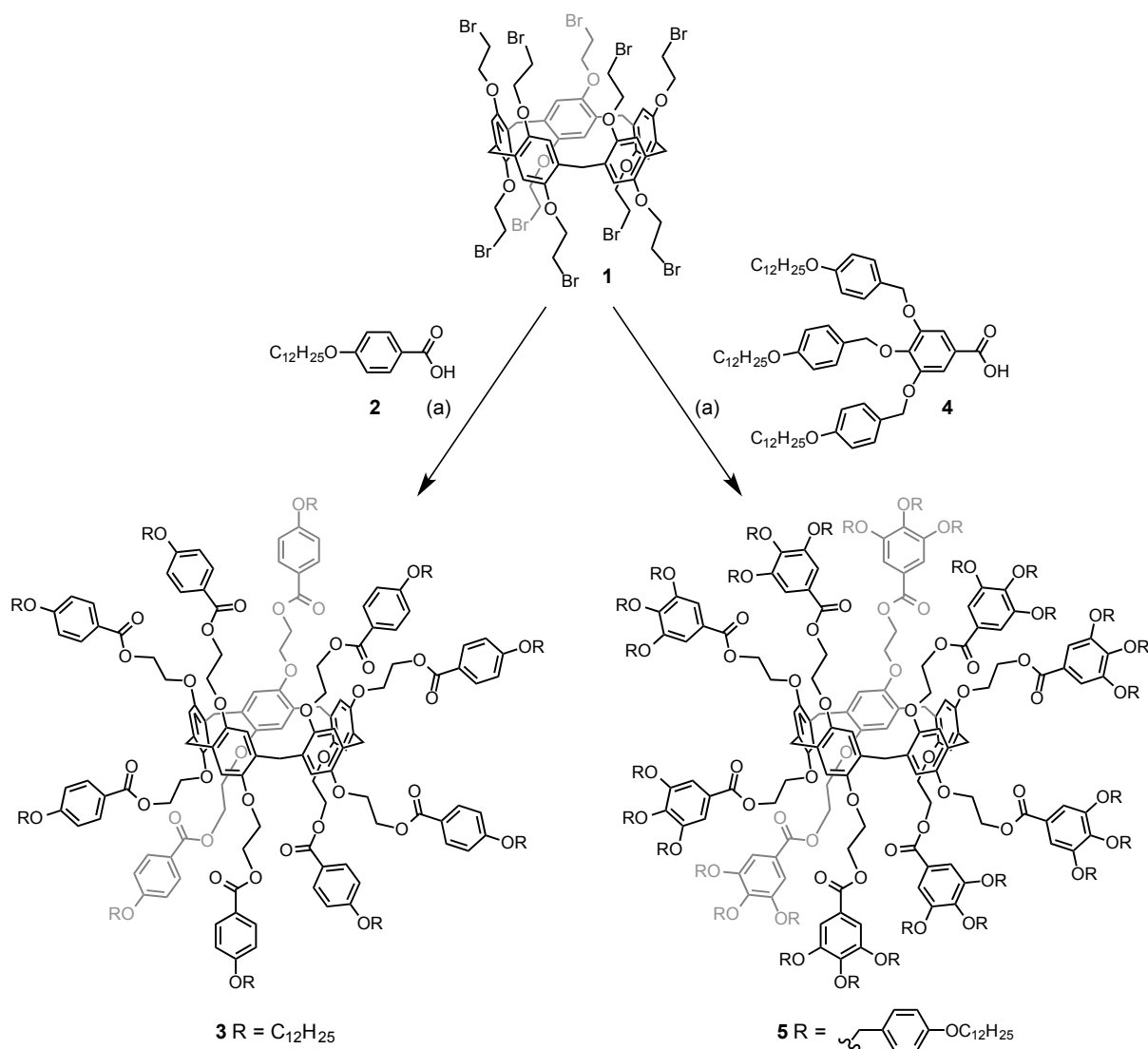


Figure 1. Typical examples of dendronized [60]fullerene and supramolecular organisation model within the columnar phase. Color code: gray as C, white as H, red as O, and blue as N; Orange as dendron aromatic rings, green as fullerene core, and yellow as the cyclopropane rings on the fullerene surface (adapted from reference 4).

2.2. Synthesis

A first synthetic approach for the grafting of peripheral poly(benzylether) dendrons onto the pillar[5]arene scaffold was based on the acylation of decabromide **1** with carboxylates (Scheme 1). The reaction conditions were first adjusted with reagent **2**. Under

optimized conditions, treatment of **1** (1 equiv.) with an excess of **2** (12 equiv.) and K_2CO_3 (24 equiv.) in DMF at $80^\circ C$ for 96 h gave compound **3** in 80% yield. The functionalization of pillar[5]arene **1** with dendron **4** was then performed under the same conditions. After work-up and purification, compound **5** was thus obtained in 57% yield.



Scheme 1. Preparation of compounds **3** and **5**. *Reagents and conditions:* (a) K_2CO_3 , DMF, $80^\circ C$ [from **2**: **3** (80%); from **4**: **5** (57%)].

The structure and purity of compounds **3** and **5** were confirmed by 1H and ^{13}C NMR spectroscopy and elemental analysis. The 1H NMR spectra of **3** and **5** are depicted in Figure 2. For both compounds, unambiguous assignments were achieved on the basis of 2D-COSY and NOESY spectra recorded at room temperature in CD_2Cl_2 .

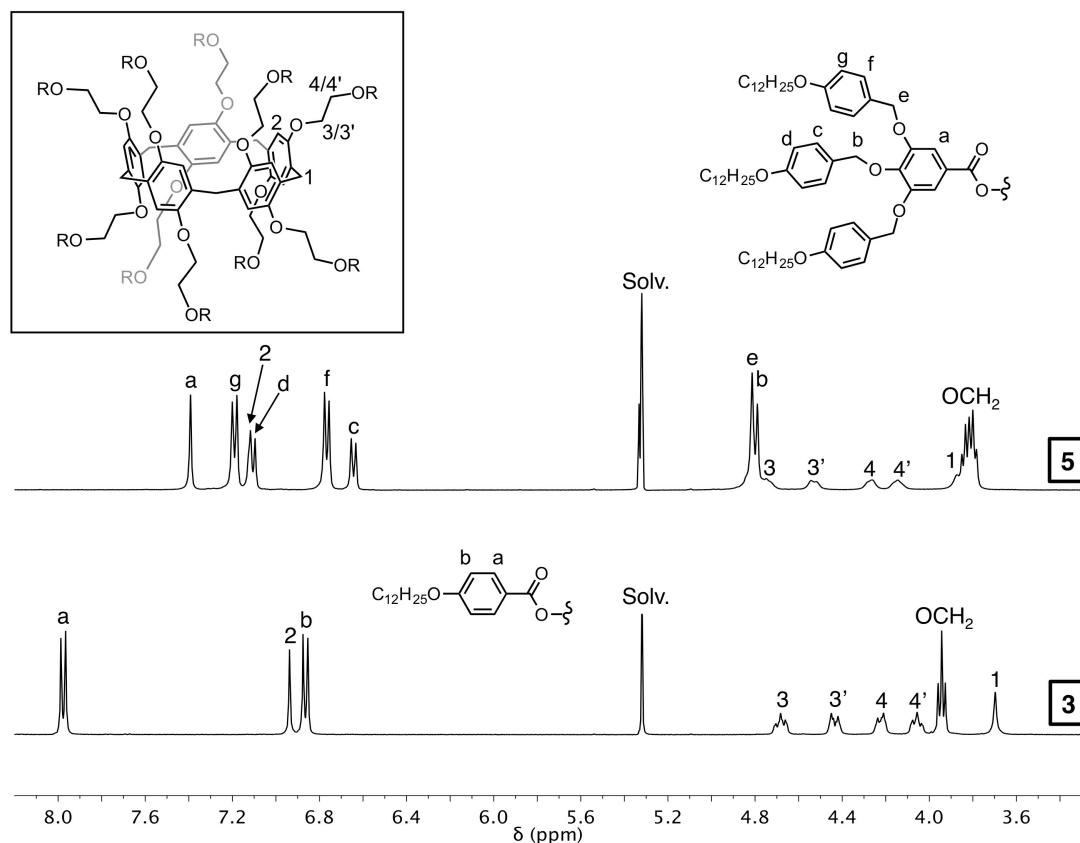


Figure 2. ^1H NMR (CD_2Cl_2 , 400 MHz) of compounds **3** and **5**.

The spectrum of **3** shows all the expected features of a D_{5h} symmetrical compound. Effectively, a single set of signals is observed for the ten equivalent *p*-dodecyloxybenzoate groups. The spectrum is also characterized by two singlets at $\delta = 6.94$ and 3.69 ppm corresponding to the resonances of the protons of the pillar[5]arene core unit (H-1 and H-2). Compound **3** is chiral and both CH_2 groups of the ten equivalent ethylene linkers are diastereotopic. Accordingly, four sets of signals are observed for the resonances of these protons (H-3/3'/4/4'). The ^1H -NMR of compound **5** is also consistent with the proposed structure. In addition to the signals corresponding to the pillar[5]arene core unit, the resonances arising from the ten equivalent dendrons are clearly observed. Effectively, two singlets are observed for the benzylic CH_2 groups (H-b and H-e) as well as five aromatic signals in a typical pattern for a first generation Percec-type dendron.⁴

The structure of compound **3** was also confirmed by its MALDI-TOF mass spectra showing the expected molecular ion peak at $m/z = 3933.67$ ($[\text{M}+\text{H}]^+$, calcd for $\text{C}_{245}\text{H}_{351}\text{O}_{40}$: 3933.54). Under the same experimental conditions, the molecular ion peak could not be

detected for compound **5**. This was not result of high levels of fragmentation as characteristic fragments were also not observed but it might be related to aggregation effects preventing the transfer of the compounds/fragments in the gas phase during the MS analysis. A similar behavior has been reported for analogous compounds constructed on a hexasubstituted fullerene core.⁴ The monodispersity of compound **5** was however clearly supported by its chromatogram recorded on a HPLC equipped with a PLgel size exclusion column (Figure 3). Comparison with the chromatogram recorded for compound **3** under the same conditions reveals a shorter retention time for **5**. This is in perfect agreement with the larger size of compound **5** when compared to **3**.

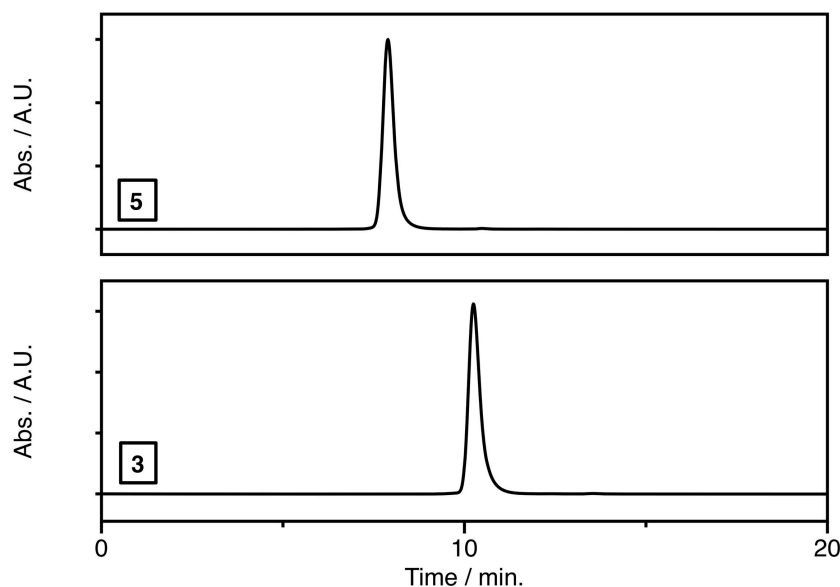
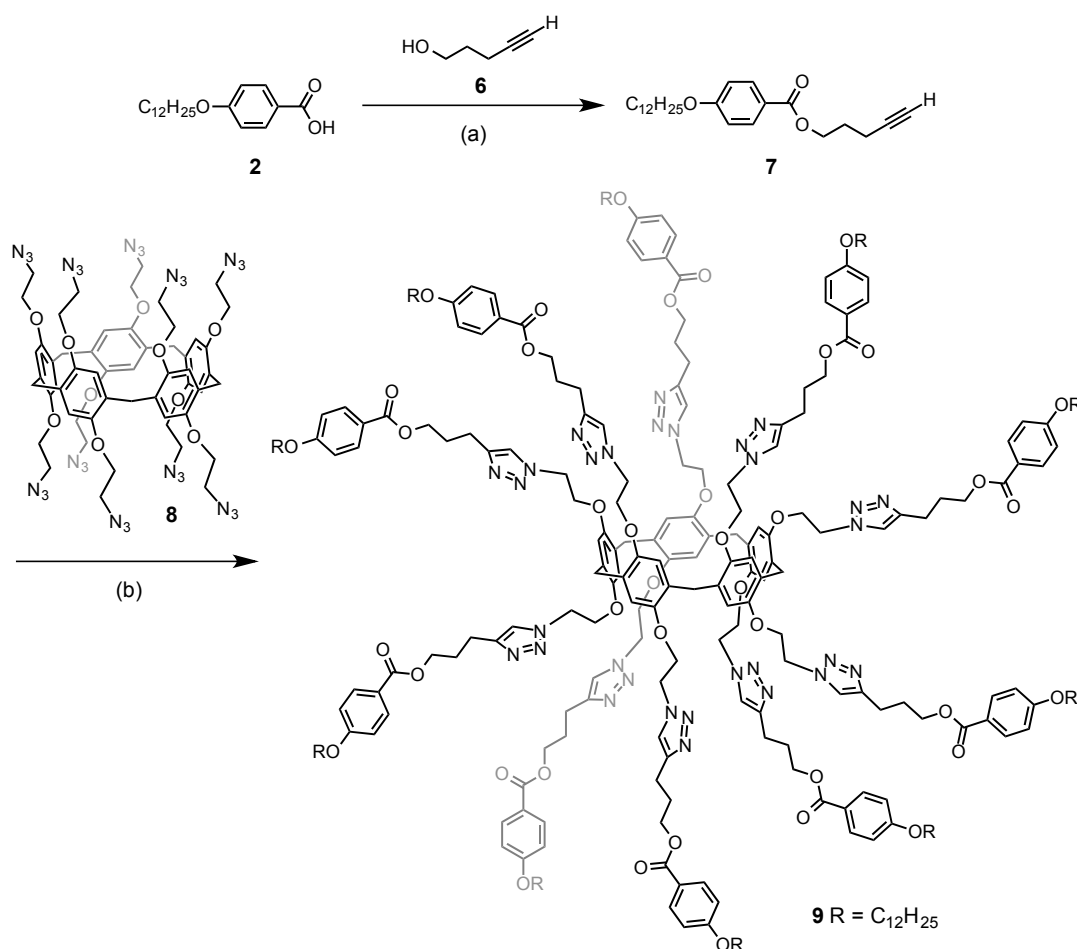


Figure 3. HPLC traces on a size exclusion column (PLgel, CH₂Cl₂, UV detector at $\lambda = 254$ nm) obtained for compounds **3** and **5**.

A second series of compounds was prepared from dodecaazide **8** (Schemes 2 and 3). Compound **8** was obtained by reaction of dodecabromide **1** with sodium azide in DMF at room temperature as described in the literature.¹ Owing to the high number of azide residues, compound **8** was handled with special care: upon evaporation, polyazide **8** was not dried under high vacuum and the use of metallic spatula avoided. Furthermore, this compound was always prepared on a small scale (< 500 mg).

The *p*-dodecyloxybenzoate moiety was first equipped with a terminal alkyne function to allow their grafting onto clickable pillar[5]arene building block **8** (Scheme 2). This was achieved by reaction of *p*-dodecyloxybenzoic acid (**2**) with 4-pentyn-1-ol (**6**) under

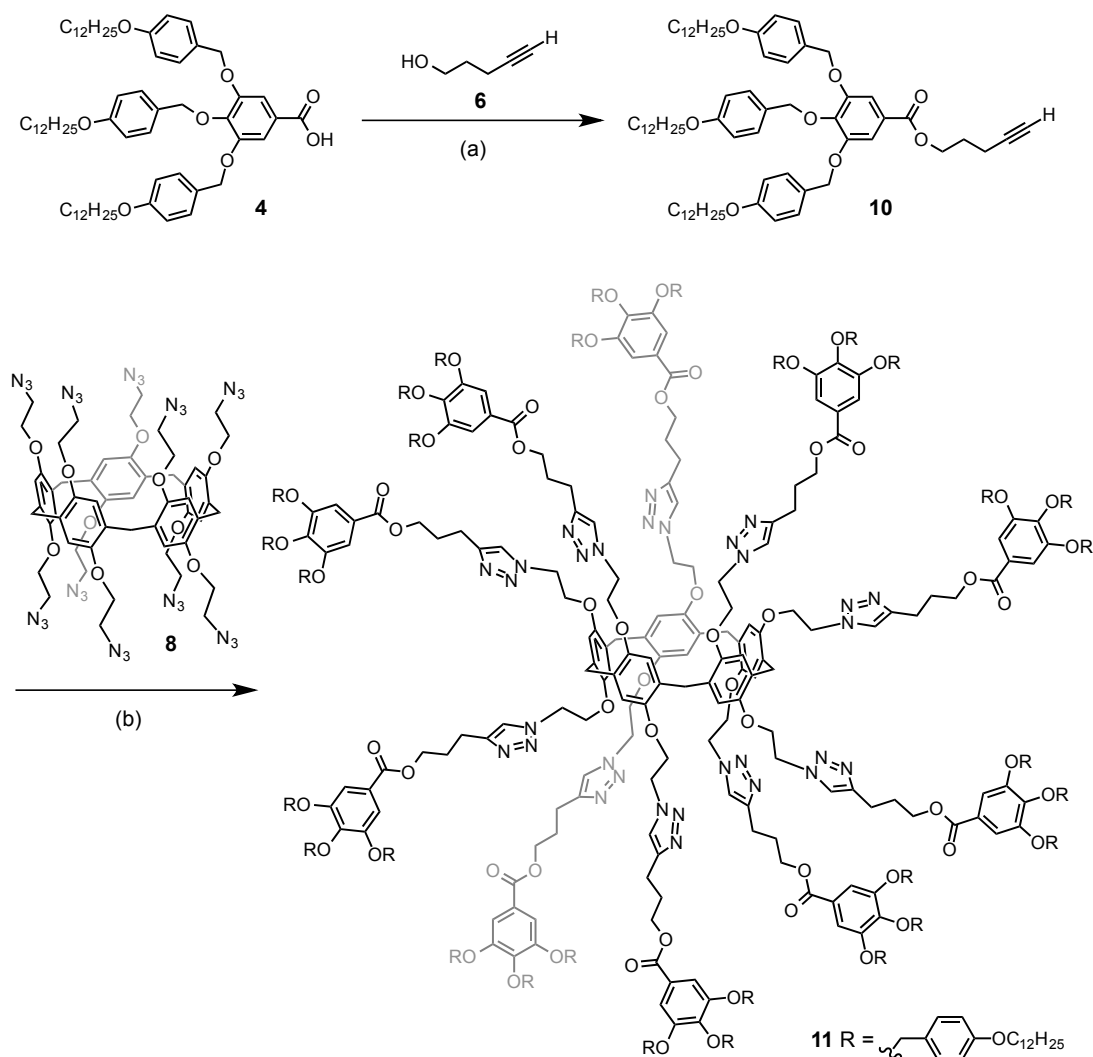
esterification conditions using *N*-(3-dimethylaminopropyl)-*N'*-ethylcarbodiimide hydrochloride (EDC) and 4-(dimethylamino)pyridinium *p*-toluenesulfonate (DPTS).⁵ Compound **7** was thus obtained in 93% yield. The functionalization of pillar[5]arene **8** with **7** was performed under the typical CuAAC conditions reported by Sharpless⁶ (CuSO₄·5H₂O/sodium ascorbate/CH₂Cl₂/H₂O). After purification by column chromatography on SiO₂, compound **9** was isolated in 41% yield. This moderate yield is explained by difficulties encountered during the purification due to the presence of an undefined polar impurity that was difficult to separate from the desired product.



Scheme 2. Preparation of compound **9**. *Reagents and conditions:* (a) EDC, DPTS, CH₂Cl₂, 0 to 25°C (93%); (b) CuSO₄·5H₂O, sodium ascorbate, CH₂Cl₂, H₂O, 25°C (41%).

Compound **11** was prepared by following the same synthetic strategy (Scheme 3). Esterification of carboxylic acid **4** with alcohol **6** afforded clickable dendron **10** in 81% yield.

Reaction of **8** with an excess of **10** in the presence of $\text{CuSO}_4 \cdot 5\text{H}_2\text{O}$ and sodium ascorbate gave dendronized pillar[5]arene **11** in 41% yield.



Scheme 3. Preparation of compound **11**. *Reagents and conditions:* (a) EDC, DPTS, CH_2Cl_2 , 0 to 25°C (81%); (b) $\text{CuSO}_4 \cdot 5\text{H}_2\text{O}$, sodium ascorbate, CH_2Cl_2 , H_2O , 25°C (41%).

The structure of compounds **9** and **11** was confirmed by their ^1H and ^{13}C NMR spectra. Inspection of the ^1H NMR spectra indicates total disappearance of the CH_2 -azide signal observed at $\delta = 3.67$ ppm for **8** and the characteristic signal of the ten equivalents 1,2,3-triazole unit is observed at $\delta = 7.61$ and 7.66 ppm for **9** and **11**, respectively. The complete peripheral functionalization of the pillar[5]arene core was further confirmed by the IR data showing that no azide residues (2089 cm^{-1}) remain in the final products (Figure 4). The MALDI-TOF mass spectrum of **9** shows the expected pseudo-molecular ion peak at $m/z =$

5027.08 ($[M+H]^+$, calcd for $C_{295}H_{421}O_{40}N_{30}$: 5027.19). As observed for compound **5**, aggregation effects prevented the observation of the molecular ion peak of compound **11**. The monodispersity of **11** was however attested by the elemental analysis results as well as by the HPLC trace obtained on a gel permeation chromatography column.

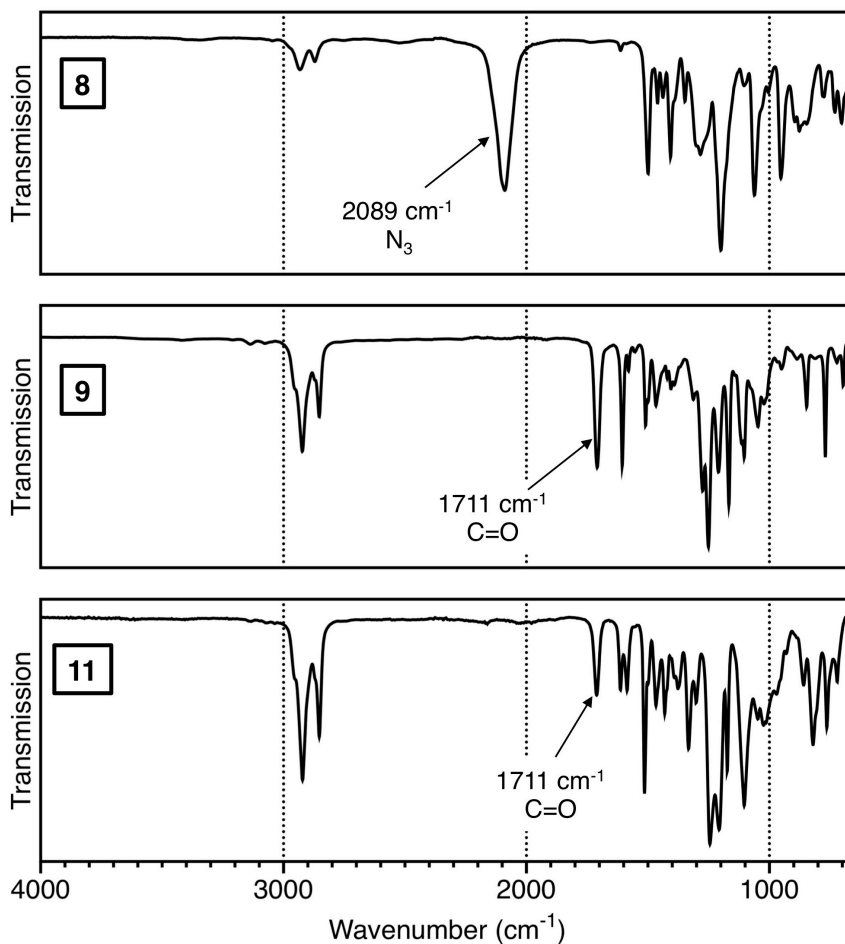


Figure 4. IR spectra of compounds **8**, **9** and **11**.

2.3. Host-guest complexes

The host-guest complexes described herein have been prepared and investigated by Iwona Nierengarten and Sebastiano Guerra.

Pillar[5]arenes exhibit interesting host-guest properties with electron-accepting molecules but also with simple alkyl-substituted guests.⁷ We became thus also interested in preparing inclusion complexes from pillar[5]arene **3**, **5**, **9** and **11** in order to modulate their

thermal properties. In this perspective, we have selected 1,6-dicyanohexane as a guest molecule.⁸ In the solid state, dipole-dipole interactions are often observed between nitrile moieties of neighboring molecules oriented in an antiparallel fashion. This effect plays also an important role in the supramolecular organization of liquid-crystalline nitrile derivatives, cyanobiphenyl derivatives being emblematic examples.⁹ In the case of inclusion complexes obtained from 1,6-dicyanohexane and pillar[5]arene derivatives **3**, **5**, **9** and **11**, one may anticipate that the CN groups of neighboring inclusion complexes will give rise to intermolecular dipole-dipole interactions within the columnar stacks and thus stabilize the supramolecular organization.

2.3.1. NMR binding studies

The formation of inclusion complexes from α,ω -dicyanoalkanes with 1,4-dialkoxypillar[5]arene has been investigated in DMSO-*d*₆/CDCl₃ by C. Li and co-workers.⁸ Under these conditions, association constants (K_A) of 1.5×10^4 and $6.5 \times 10^2 \text{ M}^{-1}$ have been derived from the NMR binding studies of 1,4-diethoxypillar[5]arene with 1,4-dicyanobutane and 1,6-dicyanohexane, respectively. The value of the binding constant is also influenced by the size of the peripheral alkyl substituents of the pillar[5]arene host. In the case of the 1,4-dicyanobutane guest, a decrease of the K_A value has been observed by increasing the chain length. Effectively, K_A values of 5.4×10^4 and $3.3 \times 10^2 \text{ M}^{-1}$ have been obtained for 1,4-dibutylpillar[5]arene and 1,4-dioctylpillar[5]arene, respectively.

For solubility reasons, the experimental conditions used by C. Li and co-workers are not applicable to investigate the binding of 1,6-dicyanohexane with pillar[5]arene derivatives **3**, **5**, **9** and **11**. In order to have an appropriate reference experiment, we started to investigate a model inclusion complex resulting from the association of 1,4-dimethoxypillar[5]arene (**12**) and 1,6-dicyanohexane (**13**) (Figure 5). The formation of a host-guest complex was evidenced by NMR binding studies in CDCl₃ at 25°C. Continuous up-field shifts were observed for all the signals of **13** upon successive additions of **12**. Formation of inclusion complexes of **13** with **12** locates the $-(\text{CH}_2)_6-$ chain of **13** within the cavity of the pillar[5]arene host and thus the methylene protons are exposed to the strong shielding effect from the aromatic subunits of the host. This is in full agreement with the proposed formation of an inclusion complex.¹⁰ This first series of experiments did not allow us to derive a binding constant value due to the

limited solubility of pillar[5]arene **12** in CDCl_3 preventing to reach a sufficient saturation level at the end of the titration. This prompted us to perform the titration in the other way around, *i.e.* by adding increasing amount of guest **13** to a solution of host **12**. Continuous chemical shift changes were observed for all the signals of **12** upon successive additions of guest **13** (Figure 5). The association constant for the 1:1 complex [**13** \subset **12**] was then calculated based on the complexation-induced changes in chemical shifts by using curve-fitting analysis (Figure 6). The $\log K_a$ value was found to be 2.92 (8).

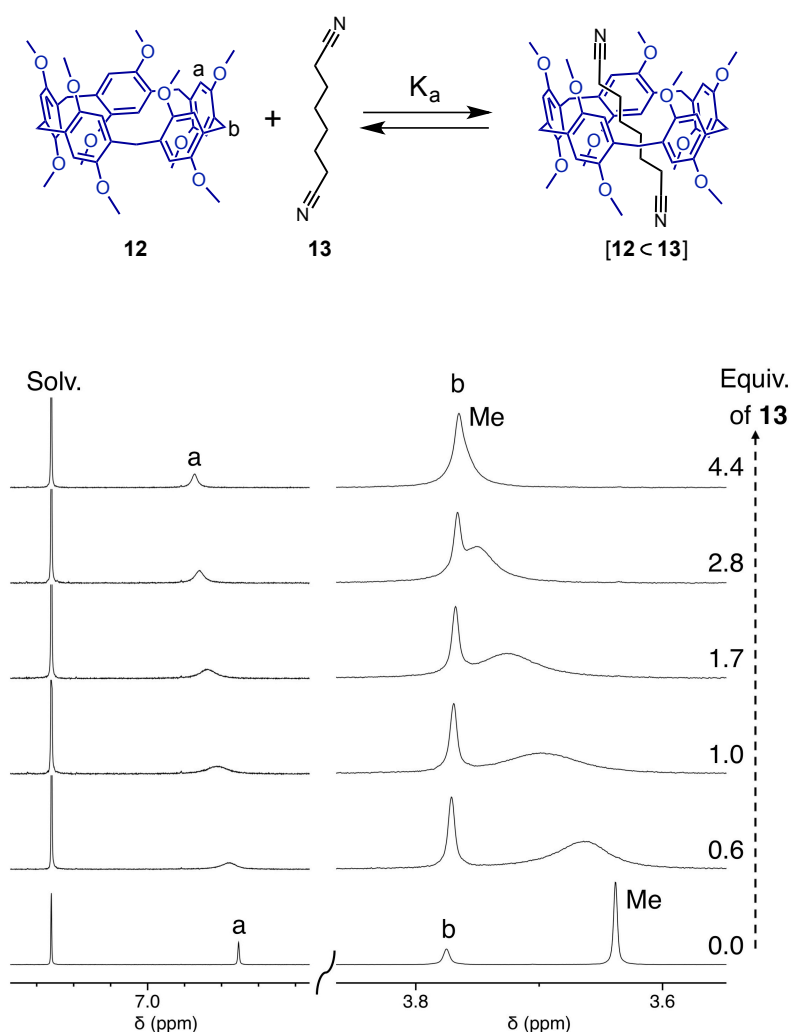


Figure 5. ^1H NMR (300 MHz, CDCl_3 , 298K) spectra recorded upon successive additions of 1,6-dicyanohexane (**13**) to a solution of pillar[5]arene **12** (1 mM).

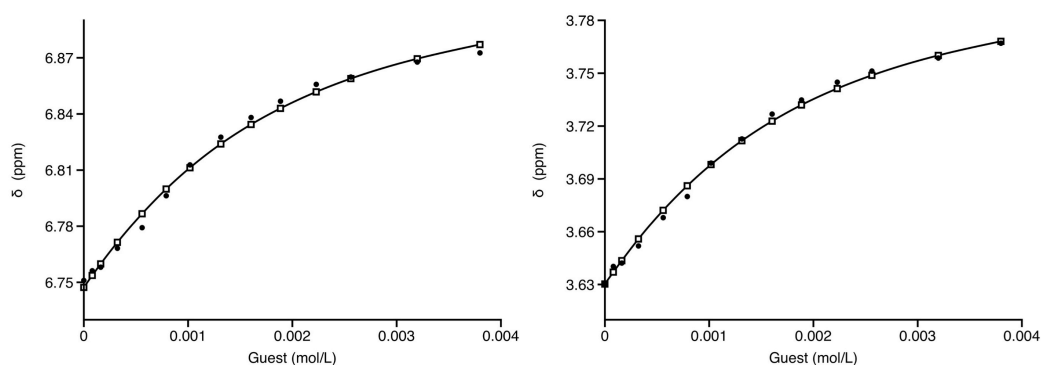


Figure 6. Chemical shifts of the signals corresponding to H-a (left) and the Me group (right) in **12** as a function of guest (**13**) concentration (calculated: \square , experimental: \bullet).

NMR binding studies were performed under the same conditions with pillar[5]arene hosts **3**, **5**, **9** and **11**. As typical examples, the ^1H NMR spectra recorded upon successive addition of **13** to a solution of **3** and the corresponding binding isotherm are shown in Figure 7. The binding constants derived from the titrations are reported in Table 1.

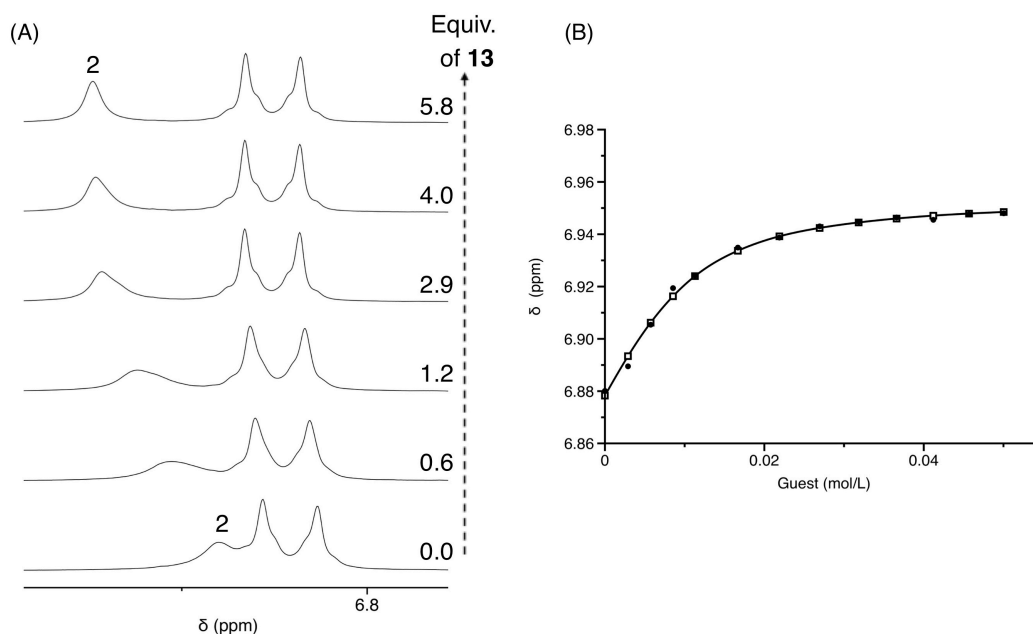


Figure 7. (A) ^1H NMR (300 MHz, CDCl_3 , 298K) spectra recorded upon successive additions of 1,6-dicyanohexane (**13**) to a solution of pillar[5]arene **3** (10 mM). (B) Chemical shift of the signal corresponding to H-2 (for the numbering, see Figure 1) in **3** as a function of guest (**13**) concentration (calculated: \square , experimental: \bullet).

Table 1. Values of the association constants ($\log K_a$) calculated for the 1:1 complexes of 1,6-dicyanohexane **13** with the pillar[5]arene hosts (**3**, **5**, **9**, **11** and **12**).

Pillar[5]arene host	$\log K_a$ (error)
Compound 3	2.44 (4)
Compound 5	0.7 (1)
Compound 9	3.56 (3)
Compound 11	3.28 (8)
Compound 12	2.92 (8)

When compared to model compound **12**, the K_A values obtained for compounds **3** and **5** are significantly decreased, the effect being more pronounced for the largest compound. In contrast, the same comparison reveals increased K_A values for compounds **9** and **11** despite the increased size of their peripheral groups. These observations show that the nature of the substituents of the pillar[5]arene host has an influence on the stability of the inclusion complexes obtained with 1,6-dicyanohexane. In other words, electronic interactions between the encapsulated guest and the peripheral units of the host must play an important role. The increased stability observed for [**13** \subset **9**] and [**13** \subset **11**] suggests the establishment of secondary interactions. For instance, intramolecular π - π interactions between the nitrile subunits of **13** and 1,2,3-triazole groups of **9** or **11** could explain well the higher stability of [**13** \subset **9**] and [**13** \subset **11**] when compared to [**13** \subset **12**]. On the other hand, the ester functions in the macrocyclic component of [**13** \subset **3**] and [**13** \subset **5**] destabilize the inclusion complexes. The dipole moments of these ester groups may generate repulsive interactions with the nitrile functions of the guest and thus contribute to substantially destabilize [**13** \subset **3**] and [**13** \subset **5**] when compared to [**13** \subset **12**].

Inclusion complexes [**13** \subset **3**], [**13** \subset **5**], [**13** \subset **9**] and [**13** \subset **11**] were also prepared in the solid state to investigate their thermal properties. Equimolar CHCl_3 solutions of **13** and the appropriate pillar[5]arene derivative (**3**, **5**, **9** or **11**) were allowed to stand at room temperature until complete evaporation of the solvent. The 1:1 host-guest complexes thus obtained were

further dried under high vacuum for 12 h. In all the cases, the samples were homogeneous and NMR analysis confirmed the 1:1 ratio of both components.

2.3.2. X-ray crystal structure of inclusion complex [13 C 12]

For inclusion complex [13 C 12], crystals suitable for X-ray crystal-structure analysis were obtained by slow diffusion of *n*-hexane into a CH₂Cl₂ solution of an equimolar mixture of 12 and 13. The structure of [13 C 12] is shown in Figure 8. The two central methylene groups of the 1,3-dicyanohexane guest are located within the cavity of the pillar[5]arene host and three out of their four hydrogen atoms point towards an aromatic subunit of the pillar[5]arene. The short C-H \cdots π -plane distances (2.757 to 2.891 Å) indicate the occurrence of intramolecular C-H \cdots π interactions in [13 C 12] as already observed in the X-ray crystal structures of pillar[5]arene inclusion complexes¹¹ and pillar[5]arene-containing [2]rotaxanes.¹²

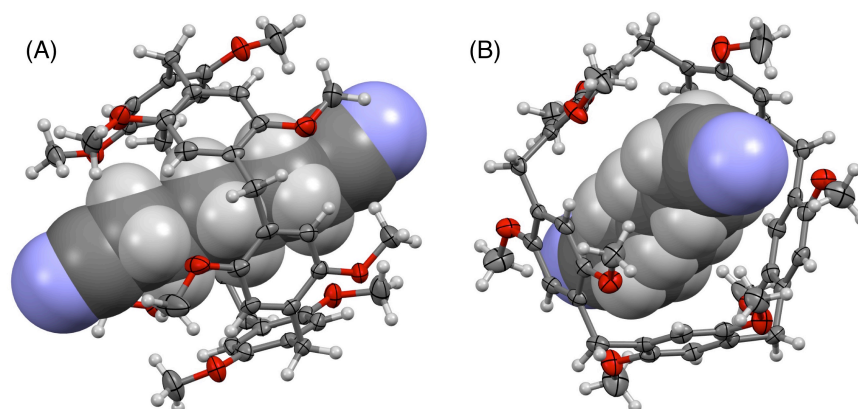


Figure 8. ORTEP plot of the X-ray crystal structure of [13 C 12] (thermal ellipsoids are shown at 50% probability level; N: blue, O: red, C: gray). For clarity, the 1,6-dicyanohexane guest is represented in spacefilling and the co-crystallized CH₂Cl₂ molecule omitted.

(A) Side view (view down the crystallographic *c* axis).

(B) Top view (view down the crystallographic *a* axis).

Interestingly, supramolecular complex [13 C 12] crystallized as a conglomerate in the chiral orthorhombic space group *C*222₁. In other words, only one enantiomer of the pillar[5]arene macrocycle is present in the crystal lattice. As shown in Figure 9, observation of the crystal lattice down the crystallographic *a* or *b* axis reveals alternating layers of [13 C 12]

supramolecules. Layers A/B are related to the A'/B' ones by a crystallographic C_2 axis. Within each layer, all of the molecules are oriented in the same directions. However, molecules of neighboring layers are not parallel. Indeed, there are four distinct orientations for the [13 C 12] supramolecules in the crystal lattice, each orientation being specific of one layer (A, B, A' or B').

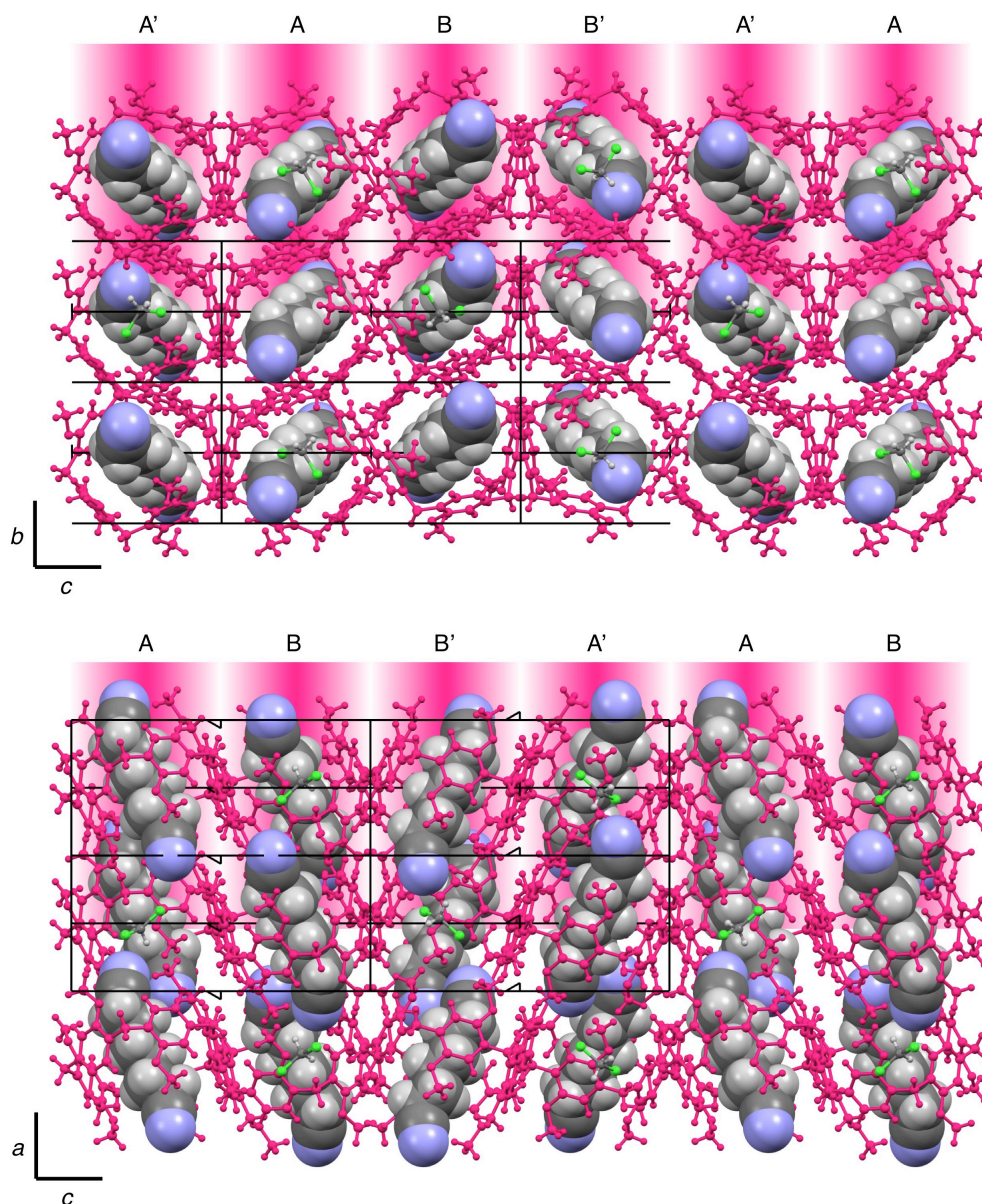


Figure 9. Stacking within the [13 C 12](CH_2Cl_2) lattice showing successive A/B/B'/A' layers (top: view down the crystallographic a axis; bottom: view down the crystallographic b axis); the pillar[5]arene moieties are shown in pink. For the 1,6-dicyanohexane guests and the co-crystallized CH_2Cl_2 molecules: N: blue, C: gray, Cl: green. The crystallographic C_2 axis are represented as black lines.

The supramolecular organization within one layer is depicted in Figure 10 (observation of the crystal lattice down the crystallographic c axis). The [13 C 12] supramolecules are tilted by about 25° with respect to the crystallographic a axis and form parallel columns separated by CH_2Cl_2 molecules. Interestingly, nitrile groups of neighboring [13 C 12] supramolecules adopt an anti-parallel orientation within these columns and their N atoms are separated by 5.159 \AA . Actually, the [13 C 12] ensembles are self-organized in infinite supramolecular polymeric columns through dipole-dipole interactions between the nitrile functions of their 1,6-dicyanohexane subunits.

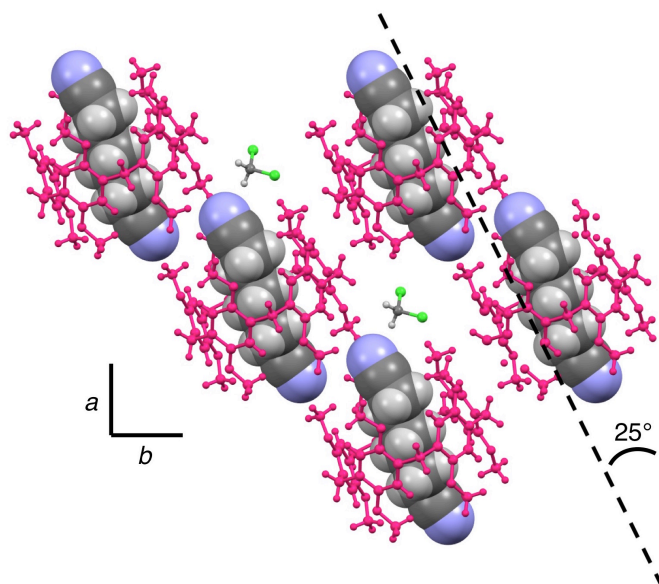


Figure 10. Stacking within the [13 C 12](CH_2Cl_2) lattice showing a tilted pseudo-columnar organization of the molecules in which the neighboring anti-parallel nitrile subunits give rise to dipole-dipole interactions (view down the crystallographic c axis)

2.4. Liquid-crystalline properties

The thermal properties of the compounds have been investigated in the group of Prof. Robert Deschenaux (University of Neuchâtel, Switzerland). The X-ray diffraction

investigations have been carried out in the group of Prof. Joaquín Barberá (University of Zaragoza, Spain).

The liquid-crystalline and thermal properties of compounds **3**, **5**, **9**, **11**, [**13 C 3**], [**13 C 5**], [**13 C 9**] and [**13 C 11**] were investigated by polarized optical microscopy (POM), differential scanning calorimetry (DSC) and powder X-ray diffraction (XRD). Their thermal properties are summarized in Table 2.

Table 2. Thermal properties deduced from the POM and DSC investigations for the pillar[5]arene derivatives (**3**, **5**, **9** and **11**) and the corresponding inclusion complexes ([**13 C 3**], [**13 C 5**], [**13 C 9**] and [**13 C 11**]).

Compound	Phase transition (temperature) ^[a]	ΔH (kJ/mol)
3	Cr \rightarrow I (42°C)	24.8
5	Col _h \rightarrow I (130°C)	17.7
9	T_g (44°C) Sm \rightarrow I (95°C)	6.3
11	Col _h \rightarrow I (136°C)	9.9
[13 C 3]	T_g (50°C) ^[b]	
[13 C 5]	Col _h \rightarrow I (123°C)	21.9
[13 C 9]	T_g (50°C) ^[b]	
[13 C 11]	Col _h \rightarrow I (128°C)	10.3

[a] Cr: crystalline solid; Sm: smectic phase; Col_h: hexagonal columnar phase; I: isotropic liquid, T_g : glass transition temperature. Temperatures are given as the onset of the peak obtained during the second heating run. T_g values are determined during the first cooling run.

[b] The supramolecular complexes [**13 C 3**] and [**13 C 9**] are not thermally stable and irreversible phase separation was observed upon isotropisation.

2.4.1. *p*-Dodecyloxybenzoate derivatives (**3**, **9**, [**13 C 3**] and [**13 C 9**]).

No liquid-crystalline behavior could be observed for **3** and the only phase transition detected for this compound was a melting point. In contrast, a mesophase was observed for

compound **9**. POM observations of **9** revealed effectively the slow apparition of a fluid birefringent phase during the first heating. No clear glass transition could be observed and the clearing point was determined to be 95°C. Whereas the birefringent optical texture was non-characteristic on cooling the sample from the liquid isotropic phase, the X-ray diffraction patterns recorded for **9** were typical of a smectic type organization (*vide infra*). Supramolecular complexes [**13** ⊂ **3**] and [**13** ⊂ **9**] were not thermally stable and no liquid-crystalline behavior could be evidenced for these compounds. In both cases, a clear phase separation was observed by POM as soon as the samples became liquid.

The XRD patterns recorded for compound **9** contained a set of two sharp maxima in the small-angle region with a reciprocal spacing ratio 1:2, characteristic of a lamellar organization. The two maxima are assigned respectively to the first and second layer reflection orders. In addition to these reflections, a broad, diffuse halo is observed in the large-angle region of the patterns, corresponding to the liquid-like state of the conformationally-disordered hydrocarbon chains. The presence of this diffuse scattering and the absence of other reflections confirm the liquid-crystalline nature of this phase. The patterns are consistent both with a smectic A and with a smectic C mesophase, more ordered smectic mesophases being excluded by the diffuse halo observed in wide angle region. The distinction between smectic A and smectic C mesophases is very difficult on the basis of the X-ray diffraction studies. The experimentally measured layer spacing (48.2 Å) is however shorter than the length of a molecule estimated in its most-extended conformation (*ca.* 65 Å, see Figure 11A). This observation would be in favor of a tilted smectic mesophase. This view was further supported by the cross-sectional area value (173 Å²) deduced from the experimentally measured layer spacing for compound **9**. The cross-sectional area *per* (pro)mesogenic unit (or *per* chain) can be obtained by dividing the total cross-section by the number of units oriented in opposite directions on both rims of the pillar[5]arene core, *i.e.* five. This gives a value of about 35 Å², which in principle is too large for an orthogonal mesophase (smectic A). Indeed, the large value obtained for the cross-sectional area of the mesogenic unit projected on the smectic plane is in favor of a tilted smectic mesophase (smectic C). A hypothetical model for such a lamellar organization of compound **9** is depicted in Figure 11B.

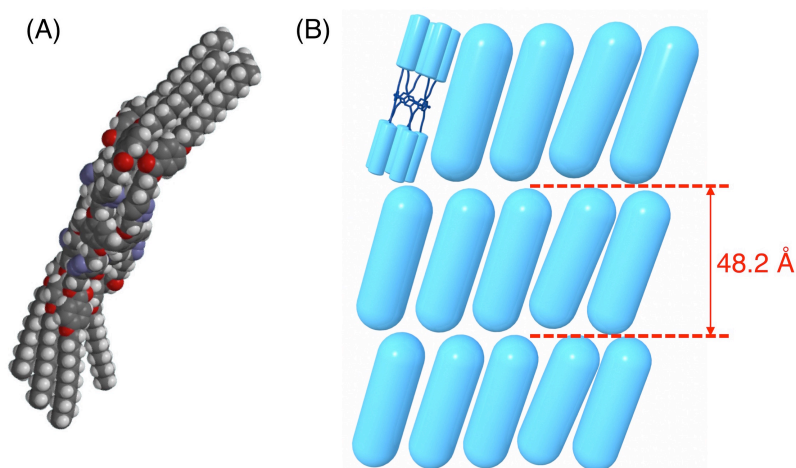


Figure 11. (A) Calculated structure of compound **9** (the molecular modeling has been performed with *Spartan'10* Macintosh Parallel Edition, Wavefunction Inc., USA at the PM6 level). (B) Schematic representation of the supramolecular organization of compound **9** in a tilted smectic mesophase.

2.4.2. Dendronized compounds (**5**, **11**, [**13** \subset **5**] and [**13** \subset **11**]).

Mesomorphic properties have been evidenced for pillar[5]arene derivatives **5** and **11**. Whereas the clearing temperatures were evidenced by DSC in both cases, no glass transitions could be clearly observed. Inclusion complexes [**13** \subset **5**] and [**13** \subset **11**] were found to be thermally stable and no phase separation was observed even on repeated heating-cooling cycles. In both cases, DSC thermograms registered during the second heating-cooling cycle revealed a reversible transition from the liquid-crystalline phase into an isotropic liquid. POM observations revealed birefringent phases for **5**, **11**, [**13** \subset **5**] and [**13** \subset **11**]. For all these compounds, the optical textures observed on cooling the samples from the isotropic phases displayed pseudo focal conic fan, characteristic for a columnar arrangement (Figure 12). It can also be noted that the birefringent fluids of the supramolecular complexes [**13** \subset **5**] and [**13** \subset **11**] were more viscous when compared to those of **5** and **11**.

The X-ray patterns unambiguously confirmed that the mesophases of **5**, **11**, [**13** \subset **5**] and [**13** \subset **11**] are columnar hexagonal (Col_h). In all the cases, three sharp maxima were observed in the small-angle region (Table 3). The reciprocal ratio of the three peaks are $1:\sqrt{3}:\sqrt{4}$, corresponding to the (1 0), (1 1) and (2 0) reflections of a two-dimensional

hexagonal lattice of packed columns. Apart from these reflections, a broad diffuse halo is also detected in the large-angle region of the patterns, corresponding to the interferences between the molten hydrocarbon chains. The diffuse character of this scattering and the absence of other reflections confirm the liquid-crystalline nature of the mesophases.

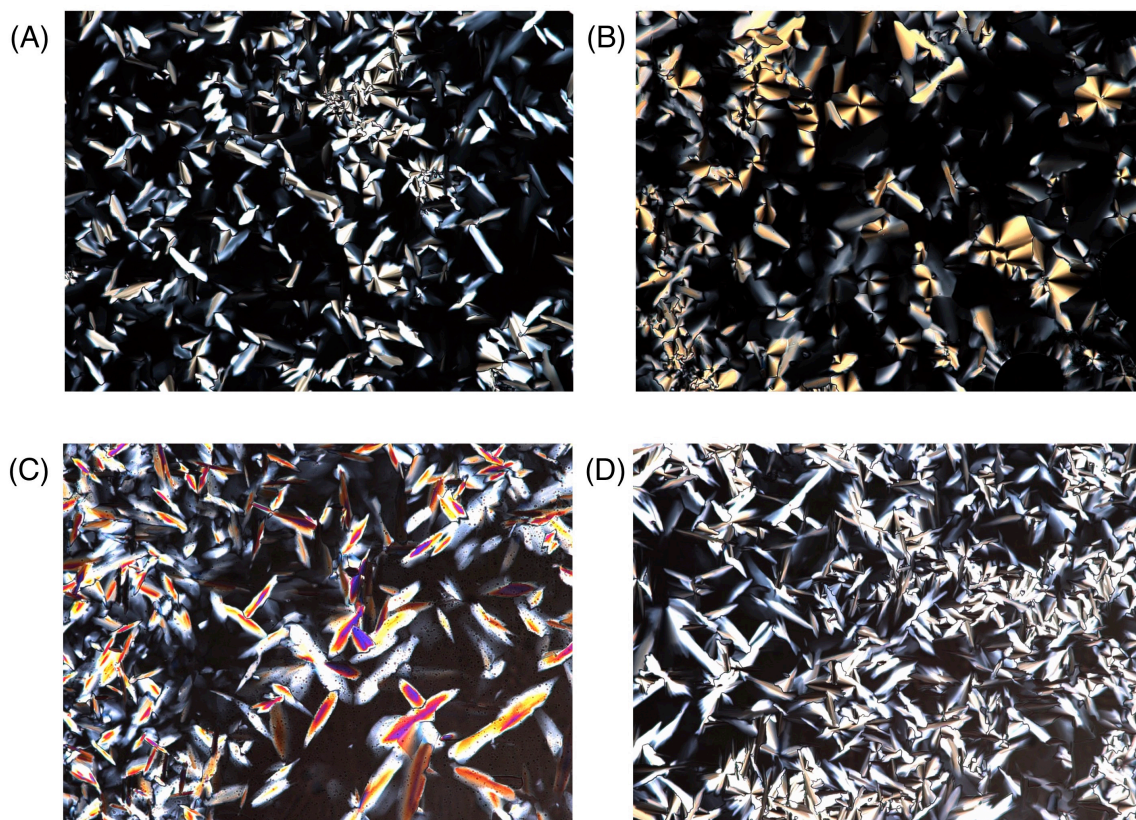


Figure 12. Thermal polarized optical micrographs of the textures displayed in the hexagonal columnar phase for (A) **5** at 109°C, (B) **11** at 112°C, (C) [**13** \subset **5**] at 112°C and (D) [**13** \subset **11**] at 120°C.

Importantly, the measured lattice parameter (a) follows the trend of the pillar[5]arene-dendron spacer length when going from **5** to **11**. Similar a values are also obtained when comparing the pillar[5]arene derivatives (**5** and **11**) with their inclusion complexes ([**13** \subset **5**] and [**13** \subset **11**], respectively). The measured lattice parameters (a) are consistent with the dimensions of the molecules deduced from molecular modeling studies. As shown in Figure 13A for compound **11**, one molecule forms an entire disk where the central pillar[5]arene core is surrounded by its 10 dendrons forming a ring with all the 30 alkyl chains pointing out of the

disc. Indeed, the discotic conformation adopted by the system results from the self-assembling capabilities of the peripheral dendrons through the establishment of intramolecular inter-dendron π - π and van der Waals interactions.²⁻⁴

Table 3. Structural data for the mesophases of **5**, **11**, [**13** C **5**] and [**13** C **11**] measured by powder X-ray diffraction. The columns list, respectively, the compound name, the temperature of the experiment, the mesophase type, the measured parameters (a : lattice constant in the columnar mesophase), the experimentally measured spacing, the calculated spacing, the Miller indices, and the estimated disc thickness.

Compound	Temperature (°C)	Phase	Structural parameter (Å) ^[a]	d_{exp} (Å)	d_{cal} (Å)	hkl	h (Å) ^[b]
5	r.t.	Col _h	$a = 50.0$	43.2	43.3	1 0 0	8.3
				25.3	25.0	1 1 0	
				21.5	21.7	2 0 0	
				4.45 ^[c]			
11	r.t.	Col _h	$a = 58.9$	51.2	51.0	1 0 0	6.4
				29.4	29.4	1 1 0	
				25.3	25.5	2 0 0	
				4.4 ^[c]			
[13 C 5]	r.t.	Col _h	$a = 49.3$	42.8	42.7	1 0 0	8.6
				24.7	24.65	1 1 0	
				21.2	21.3	2 0 0	
				4.4 ^[c]			
[13 C 11]	r.t.	Col _h	$a = 57.8$	50.0	50.1	1 0 0	6.7
				29.0	28.9	1 1 0	
				25.0	25.0	2 0 0	
				4.4 ^[c]			

^[a] Hexagonal lattice constant calculated from the observed spacing as $a = 2 (d_{100} + 3^{1/2}d_{110} + 4^{1/2}d_{200}) / (3\sqrt{3})$. Layer thickness calculated as $d = (d_{001} + 2d_{002}) / 2$. ^[b] Calculated thickness of the molecular disk, assuming a density $\rho = 1 \text{ g cm}^{-3}$ [$h = 10 \times M / 6.023 \times (\sqrt{3}/2) \times a^2$], M = molecular mass. ^[c] Diffuse maximum.

The dendronized pillar[5]arene derivatives form columns in which each disks are constituted by a single molecule (Figures 13B and 13C). The pillar[5]arene cores located at the center of the column are piled up thus forming a nanotubular wire alongside the column directive vector. Finally, these columnar assemblies are organized into a hexagonal array in the Col_h mesophase as shown in Figure 13D.

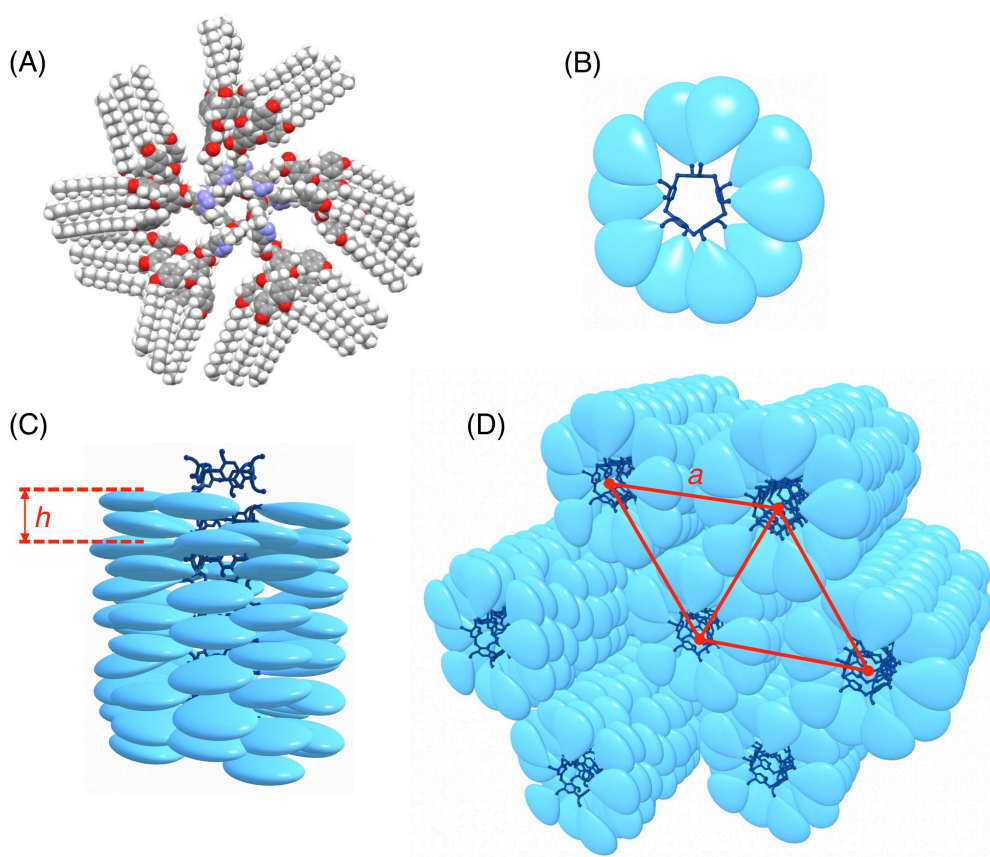


Figure 13. (A) Calculated structure of compound **11** (the molecular modeling has been performed with *Spartan'10* Macintosh Parallel Edition, Wavefunction Inc., USA at the PM6 level). (B) Schematic representation of compound **11** (dark blue: pillar[5]arene core, pale blue: peripheral dendrons). (C) Schematic representation of the columnar stacks of compound **11**. (D) Schematic representation of the supramolecular arrangement of compound **11** into the hexagonal columnar phase.

For all the compounds, the molecule thicknesses along the column axis (h) were estimated on the basis of the X-ray data (Table 3). The h values estimated in the four cases are larger than those typically observed in classical disk-like systems and are consistent with the proposed model for the Col_h mesophase. The stacking distances h found for **5** and [**13 C 5**] are however significantly shorter than those of **11** and [**13 C 11**]. In the case of **11** and [**13 C 11**], the linker connecting the dendron to the macrocyclic core is longer thus bringing a higher conformational flexibility and thus the possibility of a flatter arrangement of the molecule. The estimated molecule thicknesses h are also slightly larger for [**13 C 5**] and

[**13** ⊂ **11**] than for their respective free pillar[5]arenes, **5** and **11**, respectively. At the same time, the lattice constants a measured for the inclusion complexes are slightly smaller. This effect results from the space demand of the 1,6-dicyanohexane guests located in the middle of the macrocycle as shown in Figure 14. In this way, the 1,6-dicyanohexane moieties contribute to make the complex thicker, and hence the lattice constant smaller to preserve the density. This model for the supramolecular organization of [**13** ⊂ **5**] and [**13** ⊂ **11**] is actually similar to the infinite polymeric columns observed within the crystal lattice of [**13** ⊂ **12**]. Moreover, the existence of dipole-dipole interactions between neighboring guest molecules in the center of the columns should contribute to rigidify the supramolecular columns. Actually, this effect may explain the very high viscosity observed for the birefringent fluids observed for inclusion complexes [**13** ⊂ **5**] and [**13** ⊂ **11**].

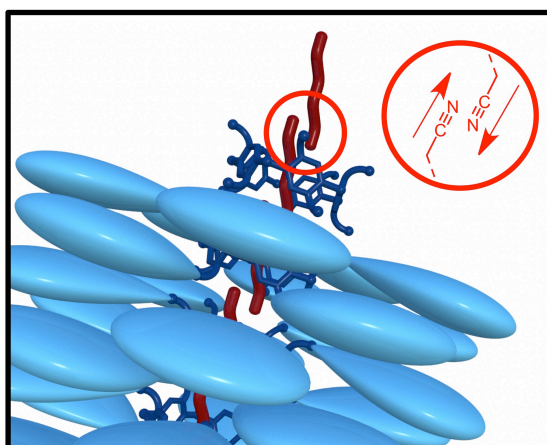


Figure 14. Schematic representation of the columnar stacks of the inclusion complexes [**13** ⊂ **5**] and [**13** ⊂ **11**] (dark blue: pillar[5]arene core, pale blue: peripheral dendrons, dark red: 1,6-dicyanohexane guest). Dipole-dipole interactions between neighboring guest molecules in the columnar phases contribute to rigidify the columns.

2.5. Conclusion

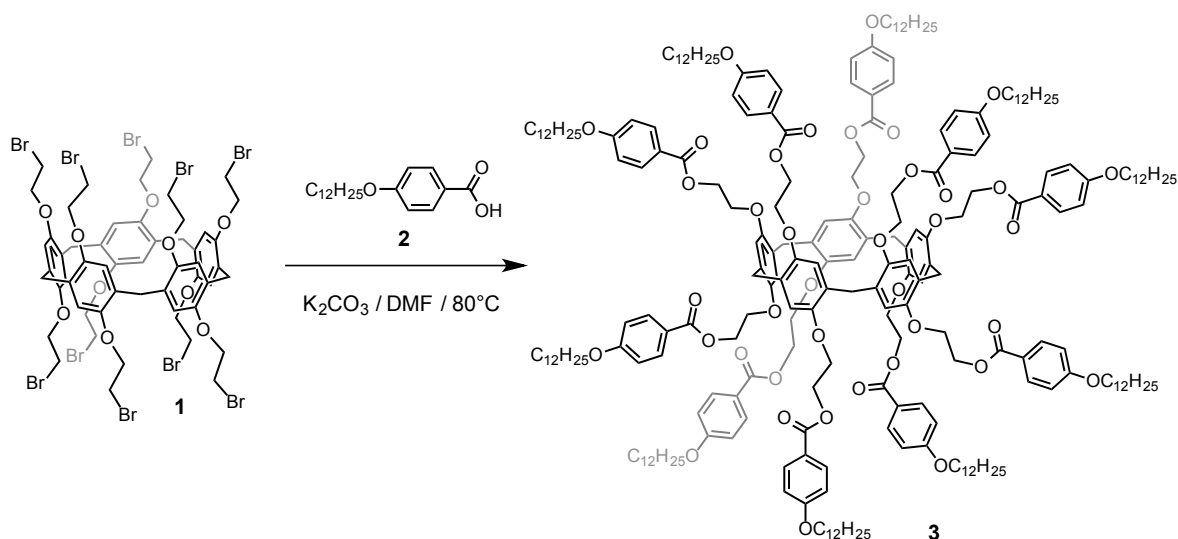
New liquid-crystalline pillar[5]arene derivatives have been prepared by grafting either *p*-dodecyloxybenzoate groups or percec-type dendrons on the macrocyclic scaffold. The supramolecular organization of the compounds within the mesophases is strongly dependent

on the type of peripheral units. In the case of compound **9**, the five *p*-dodecyloxybenzoate groups located on each rim of the pillar[5]arene core are oriented in opposite directions and the molecules adopt a tubular shape suited for the self-organization into a smectic mesophase. In contrast, the conformation adopted by compounds **5** and **11** is mainly dominated by the self-assembling capabilities of the peripheral dendrons and the molecules adopt a disc-shaped structure perfectly suited for the self-organization into a columnar liquid-crystalline phase. In this way, the pillar[5]arene cores are piled up thus forming a nanotube alongside the column directive vector. The capability of pillar[5]arenes to form inclusions complexes has been also exploited. Specifically, detailed binding studies have been carried out in solution with 1,6-dicyanohexane as the guest. Inclusion complexes have been prepared in the solid state and mesomorphic properties evidenced for [**13** ⊂ **5**] and [**13** ⊂ **11**]. The supramolecular organization in the Col_h mesophase deduced from the XRD data for [**13** ⊂ **5**] and [**13** ⊂ **11**] is indeed similar to the one observed within the crystal lattice of a model inclusion complex prepared from 1,4-dimethoxypillar[5]arene and 1,6-dicyanohexane.

2.6. Experimental section

General methods. Reagents were purchased as reagent grade and used without further purification. Compounds **1**,¹ **4**,¹³ **8**,¹ and **12**¹⁴ were prepared according to previously reported procedures. Acetonitrile (CH₃CN) and dichloromethane (CH₂Cl₂) were distilled over CaH₂ under Ar. All reactions were performed in standard glassware under an inert Ar atmosphere. Evaporation and concentration were done at water aspirator pressure and drying in vacuo at 10⁻² Torr. Column chromatography: silica gel 60 (230-400 mesh, 0.040-0.063 mm) was purchased from E. Merck. Thin Layer Chromatography (TLC) was performed on aluminum sheets coated with silica gel 60 F₂₅₄ purchased from E. Merck. NMR spectra were recorded with a Bruker AC 300 or AC 400 spectrometer with solvent peaks as reference. The ¹H signals were assigned by 2D experiments (COSY and NOESY). IR spectra (cm⁻¹) were recorded with a Perkin–Elmer Spectrum One spectrophotometer. MALDI-TOF mass spectra were carried out by the analytical service of the School of Chemistry (Strasbourg, France). Elemental analyses were performed by the analytical service of the Chemistry Department of the University of Strasbourg (France). Compounds **4** and **10** have been prepared by Sebastiano Guerra.

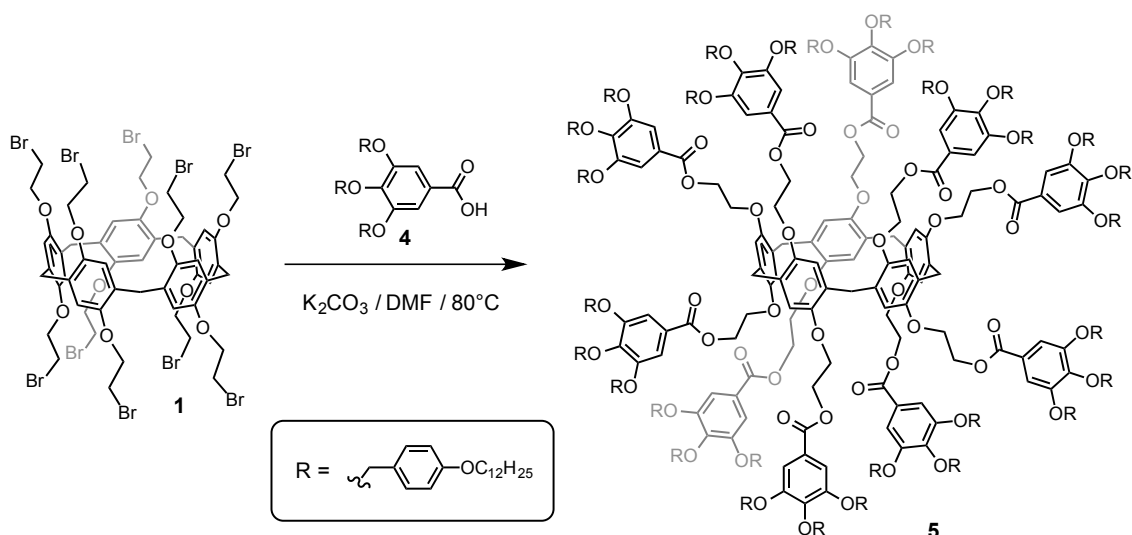
Compound 3



K₂CO₃ (649 mg, 4.7 mmol) was added to a solution of **2** (863 mg, 2.80 mmol) and **1** (400 mg, 0.23 mmol) in DMF (45 mL). The mixture was stirred at 80°C for 96 h under argon

atmosphere, then concentrated. Column chromatography (SiO₂, cyclohexane/CH₂Cl₂ 4:1) gave **3** (0.84 g, 80%) as a colorless glassy product. IR (neat): 2922 (C-H), 2853 (C-H), 1714 (C=O) cm⁻¹. ¹H NMR (400 MHz, CD₂Cl₂): δ = 7.98 (d, *J* = 8 Hz, 20H), 6.94 (s, 10H), 6.87 (d, *J* = 8 Hz, 20H), 4.68 (m, 10H), 4.43 (m, 10H), 4.22 (m, 10H), 4.06 (m, 10H), 3.94 (t, *J* = 6 Hz, 20H), 3.69 (s, 10H), 1.75 (m, 20H), 1.41 (m, 20H), 1.27 (m, 160H), 0.88 (t, *J* = 6 Hz, 30H) ppm. ¹³C NMR (100 MHz, CDCl₃): δ = 166.3, 163.1, 150.0, 131.7, 129.1, 122.2, 115.8, 114.1, 68.3, 67.3, 63.4, 32.0, 29.8, 29.7, 29.6, 29.5, 29.4, 29.2, 26.0, 22.8, 14.2 ppm. MALDI-TOF-MS: *m/z* 3933.67 ([M+H]⁺, calcd for C₂₄₅H₃₅₁O₄₀: 3933.54, 5%), 3672.15 ([M+H]⁺-PhOC₁₂H₂₅, calcd for C₂₂₇H₃₂₂O₃₉: 3672.32, 100%). Elemental analysis: (%) calcd for C₂₄₅H₃₅₀O₄₀ (3935.39): C, 74.77; H, 8.96; found: C, 74.72; H, 9.13.

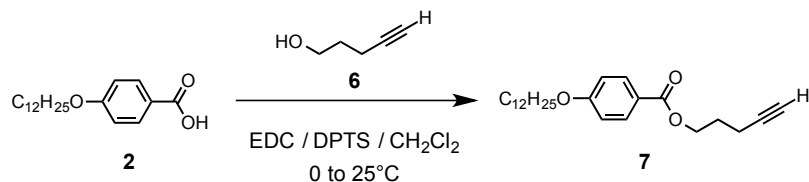
Compound 5



K₂CO₃ (417 mg, 3.018 mmol) was added to a mixture of **1** (257 mg, 0.151 mmol) and **4** (1.8 g, 1.811 mmol) in DMF (35 mL). The mixture was heated at 80 °C for 10 days, then concentrated. Column chromatography (SiO₂, Cyclohexane/CH₂Cl₂ 5:5) gave **5** (0.93 g, 57%) as a colourless glassy product. IR (neat): 2922 (C-H), 2853 (C-H), 1714 (C=O) cm⁻¹. ¹H NMR (400 MHz, CD₂Cl₂): δ = 7.39 (s, 20H), 7.19 (d, *J* = 8 Hz, 40H), 7.11 (d, *J* = 8 Hz, 30H), 6.77 (d, *J* = 8 Hz, 40H), 6.64 (d, *J* = 8 Hz, 20H), 4.80 (d, *J* = 9 Hz, 60H), 4.75 (m, 10H), 4.53 (m, 10H), 4.27 (m, 10H), 4.15 (m, 10H), 3.82 (m, 70H), 1.69 (m, 60H), 1.32 (m, 540H), 0.88 (t, *J* = 7 Hz, 90H) ppm. ¹³C NMR (100 MHz, CDCl₃): δ = 166.0, 158.9, 158.8, 152.7, 150.0, 142.8, 130.0, 129.6, 129.3, 128.4, 124.7, 114.3, 114.0, 109.0, 74.8, 70.9, 67.9, 31.9, 29.8, 29.7, 29.7,

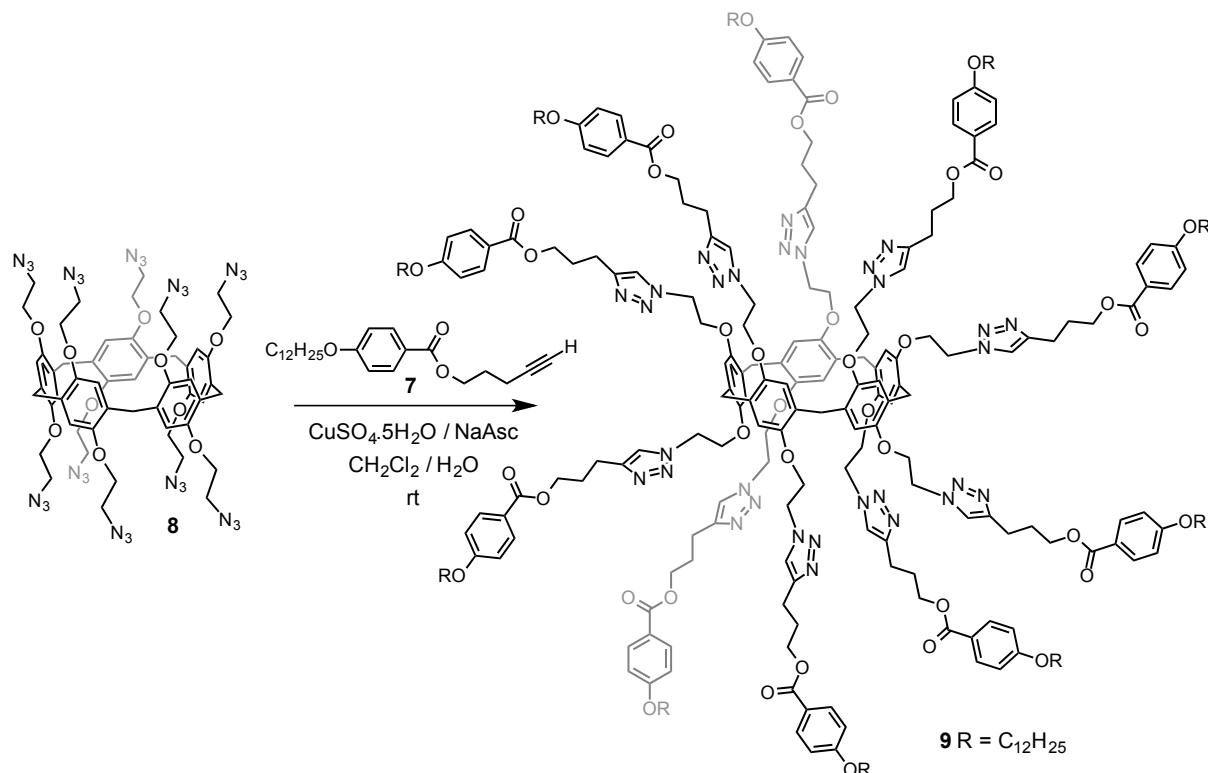
29.6, 29.6, 29.5, 29.4, 29.4, 29.3, 26.1, 26.0, 22.7, 14.1 ppm. Elemental analysis: (%) calcd for $C_{695}H_{1010}O_{90}$ (10805.43): C, 77.25; H, 9.42; found: C, 76.98; H, 9.61.

Compound 7



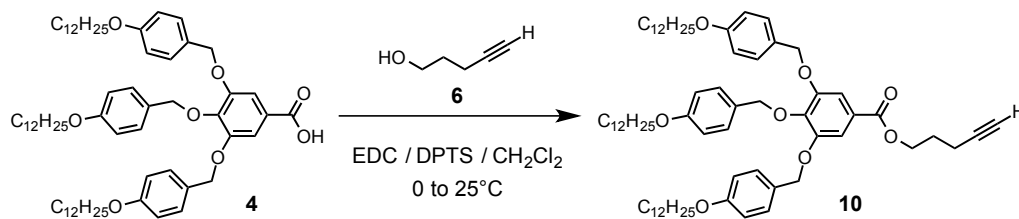
EDC (1.4 g, 9.04 mmol) was added to a mixture of 4-(Dodecyloxy)benzoic acid **1** (2.31 g, 7.54 mmol), 4-Pentyn-1-ol **6** (697 mg, 8.29 mmol) and DPTS (2.21 g, 7.53 mmol) in dry CH_2Cl_2 (150 mL) at 0°C. The resulting mixture was stirred for 3h at rt under argon, then H_2O was added. The aqueous layer was extracted with CH_2Cl_2 . The combined organic layers were washed with H_2O , dried over $MgSO_4$, filtered and concentrated. Column chromatography (SiO_2 , CH_2Cl_2 /Cyclohexane: 1:1) gave **7** (2.61 g, 93%) as a glassy product. IR (neat): 3312 ($\equiv C-H$), 2925 (C-H), 2855 (C-H), 2126 ($C\equiv C$), 1715 (C=O) cm^{-1} . 1H NMR (300 MHz, $CDCl_3$): δ = 7.98 (d, J = 7 Hz, 2H), 6.89 (d, J = 7 Hz, 2H), 4.39 (t, J = 6 Hz, 2H), 4.00 (t, J = 6 Hz, 2H), 2.37 (td, J = 7 Hz, 2H), 1.99 (m, 3H), 1.79 (m, 2H), 1.46 (m, 2H), 1.28 (m, 16H), 0.88 (t, J = 6 Hz, 3H) ppm. ^{13}C NMR (75 MHz, $CDCl_3$): δ = 166.3, 163.0, 131.6, 122.4, 114.1, 83.1, 69.0, 68.2, 63.1, 31.9, 29.7, 29.6, 29.5, 29.5, 29.4, 29.3, 29.1, 27.8, 26.0, 22.7, 15.4, 14.1 ppm. MALDI-TOF-MS: m/z 373.28 ($[M+H]^+$, calcd for $C_{24}H_{37}O_3$: 373.27), 289.25 ($[M+H]^+ - HCC(CH_2)_3$, calcd for $C_{19}H_{29}O_2$: 289.21).

Compound 9



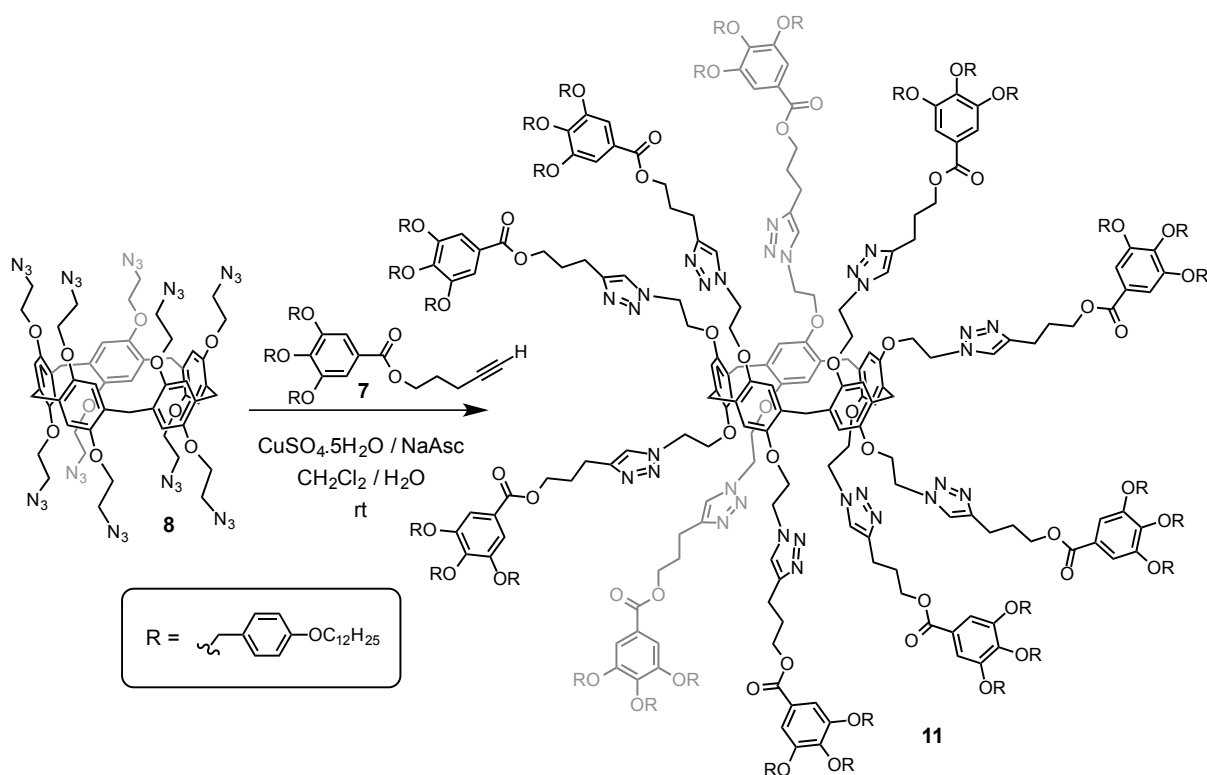
CuSO₄·5H₂O (2.8 mg, 0.008 mmol) and sodium ascorbate (5.3 mg, 0.02 mmol) were added to a mixture of **7** (400 mg, 1.07 mmol) and **8** (116 mg, 0.089 mmol) in CH₂Cl₂/H₂O (1:1). The resulting mixture was vigorously stirred at room temperature under Ar. After 12 days, H₂O was added. The aqueous layer was extracted with CH₂Cl₂ (3x). The combined organic layers were dried (MgSO₄), filtered and concentrated. Column chromatography (SiO₂, CH₂Cl₂ containing 2% methanol) gave **9** (180 mg, 41%) as a colorless glassy product. IR (neat): 2923 (C-H), 2853 (C-H), 1708 (C=O) cm⁻¹. ¹H NMR (400 MHz, CDCl₃): δ = 7.91 (d, *J* = 7 Hz, 20H), 7.61 (sbroad, 10H), 6.84 (d, *J* = 7 Hz, 20H), 6.60 (sbroad, 10H), 4.66 (m, 20H), 4.23 (m, 30H), 3.94 (m, 20H), 3.23 (sbroad, 10H), 2.83 (sbroad, 20H), 2.09 (m, 20H), 1.69 (m, 30H), 1.28 (m, 180H), 0.87 (t, *J* = 6 Hz, 30H) ppm. ¹³C NMR (100 MHz, CDCl₃): δ = 166.3, 166.0, 150.0, 147.3, 131.5, 122.3, 121.5, 115.8, 114.1, 68.2, 67.3, 63.7, 50.0, 31.9, 29.7, 29.7, 29.6, 29.4, 29.3, 29.1, 28.5, 25.9, 22.7, 22.4, 14.1 ppm. MALDI-TOF-MS: *m/z* 5027.08 ([M+H]⁺, calcd for C₂₉₅H₄₂₁O₄₀N₃₀: 5027.19). Elemental analysis: (%) calcd for C₂₉₅H₄₂₀O₄₀N₃₀·0.5CH₂Cl₂ (5069.15): C, 70.02; H, 8.37; N, 8.29; found: C, 70.07; H, 8.69, N, 8.17.

Compound 10



EDC (170 mg, 1.71 mmol) was added to a mixture of acid **4** (1.44 g, 1.45 mmol), 4-pentyn-1-ol **6** (121.97 mg, 1.45 mmol) and DPTS (430 mg, 1.45 mmol) in dry CH₂Cl₂ (100 mL) at 0°C. The resulting mixture was stirred for 12h at rt under Ar, then H₂O was added. The aqueous layer was extracted with CH₂Cl₂. The combined organic layers were washed with water, dried over MgSO₄, filtered and concentrated. Column chromatography (SiO₂, CH₂Cl₂) followed by precipitation from MeOH gave **10** (1.18 g, 81%) as a colorless solid. IR (neat): 3299 (C≡C-H), 2918 (C-H), 2851 (C-H), 2120 (C≡C), 1723 (C=O) cm⁻¹. ¹H NMR (400 MHz, CD₂Cl₂): δ = 7.38 (s, 2H), 7.36 (d, *J* = 7 Hz, 4H), 7.25 (d, *J* = 7 Hz, 2H), 6.92 (d, *J* = 7 Hz, 4H), 6.77 (d, *J* = 7 Hz, 2H), 5.06 (s, 4H), 5.00 (s, 2H), 4.37 (t, *J* = 6 Hz, 2H), 3.98 (t, *J* = 7 Hz, 4H), 3.93 (t, *J* = 7 Hz, 2H), 2.37 (td, *J* = 7 and 1 Hz, 2H), 2.04 (t, *J* = 1 Hz, 1H), 1.99 (m, 2H), 1.78 (m, 6H), 1.47 (m, 6H), 1.29 (m, 48H), 0.90 (t, *J* = 7 Hz, 9H) ppm. ¹³C NMR (100 MHz, CD₂Cl₂): δ = 165.9, 159.2, 159.1, 152.6, 142.2, 130.2, 129.5, 129.4, 128.6, 125.2, 114.4, 114.0, 108.7, 83.2, 74.6, 70.9, 68.8, 68.1, 68.0, 63.5, 31.9, 29.8, 29.7, 29.7, 29.6, 29.6, 29.5, 29.4, 29.4, 29.3, 29.3, 27.8, 26.1, 26.0, 22.7, 15.3, 13.9 ppm. MALDI-TOF-MS: *m/z* 1081.74 ([M+Na]⁺, calcd for C₆₉H₁₀₂O₈Na: 373.27, 100%), 1097.78 ([M+K]⁺, calcd for C₆₉H₁₀₂O₈K: 1097.72, 30%).

Compound 11



$\text{CuSO}_4 \cdot 5\text{H}_2\text{O}$ (2 mg, 0.003 mmol) and sodium ascorbate (3 mg, 0.009 mmol) were added to a mixture of **8** (40 mg, 0.031 mmol) and **10** (400 mg, 0.37 mmol) in $\text{CH}_2\text{Cl}_2/\text{H}_2\text{O}$ (1:1). The resulting mixture was vigorously stirred at rt under Ar. After 7 days, H_2O was added. The aqueous layer was extracted with CH_2Cl_2 (3 \times). The combined organic layers were dried (MgSO_4), filtered and concentrated. Column chromatography (SiO_2 , CH_2Cl_2 containing 2% methanol) gave **11** (140 mg, 41 %) as a colorless glassy product. IR (neat): 2922 (C-H), 2853 (C-H), 1711 (C=O) cm^{-1} . ^1H NMR (300 MHz, CD_2Cl_2): δ = 7.66 (s, 10H), 7.33 (s, 20H), 7.28 (d, J = 8 Hz, 40H), 7.16 (d, J = 8 Hz, 20H), 6.84 (d, J = 8 Hz, 40H), 6.68 (m, 30H), 4.94 (s, 40H), 4.87 (s, 20H), 4.72 (m, 20H), 4.27 (m, 40H), 3.89 (m, 60H), 3.31 (s broad, 10H), 2.83 (t, J = 8 Hz, 20H), 2.09 (m, 20H), 1.72 (m, 60H), 1.32 (m, 540H), 0.87 (m, 90H) ppm. ^{13}C NMR (75 MHz, CD_2Cl_2): δ = 164.6, 157.5, 157.4, 151.1, 145.6, 141.2, 128.6, 128.0, 127.8, 127.0, 123.6, 120.8, 119.9, 112.9, 112.5, 107.6, 73.2, 69.6, 66.5, 66.4, 62.7, 30.4, 28.2, 28.2, 28.1, 27.9, 27.8, 27.7, 26.9, 24.5, 21.2, 20.8, 12.6 ppm. Elemental analysis: (%) calcd for $\text{C}_{745}\text{H}_{1080}\text{O}_{90}\text{N}_{30} \cdot 2\text{CH}_2\text{Cl}_2$ (12066.59): C, 74.35; H, 9.06; N, 3.48; found: C, 74.01; H, 9.37, N, 3.42.

Binding studies

All the ^1H NMR titration experiments were performed on a Bruker AC 300 at 25(1)°C, in CDCl_3 purchased from Sigma Aldrich Chemical Company. The appropriate amount of $\text{NC}-(\text{CH}_2)_6-\text{CN}$ (**13**) stock solution (in CDCl_3) was added to appropriate solution of compound **3**, **5**, **9**, **11** or methoxy-pillar[5]arene **12** in CDCl_3 . The association constants (K_a) of complexes [**13** \subset **3**], [**13** \subset **5**], [**13** \subset **9**], [**13** \subset **11**] and [**13** \subset **12**] were determined based on the changes in chemical shifts of the protons of the signals of the hosts (**3**, **5**, **9**, **11** or **12**). The calculations were done using the nonlinear least-square regression analysis program HypNMR.¹⁵

X-ray crystal structure of host-guest complex [**13** \subset **12**]

Crystals suitable for X-ray crystal-structure analysis were obtained by slow diffusion of n-hexane into a CH_2Cl_2 solution of an equimolar mixture of **12** and 1,6-dicyanohexane. Data were collected at 173(2) K on a Bruker APEX-II Duo KappaCCD diffractometer (Mo- $\text{K}\alpha$ radiation, $\lambda = 0.71073$ Å). The structure was solved by direct methods (SHELXS-97) and refined against F^2 using the SHELXL-2013 software. The non-hydrogen atoms were refined anisotropically, using weighted full-matrix least-squares on F^2 . The H-atoms were included in calculated positions and treated as riding atoms using SHELXL default parameters. Crystallographic data: formula: $(\text{C}_{45}\text{H}_{50}\text{O}_{10})\cdot(\text{C}_8\text{H}_{12}\text{N}_2)\cdot(\text{CH}_2\text{Cl}_2)$ ($M = 971.97$ g.mol $^{-1}$); colorless crystal, $0.35 \times 0.32 \times 0.30$ mm; crystal system: orthorhombic, space group $C222_1$; $a = 16.4825(12)$ Å; $b = 17.1577(13)$ Å; $c = 36.368(3)$ Å; $\alpha = \beta = \gamma = 90^\circ$; $V = 10285.0(14)$ Å 3 ; $Z = 8$; $F(000) = 4128$; a total of 12457 reflections collected; $1.713^\circ < \theta < 28.044^\circ$, 12457 independent reflections with 8361 having $I > 2\sigma(I)$; 623 parameters; Final results : $R_1(F^2) = 0.0673$; $wR_2(F^2) = 0.1716$, $\text{Goof} = 1.022$.

References

- 1) a) I. Nierengarten, S. Guerra, M. Holler, J.-F. Nierengarten, R. Deschenaux, *Chem. Commun.* **2012**, 48, 8072; b) I. Nierengarten, S. Guerra, M. Holler, L. Karmazin-Brelot, J. Barbera, R. Deschenaux, J.-F. Nierengarten, *Eur. J. Org. Chem.* **2013**, 3675.
- 2) B. M. Rosen, C. J. Wilson, D. A. Wilson, M. Peterca, M. R. Imam, V. Percec, *Chem. Rev.* **2009**, 109, 6275.
- 3) a) V. Percec, C. H. Ahn, G. Ungar, D. J. P. Yeardley, M. Moller, S. S. Sheiko, *Nature* **1998**, 391, 161; b) V. Percec, C.-H. Ahn, W.-D. Cho, A. M. Jamieson, J. Kim, T. Leman, M. Schmidt, M. Gerle, M. Möller, S. A. Prokhorova, S. S. Sheiko, S. Z. D. Cheng, A. Zhang, G. Ungar, D. J. P. Yeardley, *J. Am. Chem. Soc.* **1998**, 120, 8619.
- 4) S. Guerra, J. Iehl, M. Holler, M. Peterca, D. A. Wilson, B. E. Partridge, S. Zhang, R. Deschenaux, J.-F. Nierengarten, V. Percec, *Chem. Sci.* **2015**, 6, 3393.
- 5) S. Campidelli, P. Bourgun, B. Guintchin, J. Furrer, H. Stoeckli-Evans, I. M. Saez, J. W. Goodby, R. Deschenaux, *J. Am. Chem. Soc.* **2010**, 132, 3574.
- 6) V. V. Rostovtsev, L. G. Green, V. V. Fokin, K. B. Sharpless, *Angew. Chem. Int. Ed.* **2002**, 41, 2596.
- 7) a) M. Xue, Y. Yang, X. Chi, Z. Zhang, F. Huang, *Acc. Chem. Res.* **2012**, 45, 1294; b) T. Ogoshi, *J. Incl. Phenom. Macrocycl. Chem.* **2012**, 72, 247; c) T. Ogoshi, T.-a. Yamagishi, *Eur. J. Org. Chem.* **2013**, 2961; e) H. Zhang, Y. Zhao, *Chem. Eur. J.* **2013**, 19, 16862; d) D. Cao, H. Meier, *Asian J. Org. Chem.* **2014**, 244.
- 8) X. Shu, S. Chen, J. Li, Z. Chen, L. Weng, X. Jia, C. Li, *Chem. Commun.* **2012**, 48, 2967.
- 9) G. W. Gray, K. J. Harrison, J. A. Nash, *Electronic Lett.* **1973**, 9, 130.
- 10) R. Milev, A. Lopez-Pacheco, I. Nierengarten, T. M. N. Trinh, M. Holler, R. Deschenaux, J.-F. Nierengarten, *Eur. J. Org. Chem.* **2015**, 479.
- 11) For other examples of X-ray crystal structures of inclusion complexes of pillar[5]arene derivatives, see: a) L. Gao, C. Han, B. Zheng, S. Dong, F. Huang, *Chem. Commun.* **2013**, 49, 472; b) X. Shu, J. Fan, J. Li, X. Wang, W. Chen, X. Jia, C. Li, *Org. Biomol. Chem.* **2012**, 10, 3393; c) C. Han, G. Yu, B. Zheng, F. Huang, *Org. Lett.* **2012**, 14, 1712; d) L. Liu, L. Wang, C. Liu, Z. Fu, H. Meier, D. Cao, *J. Org. Chem.* **2012**, 77, 9413-9417.
- 12) T. M. N. Trinh, I. Nierengarten, M. Holler, J.-L. Gallani, J.-F. Nierengarten, *Chem. Eur. J.* **2015**, 21, 8019.

- 13) V. Percec, C.-H. Ahn, W.-D. Cho, A. M. Jamieson, J. Kim, T. Leman, M. Schmidt, M. Gerle, M. Möller, S. A. Prokhorova, S. S. Sheiko, S. Z. D. Cheng, A. Zhang, G. Ungar, D. J. P. Yeardley, *J. Am. Chem. Soc.* **1998**, *120*, 8619.
- 14) T. Ogoshi, T. Aoki, K. Kitajima, S. Fujinami, T.-a. Yamagishi, Y. Nakamoto, *J. Org. Chem.* **2011**, *76*, 328.
- 15) a) C. Frassinetti, S. Ghelli, P. Gans, A. Sabatini, M. S. Moruzzi, A. Vacca, *Anal. Biochem.* **1995**, *231*, 374; b) C. Frassinetti, L. Alderighi, P. Gans, A. Sabatini, A. Vacca, S. Ghelli, *Anal. Bioanal. Chem.* **2003**, *376*, 1041.

3. Porphyrin-substituted pillar[5]arenes

3.1. Introduction

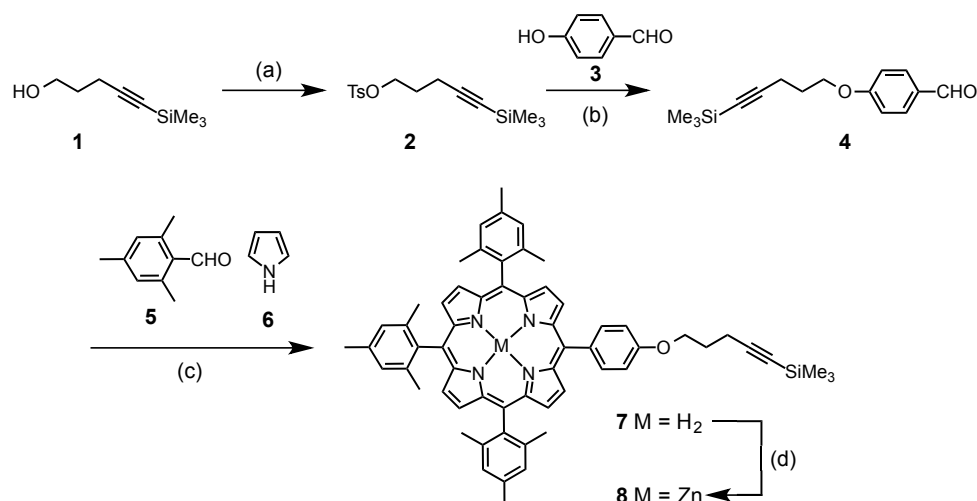
Tetrapyrrolic compounds are an important class of molecules whose derivatives play key roles in several natural processes. Such compounds serve often as cofactors in proteins. Heme is a typical example.¹ This iron porphyrin participates in the storage and the transport of molecular oxygen (O₂). Tetrapyrrolic compounds are also essential components of the natural photosynthetic systems.² For example, in the light-harvesting complexes of purple bacteria, wheel-like supramolecular assemblies of many bacteriochlorophyll subunits are achieved with the assistance of proteins.² The chlorophyll pigments collect efficiently the sunlight and channel the absorbed energy to a single reaction center. Over the two last decades, chemists have prepared a large variety of molecular and supramolecular systems capable of mimicking the light-harvesting effect of the photosynthetic system.³ Owing to their high number of peripheral groups, dendrimers are perfectly suited scaffolds to assemble a large number of pigments and numerous examples of dendritic light-harvesting systems have been reported.⁴ On the other hand, porphyrin building blocks have been often used as chromophores for the construction of photoactive molecular devices. Indeed, their electronic properties can be finely tuned by changing the nature of their substituents or by metalation.⁵

As part of this research, we became interested in the functionalization of our pillar[5]arene scaffolds with peripheral porphyrin subunits. Not only, the preparation of such molecules represents an interesting synthetic challenge, but investigation of their electronic properties might also reveal unprecedented features.

3.2. Synthesis

3.2.1. Preparation of the clickable porphyrin building blocks

The preparation of the first clickable porphyrin building block is depicted in Schemes 1 and 2. Treatment of alcohol **1** with *p*-toluenesulfonyl chloride (*p*-TsCl) gave tosylate **2** in 77% yield. Reaction of *p*-hydroxybenzaldehyde (**3**) with tosylate **2** under classical Williamson etherification conditions (K_2CO_3 , DMF, 80°C) afforded **4** in 85% yield.

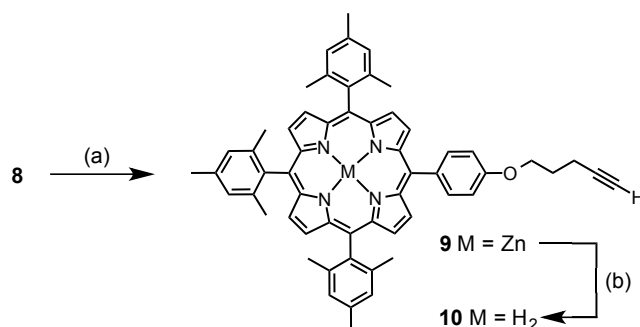


Scheme 1. Preparation of compound **8**. *Reagents and conditions:* (a) *p*-TsCl, *pyr*, CH_2Cl_2 , rt (77%); (b) K_2CO_3 , DMF, 80°C (85%); (c) $BF_3 \cdot Et_2O$, $CHCl_3$, rt, then chloranil (15%); (d) $Zn(OAc)_2 \cdot 2H_2O$, $CHCl_3/MeOH$, Δ (83%).

Porphyrin **7** was obtained by using the reaction conditions developed by Lindsey for the synthesis of sterically hindered porphyrins.⁶ A key feature of these conditions involves BF_3 -ethanol co-catalysis. The condensation of **4** (1 equiv.), mesitaldehyde (**5**, 3 equiv.) and pyrrole (**6**, 4 equiv.) was performed in $CHCl_3$ (commercial $CHCl_3$ containing 0.75% ethanol as stabilizer) at room temperature in the presence of $BF_3 \cdot Et_2O$. After 3 h, *p*-chloranil (tetrachlorobenzoquinone) was added to irreversibly convert the porphyrinogen to the porphyrin. Free base porphyrin **7** was subsequently isolated in 15% yield by tedious chromatographic separations. Metalation of **7** with $Zn(OAc)_2$ gave **8** in 83% yield. The

metalation is conveniently followed by the changes in the absorption spectra. Actually, four bands (Q bands), responsible for the red-purple color in solution, are observed in the visible region (515, 549, 593 and 648 nm) of the absorption spectrum of free base porphyrin **7**. A very sharp and intense band (B band also called Soret band) is also present in the near UV region (419 nm). Upon metalation, the four Q bands collapse into two bands (550 and 587 nm) due to the higher symmetry of the porphyrin core when metalated (D_{4h} vs. C_{2v}), but the Soret band (422 nm) is barely affected.⁷ The changes in the visible region result also in a clear color change when going from **7** to **8**. Effectively solutions of free base porphyrin **7** are red-purple while solutions of Zn(II)-porphyrin **8** are pink-purple.

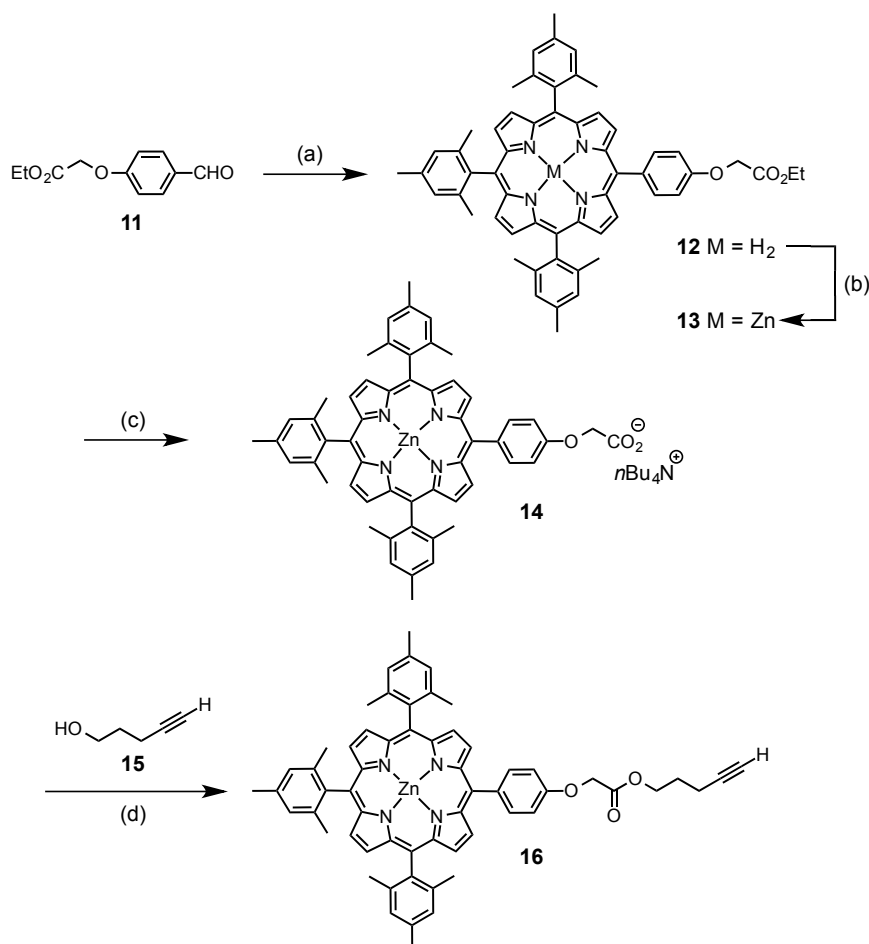
Reaction of trimethylsilyl (TMS)-protected alkyne **8** with tetrabutylammonium fluoride (TBAF) in THF afforded Zn(II)-porphyrin **9** bearing a terminal alkyne function (Scheme 2). Inspection of the ^1H NMR spectrum of **9** indicates the disappearance of the diagnostic TMS signal observed at $\delta = 0.20$ ppm for **8** and the concomitant apparition of a triplet ($J = 3$ Hz) at $\delta = 2.04$ ppm corresponding to the resonance of the terminal alkyne proton. Moreover, in the IR spectrum of **9**, the C-H stretching band characteristic of the terminal alkyne function is observed at 3302 cm^{-1} . Finally, Zn(II)-porphyrin **9** was also demetalated by treatment with trifluoroacetic acid (TFA) to afford the corresponding free-base porphyrin (**10**) that was used as a reference compound for the photophysical studies.



Scheme 2. Preparation of compound **10**. *Reagents and conditions:* (a) TBAF, THF, 0°C (91%); (b) TFA, CH_2Cl_2 , rt (96%).

The preparation of a second clickable Zn(II)-porphyrin building block having a slightly longer spacer between the porphyrin core and the terminal alkyne function was also achieved (Scheme 3). Aldehyde **11** was prepared from **3** and ethyl bromoacetate according to

a previously reported method.⁸ A₃B porphyrin **12** was then obtained in 14% yield by reaction of **11** (1 equiv.) and **5** (3 equiv.) with pyrrole (**6**, 4 equiv.) under typical Lindsey conditions. Subsequent treatment with Zn(OAc)₂ afforded the corresponding Zn(II)-porphyrin (**13**) in 99% yield.



Scheme 3. Preparation of compound **11**. *Reagents and conditions:* (a) **5**, **6**, BF₃·Et₂O, CHCl₃, rt, then chloranil (14%); (b) Zn(OAc)₂·2H₂O, CHCl₃/MeOH, Δ (99%); (c) K₂CO₃, H₂O, THF, Δ then *n*Bu₄NOH (85%); (d) DCC, DMAP, HOBT, CH₂Cl₂, 0 to 25°C (95%).

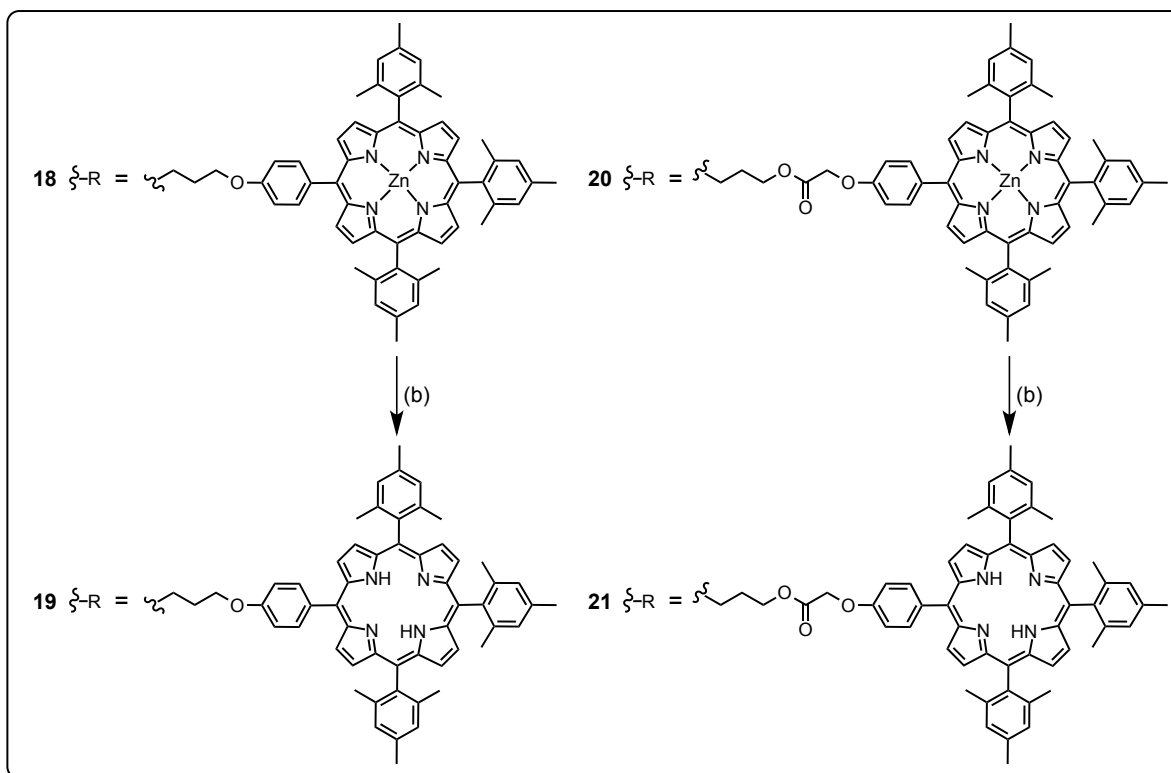
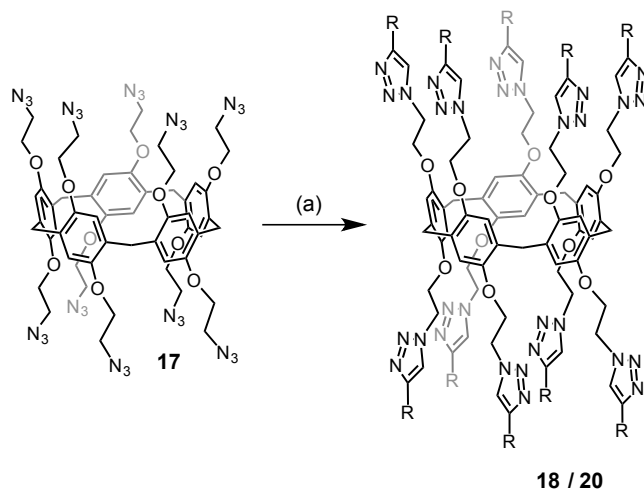
Hydrolysis of the ester function of **13** was achieved by treatment with K₂CO₃ in a mixture THF and water. The resulting carboxylate is poorly soluble in CH₂Cl₂ as its potassium salt. In order to obtain a good solubility in organic solvents, tetrabutylammonium hydroxide was added to the reaction mixture and carboxylate **14** was conveniently extracted with CH₂Cl₂ as its tetrabutylammonium salt. Finally, reaction of **14** with alcohol **15** under esterification conditions using *N,N'*-dicyclohexylcarbodiimide (DCC), 4-(dimethylamino)

pyridine (DMAP) and 1-hydroxybenzotriazole (HOBt) afforded clickable Zn(II)-porphyrin **16** in 95% yield.

3.2.2. Preparation of porphyrin-substituted pillar[5]arenes

The grafting of the Zn(II)-porphyrin building blocks (**9** and **16**) onto the pillar[5]arene scaffold was achieved under copper-catalyzed alkyne-azide cycloaddition (CuAAC) conditions (Scheme 4). Pillar[5]arene building block **17** bearing ten peripheral azide function was prepared according to a previously reported procedure.⁹ The copper-mediated Huisgen 1,3-dipolar cycloaddition of azides and alkynes resulting in 1,2,3-triazoles,¹⁰ one of the most popular click reactions,¹¹ is indeed an ideal tool to efficiently produce functionalized pillar[5]arenes from compound **17**.^{9,12} It should be however noted that owing to its high nitrogen content, this compound must be handled with special care. Upon evaporation, compound **17** was never dried under high vacuum and the use of metallic spatula avoided. Furthermore this compound was always prepared on a relatively small scale (< 500 mg). The reaction of **17** with terminal alkyne **9** was achieved under the typical CuAAC conditions developed for the functionalization of multi-azide cores¹²⁻¹³ (CuSO₄·5H₂O, sodium ascorbate, CH₂Cl₂/H₂O). It can be noted that it was difficult to follow the progress of the reaction by simple thin layer chromatography (TLC) analysis. Indeed, IR spectroscopy was a precious complementary tool to indicate the total consumption of the azide residues by monitoring the disappearance of the diagnostic azide band at 2089 cm⁻¹. In this particular case, completion of the reaction was clearly observed after 48 h. After work-up and purification, compound **18** was obtained in 96% yield. The ten peripheral Zn(II)-porphyrin moieties were then demetalated by treatment of **18** with TFA to afford **19**.

The reaction conditions used for the preparation of **18** were then applied to the second clickable Zn(II)-porphyrin derivative (**16**). A mixture of **17** (1 equiv.), **16** (12 equiv.), CuSO₄·5H₂O (0.4 equiv.), sodium ascorbate (0.3 equiv.) in CH₂Cl₂/H₂O was vigorously stirred at room temperature for 6 days. After work-up and purification by column chromatography on SiO₂ followed by gel-permeation chromatography (Biobeads SX-1, CH₂Cl₂), pillar[5]arene derivative **20** was obtained in 66% yield. Finally, treatment of **20** with TFA afforded the corresponding free base porphyrin-substituted pillar[5]arene derivative (**21**) in 97% yield.



Scheme 4. Preparation of porphyrin-substituted pillar[5]arene derivatives.

Reagents and conditions: (a) **9** or **16**, $\text{CuSO}_4 \cdot 5\text{H}_2\text{O}$, sodium ascorbate, CH_2Cl_2 , H_2O , 25°C [from **9**: **18** (96%); from **16**: **20** (66%)]; (b) TFA, CH_2Cl_2 , rt [from **18**: **19** (92%); from **20**: **21** (97%)].

3.3. Characterization of the porphyrin-substituted pillar[5]arene derivatives

Compounds **18-21** were characterized by ^1H and ^{13}C NMR, IR and UV/vis spectroscopies. For all the compounds, the proposed structures were also confirmed by MALDI-TOF mass spectrometry. As a typical example, the mass spectrum recorded for compound **20** is depicted in Figure 1. The spectrum is dominated by the pseudo-molecular ion peak $[\text{MH}]^+$ at $m/z = 10751.6$. The doubly charged pseudo-molecular ion peak $[\text{MH}_2]^{2+}$ is also detected at $m/z = 5377.9$. Moreover, characteristic fragments resulting from the cleavage of an ester function ($[\text{MH} - \text{ZnP-PhOCH}_2\text{CO}_2]^+$ at $m/z = 9872.5$) or from an ether unit ($[\text{M} - \text{ZnP-PhOCH}_2\text{CO}_2]^+$ at $m/z = 9830.7$) are observed; the degree of fragmentation remains however limited despite the high molecular weight of compound **20**. All these peaks can only arise from a fully clicked product. An additional minor peak is however detected at $m/z = 9805.9$. The latter might be ascribed to a minor byproduct, namely a defected compound to which only 9 terminal alkyne moieties have been clicked. However, the typical signature of azide residues at 2089 cm^{-1} could not be detected in the IR spectrum of the final product, thus the minor peak observed at $m/z = 9805.9$ corresponds more likely to a fragment resulting from a retro-click reaction, such fragmentation pattern being typical for 1,2,3-triazoles.¹⁴

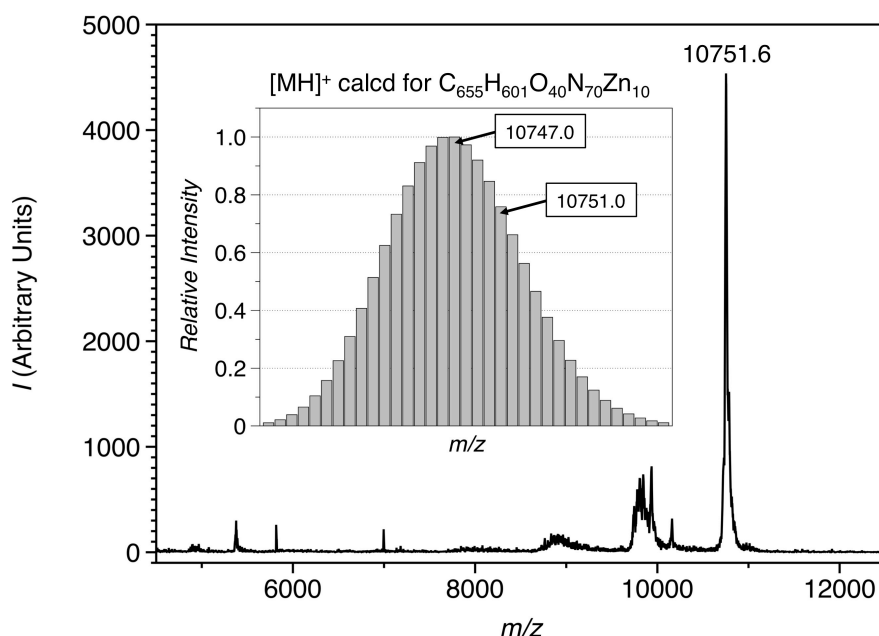


Figure 1. MALDI-TOF mass spectrum of compound **20**. Inset: calculated isotopic pattern for the pseudomolecular ion peak $[\text{MH}]^+$ ($\text{C}_{655}\text{H}_{601}\text{O}_{40}\text{N}_{70}\text{Zn}_{10}$).

For both free-base porphyrin derivatives (**19** and **21**), the ^1H NMR spectra recorded at room temperature revealed a single set of signals for all the peripheral porphyrin moieties thus showing that they are all equivalent. This is in perfect agreement with the 5-fold symmetrical structures of compounds **19** and **21**. In addition to the signals corresponding to the 10 equivalent peripheral moieties, the resonances arising from the pillar[5]arene core are clearly observed for both **19** and **21**. Actually, the ten aromatic protons of the macrocyclic core are equivalent and give rise to a singlet at $\delta = 6.81$ for **19** and 6.69 ppm for **21**. Similarly, a singlet is observed for the methylene bridging moieties of the pillar[5]arene core ($\delta = 3.45$ and 3.34 ppm for **19** and **21**, respectively).

Whereas well resolved signals are observed in the ^1H NMR spectrum of the free base porphyrin derivatives (**19** and **21**) recorded at room temperature, the spectra of the corresponding Zn(II)-porphyrin analogues (**18** and **20**) are broad under the same conditions. This is shown in Figure 2 for compound **18**. Variable NMR studies revealed however a perfectly reversible narrowing of the signals and ^1H NMR spectra of **18** and **20** recorded at high temperature shows the expected set of signals. These observations suggest a fast dynamic exchange between different conformers on the NMR timescale. This is in principle possible by rotational motions of the hydroquinone subunits of the pillar[5]arene moiety. Simple steric considerations reveal however that the porphyrin groups are by far too large to allow the oxygen-through-the-annulus movements of the hydroquinone units as evidenced for pillar[5]arenes with small alkyloxy substituents.¹⁵ Moreover the dynamic motions at the origin of the broadening of the spectra of **18** and **20** are specific to the presence of the Zn(II) centers. Effectively, as shown in Figure 2, the ^1H NMR spectra of free-base porphyrin **19** reveals only minor changes as a function of the temperature. In this particular case, limited molecular motions of the peripheral groups at low temperature results in a slight broadening of the signals corresponding to the protons located close to the core moiety of the molecule. At higher temperature, the increased thermal agitation of the peripheral substituents contributes to sharpen these signals ($\text{H}_{\text{a-b}}$ and H_{12} , see Figure 2). Moreover, agitation also contributes to simplify the pattern observed for the signals of some specific protons. For example, the two CH_2 groups of the ethylene linker are both diastereotopic ($\text{H-13/13}'$ and $\text{H-14/14}'$, see Figure 2) and accordingly give rise to four sets of signals at 30°C. In contrast, only two signals are observed at 105°C for the same groups (H-13 and H-14 , see Figure 2) and both methylene subunits appear as enantiotopic under these conditions. As already observed for

glycopillar[5]arenes,¹⁶ the thermal agitation of the peripheral substituents prevents the transfer of the chiral information between the peripheral subunits and the central core.

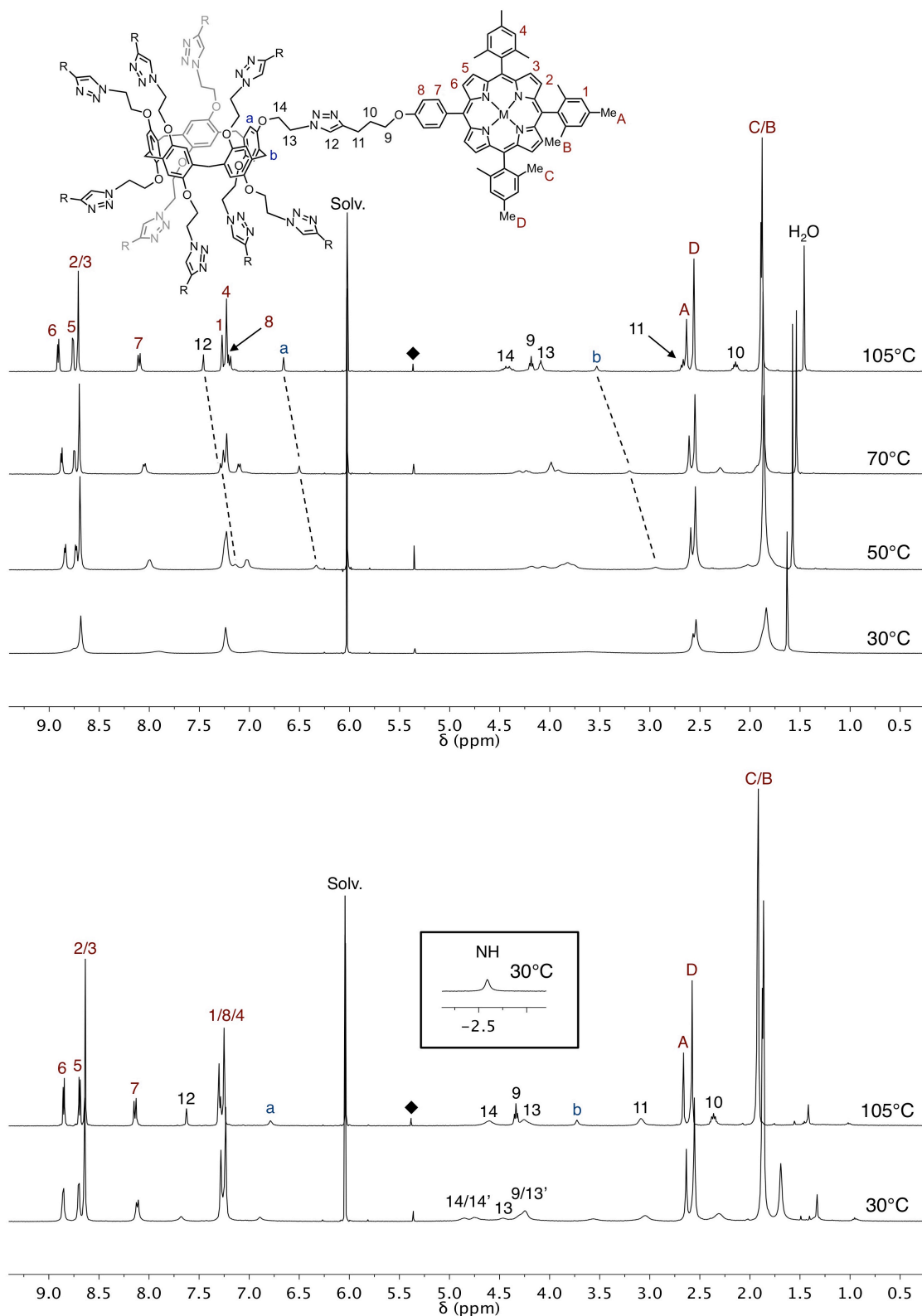


Figure 2. ¹H NMR spectra (400 MHz, CDCl₂CDCl₂) of compounds **18** (top) and **19** (bottom) recorded at different temperatures (◆: CH₂Cl₂).

In the case of **18** and **20**, the dramatic changes observed in the ^1H NMR spectra as a function of the temperature cannot be simply explained by an increased thermal agitation of the peripheral substituents. The Zn(II) centers play obviously a key role in the dynamic motions contributing to the broadening of the spectra at low temperature. Actually, the presence of 1,2,3-triazole moieties in **18** or **20** could result in intramolecular interactions with neighboring Zn(II)-porphyrin subunits as schematically depicted in Figure 3. Aromatic compounds with a donating nitrogen moiety are well known ligands of Zn(II)-porphyrins.¹⁷ Pyridine and imidazole derivatives are typical examples. Even if 1,2,3-triazoles are weaker ligands owing to their lower basicity, their binding to Zn(II)-porphyrins has been already documented in the literature.¹⁸

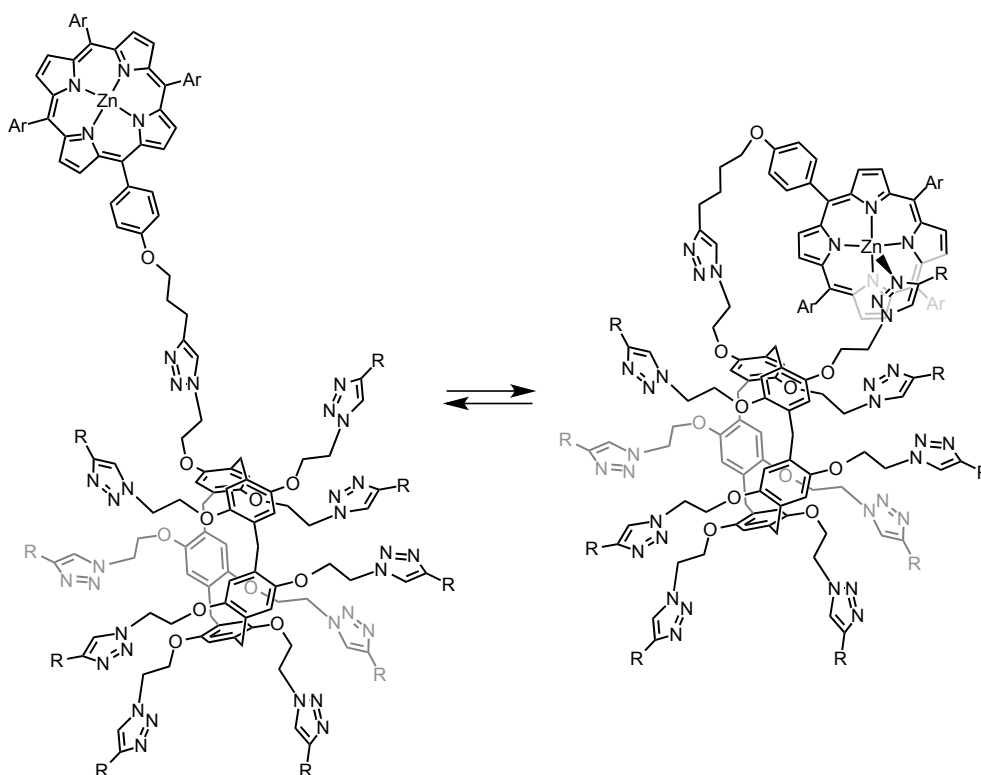


Figure 3. Schematic representation of the dynamic conformational changes resulting from the intramolecular coordination of a 1,2,3-triazole moiety to a Zn(II)-porphyrin subunit of compound **18**.

The binding constant for the intramolecular equilibrium between coordinated and uncoordinated Zn(II)-porphyrins in **18** is temperature dependent. At high temperature, the dynamic equilibrium is displaced in favor of uncomplexed species and the conformation of **18**

must be similar to that of its analogous free-base analogue (**19**). Indeed, as shown in Figure 2, the ^1H NMR spectra recorded at 105°C for **18** and **19** are very similar. In contrast, at low temperature, association is favored thus generating important conformational changes in **18**. The coordination of the Zn(II)-porphyrin moieties implies a folding of the molecule and aromatic porphyrin rings are located closer to the core moiety of the molecule. This view is clearly supported by the dramatic shielding observed for the signals of some protons by decreasing the temperature (H-a, H-b and H-12, see Figure 2). Indeed, these chemical shift changes result from the ring current effect of the aromatic porphyrin moieties that are spatially close to H-a, H-b or H-12 when intramolecular coordination of Zn(II) centers with 1,2,3-triazole groups occurs. ^1H NMR spectra of **18** were also recorded at a low temperature (from room temperature to -70°C). A continuous broadening was observed thus showing that the coordination/decoordination process remains faster than the NMR timescale even at -70°C and/or that compound **18** does not adopt a preferential folded conformation at -70°C . A similar behavior has been also observed for compound **20** with longer spacer subunits.

The occurrence of intramolecular interactions of 1,2,3-triazole groups with neighboring Zn(II)-porphyrin subunits in **18** and **20** was further supported by their absorption spectra recorded in CH_2Cl_2 at room temperature (Figures 4A and 4B). In both cases, the absorption bands of the Zn(II)-porphyrin moieties are effectively broadened and red-shifted when compared to those of appropriate model compounds. This is a clear signature¹⁹ for the apical coordination of Zn(II)-porphyrin moieties in **18** and **20** by a nitrogen ligand. Moreover, no evidence of molecular aggregation (*e.g.* intermolecular coordination) could be detected within the range of concentrations used for the optical measurements (10^{-5} to 10^{-7} M) as the absorbance follows the Beer-Lambert law for both **18** and **20**. Therefore, the apical coordination of the Zn(II)-porphyrin moieties by 1,2,3-triazoles in **18** and **20** occurs in an intramolecular manner. It can be also noted that the shape of the absorption spectra of both **18** and **20** is significantly affected by the nature of the solvent. This is shown in Figure 4C for compound **18**. Indeed, the affinity of the 1,2,3-triazole ligands for the Zn(II)-porphyrin moieties is not the same in the different solvents. As a result, the amount of coordinated Zn(II)-porphyrins is solvent-dependent thus explaining the differences observed in the absorption spectra recorded for **18** in CHCl_3 , CH_2Cl_2 and toluene. Close inspection of the shape of the Soret band suggests a higher degree of association in the less polar solvent (toluene). In this solvent, the red-shifted absorption maxima of the Soret band that is typical for coordinated Zn(II)-porphyrins becomes effectively more pronounced. This observation is

consistent with the solvent-dependence of the binding constant (K_A) reported in the literature for complexes resulting from the intermolecular association of N-ligands and Zn(II)-porphyrin derivatives.¹⁹ The K_A values are in general higher in less polar solvents.

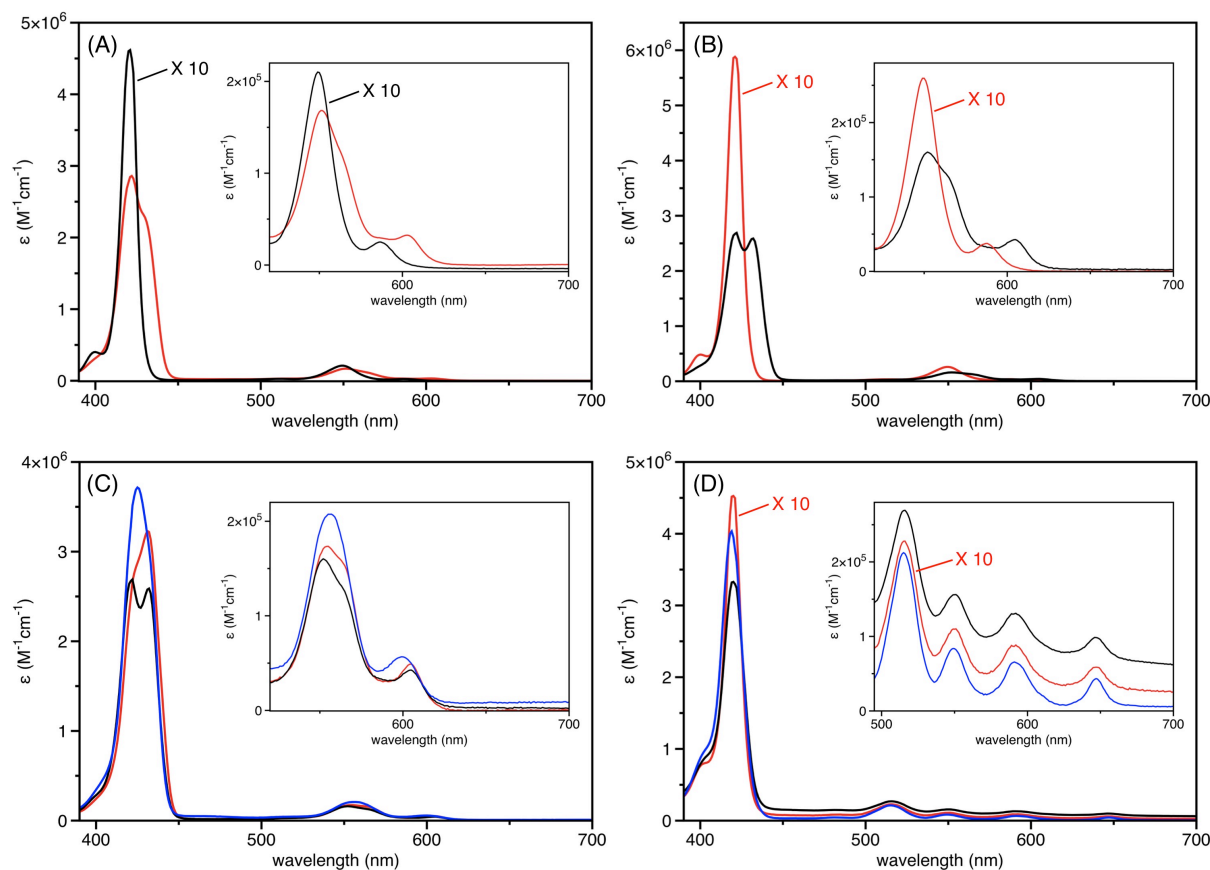
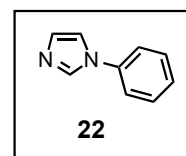


Figure 4. (A) Absorption spectra of compounds **20** (red) and **16** (black) recorded in CH_2Cl_2 at 25°C . (B) Absorption spectra of compounds **18** (black) and **9** (red) recorded in CH_2Cl_2 at 25°C . (C) Absorption spectra of compounds **18** recorded in different solvents at 25°C (blue: CHCl_3 , red: CH_2Cl_2 , red: toluene). (D) Absorption spectra of compounds **19** (blue), **21** (black) and **10** (red) recorded in CH_2Cl_2 at 25°C .

The absorption spectra of the free-base porphyrin-substituted pillar[5]arene derivatives **19** and **21** are depicted in Figure 4D. In contrast to what was observed for their Zn(II) analogues, the absorption spectra of **19** and **21** are only very slightly broadened when compared to model free-base porphyrin **10**. Indeed, their absorption spectra corresponds well

to the sum of their constitutive subunits (10 x **10**) thus showing rather limited electronic interactions (if any) among the free-base porphyrin moieties in **19** and **21** (Figure 4D). These observations further support our interpretation of the UV/vis data of the Zn(II) analogues **18** and **20**. The splitting of the Soret band and the overall broadening of the absorption spectra observed for **18** and **20** are not related to electronic interactions between their peripheral porphyrin subunits but result from an intramolecular coordination-driven conformational folding of the molecules. Indeed, the molecular motions resulting from the coordination/decoordination phenomena observed for compounds **18** and **20** mimic the blooming of a flower. As deduced from the variable temperature NMR studies, the folded conformation is favored at low temperature. By increasing the temperature, the intramolecular coordination is disfavored and the molecules adopt an open conformation like a flower that bloom. In order to gain more control on this conformational change, we became interested in using an external input to trigger the blooming of molecular flowers **18** and **20**. For this purpose, 1-phenylimidazole (**22**) was selected as an external chemical input. Indeed, compound **22** is a stronger ligand for Zn(II)-porphyrins¹⁷⁻¹⁹ when compared to 1,2,3-triazoles and one may anticipate that a preferential coordination of the Zn(II)-porphyrin groups in **18** or **20** will occur in the presence of an excess of **22**. As shown in Figure 5, dramatic changes were evidenced in the UV/vis spectrum of **20** upon addition of an excess of imidazole derivative **22** (14 equiv.). The Soret band is red-shifted and becomes narrow. A similar effect is also observed for the Q bands. These are diagnostic signatures for an effective apical coordination of **22** onto the Zn(II)-porphyrin subunits of **20**. Importantly, the absorption spectrum of **20** upon addition of **22** corresponds well to the one recorded for model porphyrin **16** in the presence of imidazole **22** (Figure 5B, inset) thus suggesting that the intramolecular coordination of Zn(II)-porphyrin moieties by 1,2,3-triazole subunits is not effective anymore. Coordination of the Zn(II)-porphyrins of compound **20** by imidazole ligand **22** is thus capable of preventing the coordination-induced folding in the multi-Zn(II)-porphyrin array. As schematically shown in Figure 5A, addition of ligand **22** to **20** allows for a complete unfolding of the compound thus mimicking the blooming of a flower.



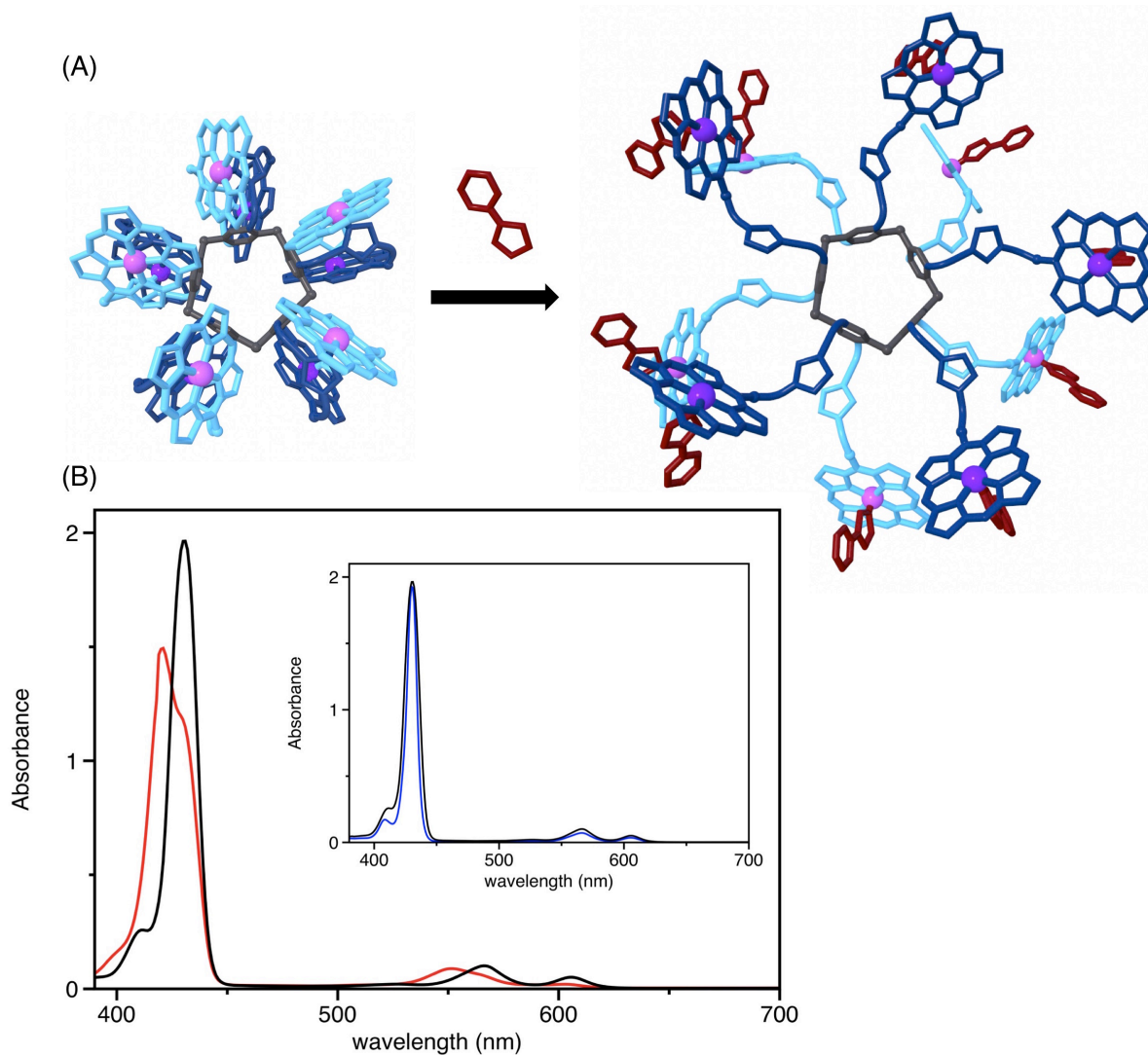


Figure 5. (A) Schematic representation of the blooming of molecular flower **20** upon addition of 1-phenylimidazole (**22**). (B) Absorption spectra of compound **20** before (red) and after (black) addition of 14 equiv. of **22** (CH_2Cl_2 , 25°C , $[\mathbf{20}] = 0.48 \mu\text{M}$); inset: comparison of the absorption spectra of pillar[5]arene **22** (black) and model porphyrin **16** (blue) in the presence of 14 equiv. of **22** (CH_2Cl_2 , 25°C , $[\mathbf{20}] = 0.48 \mu\text{M}$, $[\mathbf{16}] = 3.6 \mu\text{M}$).

3.4. Conclusion

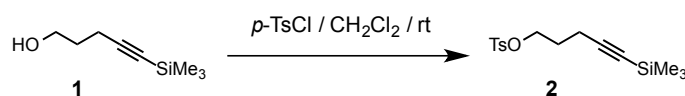
Pillar[5]arene derivatives bearing peripheral porphyrin subunits have been efficiently prepared from a clickable pillar[5]arene building block (**17**) and Zn(II)-porphyrin derivatives bearing a terminal alkyne function (**9** and **16**). The characterization of the resulting deca-Zn(II)-porphyrin arrays (**18** and **20**) has been complicated owing to an intramolecular

complexation of the peripheral Zn(II)-porphyrin moieties by 1,2,3-triazole subunits. As a result of this intramolecular coordination, the ^1H NMR spectra of **18** and **20** are broad at room temperature. Variable temperature NMR studies have shown that the conformational equilibrium resulting from the coordination-driven molecular folding is dynamic and well-resolved ^1H NMR spectra have been recorded at high temperature. Actually, the thermodynamic equilibrium is displaced in favor of uncoordinated species at high temperature and molecules **18** and **20** adopt an open conformation similar to the one of their free-base porphyrin analogues (**19** and **21**) under these conditions. In contrast, coordination of the Zn(II)-porphyrin moieties by 1,2,3-triazole groups is favored at low temperature and thus the molecules adopt a folded conformation. Finally, we have shown that the coordination-driven folding of **18** and **20** can be controlled by an external chemical stimulus. Specifically, addition of an imidazole derivative (**22**) to solution of **18** or **20** prevents the intramolecular coordination at the origin of the folding. As a result, unfolding of molecules **18** and **20** occurs. The resulting molecular motions triggered by the addition of the imidazole ligand mimics the blooming of a flower.

3.5. Experimental section

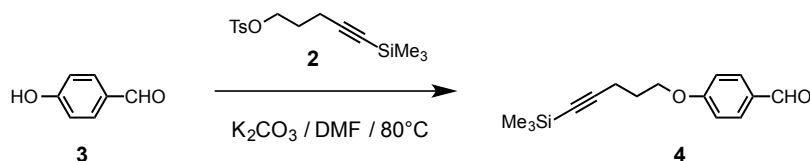
General methods. Reagents were purchased as reagent grade and used without further purification. Compounds **11**⁸ and **17**⁹ were prepared according to previously reported procedures. Acetonitrile (CH₃CN) and dichloromethane (CH₂Cl₂) were distilled over CaH₂ under Ar. All reactions were performed in standard glassware under an inert Ar atmosphere. Evaporation and concentration were done at water aspirator pressure and drying in vacuo at 10⁻² Torr. Column chromatography: silica gel 60 (230-400 mesh, 0.040-0.063 mm) was purchased from E. Merck. Thin Layer Chromatography (TLC) was performed on aluminum sheets coated with silica gel 60 F₂₅₄ purchased from E. Merck. NMR spectra were recorded with a Bruker AC 300 or AC 400 spectrometer with solvent peaks as reference. The ¹H signals were assigned by 2D experiments (COSY and NOESY). IR spectra (cm⁻¹) were recorded with a Perkin–Elmer Spectrum One spectrophotometer. MALDI-TOF mass spectra were carried out by the analytical service of the School of Chemistry (Strasbourg, France). Elemental analyses were performed by the analytical service of the Chemistry Department of the University of Strasbourg (France). The steady-state measurements have been carried out by Iwona Nierengarten and Matthieu Chesse. Compounds **2-10** and **18-19** have been prepared and characterized by Thi Minh Nguyet Trinh.

Compound 2



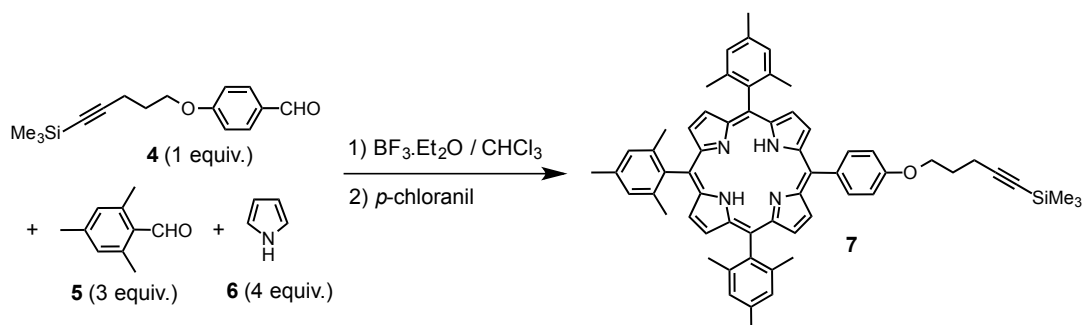
Pyridine (1.5 mL, 18.60 mmol) was added to a solution of **1** (2.40 g, 15.50 mmol) and *p*-TsCl (3.55 g, 18.60 mmol) in CH₂Cl₂ (100 mL). The resulting mixture was stirred for 16 h at room temperature. The reaction mixture was filtered on SiO₂ (CH₂Cl₂) and the solvent evaporated. Column chromatography (SiO₂, cyclohexane/CH₂Cl₂ 1:1) gave **2** (3.71 g, 77%) as a colourless oil. IR (neat): 2176 (C≡C). ¹H-NMR (400 MHz, CDCl₃): δ = 7.80 (d, *J* = 8 Hz, 2H), 7.35 (d, *J* = 8 Hz, 2H), 4.13 (t, *J* = 6 Hz, 2H), 2.45 (s, 3H), 2.28 (t, *J* = 7 Hz, 2H), 1.85 (quint., *J* = 7 Hz, 2H), 0.09 (s, 9H) ppm. ¹³C-NMR (100 MHz, CDCl₃): δ = 147.7, 133.1, 129.9, 127.9, 104.8, 85.9, 68.9, 27.9, 21.6, 16.1 ppm.

Compound 4



A mixture of **2** (3.8 g, 12.24 mmol), **3** (1.50 g, 12.24 mmol) and K_2CO_3 (5.08 g, 4.90 mmol) in DMF (20 mL) was stirred at 80°C for 16 h. The resulting mixture was cooled to room temperature and diluted with ether. The organic layer was washed with water, dried ($MgSO_4$), filtered and concentrated. Column chromatography (SiO_2 , cyclohexane/ CH_2Cl_2 2:3) gave **4** (2.70 mg, 85%) as a colourless solid. IR (neat): 2175 ($C\equiv C$). 1H NMR (400 MHz, $CDCl_3$): δ = 9.89 (s, 1H), 7.84 (d, J = 8 Hz, 2H), 7.00 (d, J = 8 Hz, 2H), 4.16 (t, J = 6 Hz, 2H), 2.45 (t, J = 7 Hz, 2H), 2.02 (quint., J = 7 Hz, 2H), 0.14 (s, 9H) ppm. ^{13}C -NMR (100 MHz, $CDCl_3$): δ = 190.7, 163.9, 131.9, 129.8, 114.6, 105.6, 85.5, 66.6, 27.9, 16.4, 0.0 ppm.

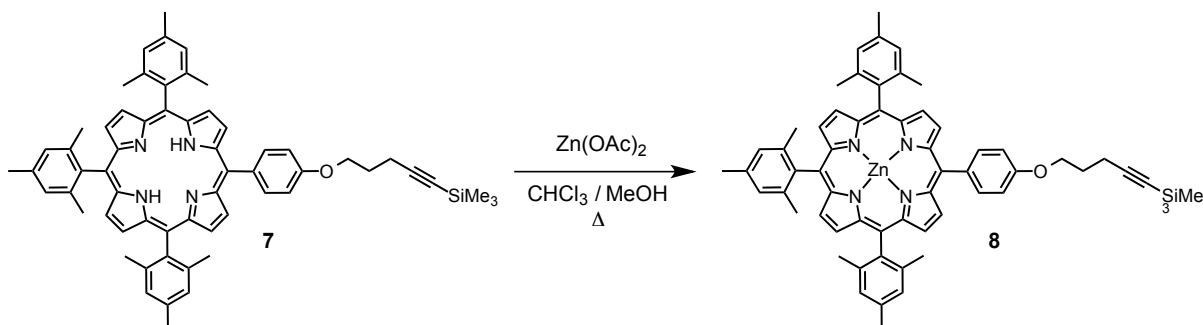
Compound 7



$BF_3 \cdot Et_2O$ (0.37 mL, 2.97 mmol) was added to a solution of **4** (850 mg, 3.26 mmol), **5** (1.44 mL, 9.79 mmol) and **6** (0.91 mL, 13.06 mmol) in $CHCl_3$ (containing 0.75% EtOH, 800 mL) under argon. After 3 h, *p*-chloranil (3.21 g, 13.06 mmol) was added and the reaction mixture stirred for 2 h. Triethylamine (0.5 mL) was then added. The reaction mixture was filtered through SiO_2 (CH_2Cl_2) and the solvent evaporated. Column chromatography (SiO_2 , cyclohexane/ CH_2Cl_2 /Toluene, 30:20:2) gave **7** (888 mg, 15%) as a purple solid. IR (neat): 2175 ($C\equiv C$). UV/Vis (CH_2Cl_2): 419 (238000), 515 (10000), 549 (3800), 593 (2800), 648 (2000). 1H NMR (400 MHz, $CDCl_3$): δ = 8.79 (d, J = 5 Hz, 2H), 8.65 (d, J = 5 Hz, 2H), 8.61

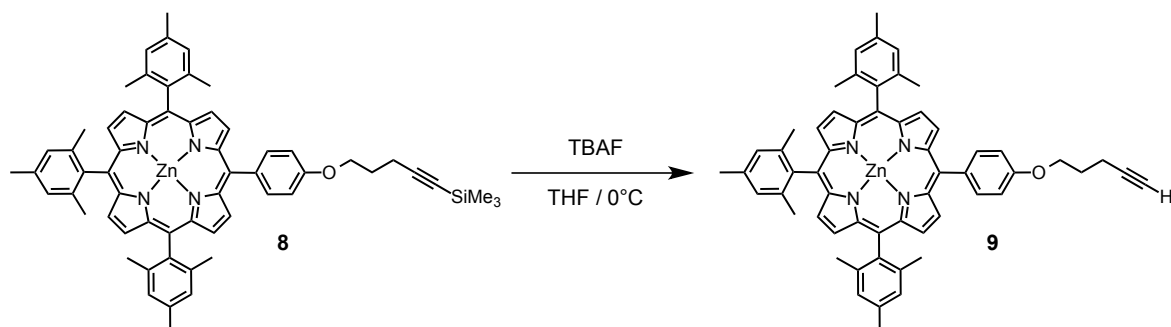
(s, 4H), 8.08 (d, $J = 8$, 2H), 7.25 (m, 8H), 4.34 (t, $J = 6$ Hz, 2H), 2.61 (m, 11H), 2.18 (quint., $J = 7$ Hz, 2H), 1.84 (2s, 18H), 0.20 (s, 9H) ppm. ^{13}C NMR (100 MHz, CDCl_3): $\delta = 158.5$, 139.2, 138.2, 137.9, 137.4, 135.1, 134.3, 129.1, 127.5, 118.9, 117.6, 117.2, 112.4, 106.1, 85.2, 66.4, 28.3, 26.7, 21.5 (two peaks), 21.2, 16.6, 0.0 ppm.

Compound 8



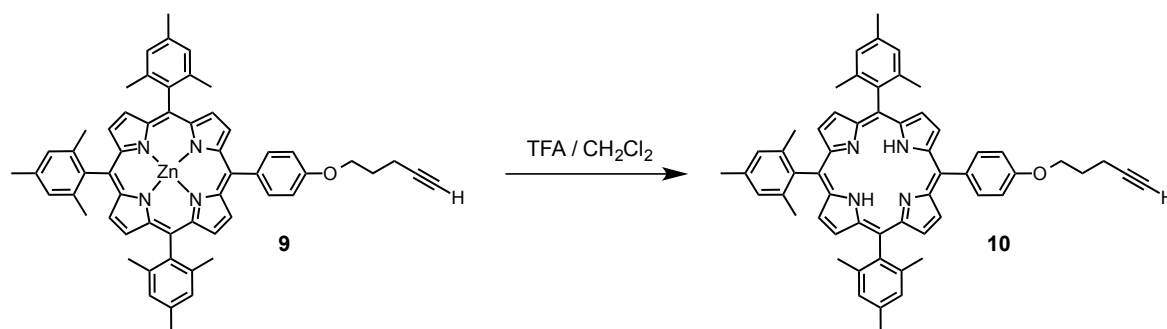
A mixture of $\text{Zn}(\text{OAc})_2 \cdot 2\text{H}_2\text{O}$ (1.08 g, 4.91 mmol) and **7** (1.1 g, 1.23 mmol) in $\text{CHCl}_3/\text{MeOH}$ 9:1 (150 mL) was heated under reflux for 3 h under argon. The resulting mixture was filtered (SiO_2 , CH_2Cl_2) and concentrated. Column chromatography (SiO_2 , cyclohexane/ CH_2Cl_2 /Toluene, 30:20:2) gave **8** (1.02 g, 83%) as a purple solid. IR (neat): 2175 ($\text{C}\equiv\text{C}$). UV/Vis (CH_2Cl_2): 399 (23600), 422 (290000), 510 (1500), 550 (11500), 587 (1700). ^1H NMR (400 MHz, CDCl_3): $\delta = 8.89$ (d, $J = 5$ Hz, 2H), 8.74 (d, $J = 5$ Hz, 2H), 8.69 (s, 4H), 8.10 (d, $J = 8$, 2H), 7.25 (m, 8H), 4.34 (t, $J = 6$ Hz, 2H), 2.61 (m, 11H), 2.18 (quint., $J = 7$ Hz, 2H), 1.84 (2s, 18H), 0.20 (s, 9H) ppm. ^{13}C NMR (100 MHz, CDCl_3): $\delta = 158.3$, 150.0, 149.6, 149.5 (two peaks), 139.0, 138.9, 138.7, 137.1, 135.1, 131.9, 130.8, 130.2, 127.4, 119.7, 118.5, 118.1, 112.3, 106.1, 85.1, 66.4, 28.3, 26.7, 21.5 (two peaks), 21.3, 16.6, 0.0 ppm.

Compound 9



A 1 M TBAF solution in THF (0.76 mL, 0.76 mmol) was added to a stirred solution of **8** (661 mg, 0.069 mmol) in dry THF (40 mL) at 0° C under argon. After 2 h, a saturated NH₄Cl aqueous solution (100 mL) was added and the THF evaporated. The resulting mixture was extracted with CH₂Cl₂. The combined organic layers were dried (Na₂CO₃), filtered and evaporated. Column chromatography (SiO₂, Cyclohexane/CH₂Cl₂ 5/5) gave **9** (556 mg, 91 %) as a purple solid. IR (neat): 3302 (≡C-H), 2175 (C≡C). UV/Vis (CH₂Cl₂): 400 (sh, 35000), 422 (460000), 508 (sh, 2000), 550 (22000), 589 (2600). ¹H NMR (400 MHz, CDCl₃): δ = 8.89 (d, *J* = 5 Hz, 2H), 8.74 (d, *J* = 5 Hz, 2H), 8.69 (s, 4H), 8.10 (d, *J* = 8, 2H), 7.25 (m, 8H), 4.34 (t, *J* = 6 Hz, 2H), 2.61 (s, 9H), 2.56 (dt, *J* = 7 Hz, 2H), 2.18 (quint., *J* = 7 Hz, 2H), 2.04 (t, *J* = 3 Hz, 1H), 1.84 (2s, 18H) ppm. ¹³C NMR (100 MHz, CDCl₃): δ = 158.5, 150.3, 149.8 (two peaks), 149.7, 139.3, 139.1, 137.3, 135.3, 132.2, 131.0, 130.4, 127.6, 118.6, 112.5, 83.7, 69.0, 66.5, 28.5, 26.9, 21.7 (two peaks), 21.5, 15.4 ppm. MALDI-TOF-MS: 884.3 ([M]⁺, calcd. for C₅₈H₅₂N₄OZn: 884.3). Elemental analysis: (%) calcd for C₅₈H₅₂N₄OZn (884.3): C, 78.59; H, 5.91; N, 6.32; found: C, 78.32; H, 5.88; N, 6.30.

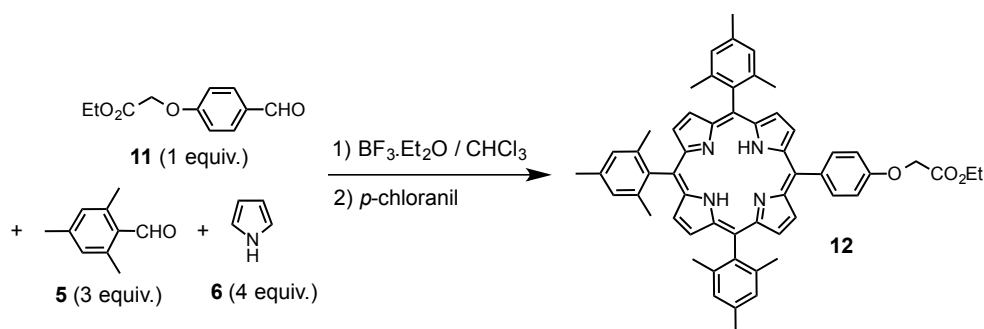
Compound 10



TFA (1.0 mL) was added to a solution of **9** (90 mg, 0.102 mmol) in CH₂Cl₂ (3 mL). The resulting mixture was stirred for 1 h and concentrated. Column chromatography (SiO₂, Cyclohexane/CH₂Cl₂ 1:1) gave **10** (76 mg, 96%) as a purple solid. IR (neat): 3311 (≡C-H). UV/Vis (CH₂Cl₂): 419 (330,000), 515 (26,000), 549 (15,600), 593 (10,800), 648 (8,000). ¹H-NMR (400 MHz, CDCl₃): δ = 8.81 (d, *J* = 5 Hz, 2H), 8.67 (d, *J* = 5 Hz, 2H), 8.63 (s, 4H), 8.10 (d, *J* = 8, 2H), 7.27 (m, 8H), 4.35 (t, *J* = 6 Hz, 2H), 2.61 (s, 9H), 2.56 (dt, *J* = 7 Hz, 2H), 2.18 (quint., *J* = 7 Hz, 2H), 2.04 (t, *J* = 3 Hz, 1H), 1.84 (2s, 18H), -2.25 (s, 2H) ppm. ¹³C-

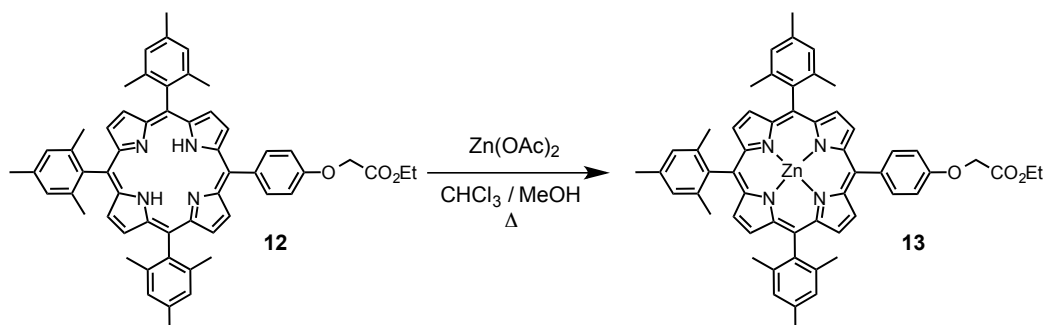
NMR (100 MHz, CDCl₃): δ = 158.7, 139.5, 138.4, 138.2, 137.7, 135.4, 134.6, 132.0-129.2 (br), 127.7, 119.2, 117.8, 117.5, 112.7, 83.6, 69.0, 66.5, 28.5, 26.9, 21.7 (two peaks), 21.5, 15.4 ppm. MALDI-TOF-MS: 823.5 ([M+H]⁺, calcd. for C₅₈H₅₅N₄O: 823.4). Elemental analysis: (%) calcd for C₅₈H₅₄N₄O (823.1): C, 84.64; H, 6.61; N, 6.81; found: C, 84.25; H, 6.61; N, 6.82.

Compound 12



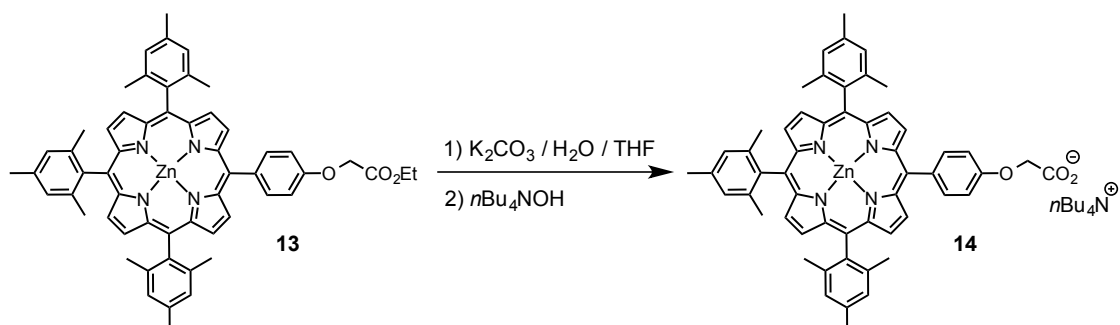
BF₃·Et₂O (0.4 mL, 3.2 mmol) was added to a solution of **11** (2 g, 9.6 mmol), **5** (4.2 mL, 28.8 mmol) and **6** (2.7 mL, 14 mmol) in CHCl₃ (containing 0.75% EtOH, 800 mL) under argon. After 3 h, *p*-chloranil (3.7 g, 15 mmol) was added and the reaction mixture was stirred for 2 h. Triethylamine (0.5 mL) was then added. The reaction mixture was filtered through SiO₂ (CH₂Cl₂) and the solvent evaporated. Column chromatography (SiO₂; CH₂Cl₂, cyclohexane/CH₂Cl₂/Toluene, 30:20:2) gave **12** (0.95 g, 14%) as a purple solid. IR (Neat): 1760 cm⁻¹ (C=O); UV-Vis (CH₂Cl₂): λ_{max} (ϵ) = 418 (480,000), 514 nm, (19,000 M⁻¹cm⁻¹); ¹H NMR (CDCl₃, 300 MHz): δ = 8.81 (d, *J* = 5 Hz, 2H), 8.70 (d, *J* = 5 Hz, 2H), 8.65 (s, 4H), 8.14 (d, *J* = 8.5 Hz, 2H), 7.30 (m, 8H), 4.94 (s, 2H), 4.43 (q, *J* = 7 Hz, 2H), 2.65 (m, 9H), 1.88 (s, 6H), 1.87 (s, 12H), 1.43 (t, *J* = 7 Hz, 3H), -2.54 (s, 2H) ppm; ¹³C NMR (CDCl₃, 75 MHz): δ = 193.2, 169.3, 158.3, 144.2, 141.7, 139.7, 138.7, 138.5, 138.4, 135.9, 135.8, 131.8, 130.9, 130.5, 128.1, 119.2, 118.3, 118.0, 113.3, 66.18, 61.8, 21.8, 21.7, 21.5, 21.2, 14.5 ppm. MALDI-TOF-MS: *m/z* calcd for C₅₇H₅₄O₃N₄ [M]⁺: 843.07; found: 843.17.

Compound 13



A mixture of $\text{Zn(OAc)}_2 \cdot 2\text{H}_2\text{O}$ (690 mg, 3.2 mmol) and **12** (888 mg, 1.1 mmol) in a $\text{CHCl}_3/\text{MeOH}$ 9:1 (100 mL) was heated under reflux for 3 h under argon. The resulting mixture was filtered (Si_2O ; CH_2Cl_2) and concentrated to give **13** (950 mg, 99%) as a purple solid. IR (neat): 1703 (C=O) cm^{-1} . UV-Vis (CH_2Cl_2): λ_{max} (ϵ) = 420 (380,000), 550 nm (15,000 $\text{M}^{-1}\text{cm}^{-1}$). ^1H NMR (CDCl_3 , 300 MHz): δ = 8.87 (d, J = 4.5 Hz, 2H), 8.76 (d, J = 4.5 Hz, 2H), 8.71 (s, 4H), 8.14 (d, J = 8.5 Hz, 2H), 7.28 (m, 8H), 4.92 (s, 2H), 4.42 (q, J = 7 Hz, 2H), 2.64 (m, 9H), 1.86 (s, 6H), 1.85 (s, 12H), 1.42 (t, J = 7 Hz, 3H) ppm. ^{13}C NMR (CDCl_3 , 75 MHz): δ = 169.1, 157.5, 150.18, 149.9, 149.8, 149.7, 143.3, 139.3, 139.1, 139.0, 137.4, 136.4, 135.3, 132.1, 131.1, 130.9, 130.5, 127.6, 119.5, 118.9, 118.8, 118.5, 112.8, 65.8, 61.5, 21.7, 21.6, 21.5, 14.3 ppm. MALDI-TOF-MS: m/z calcd for $\text{C}_{57}\text{H}_{52}\text{O}_3\text{N}_4\text{Zn}$ $[\text{M}]^+$: 906.43; found: 906.28.

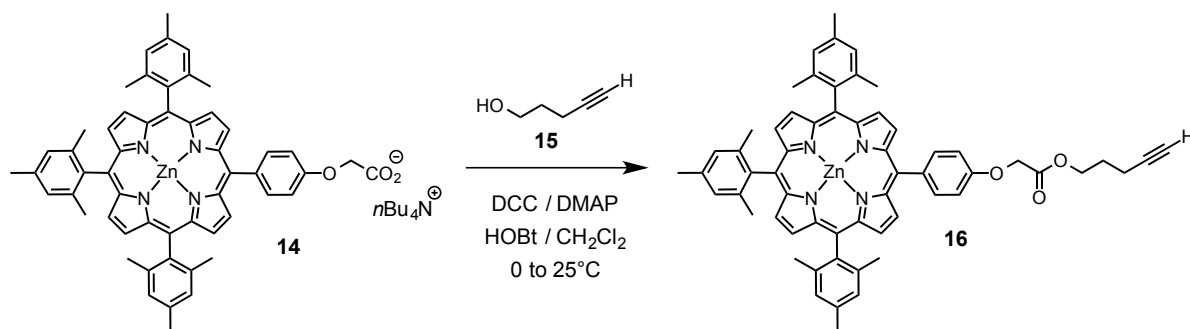
Compound 14



A mixture of K_2CO_3 (1.74 g, 12 mmol) and **13** (600 mg, 0.7 mmol) in $\text{THF}/\text{H}_2\text{O}$ 2:1 (120 mL) was heated under reflux under argon. After 3 days, the THF was evaporated and a

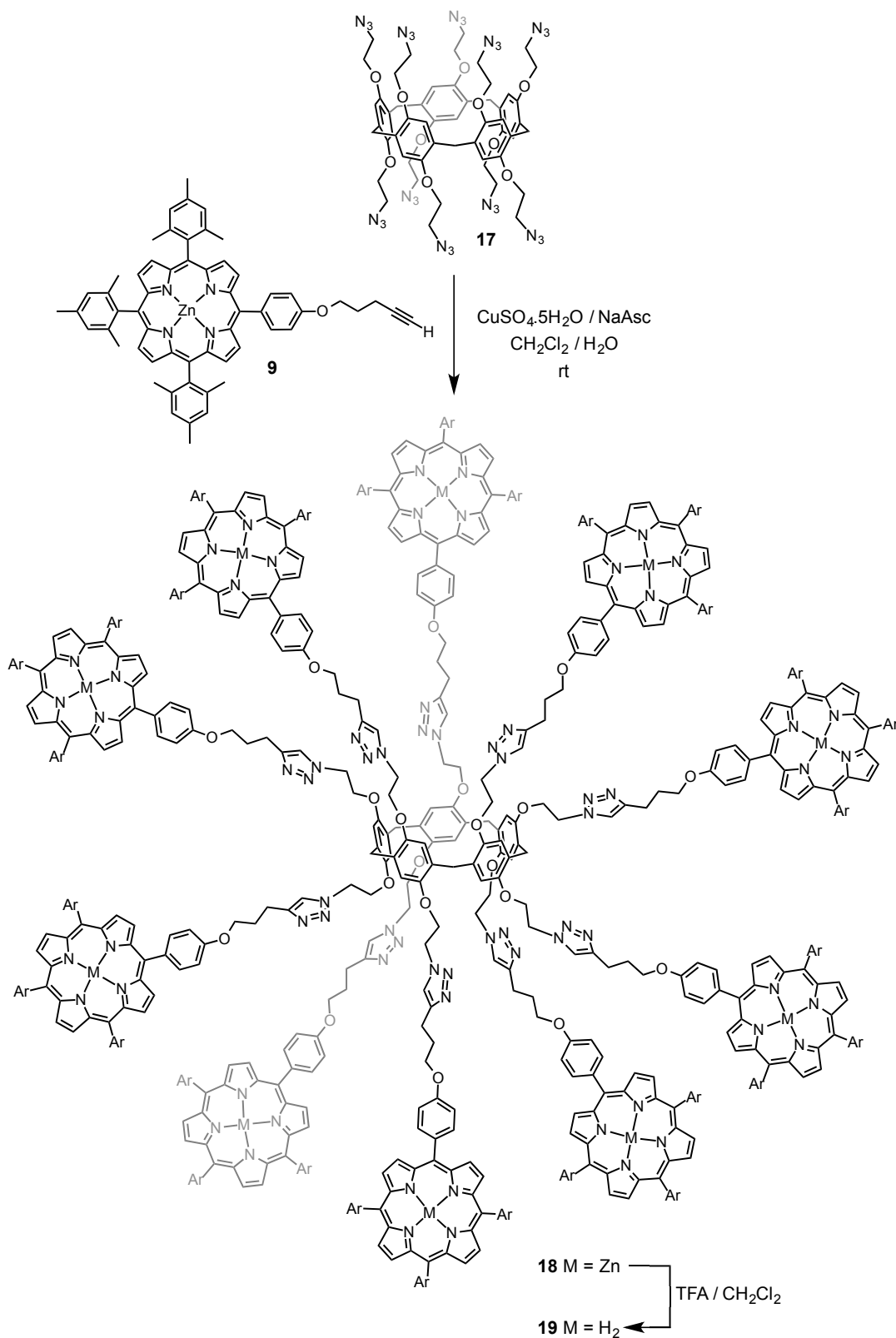
1M solution of tetrabutylammonium hydroxyde in CH_2Cl_2 (100 mL) added, the organic layer washed with water, dried (Na_2SO_4), filtered and evaporated to give **14** (711 mg, 96%) as a purple powder. IR (neat): 1703 (C=O) cm^{-1} . ^1H NMR (CDCl_3 , 300 MHz): δ = 8.91 (d, J = 5 Hz, 2H), 8.70 (d, J = 5 Hz, 2H), 8.67 (s, 4H), 8.03 (d, J = 8 Hz, 2H), 7.31 (d, J = 8 Hz, 2H), 7.26 (s, 6H), 4.64 (bs, 2H), 3.43 (m, 8H), 2.61 (s, 9H), 1.82 (s, 18H), 1.71 (m, 8H), 1.25 (m, 8H), 1.00 (t, J = 7.5 Hz, 12H) ppm. ^{13}C NMR (CDCl_3 , 75 MHz): δ = 158.3, 150.3, 150.1, 149.8, 149.7, 149.6, 143.4, 139.3, 139.1, 137.3, 137.2, 135.4, 135.2, 132.2, 132.0, 130.9, 130.5, 130.3, 130.1, 127.7, 127.6, 120.0, 118.54, 118.2, 113.0, 66.2, 59.0, 24.14, 22.7, 21.7, 21.4, 19.8, 13.7 ppm.

Compound 16



DCC (200 mg, 0.8 mmol), DMAP (25 mg, 0.2 mmol) and HOBt (37 mg, 0.2 mmol) were added to a solution of **15** (160 mg, 1.9 mmol) and **14** (711 mg, 0.6 mmol) in dry CH_2Cl_2 (110 mL) at 0°C under argon. After for 72 h at r.t., the mixture was filtered and the solvent evaporated. Column chromatography (SiO_2 ; toluene) gave **16** (570 mg, 95%) as a purple powder. IR (neat): 3299 ($\equiv\text{C-H}$), 1737 (C=O) cm^{-1} . UV-Vis (CH_2Cl_2): λ_{max} (ϵ) = 420 (610,000), 549 nm (17,000 $\text{M}^{-1}\text{cm}^{-1}$). ^1H NMR (CDCl_3 , 300 MHz): δ = 8.88 (d, J = 5 Hz, 2H), 8.77 (d, J = 5 Hz, 2H), 8.72 (s, 4H), 8.15 (d, J = 8.5 Hz, 2H), 7.29 (m, 8H), 4.94 (s, 2H), 4.47 (t, J = 7 Hz, 2H), 2.65 (s, 9H), 2.39 (dt, J = 2.5 Hz, J = 7 Hz, 2H), 2.01 (m, 3H) 1.87 (s, 6H), 1.86 (s, 12H) ppm. ^{13}C NMR (CDCl_3 , 75 MHz): δ = 169.1, 157.4, 150.1, 149.9, 149.8, 149.7, 139.3, 139.1, 139.0, 137.4, 136.5, 135.4, 132.1, 131.1, 130.9, 130.5, 128.9, 127.6, 119.5, 118.8, 118.5, 112.7, 82.7, 69.38, 65.7, 63.9, 38.75, 30.37, 28.9, 27.5, 23.7, 21.8, 21.7, 15.21 ppm. MALDI-TOF-MS: m/z calcd for $\text{C}_{60}\text{H}_{54}\text{O}_3\text{N}_4\text{Zn} [\text{M}]^+$: 944.48; found: 944.35.

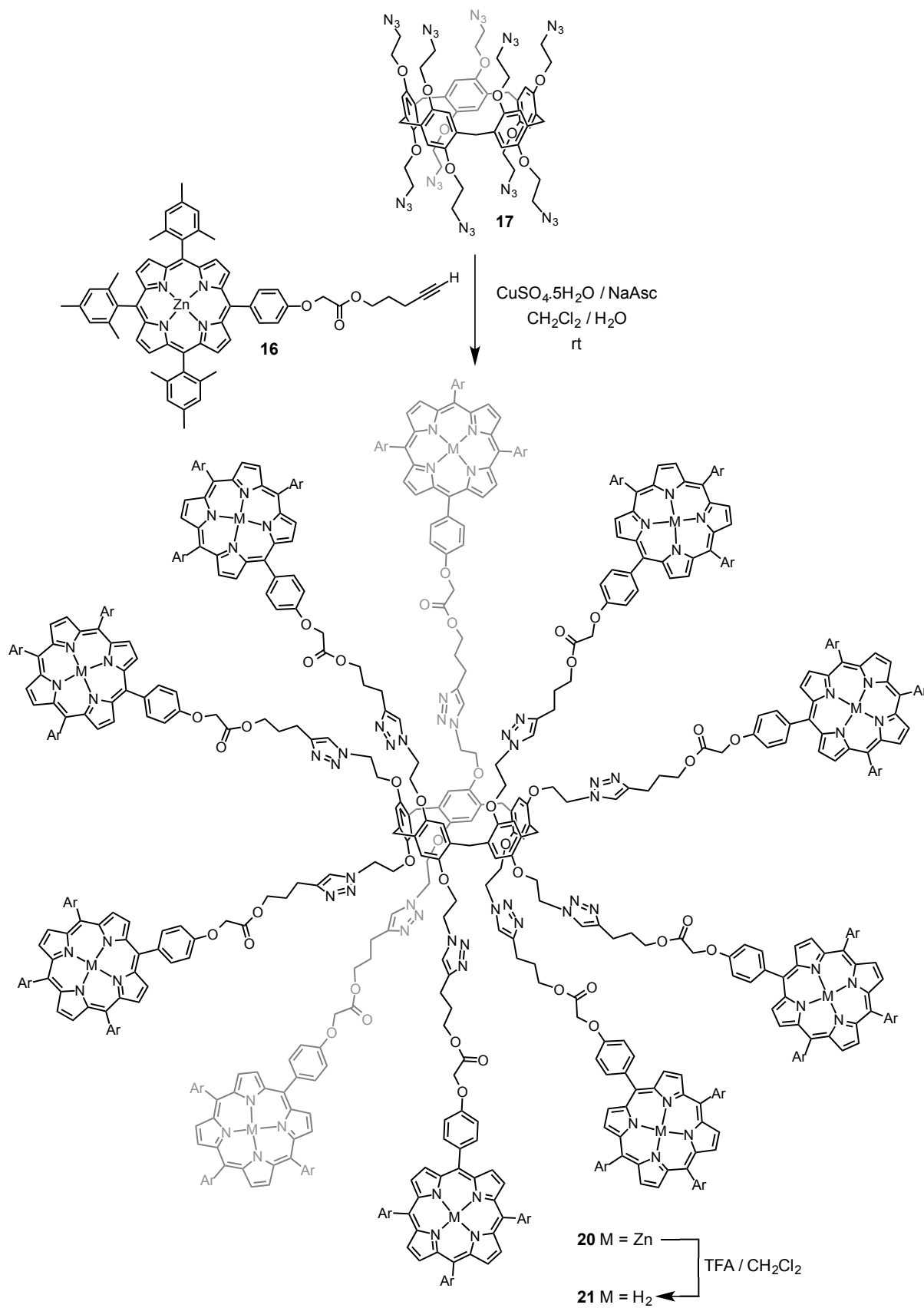
Compounds 18 and 19



A mixture of **17** (29 mg, 0.022 mmol), **9** (214 mg, 0.242 mmol), CuSO₄·5H₂O (1.6 mg, 66 μmol) and sodium ascorbate (2.6 mg, 0.013 mmol) in CH₂Cl₂/H₂O (4:1 mL) was stirred at room temperature for 48 h. The organic layer was diluted with CH₂Cl₂, washed with water and concentrated. Column chromatography (SiO₂, CH₂Cl₂ → CH₂Cl₂/MeOH 100:3) followed by gel permeation chromatography (Biobeads SX-1 CH₂Cl₂) gave **18** (261 mg, 96%) as a purple solid. UV/Vis (CH₂Cl₂): 423 (2,690,600), 432 (sh, 2,588,140), 552 (160,200), 605 (42,600). ¹H-NMR (400 MHz, CDCl₂-CDCl₂, 105°C): 8.87 (d, *J* = 5 Hz, 20H), 8.72 (d, *J* = 5 Hz, 20H), 8.67 (s, 40H), 8.06 (d, *J* = 8 Hz, 20H), 7.42 (s, 10H), 7.23-7.16 (m, 80H), 6.62 (s, 10H), 4.39 (m, 20H), 4.14 (t, *J* = 6 Hz, 20H), 4.05 (t, *J* = 5 Hz, 20H), 3.48 (s, 10H), 2.62 (m, 20H), 2.59 (s, 90H), 2.10 (quint., *J* = 7 Hz, 20H), 2.04 (t, *J* = 3 Hz, 1H), 1.84 (2s, 180H). ¹³C-NMR (100 MHz, CDCl₃): 157.7, 149.7, 149.6 (two peaks), 148.1, 145.2, 139.4, 139.2, 139.0, 138.9, 137.3, 135.5, 135.3, 131.6, 130.9 (two peaks), 130.8, 130.0, 128.1, 127.5, 119.8, 119.7, 119.1, 118.4, 118.0, 114.3, 112.3, 66.3, 64.8 (two peaks), 48.9, 48.8, 48.7, 27.9, 21.6, 21.5, 21.1. MALDI-TOF-MS: 10161.81 ([M⁺, calcd. for C₆₃₅H₅₈₀N₇₀O₂₀Zn₁₀: 10164.95 (relative intensity: 100%), 10161.95 (relative intensity: 85%)). Anal. Calcd. for C₆₃₅H₅₈₀N₇₀O₂₀·2CH₂Cl₂: C, 74.02; H, 5.70; N, 9.49. Found: C, 73.83; H, 5.72; N, 9.45.

TFA (1.2 mL) was added to a solution of **18** (115 mg, 0.011 mmol) in CH₂Cl₂ (3 mL). The resulting mixture was stirred for 1 h and concentrated. Column chromatography (SiO₂, CH₂Cl₂ → CH₂Cl₂/MeOH 100:3) followed by gel permeation chromatography (Biobeads SX-1 CH₂Cl₂) gave **19** (98 mg, 92%) a purple solid. IR: 3321 (N-H). UV/Vis (CH₂Cl₂): 420 (3,330,000), 516 (270,000), 551 (156,160), 592 (130,983), 646 (98,000). ¹H-NMR (400 MHz, CDCl₃): 8.88 (br, 20H), 8.73 (br, 20H), 8.68 (s, 40H), 8.11 (br, 20H), 7.68 (br, 10H), 7.28 (br, 80H), 6.81 (br, 10H), 4.97-4.71 (br, 20H), 4.53-4.15 (br, 40H), 3.45 (br, 10H), 3.08 (br, 20H), 2.65 (br, 30H), 2.58 (br, 60H), 2.28 (br, 20H), 1.91 (br, 60H), 1.88 (br, 120H), -2.45 (br, 20H). ¹³C-NMR (100 MHz, CDCl₃): 157.8, 149.8, 147.7, 139.5, 139.4, 138.4, 138.2, 137.7, 135.5, 134.5, 132.0-129.4 (br), 128.8, 127.8, 121.6, 119.2, 117.9, 117.6, 116.2, 112.8, 67.6, 67.1, 50.3, 29.8, 29.3, 22.5, 21.8, 21.7, 21.5 (two peaks). MALDI-TOF-MS: 9525.88 ([M+H]⁺, calcd. for C₆₃₅H₆₀₁N₇₀O₄₀: 9525.81). Anal. Calcd. for C₆₃₅H₆₀₀N₇₀O₂₀·3CHCl₃: C, 77.48; H, 6.15; N, 9.91. Found: C, 77.40; H, 6.28; N, 9.74.

Compounds 20 and 21



A mixture of **17** (38 mg, 0.03 mmol), **16** (334 mg, 0.35 mmol), CuSO₄·5H₂O (1.6 mg, 66 μmol) and sodium ascorbate (2.6 mg, 0.013 mmol) in CH₂Cl₂/H₂O (4:1 mL) was stirred at room temperature for 6 days. The organic layer was diluted with CH₂Cl₂, washed with water and concentrated. Column chromatography (SiO₂, CH₂Cl₂ → CH₂Cl₂/MeOH 100:2) followed by gel permeation chromatography (Biobeads SX-1 CH₂Cl₂) gave **20** (213 mg, 66%) as a purple solid. IR (neat): 3110 (C_{arom}-H), 2960 (C-H), 2917 (C-H), 2855 (C-H), 1742 and 1741 (C=O) cm⁻¹. UV/Vis (CH₂Cl₂): 422 (2966183), shoulder 430 (2281212), 551 (168239), shoulder 564 (117797), 603 (32450) nm (M⁻¹ cm⁻¹). ¹H NMR (400 MHz, CD₂Cl₂): δ = 8.70 (m, 20H), 8.64 (m, 60H), 7.92 (m, 20H), 7.21 (s, 20H), 7.17 (s, 40H), 6.90 (m, 30H), 5.96 (s, 10H), 4.44 (m, 20H), 3.64 (m, 60H), 2.63 (s, 10H), 2.50 (s, 30H), 2.45 (m, 60H), 1.79 (3s, 180H), 1.31 (m, 20H), 1.16 (m, 20H) ppm. ¹³C NMR (100 MHz, CD₂Cl₂): δ = 168.7, 157.1, 150.0, 149.8, 149.7, 148.5, 145.1, 139.3, 139.1, 137.3, 136.7, 135.3, 131.8, 130.9, 130.8, 130.2, 128.2, 127.5, 120.9, 119.1, 118.5, 118.3, 114.6, 112.4, 66.1, 65.3, 63.6, 49.0, 28.5, 27.2, 26.9, 21.5, 21.1, 20.9, 20.2 ppm. MALDI-TOF-MS: *m/z* 10751.63 ([M+H]⁺, calcd for C₆₅₅H₆₀₁O₄₀N₇₀Zn₁₀: 10746.01 (100%), 10751.00 (75%)). Elemental analysis: (%) calcd for C₆₅₅H₆₀₀N₇₀O₄₀Zn₁₀·2CH₂Cl₂ (10915.88): C, 72.29; H, 5.58; N, 8.98; found: C, 72.03; H, 5.94, N, 8.91.

TFA (1.3 mL) was added to a solution of **20** (82 mg, 7.6 μmol) in CH₂Cl₂ at room temperature. After 40 minutes, the mixture was evaporated. Column chromatography (SiO₂, CH₂Cl₂/MeOH 100:0 → 100:5) gave **21** (75 mg, 97%) as a purple solid. IR (neat): 1759 (C=O). UV/Vis (CH₂Cl₂): 419 (4032833), 515 (212300), 549 (83800), 591 (65600), 647 (43400). ¹H-NMR (400 MHz, CD₂Cl₂): 8.79 (d, *J* = 5 Hz, 20H), 8.63 (d, *J* = 5 Hz, 2H), 8.50 (m, 40H), 8.08 (d, *J* = 8 Hz, 20H), 7.65 (s, 10H), 7.25-7.17 (m, 80H), 6.69 (s, 10H), 4.86 - 4.65 (m, 40H), 4.36-4.21 (m, 40H), 3.34 (s, 10H), 2.80 (t, *J* = 6 Hz, 20H), 2.56 (s, 30H), 2.48 (s, 60H), 2.04 (t, *J* = 6 Hz, 20H), 1.84 (s, 60H), 1.77 (s, 120H), -2.58 (s, 20H). ¹³C-NMR (100 MHz, CDCl₃): 168.9, 157.7, 149.3, 146.9, 139.3, 139.2, 138.2, 138.0, 137.8, 137.7, 135.5, 135.4, 131.6-129.5 (br), 128.8, 127.7 (two peaks), 121.7, 118.8, 117.8, 117.6, 115.4, 112.9, 67.3, 65.5, 64.4, 50.1, 29.7, 28.3, 22.0, 21.4, 21.3, 21.1 (two peaks). MALDI-TOF-MS: 10113.86 ([M]⁺, calcd. for C₆₅₅H₆₂₀N₇₀O₄₀: 10111.88 (relative intensity: 100%), 10113.89 (relative intensity: 89%). Anal. Calcd. for C₆₅₅H₆₂₀N₇₀O₄₀·2CHCl₃: C, 76.23; H, 6.06; N, 9.47. Found: C, 76.50; H, 6.24; N, 9.26.

References

- 1) L. Zhang (Ed.), *Heme Biology – The Secret Life of Heme in Regulating Diverse Biological Processes*, World Scientific Publishing, Singapore, **2011**.
- 2) D. M. Lawlor, *Photosynthesis*, third edition, BIOS scientific publisher, Oxford, **2001**.
- 3) a) V. Balzani, S. Campagna, G. Denti, A. Juris, S. Serroni, M. Venturi, *Acc. Chem. Res.* **1998**, *31*, 26; b) V. Balzani, P. Ceroni, A. Juris, M. Venturi, S. Campagna, F. Puntoriero, S. Serroni, *Coord. Chem. Rev.* **2001**, *219-221*, 545.
- 4) a) M. Fisher, F. Vögtle, *Angew. Chem. Int. Ed.* **1999**, *38*, 884; b) A. Adronov, J. M. J. Fréchet, *Chem. Commun.* **2000**, 1701.
- 5) D. Kim (Ed.), *Multiporphyrin Arrays: Fundamentals and Applications*, Pan Stanford Publishing, Singapore, **2012**.
- 6) a) B. J. Littler, Y. Ciringh, J. S. Lindsey, *J. Org. Chem.* **1999**, *64*, 2864; b) G. R. Geier III, B. J. Littler, J. S. Lindsey, *J. Chem. Soc. Perkin Trans. 2* **2001**, 701; c) R. W. Wagner, D. S. Lawrence, J. S. Lindsey, *Tetrahedron Lett.* **1987**, *28*, 3069; d) J. S. Lindsey, R. W. Wagner, *J. Org. Chem.* **1989**, *54*, 828.
- 7) a) X. Huang, K. Nakanishi, N. Berova, *Chirality* **2000**, *12*, 237; b) T. Hashimoto, Y.-C. Choe, H. Nakano, K. Hirao, *J. Phys. Chem. A* **1999**, *103*, 1894; c) M. Gouterman, *J. Chem. Phys.* **1959**, *30*, 1139.
- 8) J. Bhaumik, Z. Yao, K. Eszter Borbas, M. Taniguchi, J. S. Lindsey, *J. Org. Chem.* **2006**, *71*, 8807.
- 9) I. Nierengarten, S. Guerra, M. Holler, L. Karmazin-Brelot, J. Barbera, R. Deschenaux, J.-F. Nierengarten, *Eur. J. Org. Chem.* **2013**, 3675.
- 10) a) R. Huisgen, *Pure Appl. Chem.* **1989**, *61*, 613; G. Huisgen, W. Szeimies, L. Moebius, *Chem. Ber.* **1967**, *100*, 2494; C. W. Tornøe, M. Meldal, *Proceedings of the 2nd International and 17th American Peptide Symposium, Peptides: The Waves of the Future*, M. Lebl, R. A. Houghton (Eds.), San Diego, **2001**, 263; V. V. Rostovtsev, L. G. Green, V. V. Fokin, K. B. Sharpless, *Angew. Chem. Int. Ed.* **2002**, *41*, 2596.
- 11) H. C. Kolb, M. G. Finn, K. B. Sharpless, *Angew. Chem. Int. Ed.* **2001**, *40*, 2004.
- 12) a) H. Zhang, N. L. Strutt, R. S. Stoll, H. Li, Z. Zhu, J. F. Stoddart, *Chem. Commun.* **2011**, *47*, 11420; b) I. Nierengarten, S. Guerra, M. Holler, J.-F. Nierengarten, R. Deschenaux, *Chem. Commun.* **2012**, *48*, 8072; c) N. L. Strutt, H. Zhang, M. A. Giesener, J. Lei, J. F. Stoddart, *Chem. Commun.* **2012**, *48*, 1647; d) H. Deng, X. Shu,

- X. Hu, J. Li, X. Jia, C. Li, *Tetrahedron Lett.* **2012**, *53*, 4609; e) G. Yu, Z. Zhang, J. He, Z. Abliz, F. Huang, *Eur. J. Org. Chem.* **2012**, 5902; f) I. Nierengarten, M. Nothisen, D. Sigwalt, T. Biellmann, M. Holler, J.-S. Remy, J.-F. Nierengarten, *Chem. Eur. J.* **2013**, *19*, 17552.
- 13) a) J. Iehl, R. Pereira de Freitas, B. Delavaux-Nicot, J.-F. Nierengarten, *Chem. Commun.* **2008**, 2450; b) J. Iehl, J. F. Nierengarten, *Chem. Eur. J.* **2009**, *15*, 7306; c) J. Iehl, J.-F. Nierengarten, *Chem. Commun.* **2010**, *46*, 4160; d) J.-F. Nierengarten, J. Iehl, V. Oerthel, M. Holler, B. M. Illescas, A. Munoz, N. Martin, J. Rojo, M. Sanchez-Navarro, S. Cecioni, S. Vidal, K. Buffet, M. Durka, S. P. Vincent, *Chem. Commun.* **2010**, *46*, 3860; e) J. Iehl, J.-F. Nierengarten, A. Harriman, T. Bura, R. Ziessel, *J. Am. Chem. Soc.* **2012**, *134*, 988; f) J. Iehl, M. Frasconi, H.-P. Jacquot de Rouville, N. Renaud, S. M. Dyar, N. L. Strutt, R. Carmieli, M. R. Wasielewski, M. A. Ratner, J.-F. Nierengarten, J. F. Stoddart, *Chem. Sci.* **2013**, *4*, 1462; g) I. Nierengarten, J.-F. Nierengarten, *Chem. Asian J.* **2014**, *9*, 1436.
- 14) J. Iehl, M. Holler, J.-F. Nierengarten, K. Yoosaf, J. M. Malicka, N. Armaroli, J.-M. Strub, A. Van Dorselaer, B. Delavaux-Nicot, *Aust. J. Chem.* **2011**, *64*, 153.
- 15) T. Ogoshi, K. Kitayama, T. Aoki, S. Fujinami, T. Yamagashi, Y. Nakamoto, *J. Org. Chem.* **2010**, *75*, 3268.
- 16) I. Nierengarten, K. Buffet, M. Holler, S. P. Vincent, J.-F. Nierengarten, *Tetrahedron Lett.* **2013**, *54*, 2398.
- 17) A. Matea-Alonso, C. Sooambar, M. Prato, *C. R. Chimie* **2006**, *9*, 944-951 and references therein.
- 18) a) N. T. Nguyen, G. M. Mamardashvili, O. M. Kulikova, I. G. Scheblykin, N. Z. Mamardashvili, W. Dehaen, *RSC Adv.* **2014**, *4*, 19703; b) C. Maeda, P. Kim, S. Cho, J. K. Park, J. M. Lim, D. Kim, J. Vura-Weis, M. R. Wasielewski, H. Shinokubo, A. Osuka, *Chem. Eur. J.* **2010**, *16*, 5052; c) C. Maeda, S. Yamaguchi, C. Ikeda, H. Shinokubo, A. Osuka, *Org. Lett.* **2008**, *10*, 549; d) J.-P. Collin, F. Durola, V. Heitz, F. Reviriego, J.-P. Sauvage, Y. Trolez, *Angew. Chem. Int. Ed.* **2010**, *49*, 10172.
- 19) a) N. Armaroli, F. Diederich, L. Echegoyen, T. Habicher, L. Flamigni, G. Marconi, J.-F. Nierengarten, *New J. Chem.* **1999**, *23*, 77; b) F. D'Souza, G. R. Deviprasad, M. S. Rahman, J.-P. Choi, *Inorg. Chem.* **1999**, *38*, 2157; c) A. Trabolsi, M. Elhabiri, M. Urbani, J. L. Delgado de la Cruz, F. Ajamaa, N. Solladie, A.-M. Albrecht-Gary, J.-F. Nierengarten, *Chem. Commun.* **2005**, 5736; d) W.-S. Li, K. S. Kim, D.-L. Jiang, H.

Tanaka, T. Kawai, J. H. Kwon, D. Kim, T. Aida, *J. Am. Chem. Soc.* **2006**, *128*, 10527;
e) A. Trabolsi, M. Urbani, J. L. Delgado, F. Ajamaa, M. Elhabiri, N. Solladié, J.-F. Nierengarten, A.-M. Albrecht-Gary, *New J. Chem.* **2008**, *32*, 159; f) K. Yoosaf, J. Iehl, I. Nierengarten, M. Hmadeh, A.-M. Albrecht-Gary, J.-F. Nierengarten, N. Armaroli, *Chem. Eur. J.* **2014**, *20*, 223.

4. Pillar[5]arene-based rotaxanes

4.1. Introduction

The development of new building blocks bearing complementary reactive groups with a controlled spatial repartition on the scaffold is a key step for the preparation of multifunctional molecules with unique properties.¹ In this perspective, the existing pillar[5]arene scaffolds prepared so far² have some limitations. Indeed, whereas building blocks with 10 identical peripheral groups are conveniently prepared, pillar[5]arenes combining two different 1,4-dialkoxybenzene moieties is only possible under statistical conditions.³ Actually, a controlled synthesis appears difficult as cleavage of the Ar-CH₂ bonds occurs under the Friedel-Crafts conditions used for their preparation⁴ and scrambling cannot be avoided. In order to overcome this problem, we propose to take profit of the capability of pillar[5]arenes to form host-guest complexes with alkyl chains⁵ to build rotaxanes.⁶ In this way, the macrocyclic pillar[5]arene component can carry ten copies of a first functional group, whereas the molecular axis of the rotaxane can be symmetrically or unsymmetrically substituted and thus carry one or two additional functional subunits. The structure of the scaffold provides a perfect control of the spatial organization of the different functional subunits as the ten peripheral groups attached on the macrocyclic core generates an equatorial belt, whereas the two stoppers are located at the opposite poles of the ring. This synthetic approach combining recent concepts for the preparation of multifunctional nanomolecules¹ (click chemistry on multifunctional scaffolds) with supramolecular chemistry⁷ (self-assembly to prepare rotaxanes) should give easy access to a large variety of very sophisticated

supramolecular ensembles for various applications. Indeed, the rotaxane scaffolds proposed herein are ideally suited for the synthesis of multicomponent photoactive molecular devices. In this respect, we propose to functionalize the pillar[5]arene with peripheral Zn-porphyrin moieties described in the previous section with a complementary photoactive subunit. For instance, by using a free base-porphyrin stopper, one may anticipate that the light energy absorbed by the peripheral Zn-porphyrin moieties will be transferred to the free base porphyrin stopper.⁸ The system will thus mimic the natural light-harvesting antennae of the photosynthetic center.⁹

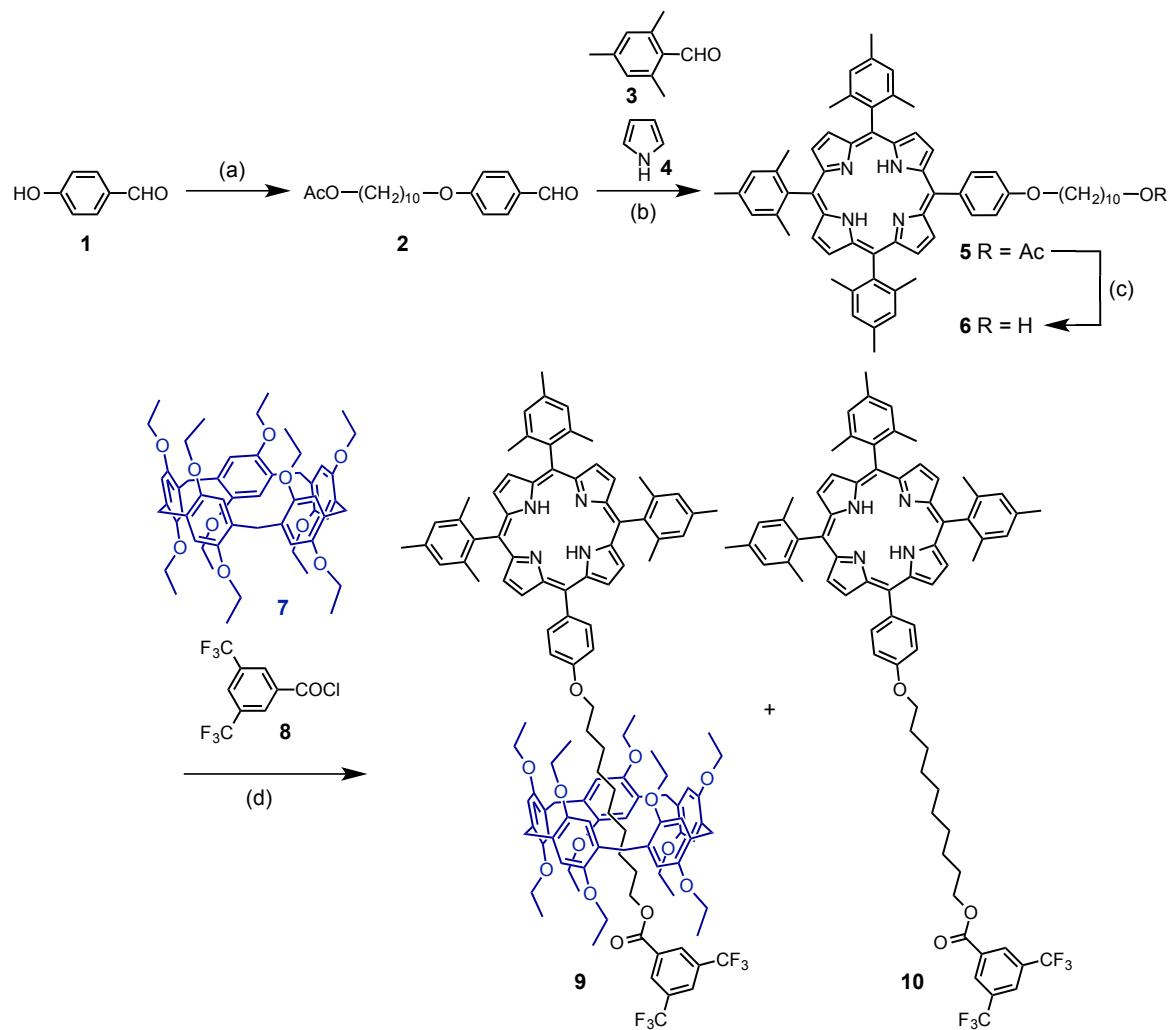
4.2. Synthesis

The reaction conditions for the preparation of [2]rotaxanes bearing a free-base porphyrin stopper were first adjusted from pillar[5]arene **7** and porphyrin **6** (Scheme 1). The 10-hydroxydecyloxy subunit of compound **6** is actually perfectly suited to form inclusion complexes with pillar[5]arene derivatives and treatment with an acyl chloride reagent under the conditions developed by Huang and co-workers¹⁰ should lead to the formation of a [2]rotaxane.

The porphyrin precursor was prepared in 3 steps from 1,10-dibromodecane. A statistical synthetic approach was used to unsymmetrically functionalize 1,10-dibromodecane. Treatment of 1,10-dibromodecane (1 equiv.) with *p*-hydroxybenzaldehyde (**1**, 1 equiv.) and sodium acetate (1 equiv.) in the presence of K₂CO₃ in DMF at 60°C afforded a mixture of 3 products and the separation of **2** from the two symmetrical byproducts, namely 1,10-decanediol diacetate and 4,4'-(decane-1,10-diylbis(oxy))dibenzaldehyde, was conveniently achieved by column chromatography on SiO₂. Compound **2** was thus obtained in 38% yield. Reaction of **2** (1 equiv.), mesitaldehyde (**3**, 3 equiv.) and pyrrole (**4**, 4 equiv.) in CHCl₃ in the presence of BF₃·Et₂O followed by *p*-chloranil oxidation gave free-base porphyrin **5** in 13% yield. Finally, treatment of **5** with KOH in H₂O/THF provided alcohol **6**.

The preparation of a model [2]rotaxane was then attempted by reaction of **6** with acyl chloride **8** in the presence of pillar[5]arene **7**. In order to obtain the desired [2]rotaxane in good yields, the reaction conditions must favor the assembly of a pseudo-rotaxane intermediate from **6** and **7**. For this reason, the reaction was carried out at -15°C and at the highest possible concentration.¹⁰⁻¹¹ Moreover, pillar[5]arene **7** was also used in excess (2 equiv.). It can be also noted that the choice of CHCl₃ as solvent is critical to obtain the desired

[2]rotaxane in good yields. Indeed, this solvent is unable to form inclusion complexes with macrocycle **7** and there is no competition for the binding of reagent **6**.¹¹



Scheme 1. Preparation of compounds **9** and **10**. *Reagents and conditions:* (a) 1,10-dibromodecane, AcONa, K₂CO₃, DMF, 60°C (38%); (b) BF₃·Et₂O, CHCl₃, rt, then chloranil (13%); (c) KOH, H₂O, THF, 80°C (97%); (d) CHCl₃, Et₃N, -15°C to rt (**9**: 77%, **10**: 3%).

Under these conditions, [2]rotaxane **9** was obtained in a remarkable 77% yield. Axle **10** was also formed and this byproduct was isolated in 3% yield. The chemical structure of compound **9** was easily confirmed by its ¹H NMR spectrum showing the diagnostic signals of both the macrocycle and the axle (Figure 1). Importantly, when compared to compound **10**, a dramatic shielding of all the signals arising from the -(CH₂)₁₀- chain is observed for [2]rotaxane **9** due to the ring current effect of the pillar[5]arene aromatic subunits on the methylene moieties of the axle. The MALDI-TOF mass spectrum further confirmed the

structure of **9** with an intense signal at $m/z = 2044.6$ corresponding to the expected molecular ion peak ($[M]^+$, calcd. for $C_{127}H_{140}N_4O_{13}F_6$: 2044.5).

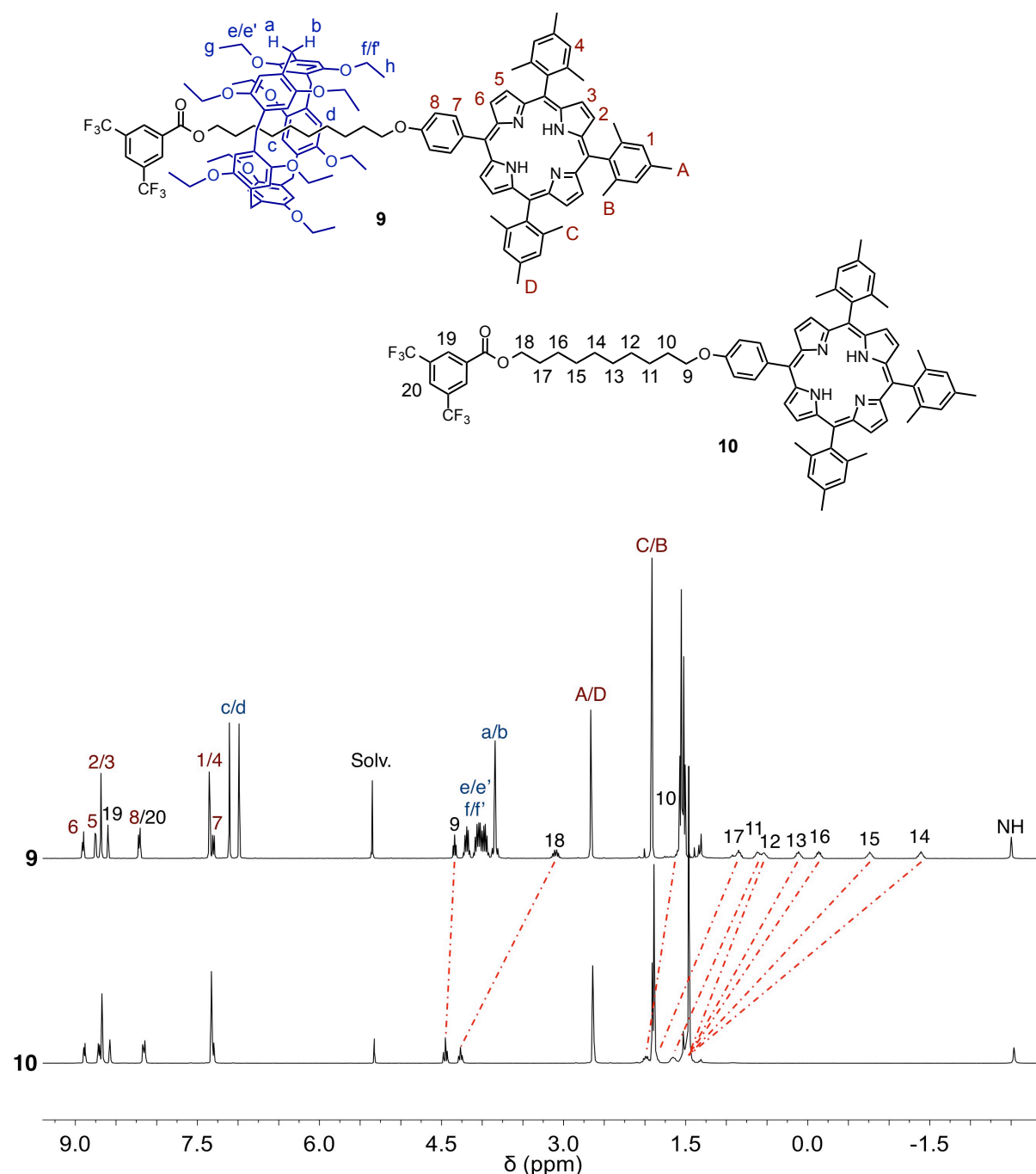
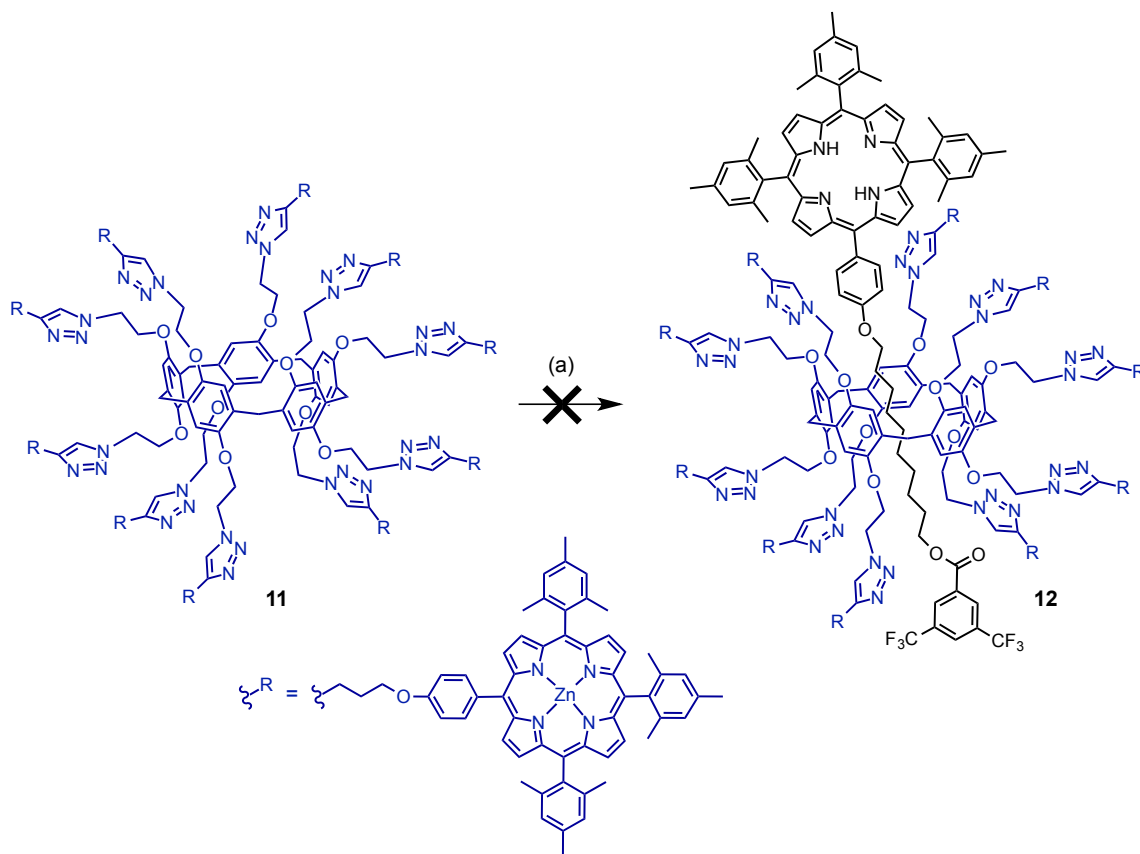


Figure 1. ^1H NMR spectra (400 MHz, CD_2Cl_2) of compounds **9** and **10**.

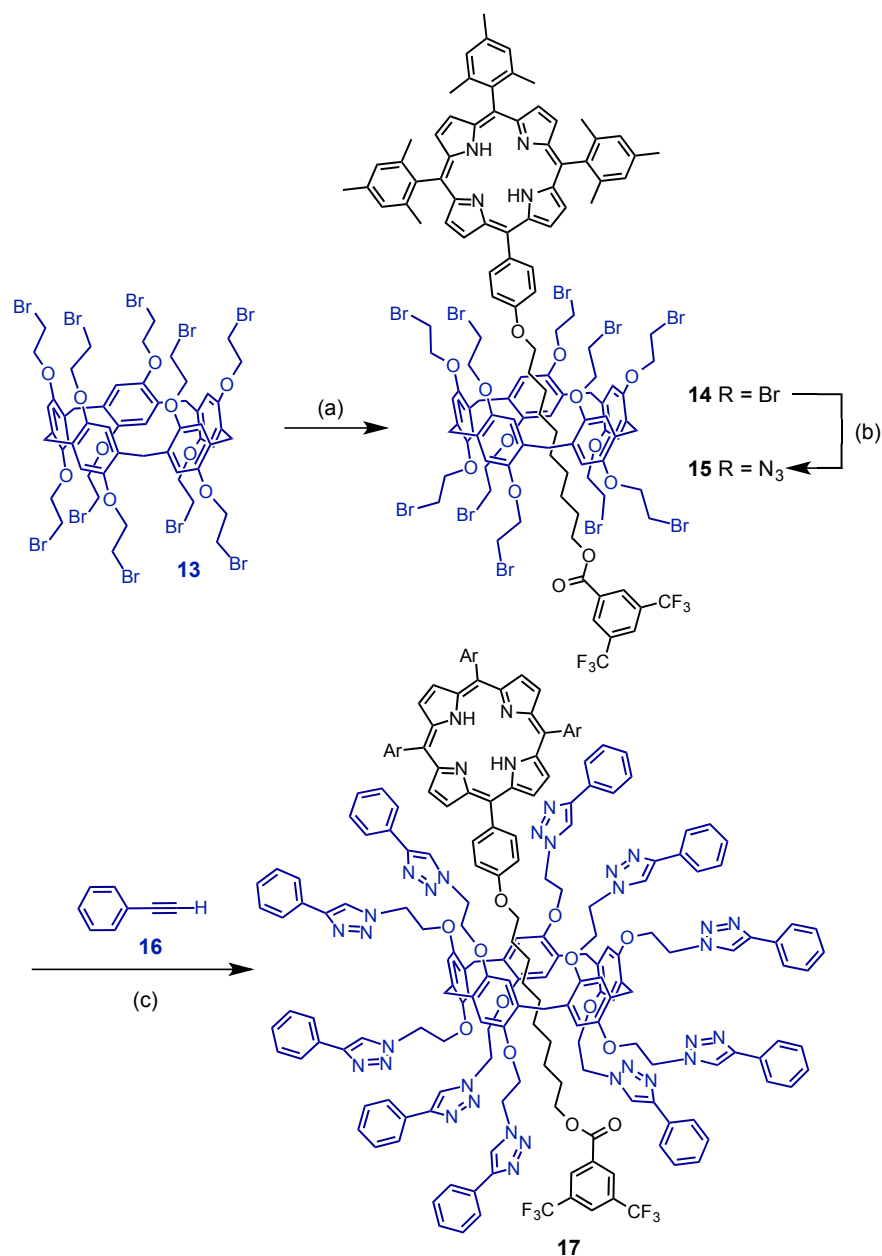
The condition reactions used for the preparation of [2]rotaxane **9** from **7** were then applied to pillar[5]arene **11** decorated with ten peripheral Zn(II)-porphyrin groups (Scheme 2).



Scheme 2. Attempted preparation of compound **12** from Zn(II)-porphyrin-substituted pillar[5]arene **11**. *Reagents and conditions:* (a) **6**, **8**, CHCl_3 , Et_3N , -15°C to rt.

Reaction of **6** and **8** was carried out in CHCl_3 in the presence of pillar[5]arene **11**. The expected [2]rotaxane (**12**) was however not formed under these conditions and axle **10** was the only product of the reaction. Indeed, it appears that steric effects resulting from the presence of the bulky peripheral groups on the pillar[5]arene building block prevent the acylation of the pseudorotaxane intermediate. Actually, it is well known that the size of the peripheral groups on both rims of the pillar[5]arene building blocks are affecting the outcome of such reactions.¹¹ When their size is increased, the reaction of the pseudo-rotaxane intermediate is slower due to steric effects and the unthreaded axle is consumed faster. As a result, the equilibrium is progressively displaced in favor of the unthreaded intermediate thus contributing to increase the yield in axle while lowering the yield in [2]rotaxane. In the particular case of pillar[5]arene **11**, the peripheral groups are so large that the formation of the desired [2]rotaxanes is completely prevented.

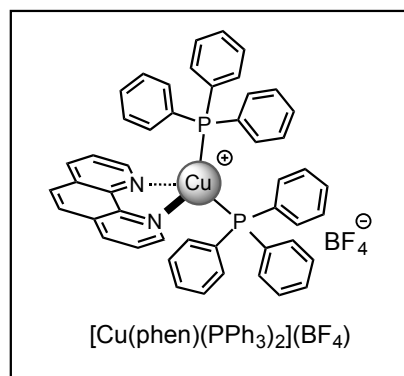
In order to achieve the preparation of compound **12**, it was decided to change the order of the different synthetic steps. Specifically, a clickable [2]rotaxane scaffold will be prepared first and the functionalization of its pillar[5]arene subunit will be achieved in the final step. With this idea in mind, clickable [5]rotaxane **15** was prepared in two steps from compounds **13** and **6** (Scheme 3).



Scheme 3. Preparation of compound **17**. *Reagents and conditions:* (a) **6**, **8**, CHCl₃, Et₃N, -15°C to rt (18%); (b) NaN₃, DMF, rt (90%); (c) [Cu(phen)(PPh₃)₂](BF₄), PhMe, rt (72%).

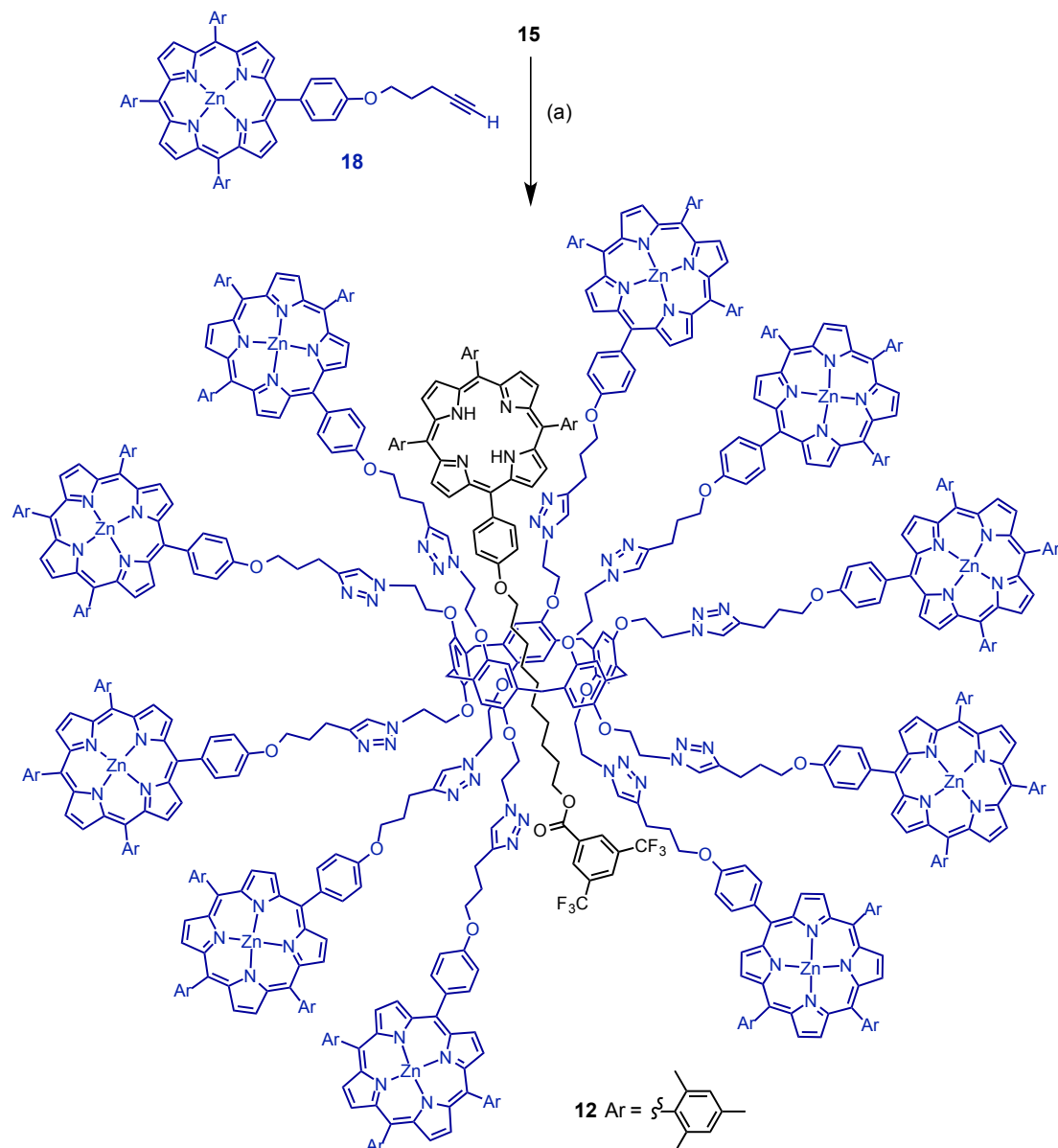
Treatment of **6** with benzoyl chloride **8** in the presence pillar[5]arene derivative **13** in CHCl_3 afforded compounds **14** and **10** in 18 and 78% yields, respectively. When compared to the preparation of [2]rotaxane **9** from 1,4-diethoxypillar[5]arene (**7**), the increased size of the peripheral substituents of the macrocyclic reagent (**13**) significantly affect the yield in [2]rotaxane. Indeed, the reaction of pseudo-rotaxane intermediate **6**⊂**13** becomes slower due to steric effects and uncomplexed **6** is consumed faster.¹¹ As a consequence, the formation of dumbbell **10** is favored thus contributing to lower the yield in [2]rotaxane.

Reaction of decabromide **14** with an excess of sodium azide (13 equiv.) in DMF at room temperature gave decaazide **15** in 90% yield. The reaction conditions for the copper-catalyzed alkyne-azide 1,3-dipolar cycloaddition (CuAAC) of compound **15** with terminal alkynes were first adjusted with phenylacetylene (**16**) (Scheme 3). Indeed, one can anticipate that the free-base porphyrin moiety of **15** will be likely metalated by the copper catalyst used for the CuAAC reactions.¹² This was effectively the case when the reaction was performed with $\text{CuSO}_4 \cdot 5\text{H}_2\text{O}$ /ascorbic acid or $[\text{Cu}(\text{CH}_3\text{CN})_4](\text{BF}_4)$ as catalyst. Gryko and co-workers have however shown that CuAAC reactions are possible without metalation of free-base porphyrin building blocks by using $[\text{Cu}(\text{phen})(\text{PPh}_3)_2]^+$ as catalyst (phen = 1,10-phenanthroline).¹² Under these conditions, we found that it was possible to prepare **17** from building block **15** and phenylacetylene (**16**) and the formation of Cu(II)-



porphyrin byproducts was effectively not observed. This can be explained by the high affinity of phen and PPh_3 for copper(I).¹³ Moreover, the remarkable stabilization of Cu(I) by these ligands also prevents the formation of Cu(II) species capable of metalating porphyrin moieties. Even if thermodynamically stable, it can be noted that the speciation of cuprous complexes such as $[\text{Cu}(\text{phen})(\text{PPh}_3)_2]^+$ is hard to control in solution and traces of $[\text{Cu}(\text{phen})(\text{PPh}_3)_2]^+$ are always present even in non-coordinating solvents.¹³⁻¹⁴ The latter Cu(I) complex is unsaturated and therefore most likely the catalytic species for the CuAAC reaction.

The reaction conditions used for the preparation of **17** from phenylacetylene and **15** were then applied to terminal alkyne **18** (Scheme 4). The clicked derivative **12** combining ten Zn(II)-porphyrin moieties with one free-base porphyrin unit was thus obtained in 60% yield.



Scheme 4. Preparation of compound **12**. *Reagents and conditions:* (a)

[Cu(phen)(PPh₃)₂](BF₄), PhMe, rt (60%).

The structure of [2]rotaxane **12** was confirmed by mass spectrometry (Figure 2). The MALDI-TOF of **12** is characterized by a singly charged peak at m/z 11320.7 and a doubly charged ion peak at m/z 5659.8 which can be assigned to $[MH]^+$ and $[MH_2]^{2+}$, respectively. Fragmentation is quite limited but typical fragments resulting from retro-click reactions are observed. Importantly, no peak corresponding to the Cu(II) analogue of **12** could be detected

thus showing that the free-base porphyrin was effectively not metalated during the CuAAC reaction.

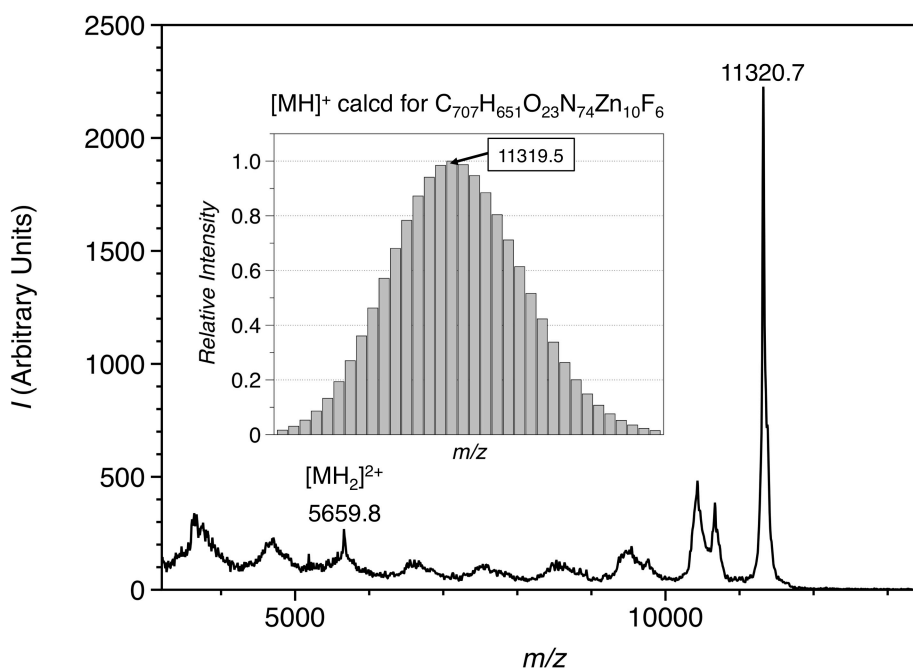


Figure 2. MALDI-TOF mass spectrum of compound **12**. Inset: calculated isotopic pattern for the pseudomolecular ion peak $[MH]^+$ ($C_{707}H_{651}O_{23}N_{74}Zn_{10}F_6$).

As observed for its constitutive pillar[5]arene subunit, *i.e.* pillar[5]arene derivative **11**, the 1H NMR spectrum of [2]rotaxane **12** is broad at room temperature due to partial intramolecular coordination of Zn(II)-porphyrin subunits by 1,2,3-triazole moieties. This prompted us to record the 1H NMR spectra of **12** at different temperatures (Figure 3). A perfectly reversible narrowing of all the signals was observed and the spectrum recorded at 100°C is sharp and well resolved. Owing to the unsymmetrical substitution of its axle component, [2]rotaxane **12** is C_5 symmetrical and the two rims of its pillar[5]arene moiety are not equivalent. Accordingly, two sets of signals are observed for the peripheral Zn(II)-porphyrin subunits. Two resonances are also observed at $\delta = 6.93$ and 6.80 ppm for the aromatic protons of the pillar[5]arene core (H- α and H- α'). Diagnostic signals of the free-base porphyrin stopper are also clearly distinguished. In particular, two AB systems are observed for the β -pyrrolic protons (H-11/12 and H-14/15). When compared to axle **10**, these signals are significantly shifted ($\Delta\delta = 0.3$ to 0.8 ppm) due to the presence of the surrounding Zn(II)-porphyrin subunits in **12**.

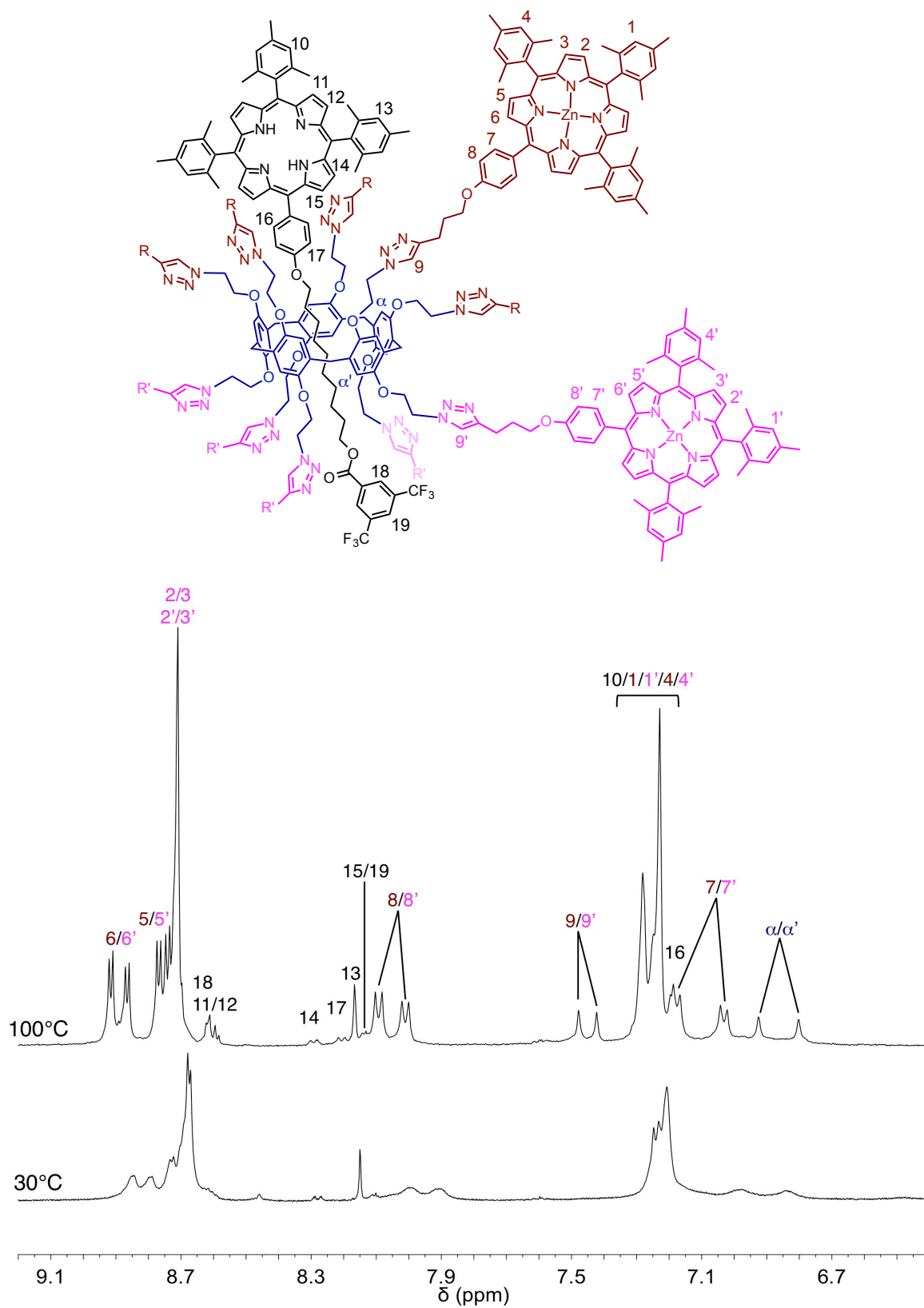


Figure 3. Aromatic region of ¹H NMR spectra (400 MHz, CDCl₂CDCl₂) of compound **12** recorded at different temperature.

4.3. Electronic properties

The ground state absorption spectra of [2]rotaxane **12** and its model compounds **9** and **11** recorded in toluene are shown in Figure 4.

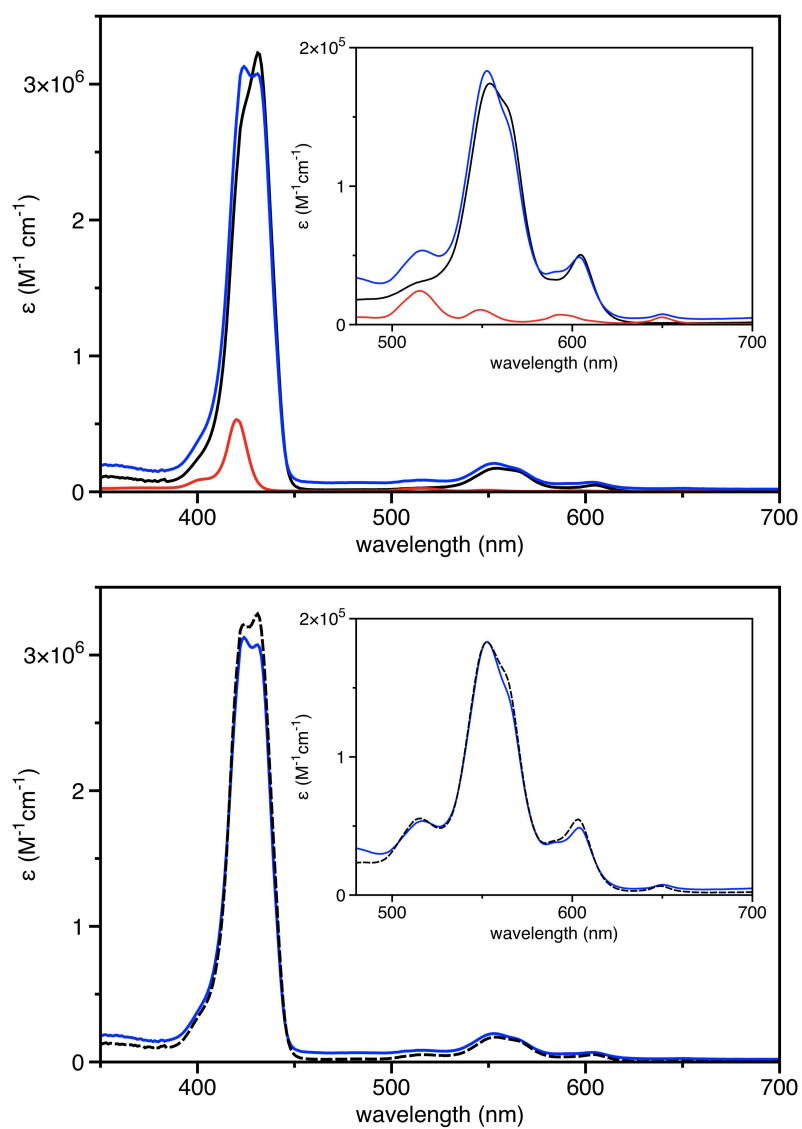


Figure 4. Top: absorption spectra of compounds **9** (red), **11** (black) and **12** (blue) recorded in toluene at 25°C. Bottom: comparison of the absorption spectrum of compound **12** (blue) with the calculated spectrum of its constitutive subunits (**9** + **11**, dotted black line).

Owing to intramolecular interactions of 1,2,3-triazole moieties with neighboring Zn(II)-porphyrin subunits, the absorption bands of multi-Zn(II)-porphyrin array **11** are broadened and red-shifted when compared to those typically observed for a Zn(II) *meso*-tetraphenylporphyrin derivative. In contrast, the absorption spectrum of model compound **9** is typical of a free-base *meso*-tetraphenylporphyrin.¹⁵ The maximum of the Soret band, corresponding to the transition to the second singlet excited state, is located at 419 nm ($\epsilon = 503\,800\text{ M}^{-1}\text{ cm}^{-1}$) in toluene. The presence of four Q bands at 515, 550, 592 and 648 nm is a diagnostic signature of a free-base porphyrin. The relative intensity of the Q bands is also typical of a porphyrin with occupied *meso*-positions (*phyllo-type* spectrum).¹⁶

The spectrum of [2]rotaxane **12** is dominated by the absorption features of its macrocyclic component bearing ten peripheral Zn(II)-porphyrin groups. Typical signatures of the free-base porphyrin unit of its axle component are however clearly detected, in particular in the 500-700 nm region. Absorption maxima corresponding to Q bands of a free-base porphyrin moiety are effectively observed at 517, 591 and 649 nm. The absorption spectrum of **12** coincides within the experimental error with the profile obtained by summation of the spectra of its component subunits (**9** and **11**) thus showing limited ground state interactions of the free-base porphyrin unit with the peripheral Zn(II)-porphyrin moieties.

Emission spectra recorded in toluene for compounds **9**, **11** and **12** are depicted in Figure 5. Upon excitation of **12** at 425 nm, more than 90% of the light is absorbed by the peripheral Zn(II)-porphyrin moieties. The intensity of the Zn(II)-porphyrin centered fluorescence in **12** is however significantly reduced when compared to **11** while, at the same time, the emission arising from the free-base porphyrin moiety is enhanced. Emission spectra of **11** and **12** recorded from solutions having the same optical density at the exciting wavelength (Figure 4B) shows that the Zn(II)-porphyrin centered fluorescence is quenched by about 75% in **12**. Notably, the intensity of the free-base-porphyrin emission is 5 times higher for **12** than that of model compound **9** when the emission spectra are recorded from solutions having the same concentration (Figure 5C). All these observations are consistent with the occurrence of a Zn(II)-porphyrin \rightarrow free-base porphyrin singlet energy transfer process *via* Förster mechanism.⁸ This energy transfer mechanism was further supported by the excitation spectra recorded for **12** (Figure 5A) at λ_{em} in the 650-750 nm region. In all the cases, the excitation spectra are similar to the absorption spectrum of **12** thus showing that the free-base

porphyrin centered fluorescence is also observed upon excitation of the Zn(II)-porphyrin moieties.

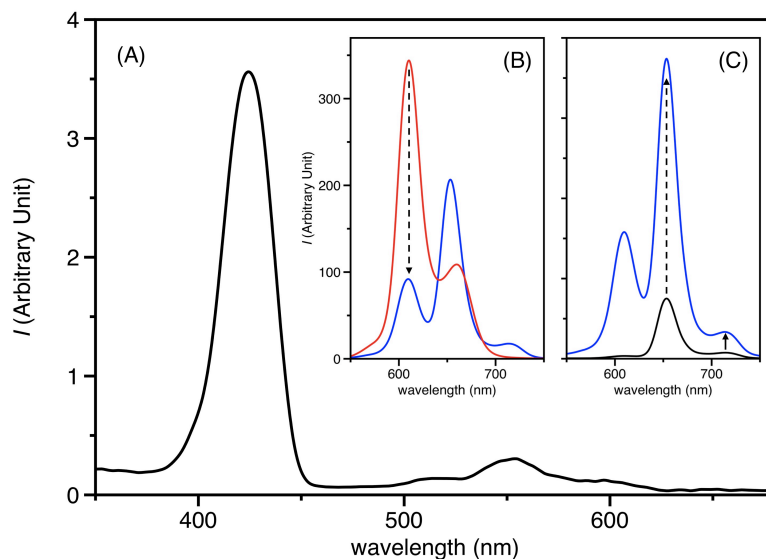


Figure 5. (A) Excitation spectrum recorded for compound **12** in toluene ($\lambda_{em} = 720$ nm). (B) Emission spectra of isoabsorbing solutions of compounds **11** (red) and **12** (blue) in toluene (25°C , $\lambda_{exc} = 425$ nm). (C) Emission spectra of compounds **9** (black) and **12** (blue) in toluene (25°C , $\lambda_{exc} = 425$ nm), the concentration of the two solutions are identical.

The steady-state properties of compounds **9**, **11** and **12** were also investigated in other solvents, namely CH_2Cl_2 and CHCl_3 . As observed in the case of compound **11** (see chapter 3) the shape of the absorption spectra of **12** is affected by the nature of the solvent and the amount of 1,2,3-triazole units coordinating Zn(II)-porphyrin moieties within **12** is not exactly the same in the different solvents. The emission spectra recorded for **12** in CH_2Cl_2 and CHCl_3 are shown in Figure 6. The results are indeed similar to those described in toluene. However, it can be noted that the spectra recorded from isoabsorbing solutions of **11** and **12** reveal that the Zn(II)-porphyrin centered fluorescence in **12** is quenched by about 70 and 58% in CH_2Cl_2 and CHCl_3 , respectively, while a quenching of 75% was observed in toluene. This difference is ascribed to the changes in the coordinated/uncoordinated Zn(II)-porphyrin ratio in **12** as a function of the solvent. In toluene, intramolecular coordination is favored and the molecules adopt on average a more folded conformation. As a result the Zn(II)-porphyrins are closer to the free-base porphyrin and the energy transfer more efficient. In contrast, in CHCl_3 , the

dynamic conformational equilibrium is in favor of a more extended conformation. The average distance between the donor units and the acceptor is thus larger and the energy transfer becomes less efficient in this solvent.

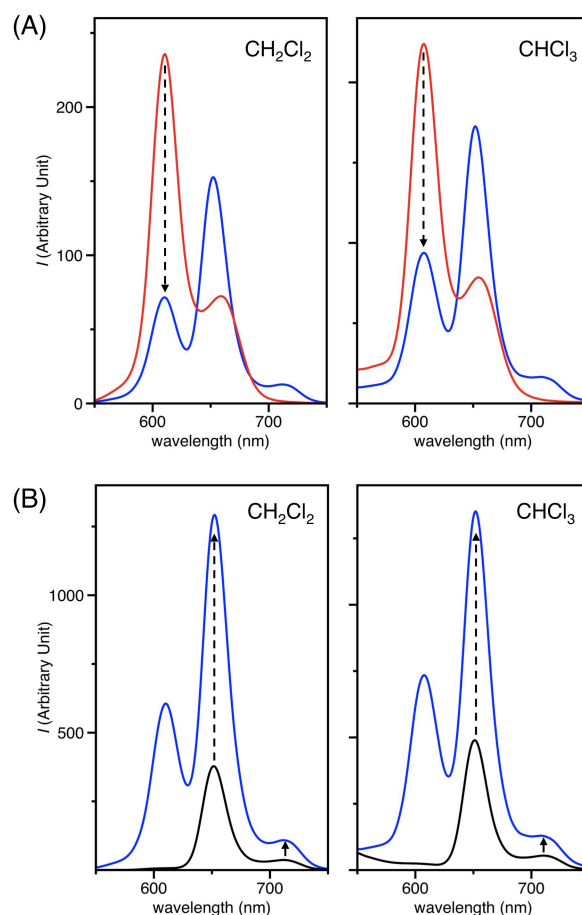


Figure 6. (A) Emission spectra of isoabsorbing solutions of compounds **11** (red) and **12** (blue) in CH₂Cl₂ and CHCl₃ (25°C, $\lambda_{\text{exc}} = 425$ nm). (B) Emission spectra of compounds **9** (black) and **12** (blue) recorded in CH₂Cl₂ and CHCl₃, the two solutions are at the same concentration in both solvents (25°C, $\lambda_{\text{exc}} = 425$ nm).

4.4. Conclusion

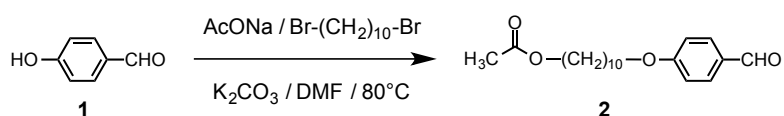
A clickable [2]rotaxane scaffold incorporating a free-base porphyrin stopper has been prepared and functionalized with ten peripheral Zn(II)-porphyrin moieties. This final step has been successfully achieved owing to the use of an appropriate copper(I) catalyst for which the unwanted insertion of copper into the free-base porphyrin stopper of the [2]rotaxane building block does not take place. The final [2]rotaxane combining Zn(II) and free-base porphyrin

moieties is a sophisticated photoactive molecular device. Steady state investigations have effectively shown that this compound is a light-harvesting device capable of channeling the light energy from the peripheral Zn(II)-porphyrin subunits to the core by singlet-singlet energy transfer.

4.5. Experimental section

General methods. Reagents were purchased as reagent grade and used without further purification. Compounds **7**,¹⁷ **13**,^{2a} and [Cu(phen)(PPh₃)₂](BF₄)¹³ were prepared according to previously reported procedures. Acetonitrile (CH₃CN) and dichloromethane (CH₂Cl₂) were distilled over CaH₂ under Ar. All reactions were performed in standard glassware under an inert Ar atmosphere. Evaporation and concentration were done at water aspirator pressure and drying in vacuo at 10⁻² Torr. Column chromatography: silica gel 60 (230-400 mesh, 0.040-0.063 mm) was purchased from E. Merck. Thin Layer Chromatography (TLC) was performed on aluminum sheets coated with silica gel 60 F₂₅₄ purchased from E. Merck. NMR spectra were recorded with a Bruker AC 300 or AC 400 spectrometer with solvent peaks as reference. The ¹H signals were assigned by 2D experiments (COSY and NOESY). IR spectra (cm⁻¹) were recorded with a Perkin–Elmer Spectrum One spectrophotometer. MALDI-TOF mass spectra were carried out by the analytical service of the School of Chemistry (Strasbourg, France). Elemental analyses were performed by the analytical service of the Chemistry Department of the University of Strasbourg (France). The steady-state measurements have been carried out by Matthieu Chesse.

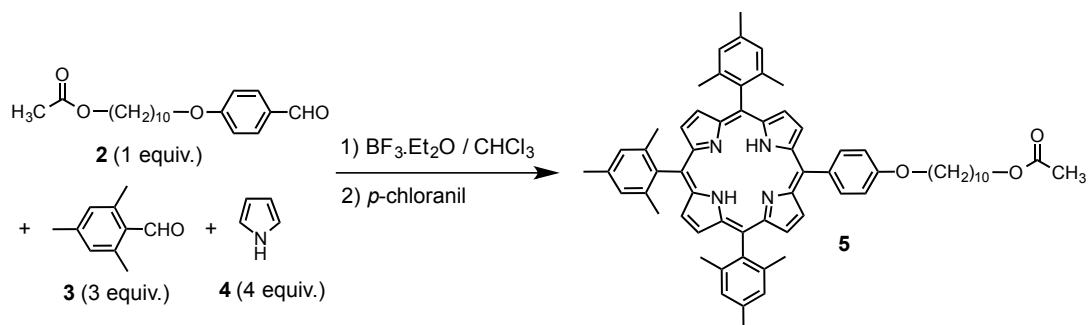
Compound 2



A mixture of 1,10-Dibromodecane (8.00 g, 26.7 mmol), **1** (3.26 g, 26.7 mmol), K₂CO₃ (3.68 g, 26.7 mmol) and sodium acetate (2.19 g, 26.7 mmol) in dry DMF (50 mL) was heated at 60 °C for 5 days. The resulting mixture was cooled to room temperature and diluted with Et₂O. The organic layer was washed with water, dried (MgSO₄), filtered and concentrated. Column chromatography (SiO₂, cyclohexane/AcOEt 9:1) gave **2** (3.28 g, 38%) as a colourless glassy product. IR (neat): $\nu = 1737$ (C=O), 1693 (C=O) cm⁻¹. ¹H NMR (400 MHz, CDCl₃): $\delta = 9.88$ (s, 1H), 7.82 (d, $J = 9$ Hz, 2H), 6.98 (d, $J = 9$ Hz, 2H), 4.05 (t, $J = 7$ Hz, 2H), 4.03 (t, $J = 6.5$ Hz, 2H), 2.04 (s, 3H), 1.81 (m, 2H), 1.61 (m, 2H), 1.46 (m, 2H), 1.31 (m, 10H) ppm.

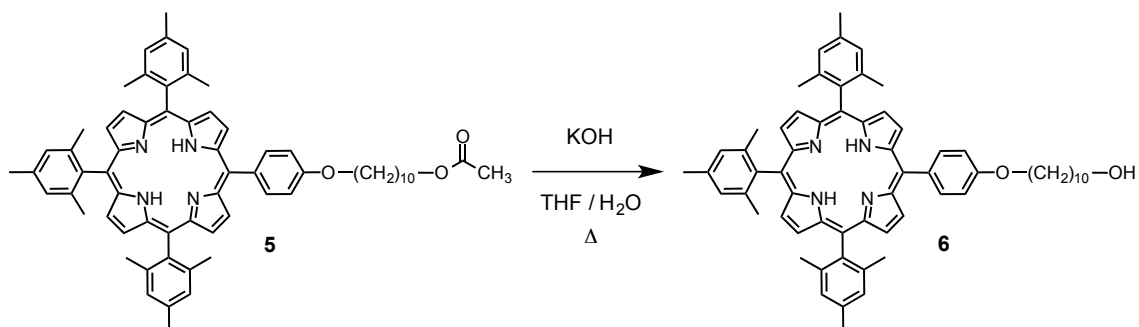
^{13}C NMR (100 MHz, CDCl_3): $\delta = 190.9, 171.4, 164.4, 132.1, 129.9, 114.9, 68.6, 64.8, 29.6, 29.5, 29.4, 29.3, 29.2, 28.7, 26.1, 26.0, 21.2$ ppm.

Compound 5

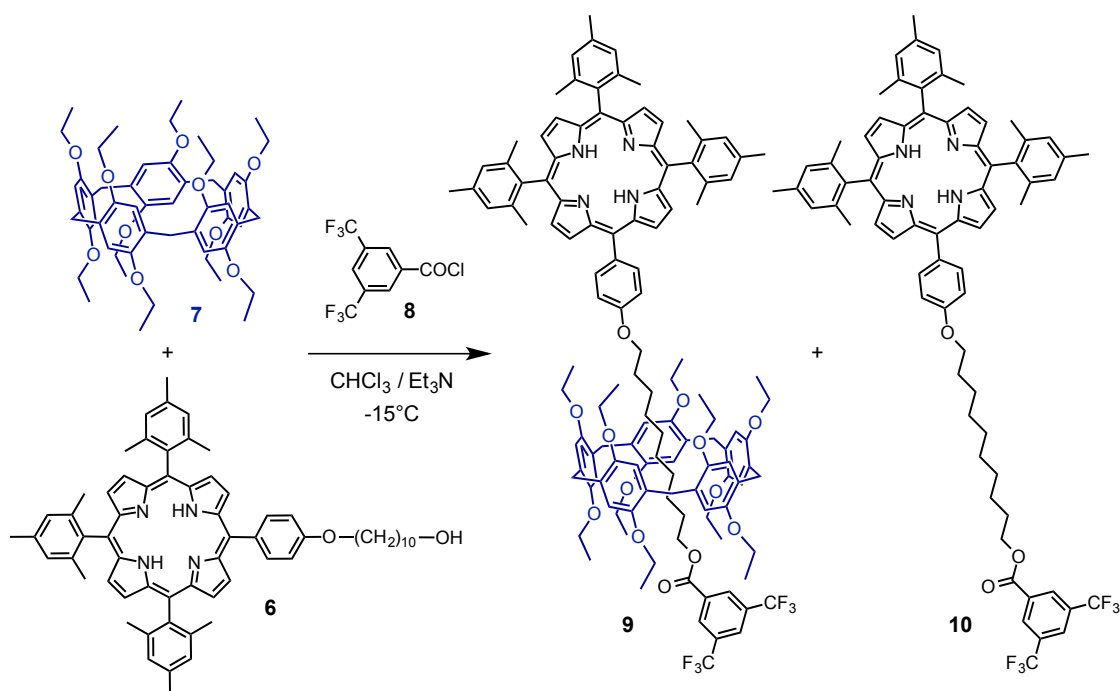


$\text{BF}_3 \cdot \text{OEt}_2$ (0.130 mL, 1.04 mmol) was added to a solution of **2** (1.0 g, 3.12 mmol), **3** (1.3 mL, 9.36 mmol) and **4** (0.8 mL, 12.6 mmol) in CHCl_3 (containing 0.75% EtOH, 400 mL) at room temperature under argon. After 3 h, *p*-chloranil (1.16 g, 4.74 mmol) was added. After 2 h, triethylamine (0.5 mL) was added. The resulting mixture was filtered (Si_2O , CH_2Cl_2) and concentrated. Column chromatography (SiO_2 , $\text{CH}_2\text{Cl}_2/\text{cyclohexane}/\text{PhMe}$, 25:25:2) gave **5** as a purple solid (0.4 g, 13%). IR (neat): $\nu = 1741 \text{ cm}^{-1}$ (C=O). UV-Vis (CH_2Cl_2): λ_{max} (ϵ) = 419 (453100), 515 (19130), 550 (7291), 593 (5399), 648 nm (3575 $\text{M}^{-1} \text{ cm}^{-1}$). ^1H NMR (400 MHz, CD_2Cl_2): $\delta = 8.84$ (d, $J = 5$ Hz, 2H), 8.66 (d, $J = 5$ Hz, 2H), 8.63 (s, 4H), 8.12 (d, $J = 8$ Hz, 2H), 7.30 (s, 8H), 4.26 (t, $J = 6$ Hz, 2H), 4.05 (t, $J = 6$ Hz, 2H), 2.62 (s, 9H), 2.03 (s, 3H), 1.98 (m, 2H), 1.85 (s, 18H), 1.65 (m, 4H), 1.28 (m, 10H), -2.58 (s, 2H) ppm. ^{13}C NMR (100 MHz, CDCl_3): $\delta = 170.9, 159.1, 139.3, 139.2, 138.3, 138.0, 137.9, 137.8, 135.4, 134.0, 128.9, 128.1, 127.7, 125.2, 119.3, 117.7, 117.4, 112.7, 68.3, 64.5, 29.5$ (2 peaks), 29.4, 29.3, 28.6, 26.1, 25.9, 21.3 (2 peaks), 21.1, 20.7 ppm. MALDI-TOF-MS: 955.46 ($[\text{M}+\text{H}]^+$, calcd. for $\text{C}_{65}\text{H}_{70}\text{N}_4\text{O}_3$: 954.54). Elem. Anal. Calcd. for $\text{C}_{63}\text{H}_{68}\text{N}_4\text{O}_2 \cdot \text{H}_2\text{O}$: C 80.21; H 7.45; N 5.75. Found: C 80.28; H 7.52; N 5.53.

Compound 6



A mixture of **5** (622 mg, 0.651 mmol) and KOH (292 mg, 5.21 mmol) in THF/H₂O 2:1 (80 mL) was heated at 80°C for 12 h under Ar. THF was evaporated and the aqueous layer extracted with CH₂Cl₂ (2 x). The combined organic layers were washed with water, dried (Na₂SO₄), filtered and concentrated. Column chromatography (SiO₂, Cyclohexane/CH₂Cl₂/PhMe 30:20:4) gave **6** (570 mg, 97%) as a purple solid. IR (neat): $\nu = 3420 \text{ cm}^{-1}$ (OH). UV-Vis (CH₂Cl₂): λ_{max} (ϵ) = 419 (512400), 515 (21700), 550 (8080), 591 (5970), 648 nm (3950 M⁻¹ cm⁻¹). ¹H NMR (300 MHz, CD₂Cl₂): δ = 8.90 (d, J = 5 Hz, 2H), 8.72 (d, J = 5 Hz, 2H), 8.68 (s, 4H), 8.16 (d, J = 9 Hz, 2H), 7.33 (s, 8H), 4.26 (t, J = 6 Hz, 2H), 3.61 (t, J = 6 Hz, 2H), 2.64 (s, 9H), 1.98 (m, 2H), 1.92 (s, 6H), 1.90 (s, 12H) 1.69-1.44 (m, 12H), -2.51 (s, 2H) ppm. ¹³C NMR (75 MHz, CDCl₃): δ = 159.7, 139.8, 138.9, 138.6, 138.4, 128.2, 119.9, 118.3, 118.0, 113.3, 68.9, 63.4, 33.5, 30.2, 30.0, 27.5, 26.7, 26.3, 21.9, 21.8, 21.7 ppm. MALDI-TOF-MS: 912.69 (M⁺, calcd. for C₆₃H₆₈N₄O₂: 912.53). Elem. Anal. Calcd. for C₆₃H₆₈N₄O₂·(H₂O)_{0.5}: C 80.05; H 7.54; N 6.08. Found: C 82.11; H 7.56; N 6.18.

Compounds **9** and **10**

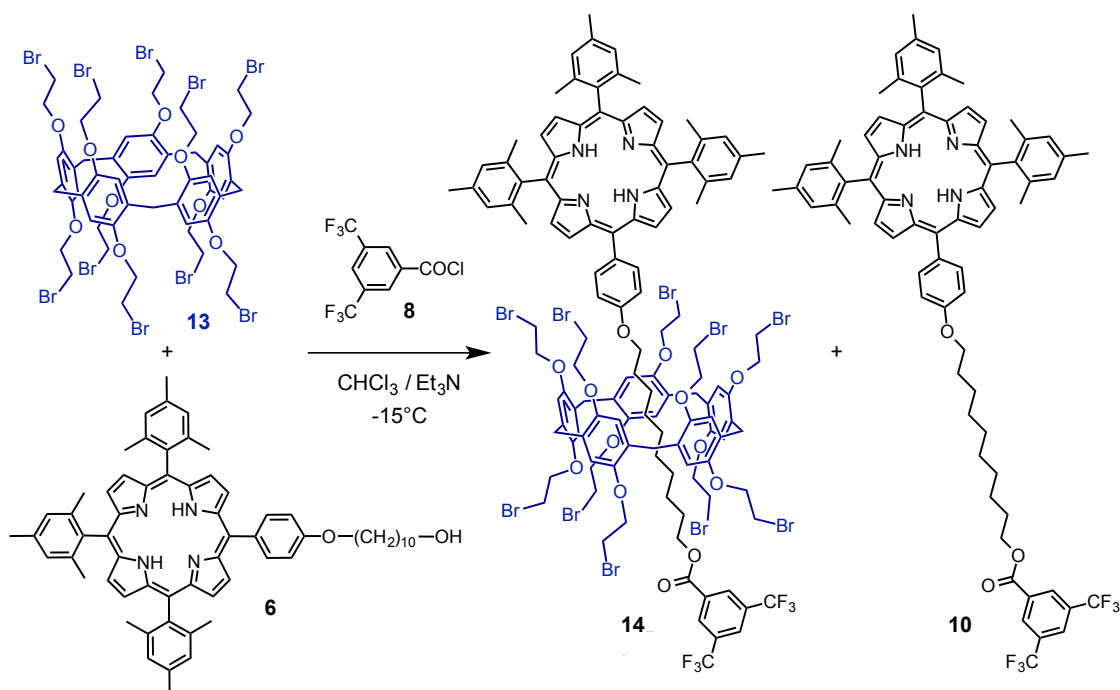
8 (42 μ L, 0.23 mmol) was added to a solution of **6** (108 mg, 0.12 mmol), **7** (206 mg, 0.23 mmol) and triethylamine (1 drop) in CHCl_3 (2 mL) at -15°C . After 30 min, the mixture was allowed to slowly warm to room temperature, then stirred for 12 h under Ar, filtered (SiO_2 , CH_2Cl_2) and evaporated. Column chromatography (SiO_2 , $\text{CH}_2\text{Cl}_2/\text{cyclohexane}$ 2:3) gave **9** (183 mg, 77%) and **10** (4 mg, 3%).

9. Purple solid. IR (neat): $\nu = 1731 \text{ cm}^{-1}(\text{C}=\text{O})$. UV-Vis (CH_2Cl_2): λ_{max} (ϵ) = 419 (503800), 515 (27501), 550 (14580), 592 (11680), 648 nm (9230 $\text{M}^{-1}\text{cm}^{-1}$). ^1H NMR (400MHz, CD_2Cl_2): $\delta = 8.90$ (d, $J = 5$ Hz, 2H), 8.74 (d, $J = 5$ Hz, 2H), 8.68 (s, 4H), 8.60 (s, 2H), 8.21 (d, $J = 9$ Hz, 3H), 7.34 (s, 6H), 7.30 (d, $J = 8$ Hz, 2H), 7.10 (s, 5H), 6.98 (s, 5H), 4.33 (t, $J = 7$ Hz, 2H), 4.19 (m, 5H), 4.01 (m, 15H), 3.84 (s, 10H), 3.09 (m, 2H), 2.66 (s, 9H), 1.91 (s, 18H), 1.55 (t, $J = 6$ Hz, 30H), 0.84 (m, 2H), 0.57 (m, 4H), 0.11 (m, 2H), -0.13 (m, 2H), -0.76 (m, 2H), -1.39 (m, 2H), -2.50 (s, 2H) ppm. ^{13}C NMR (75 MHz, CD_2Cl_2): $\delta = 164.1$, 160.0, 150.2, 150.1, 139.7, 138.4, 138.2, 135.6, 133.8, 133.2, 132.4 (q, $^2J_{\text{C-F}} = 34$ Hz), 130.0, 128.8, 128.7, 128.1, 126.7, 123.4 (q, $^1J_{\text{C-F}} = 272$ Hz), 120.0, 118.2, 117.8, 114.9, 114.4, 112.7, 69.1, 67.0, 64.1, 63.7, 31.0, 30.7, 30.2, 29.7, 29.5, 29.2, 28.8, 27.3, 26.3, 23.7, 21.6,

21.5, 15.8, 15.6 ppm. ^{19}F NMR (376 MHz, CD_2Cl_2): $\delta = -63.24$ ppm. MALDI-TOF-MS: 2044.6 (M^+ , calcd. for $\text{C}_{127}\text{H}_{140}\text{N}_4\text{O}_{13}\text{F}_6$: 2044.5). Elem. Anal. Calcd. for $\text{C}_{127}\text{H}_{140}\text{F}_6\text{N}_4\text{O}_{13}$ (2044.5): C 74.61; H 6.90; N 2.74. Found: C 74.69; H 7.11; N 2.69

10. Purple solid. IR (neat): $\nu = 1729$ cm^{-1} (C=O). UV-Vis (CH_2Cl_2): λ_{max} (ϵ) = 419 (536400), 515 (22800), 550 (7700), 593 (5410), 648 nm (3390 $\text{M}^{-1} \text{cm}^{-1}$). ^1H NMR (300MHz, CD_2Cl_2): $\delta = 8.88$ (d, 2H), 8.71 (d, 2H), 8.67 (s, 4H), 8.57 (s, 2H), 8.15 (br, 3H), 7.31 (br, 8H), 4.45 (t, $J = 7$ Hz, 2H), 4.26 (t, $J = 7$ Hz, 2H), 2.63 (s, 9H), 1.90 (s, 18H), 1.46 (br, 16H), -2.53 (s, 2H) ppm. ^{13}C NMR (75 MHz, CD_2Cl_2): $\delta = 164.3, 159.5, 139.7, 138.7, 138.2, 135.9, 134.5, 133.3, 132.3$ (q, $^2J_{\text{C,F}} = 34$ Hz), 130.2 (br), 128.1, 126.6, 125.3, 121.7, 119.8, 118.2, 113.1, 68.7, 66.8, 30.0, 29.9, 29.7, 29.0, 27.3, 26.6, 26.4, 21.8, 21.7, 21.5 ppm. ^{19}F NMR (376 MHz, CD_2Cl_2): $\delta = -63.2$ ppm. MALDI-TOF-MS: 1152.37 (M^+ , calcd. for $\text{C}_{72}\text{H}_{70}\text{N}_4\text{O}_3\text{F}_6$: 1152.53). Elemental analysis: (%) calcd for $\text{C}_{72}\text{H}_{70}\text{N}_4\text{O}_3\text{F}_6 \cdot (\text{H}_2\text{O})_2$ C 72.71, H 6.27, N 4.71; found C 72.82, H 6.19, N 4.74.

Compounds 10 and 14

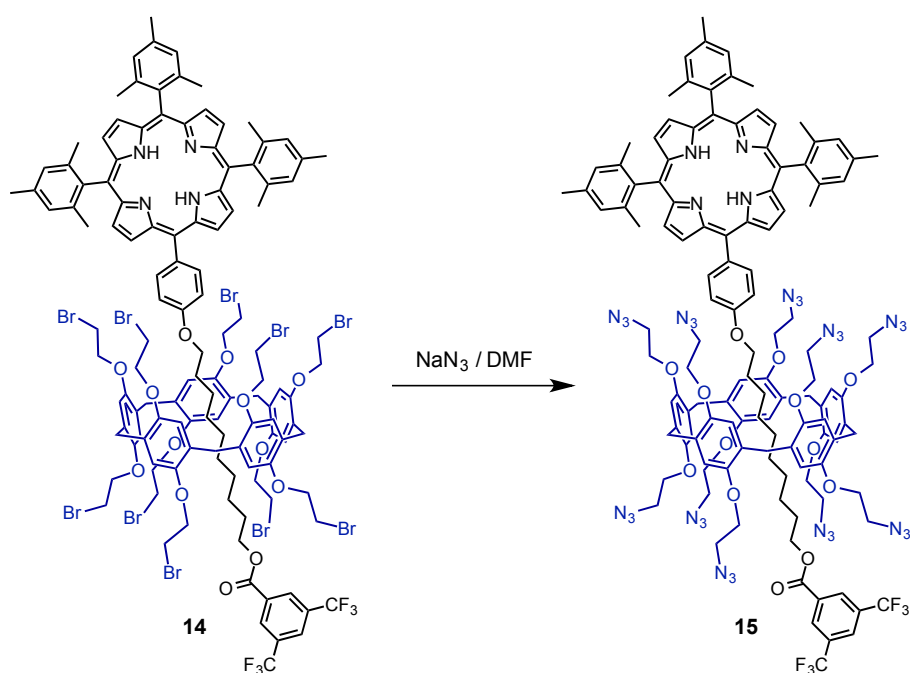


8 (90 mg, 0.329 mmol) was added to a solution of **6** (256 mg, 0.274 mmol), **13** (1.15 g, 0.687 mmol) and triethylamine (1 drop) in CHCl_3 (2 mL) at -15°C . After 30 mn, the

mixture was slowly warmed to room temperature (1 h), filtered (SiO_2 , CH_2Cl_2) and evaporated. Column chromatography (SiO_2 , $\text{CH}_2\text{Cl}_2/\text{cyclohexane}$ 2:3) gave **14** (142 mg, 18%) and **10** (230 mg, 72%).

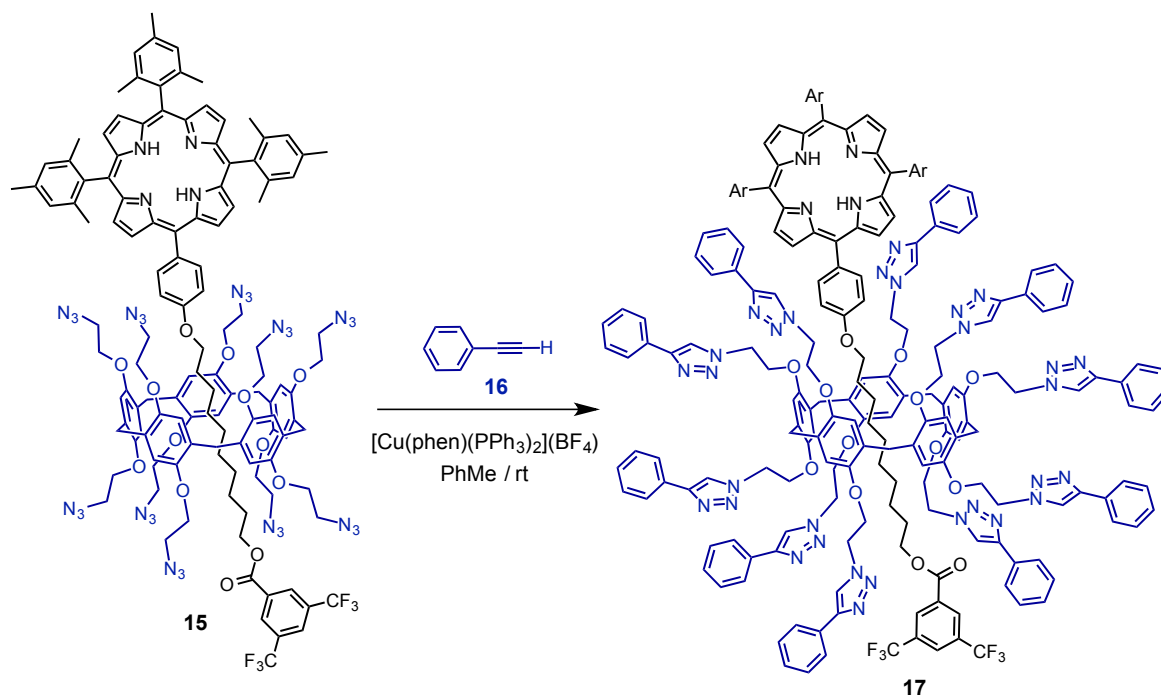
14. Purple solid. IR (neat): $\nu = 1726 \text{ cm}^{-1}(\text{C}=\text{O})$. UV-Vis (CH_2Cl_2): $\lambda_{\text{max}} (\epsilon) = 419$ (527390), 515 (22381), 550 (9069), 592 (6595), 647 nm (4472 $\text{M}^{-1} \text{cm}^{-1}$). ^1H NMR (300MHz, CD_2Cl_2): $\delta = 8.96$ (d, 2H), 8.75 (d, 2H), 8.67 (s, 4H), 8.63 (s, 2H), 8.25 (d, 2H), 8.19 (s, 1H), 7.35 (m, 8H), 7.19 (s, 5H), 7.10 (s, 5H), 4.45 (m, 10H), 4.29 (m, 12H), 3.93 (s, 10H), 3.79 (m, 20H), 3.37 (t, $J = 7 \text{ Hz}$, 2H), 2.64 (s, 9H), 1.90 (s, 18H), 1.44 (m, 2H), 0.49 (m, 2H), 0.28 (m, 6H), 0.04 (m, 2H), -0.73 (m, 2H), -2.51 (s, 2H) ppm. ^{13}C NMR (75 MHz, CD_2Cl_2): $\delta = 164.4$, 159.7, 150.2, 139.7, 138.7, 136.0, 134.3, 133.5, 132.3 (q, $^2J_{\text{C-F}} = 32 \text{ Hz}$), 130.3, 130.2, 129.6, 128.1, 126.7, 123.4 (q, $^1J_{\text{C-F}} = 274 \text{ Hz}$), 119.8, 118.2, 117.8, 116.2, 115.9, 113.0, 69.6, 69.5, 69.1, 67.3, 31.5, 31.2, 31.0, 30.7, 30.1, 30.0, 29.3, 29.2, 26.1, 24.7, 21.7, 21.6 ppm. ^{19}F NMR (376 MHz, CD_2Cl_2): $\delta = -63.03$ ppm. MALDI-TOF-MS: 2833.78 (M^+ , calcd. for $\text{C}_{127}\text{H}_{130}\text{N}_4\text{O}_{13}\text{F}_6\text{Br}_{10}$: 2833.46). Elemental analysis: (%) calcd for $\text{C}_{127}\text{H}_{130}\text{N}_4\text{O}_{13}\text{F}_6\text{Br}_{10}\cdot\text{H}_2\text{O}$: C 53.49, H 4.66, N 1.96; found C 53.29, H 4.71, N 1.99.

Compound 15



A mixture of **14** (126 mg, 0.04 mmol) and NaN_3 (35 mg, 0.53 mmol) in DMF (8 mL) was stirred for 12 hours at room temperature under Argon, then H_2O was added. The aqueous layer was extracted with Et_2O (3 x). The combined organic layers were washed with water and dried (Na_2SO_4), filtered and concentrated. Column chromatography (SiO_2 , CH_2Cl_2) gave **15** (98 mg, 90%) as a purple solid. IR (neat): $\nu = 2092 \text{ cm}^{-1}$ (N_3). ^1H NMR (400MHz, CD_2Cl_2): $\delta = 8.88$ (d, $J = 4$ Hz, 2H), 8.72 (d, $J = 4$ Hz, 2H), 8.65 (s, 4H), 8.59 (s, 2H), 8.25 (d, $J = 8$ Hz, 2H), 8.18 (s, 1H), 7.32 (m, 8H), 7.11 (s, 5H), 7.04 (s, 5H), 4.28 (m, 5H), 4.14 (m, 18H), 3.90 (s, 10H), 3.74 (m, 20H), 3.42 (m, 2H), 2.64 (m, 9H), 1.88 (s, 18H), 0.89 (m, 2H), 0.47 (m, 2H), 0.21 (m, 2H), 0.03 (m, 6H), -0.30 (m, 2H), -0.49 (m, 2H), -2.53 (s, 2H) ppm.

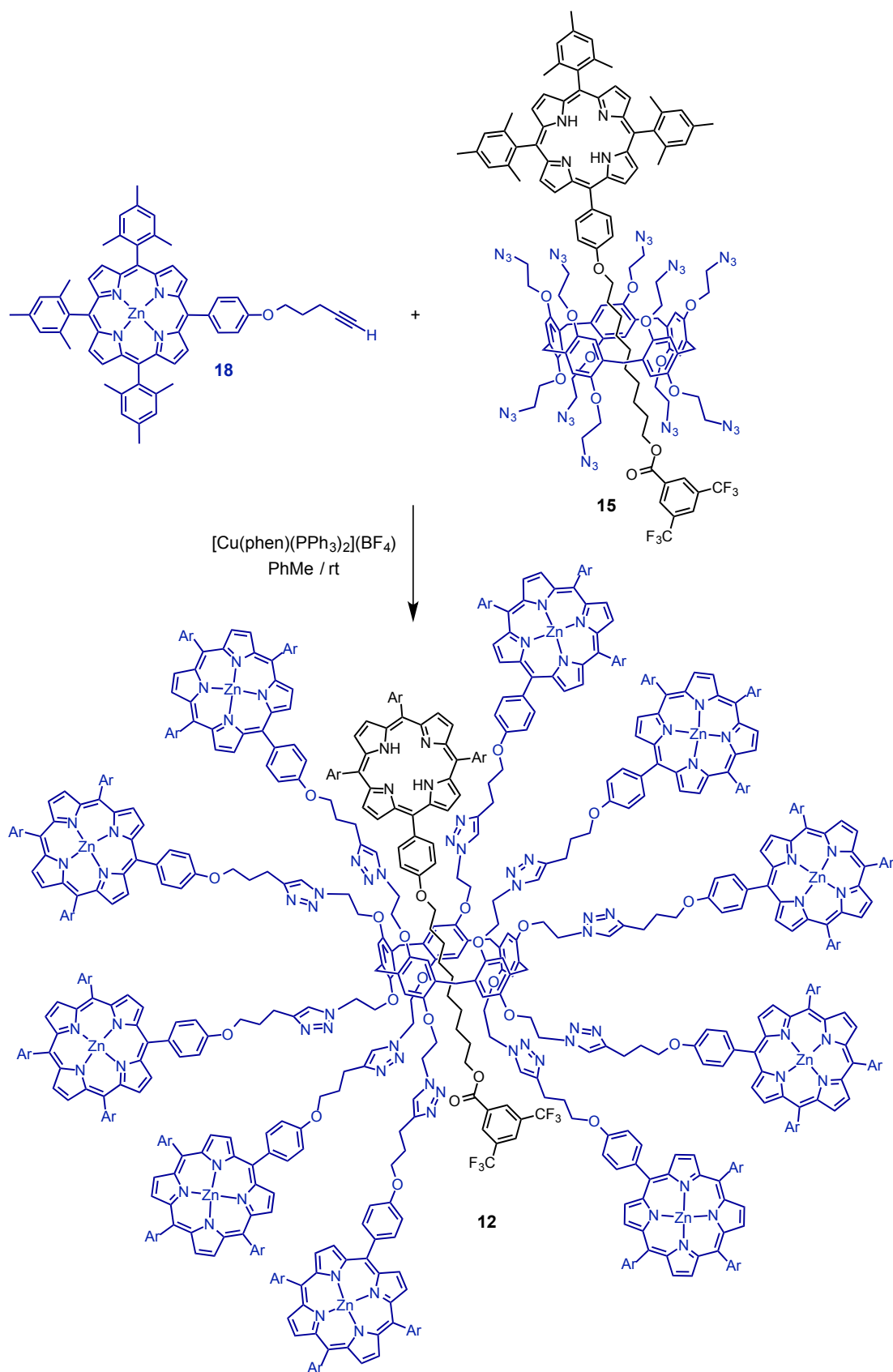
Compound 17



A mixture of **16** (20 μL , 0.23 mmol), **15** (49 mg, 0.02 mmol) and $[\text{Cu}(\text{phen})(\text{PPh}_3)_2](\text{BF}_4)$ (1.7 mg, 0.002 mmol) in toluene (1 mL) was stirred at room temperature for 7 days under argon and evaporated. Column chromatography (SiO_2 , CH_2Cl_2) gave **17** (50 mg, 72%) as a purple solid. IR (neat): $\nu = 1725 \text{ cm}^{-1}$ ($\text{C}=\text{O}$). UV-Vis (CH_2Cl_2): λ_{max} (ϵ) = 420 (450000), 517 (13279), 547 (6878), 590 (2102), 650 nm ($1368 \text{ M}^{-1} \text{ cm}^{-1}$). ^1H NMR (400 MHz, CD_2Cl_2): $\delta = 8.88$ (d, $J = 5$ Hz, 2H), 8.62 (m, 6H), 8.52 (s, 2H), 8.09 (d, $J = 8$ Hz, 2H), 8.04 (s, 1H), 7.93 (s, 6H), 7.81 (m, 18H), 7.61 (d, $J = 6$ Hz, 10H), 7.40 (t, $J = 7$

Hz, 12H), 7.32 (t, $J = 7$ Hz, 10H), 7.22 (s, 2H), 7.06 (m, 20H), 6.79 (s, 5H), 6.68 (s, 5H), 4.79 (m, 10H), 4.69(m, 5H), 4.56 (m, 5H), 4.36(m, 5H), 4.20 (m, 20H), 3.41(m, 10H), 2.61 (m, 9H), 1.87 (d, $J = 10$ Hz, 12H), 1.80 (s, 6H), 1.33 (m, 2H), 0.45(m, 2H), -0.03(m, 6H), -0.38 (m, 2H), -0.52 (m, 2H), -0.98 (m, 2H), -2.50(s, 2H) ppm. ^{13}C NMR (100 MHz, CD_2Cl_2): $\delta =$ 163.9, 159.0, 149.6 (2 peaks), 147.6, 139.3, 139.2, 139.1, 138.2, 138.0, 137.8 (2 peaks), 135.9, 133.7, 132.9, 131.6 (q, $^2J_{\text{C-F}} = 33$ Hz), 130.8, 130.6, 129.7, 128.9, 128.7, 128.1, 127.8, 127.7, 126.1, 123.0 (q, $^1J_{\text{C-F}} = 272$ Hz), 120.3, 120.1, 119.2, 117.9, 117.5, 115.7, 115.2, 112.6, 68.3, 67.5, 67.2, 66.6, 50.4 (2 peaks), 31.9, 31.1, 29.9, 29.6, 29.4, 29.3, 29.2, 28.8, 28.6, 27.8, 25.4, 24.2, 22.6, 21.3, 21.1 ppm. ^{19}F NMR (376 MHz, CD_2Cl_2): $\delta = -63.08$ ppm. MALDI-TOF-MS: 3474.1 ($[\text{M-H}]^+$, calcd. for $\text{C}_{207}\text{H}_{190}\text{N}_4\text{O}_{13}\text{F}_6$: 3475.9.5). Elem. Anal. Calcd. for $\text{C}_{207}\text{H}_{190}\text{F}_6\text{N}_4\text{O}_{13}\cdot\text{H}_2\text{O}$ (3493.96): C 71.16; H 5.53; N 13.63. Found: C 71.19; H 5.78; N 12.82.

Compound 12



A mixture of **18** (211 mg, 0.23 mmol), **15** (49 mg, 0.02 mmol) and [Cu(phen)(PPh₃)₂](BF₄) (1.7 mg, 0.002 mmol) in toluene (2.5 mL) was stirred at room temperature for 4 days under argon and evaporated. Column chromatography (SiO₂, CH₂Cl₂/cyclohexane 8:2) gave **12** (136 mg, 60%) as a purple solid. IR (neat): $\nu = 1725 \text{ cm}^{-1}$ (C=O). UV-Vis (CH₂Cl₂): λ_{max} (ϵ) = 421 (2640800), 432 (2128600), 517 (41960), 551 (150600), 605 nm (35920 M⁻¹ cm⁻¹). ¹H NMR (400MHz, C₂D₂Cl₄): $\delta = 8.91$ (d, $J = 4$ Hz, 10H), 8.90 (d, $J = 4$ Hz, 10H), 8.70 (bs, 55H), 8.60 (m, 5H), 8.16 (s, 5H), 8.08 (d, $J = 8$ Hz, 10H), 8.00 (d, $J = 8$ Hz, 10H), 7.42 (d, $J = 22$ Hz, 10H), 7.22 (bs, 72H), 7.01 (d, $J = 9$ Hz, 10H), 6.87 (s, 5H), 6.75 (s, 5H), 4.47 (m, 38H), 4.09 (m, 10H), 3.87 (m, 10H), 3.19 (m, 6H), 2.55 (bs, 90H), 1.88 (bs, 180H), 0.45 (m, 4H), 0.08 (m, 4H), -0.07 (m, 4H), -0.39 (m, 2H), -0.62 (m, 2H), -2.25 (s, 2H) ppm. ¹³C NMR (100 MHz, CD₂Cl₂): $\delta = 163.9, 158.6, 157.9$ (2 peaks), 151.4, 149.9, 149.7, 149.5, 148.6, 145.6, 139.3, 139.1, 139.0, 138.1, 137.8, 135.8, 132.7, 132.1, 131.8, 130.0, 129.5, 129.1, 128.5, 128.3, 127.4, 125.4, 126.4, 124.7, 124.2, 121.5 (q, ¹J_{C-F} = 272 Hz), 119.9, 119.3, 118.3, 118.0, 112.2, 66.2 (br), 49.1, 34.1, 33.6, 31.9, 31.1, 31.0, 30.0, 29.7, 29.3, 29.1, 28.0, 27.6, 26.9, 23.0, 22.7, 21.4, 21.0, 20.9, 20.8, 13.9 ppm. ¹⁹F NMR (376 MHz, CD₂Cl₂): $\delta = -62.95$ ppm. MALDI-TOF-MS: 11320.66 ([M+H]⁺, calcd. for C₇₀₇H₆₅₁N₇₄O₂₃Zn₁₀F₆: 11319.5). Elem. Anal. Calcd. for C₇₀₇H₆₅₀N₇₄O₂₃Zn₁₀F₆ (11319): C 75.02; H 5.87; N 9.15. Found: C 74.34; H 6.29; N 8.23.

References

- 1) a) J. Iehl, J. F. Nierengarten, *Chem. Eur. J.* **2009**, *15*, 7306; b) J. Iehl, J.-F. Nierengarten, A. Harriman, T. Bura, R. Ziessel, *J. Am. Chem. Soc.* **2012**, *134*, 988; c) P. Fortgang, E. Maisonhaute, C. Amatore, B. Delavaux-Nicot, J. Iehl, J.-F. Nierengarten, *Angew. Chem. Int. Ed.* **2011**, *50*, 2364; d) I. Nierengarten, J.-F. Nierengarten, *Chem. Rec.* **2015**, *15*, 31.
- 2) a) I. Nierengarten, S. Guerra, M. Holler, J.-F. Nierengarten, R. Deschenaux, *Chem. Commun.* **2012**, *48*, 8072; b) I. Nierengarten, S. Guerra, M. Holler, L. Karmazin-Brelot, J. Barbera, R. Deschenaux, J.-F. Nierengarten, *Eur. J. Org. Chem.* **2013**, 3675; c) I. Nierengarten, K. Buffet, M. Holler, S. P. Vincent, J.-F. Nierengarten, *Tetrahedron Lett.* **2013**, *54*, 2398; d) I. Nierengarten, M. Nothisen, D. Sigwalt, T. Biellmann, M. Holler, J.-S. Remy, J.-F. Nierengarten, *Chem. Eur. J.* **2013**, *19*, 17552.
- 3) a) Z. Zhang, B. Xia, C. Han, Y. Yu, F. Huang, *Org. Lett.* **2010**, *12*, 3285; b) L. Liu, D. Cao, Y. Jin, H. Tao, Y. Kou, H. Meier, *Org. Biomol. Chem.* **2011**, *9*, 7007.
- 4) M. Holler, N. Allenbach, J. Sonet, J.-F. Nierengarten, *Chem. Commun.* **2012**, *48*, 2576.
- 5) a) C. Li, Q. Xu, J. Li, F. Yao, X. Jia, *Org. Biomol. Chem.* **2010**, *8*, 1568; b) C. Li, L. Zhao, J. Li, X. Ding, S. Chen, Q. Zhang, Y. Yu, X. Jia, *Chem. Commun.* **2010**, *46*, 9016; c) T. Ogoshi, Y. Nishida, T.-a. Yamagishi, Y. Nakamoto, *Chem. Commun.* **2010**, *46*, 3708.
- 6) For examples of pillar[*n*]arene-containing rotaxane, see: a) N. L. Strutt, R. S. Forgan, J. M. Spruell, Y. Y. Botros, J. F. Stoddart, *J. Am. Chem. Soc.* **2011**, *133*, 5668; b) T. Ogoshi, Y. Nishida, T.-a. Yamagishi, Y. Nakamoto, *Macromolecules* **2010**, *43*, 7068; c) T. Ogoshi, D. Yamafuji, T. Aoki, T.-a. Yamagishi, *Chem. Commun.* **2012**, *48*, 6842; d) T. Ogoshi, D. Yamafuji, T. Aoki, K. Kitajima, T.-a. Yamagishi, Y. Hayashi, S. Kawauchi, *Chem. Eur. J.* **2012**, *18*, 7493; e) P. Wei, X. Yan, J. Li, Y. Ma, Y. Yao, F. Huang, *Tetrahedron* **2012**, *68*, 9179; f) T. Ogoshi, T. Aoki, R. Shiga, R. Iizuka, S. Ueda, K. Demachi, D. Yamafuji, H. Kayama, T.-a. Yamagishi, *J. Am. Chem. Soc.* **2012**, *134*, 20322; g) X.-Y. Hu, X. Wu, Q. Duan, T. Xiao, C. Lin, L. Wang, *Org. Lett.* **2012**, *14*, 4826; h) T. Ogoshi, D. Yamafuji, T.-a. Yamagishi, A. M. Brouwer, *Chem. Commun.* **2013**, *49*, 5468; i) C. Ke, N. L. Strutt, H. Li, X. Hou, K. J. Hartlieb, P. R. McGonigal, Z. Ma, J. Iehl, C. L. Stern, C. Cheng, Z. Zhu, N. A. Vermeulen, T. J. Meade, Y. Y. Botros, J. F. Stoddart, *J. Am. Chem. Soc.* **2013**, *135*, 17019; j) X. Hou, C. Ke, C. Cheng, N. Song, A. K. Blackburn, A. A. Sarjeant, Y. Y. Botros, Y.-W. Yang, J. F. Stoddart, *Chem.*

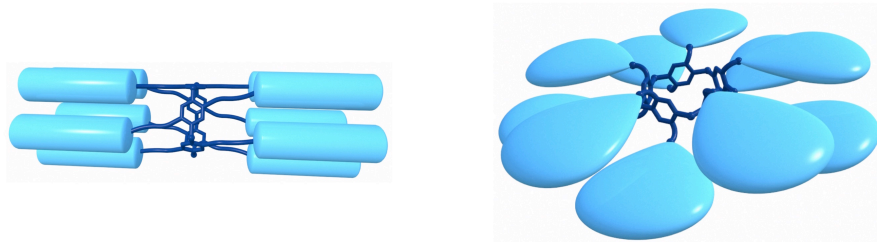
- Commun.* **2014**, *50*, 6196; k) T. M. N. Trinh, I. Nierengarten, M. Holler, J.-L. Gallani, J.-F. Nierengarten, *Chem. Eur. J.* **2015**, *21*, 8019.
- 7) For recent reviews on interlocked molecules, see: a) J. F. Stoddart, *Chem. Soc. Rev.* **2009**, *38*, 1802; b) J. A. Faiz, V. Heitz, J.-P. Sauvage, *Chem. Soc. Rev.* **2009**, *38*, 422; c) K. D. Hänni, D. A. Leigh, *Chem. Soc. Rev.* **2010**, *39*, 1240; d) R. S. Forgan, J.-P. Sauvage, J. F. Stoddart, *Chem. Rev.* **2011**, *111*, 5434; e) A. C. Fahrenbach, C. J. Bruns, D. Cao, J. F. Stoddart, *Acc. Chem. Res.* **2012**, *45*, 1581; f) A. C. Fahrenbach, C. J. Bruns, H. Li, A. Trabolsi, A. Coskun, J. F. Stoddart, *Acc. Chem. Res.* **2014**, *47*, 482; g) F. Durola, V. Heitz, F. Reviriego, C. Roche, J.-P. Sauvage, A. Sour, Y. Trolez, *Acc. Chem. Res.* **2014**, *47*, 633-645.
- 8) a) M. del Rosario Benites, T. E. Johnson, S. Weghorn, L. Yu, P. Dharma Rao, J. R. Diers, S. I. Yang, C. Kirmaier, D. F. Bocian, D. Holten, J. S. Lindsey, *J. Mater. Chem.* **2002**, *65*; b) R. W. Wagner, J. Seth, S. I. Yang, D. Kim, D. F. Bocian, D. Holten, J. S. Lindsey, *J. Org. Chem.* **1998**, *63*, 5042; c) L. Yu, J. S. Lindsey, *J. Org. Chem.* **2001**, *66*, 7402; d) J. J. S. Hsiao, B. P. Krueger, R. W. Wagner, T. E. Johnson, J. K. Delaney, D. C. Mauzerall, G. R. Fleming, J. S. Lindsey, D. F. Bocian, and R. J. Donohoe, *J. Am. Chem. Soc.* **1996**, *118*, 11166; e) J. Seth, V. Palaniappan, R. W. Wagner, T. E. Johnson, J. S. Lindsey, D. F. Bocian, *J. Am. Chem. Soc.* **1996**, *118*, 11194; f) R.W. Wagner, J. S. Lindsey, J. Seth, V. Palaniappan, D. F. Bocian, *J. Am. Chem. Soc.* **1996**, *118*, 3996; g) F. Fungo, L. A. Otero, L. Sereno, J. J. Silber, E. N. Durantini, *J. Mat. Chem.* **2000**, *10*, 645; h) A. Ambroise, J. Li, L. Yu, J. S. Lindsey, *Org. Lett.* **2000**, *2*, 2563; i) S. Prathapan, T. E. Johnson, J. S. Lindsey, *J. Am. Chem. Soc.* **1993**, *115*, 7519; j) R.W. Wagner, J. S. Lindsey, J. Seth, V. Palaniappan, D. F. Bocian, *J. Am. Chem. Soc.* **1996**, *118*, 3996.
- 9) a) V. Balzani, S. Campagna, G. Denti, A. Juris, S. Serroni, M. Venturi, *Acc. Chem. Res.* **1998**, *31*, 26; b) V. Balzani, P. Ceroni, A. Juris, M. Venturi, S. Campagna, F. Puntoriero, S. Serroni, *Coord. Chem. Rev.* **2001**, *219-221*, 545; c) M. Fisher, F. Vögtle, *Angew. Chem. Int. Ed.* **1999**, *38*, 884; d) A. Adronov, J. M. J. Fréchet, *Chem. Commun.* **2000**, 1701.
- 10) S. Dong, C. Han, B. Zheng, M. Zhang, F. Huang, *Tetrahedron Lett.* **2012**, *53*, 3668.
- 11) R. Milev, A. Lopez-Pacheco, I. Nierengarten, T. M. N. Trinh, M. Holler, R. Deschenaux, J.-F. Nierengarten, *Eur. J. Org. Chem.* **2015**, 479.
- 12) M. Chrominski, A. Zieleniewska, M. Karczewski, D. Gryco, *J. Porphyrins and Phthalocyanines* **2014**, *18*, 267.

- 13) a) R. A. Rader; D. R. McMillin, M. T. Buckner, T. G. Matthews, D. J. Casadonte, R. K. Lengel, S. B. Whittaker, L. M. Darmon, F. E. Lytle, *J. Am. Chem. Soc.* **1981**, *103*, 5906; b) A. A. Del Paggio, D. R. McMillin, *Inorg. Chem.* **1983**, *22*, 691; c) D. J. Casadonte, D. R. McMillin, *Inorg. Chem.* **1987**, *26*, 3950.
- 14) a) A. Kaeser, M. Mohankumar, J. Mohanraj, F. Monti, M. Holler, J.-J. Cid, O. Moudam, I. Nierengarten, L. Karmazin-Brelot, C. Duhayon, B. Delavaux-Nicot, N. Armaroli, J.-F. Nierengarten, *Inorg. Chem.* **2013**, *52*, 12140; b) M. Mohankumar, F. Monti, M. Holler, F. Niess, B. Delavaux-Nicot, N. Armaroli, J.-P. Sauvage, J.-F. Nierengarten, *Chem. Eur. J.* **2014**, *20*, 12083.
- 15) a) X. Huang, K. Nakanishi, N. Berova, *Chirality* **2000**, *12*, 237; b) T. Hashimoto, Y.-C. Choe, H. Nakano, K. Hirao, *J. Phys. Chem. A* **1999**, *103*, 1894; c) M. Gouterman, *J. Chem. Phys.* **1959**, *30*, 1139.
- 16) D. Dolphin (Ed.), *The Porphyrins – Structure and Synthesis, Part A*, Academic Press, New York, **1978**.
- 17) T. Ogoshi, T. Aoki, K. Kitajima, S. Fujinami, T.-a. Yamagishi, Y. Nakamoto, *J. Org. Chem.* **2011**, *76*, 328.

5. Conclusion

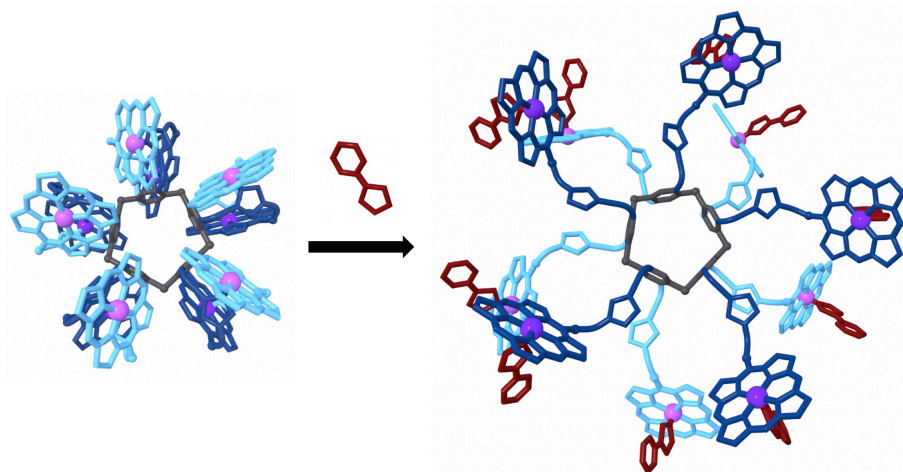
As part of the research program of our group on the use of a pillar[5]arene core as a scaffold for the preparation of nanomaterials, the present PhD thesis has been devoted to the preparation of liquid-crystalline materials (chapter 2) and derivatives (chapter 3). In these two sections, a decaazide pillar[5]arene building block has been used for the efficient grafting of peripheral subunits onto the macrocyclic core.

In chapter 2, new liquid-crystalline pillar[5]arene derivatives have been prepared by grafting either *p*-dodecyloxybenzoate groups or percec-type dendrons on the macrocyclic scaffold. The supramolecular organization of the compounds within the mesophases is strongly dependent on the type of peripheral units. In the case of the *p*-dodecyloxybenzoate derivative, the five peripheral groups located on each rim of the pillar[5]arene core are oriented in opposite directions and the molecules adopt a tubular shape suited for the self-organization into a smectic mesophase. In contrast, the conformation adopted by the dendronized compound is mainly dominated by the self-assembling capabilities of the peripheral dendrons and the molecules adopt a disc-shaped structure perfectly suited for the self-organization into a columnar liquid-crystalline phase.

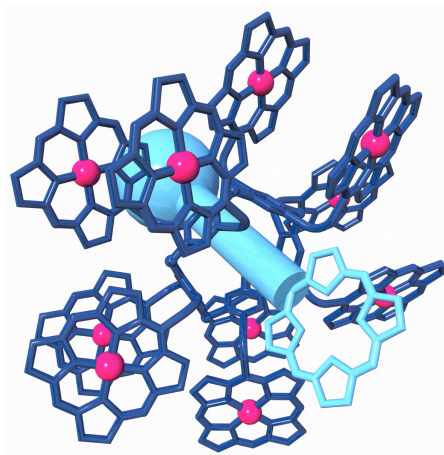


In chapter 3, pillar[5]arene derivatives bearing peripheral porphyrin subunits have been efficiently prepared from the clickable pillar[5]arene building block and Zn(II)-porphyrin derivatives bearing a terminal alkyne function. Owing to an intramolecular

complexation of the peripheral Zn(II)-porphyrin moieties by 1,2,3-triazole subunits, a dynamic conformational equilibrium leading to a folding of the molecules has been evidenced by variable temperature ^1H NMR studies. The coordination-driven folding can be prevented by an external chemical stimulus (addition of an imidazole derivative) and unfolding of the molecules occurs. The resulting molecular motions triggered by the addition of the imidazole ligand mimics the blooming of a flower.



Finally, a sophisticated photoactive molecular device has been prepared by combining recent concepts for the preparation of multifunctional nanomolecules (click chemistry on multifunctional scaffolds) with supramolecular chemistry (self-assembly to prepare rotaxanes). Specifically, a clickable [2]rotaxane scaffold incorporating a free-base porphyrin stopper has been prepared and functionalized with ten peripheral Zn(II)-porphyrin moieties (chapter 4).



Steady state investigations of the resulting final compound combining Zn(II) and free-base porphyrin moieties have shown that this compound is a light-harvesting device capable of

channeling the light energy from the peripheral Zn(II)-porphyrin subunits to the core by singlet-singlet energy transfer.

One important aspect of modern chemistry is directed towards the synthesis of complex nanomolecules that exhibit specific properties for applications in materials science and biology. However, the preparation of complex nanostructures combining the required functional groups remains often difficult and requires a large number of synthetic steps thus limiting both their accessibility and applicability. In this PhD thesis, we have shown that the preparation of easily accessible nanoscaffolds allowing for the grafting of one or more molecular entities is an appealing strategy to generate sophisticated nanomolecules. Overall, one of our main concerns has been to increase the complexity of the molecular structures without increasing the synthetic difficulties. This is an important challenge for synthetic organic chemistry in general.

S1. Supporting information (Chapter 2)

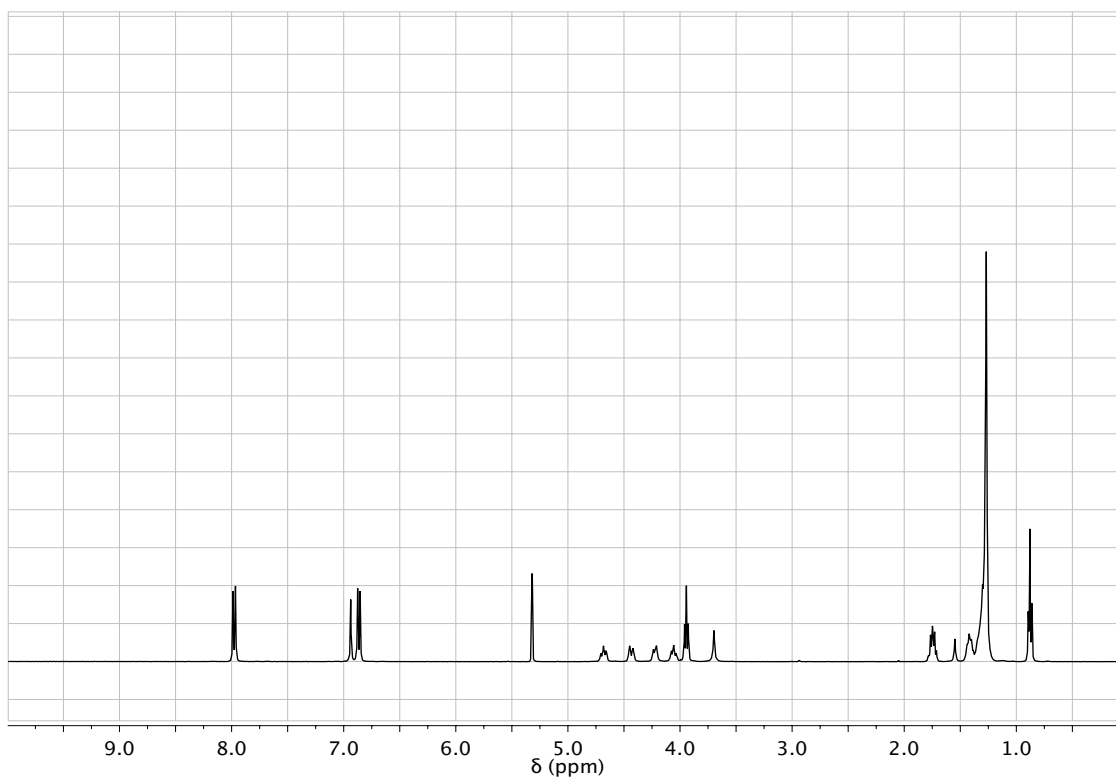
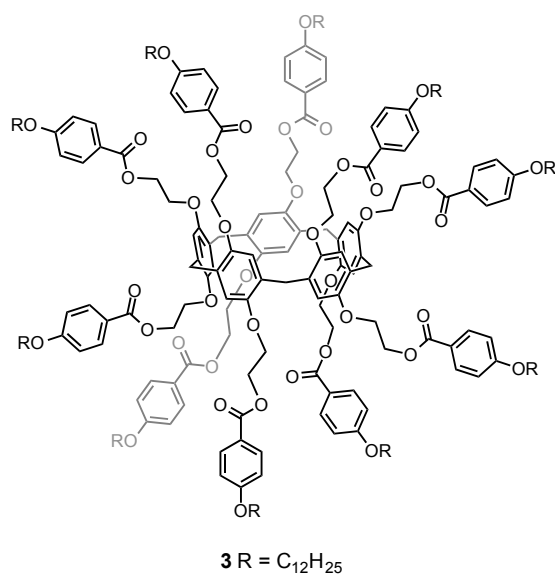
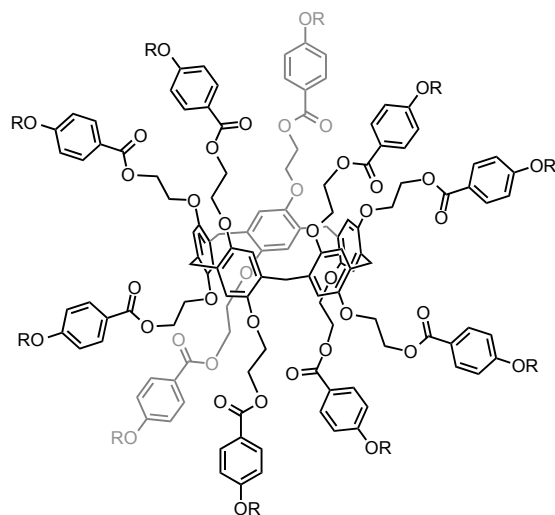


Figure S1a. ^1H NMR spectrum of compound 3 (CD_2Cl_2 , 400 MHz).



3 R = C₁₂H₂₅

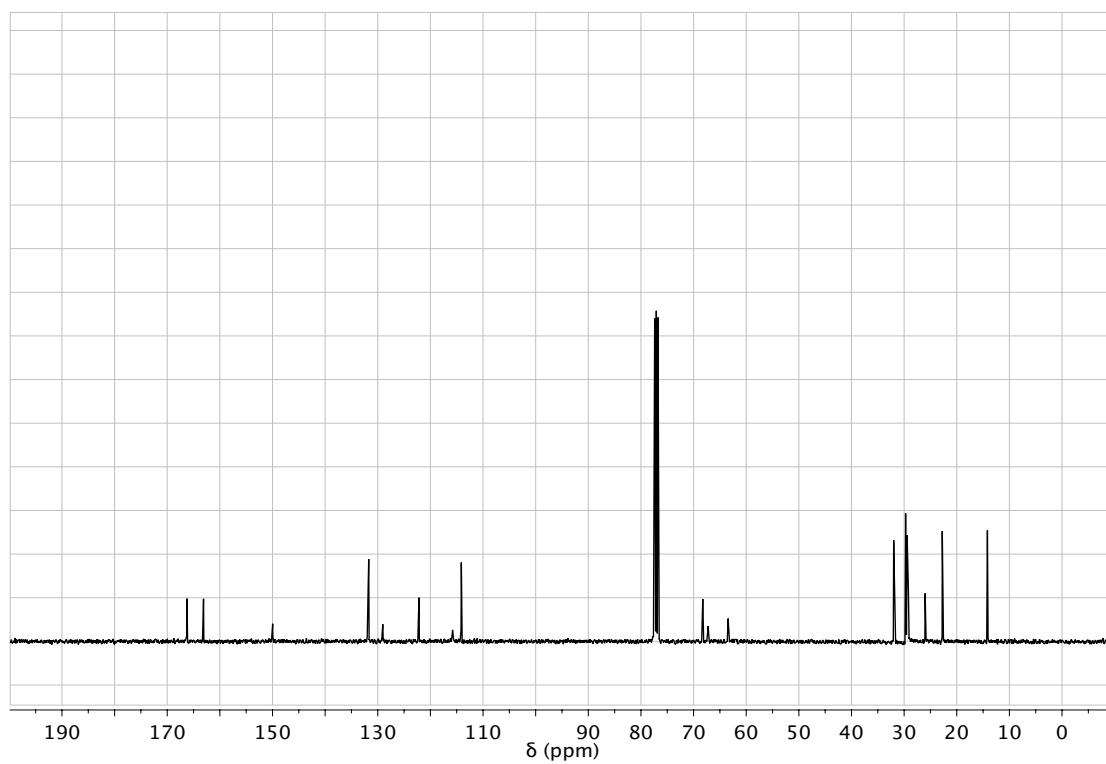
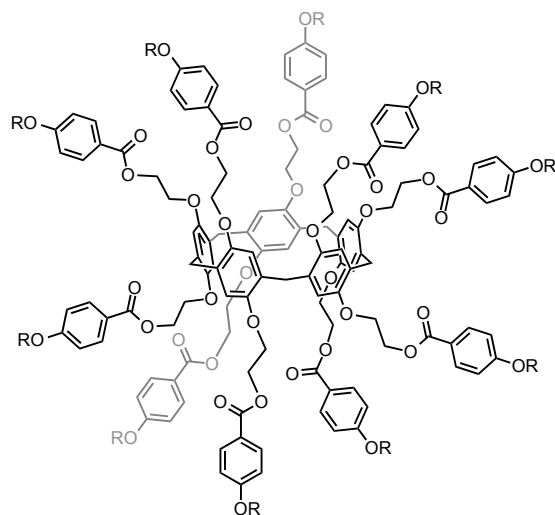


Figure S1b. ¹³C NMR spectrum of compound 3 (CDCl₃, 100 MHz).



3 R = C₁₂H₂₅

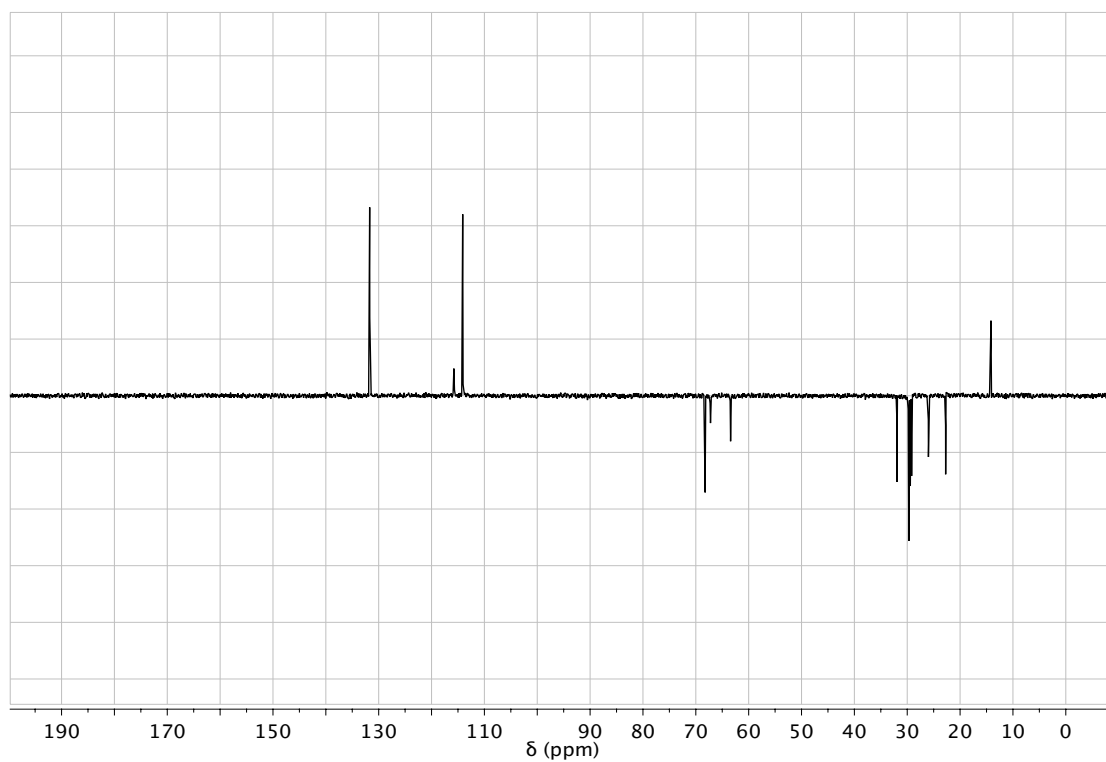
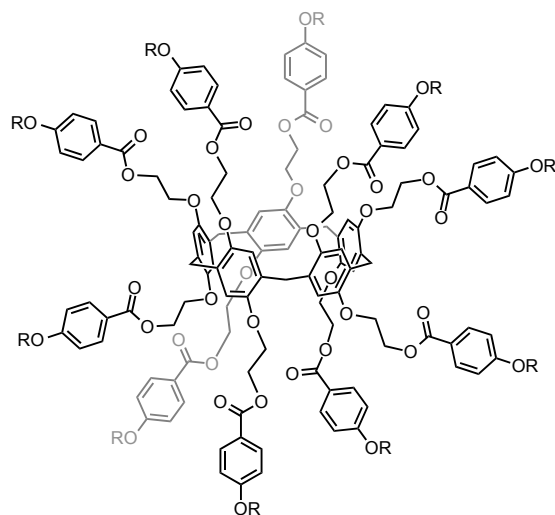


Figure S1c. DEPT spectrum of compound **3** (CDCl₃, 100 MHz).



3 R = C₁₂H₂₅

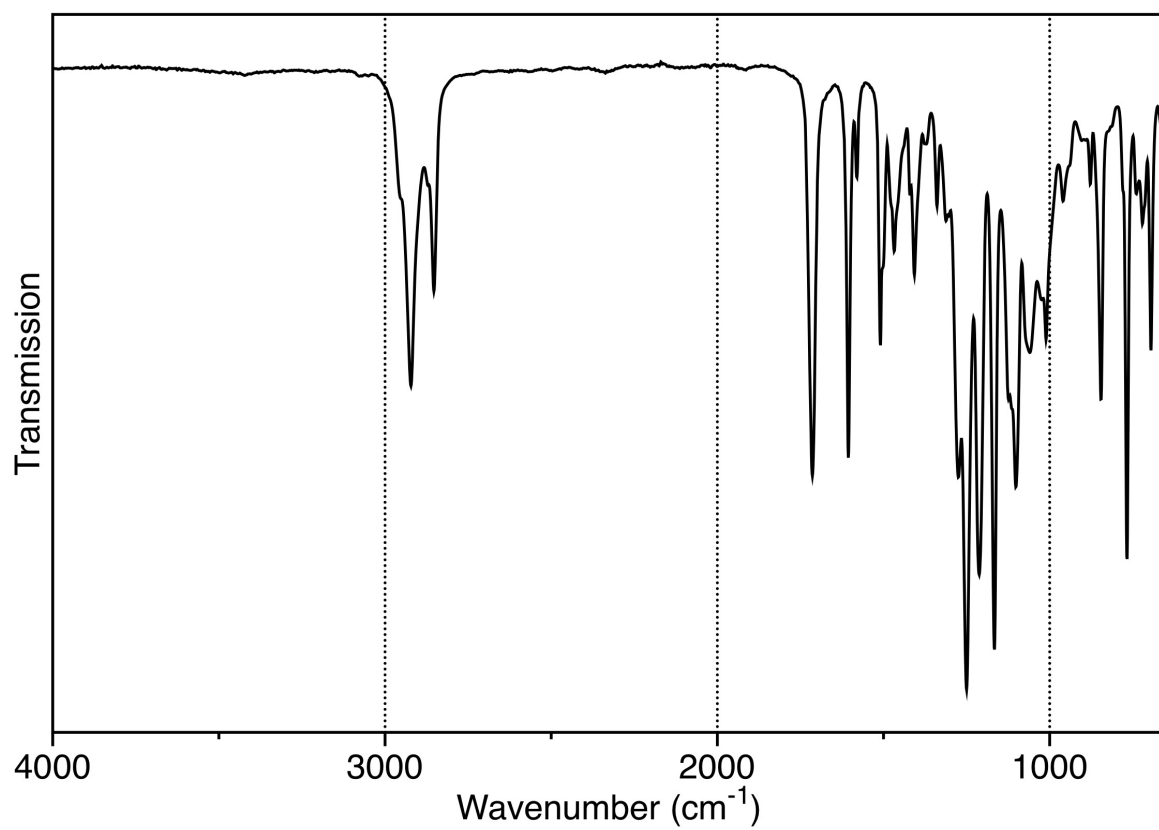
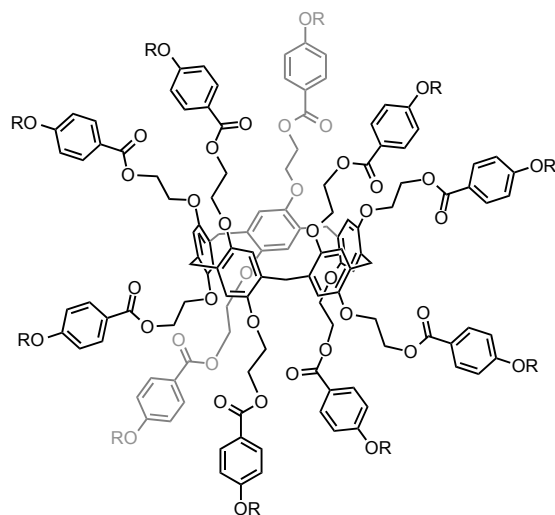


Figure S1d. IR spectrum of compound 3.



3 R = C₁₂H₂₅

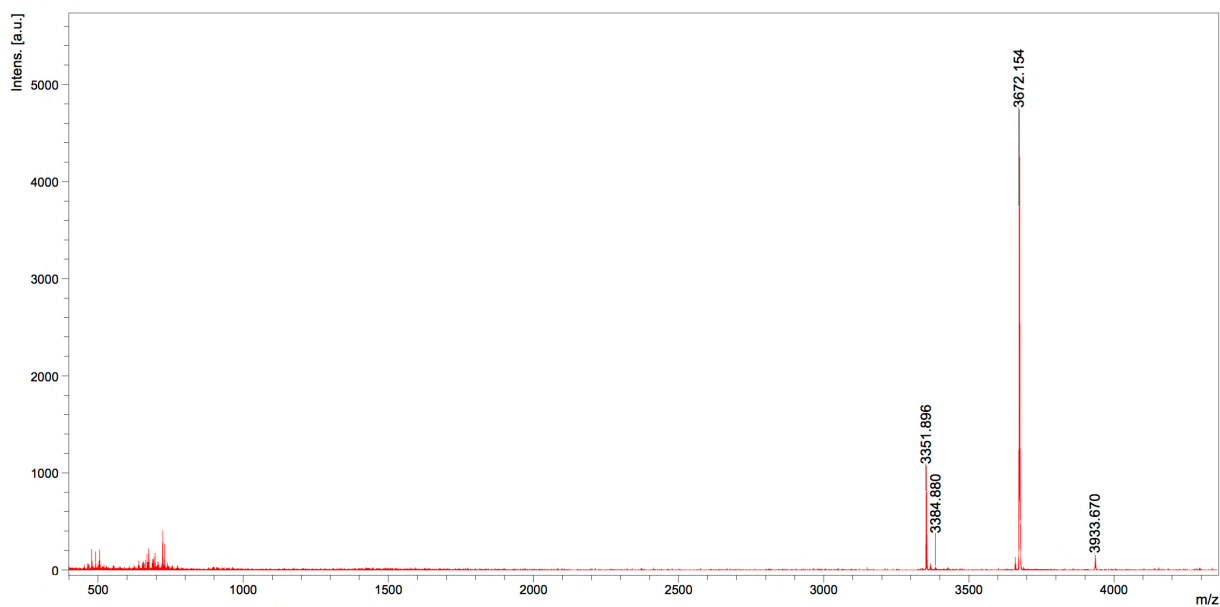


Figure S1e. MALDI-TOF mass spectrum of compound 3.

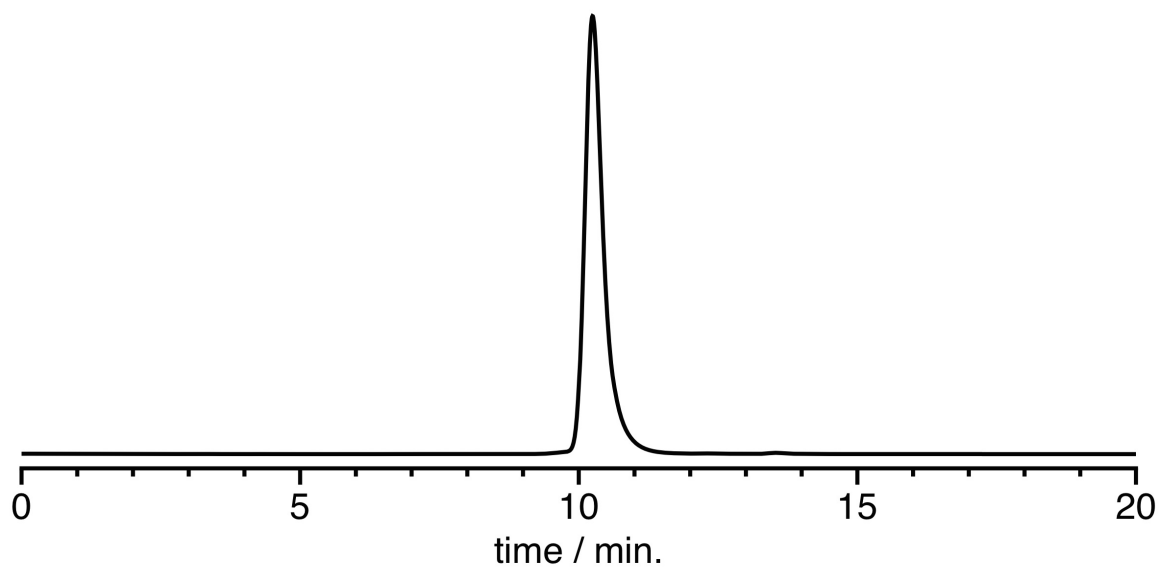
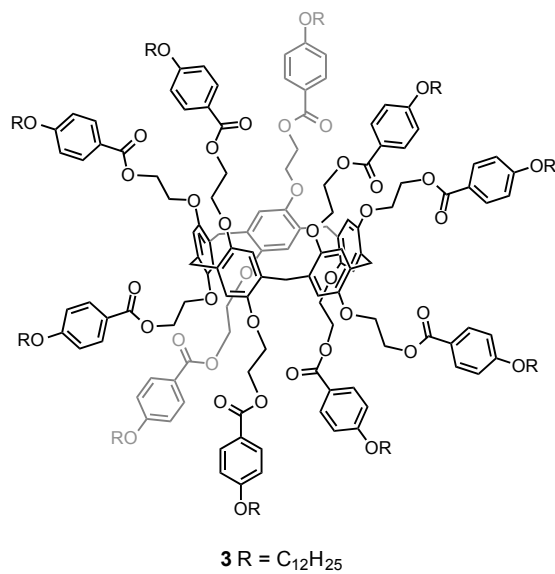


Figure S1f. HPLC trace on a size exclusion column (PLgel, CH_2Cl_2 , UV detector at $\lambda = 254$ nm) obtained for compound **3**.

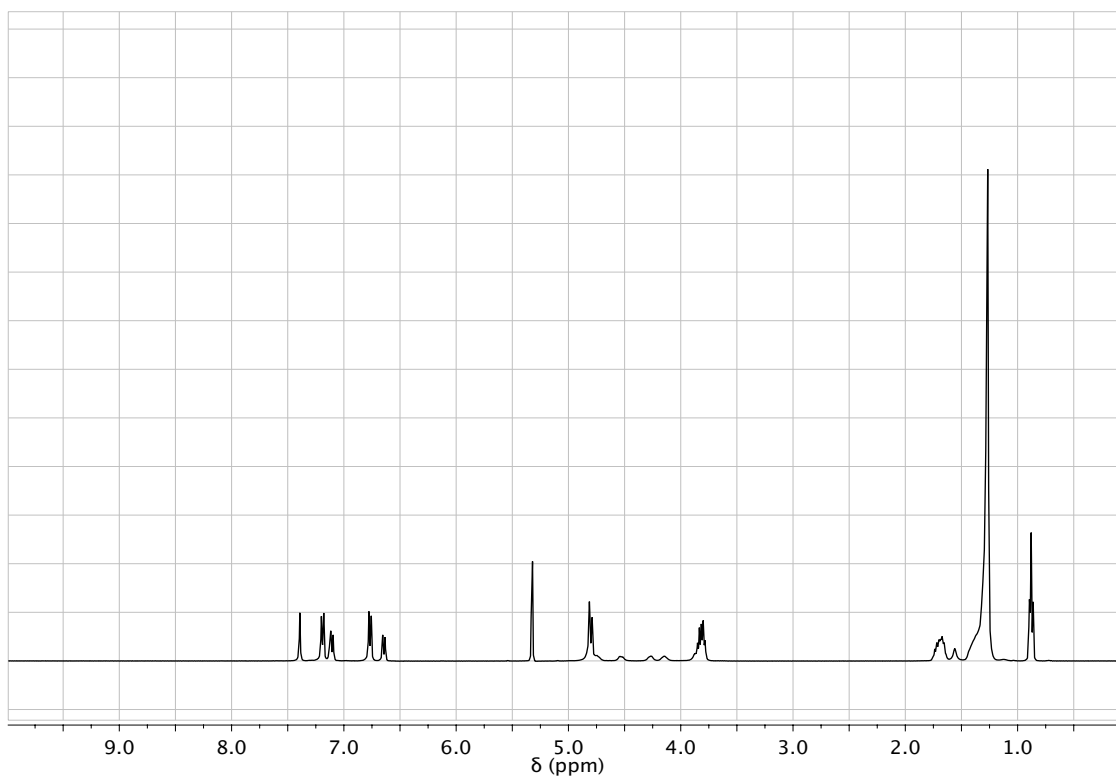
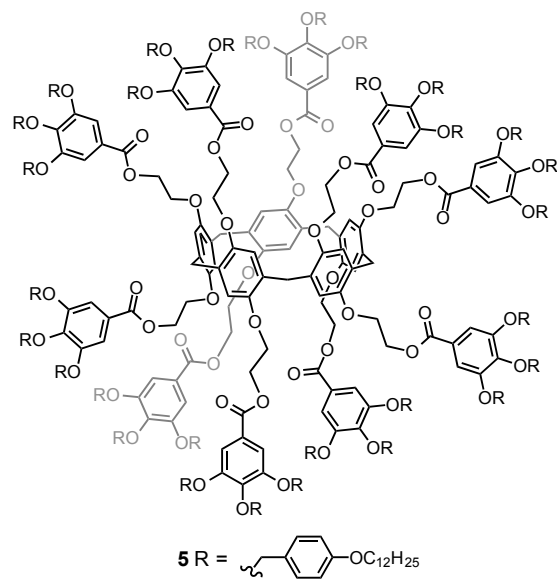


Figure S2a. ¹H NMR spectrum of compound **5** (CD₂Cl₂, 400 MHz).

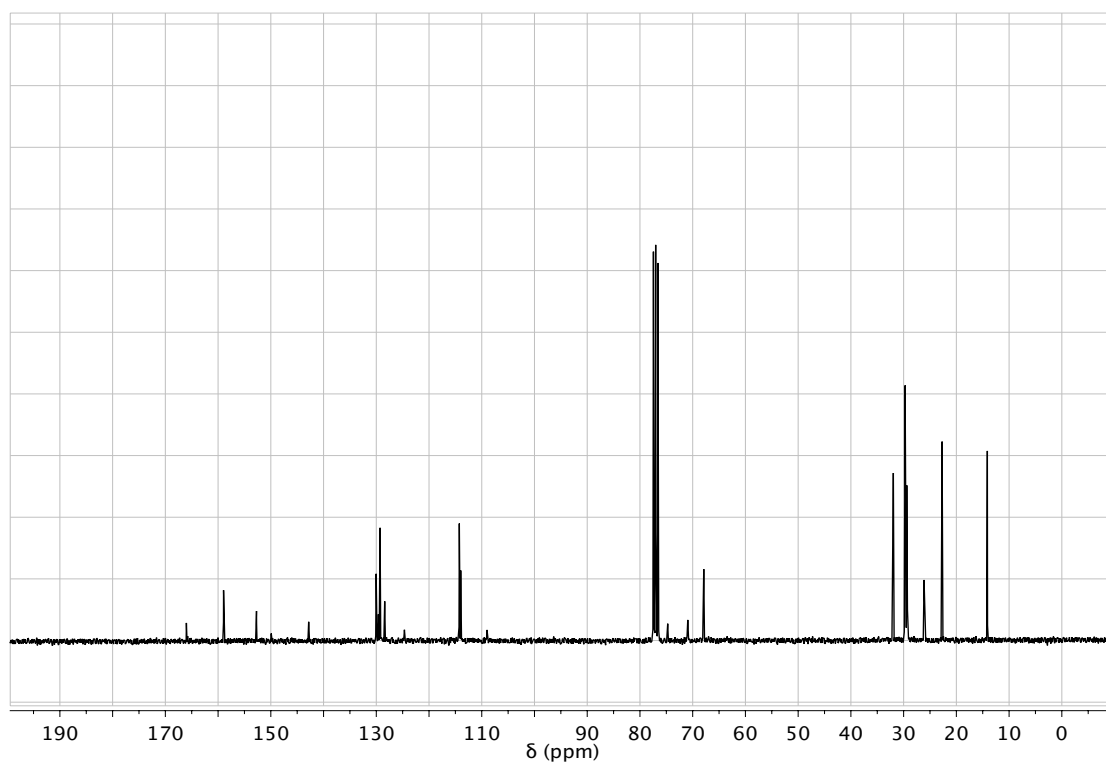
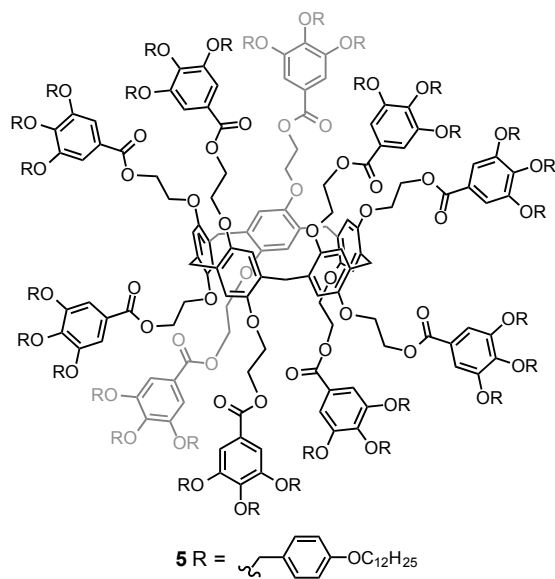


Figure S2b. ^{13}C NMR spectrum of compound **5** (CDCl_3 , 100 MHz).

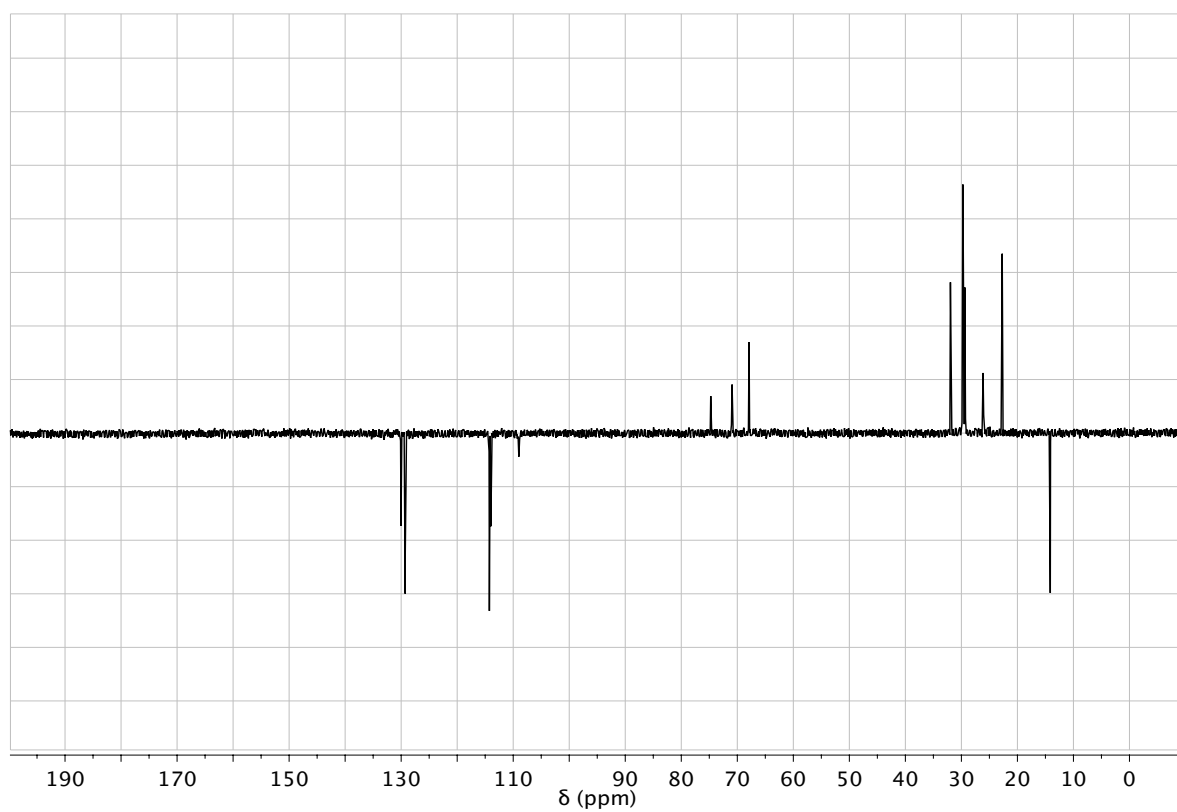
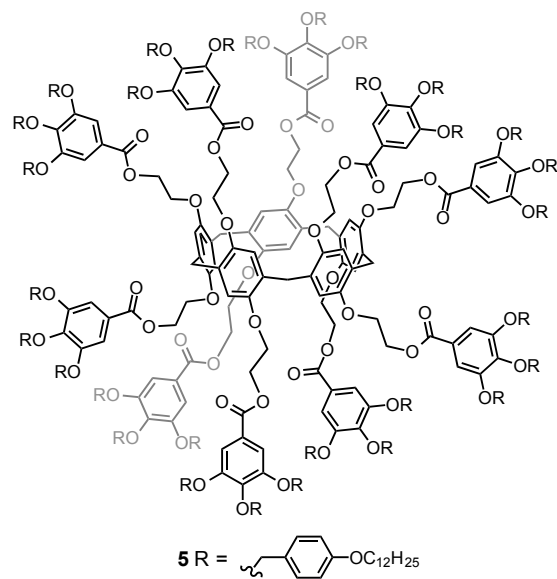


Figure S2c. DEPT spectrum of compound **5** (CDCl_3 , 100 MHz).

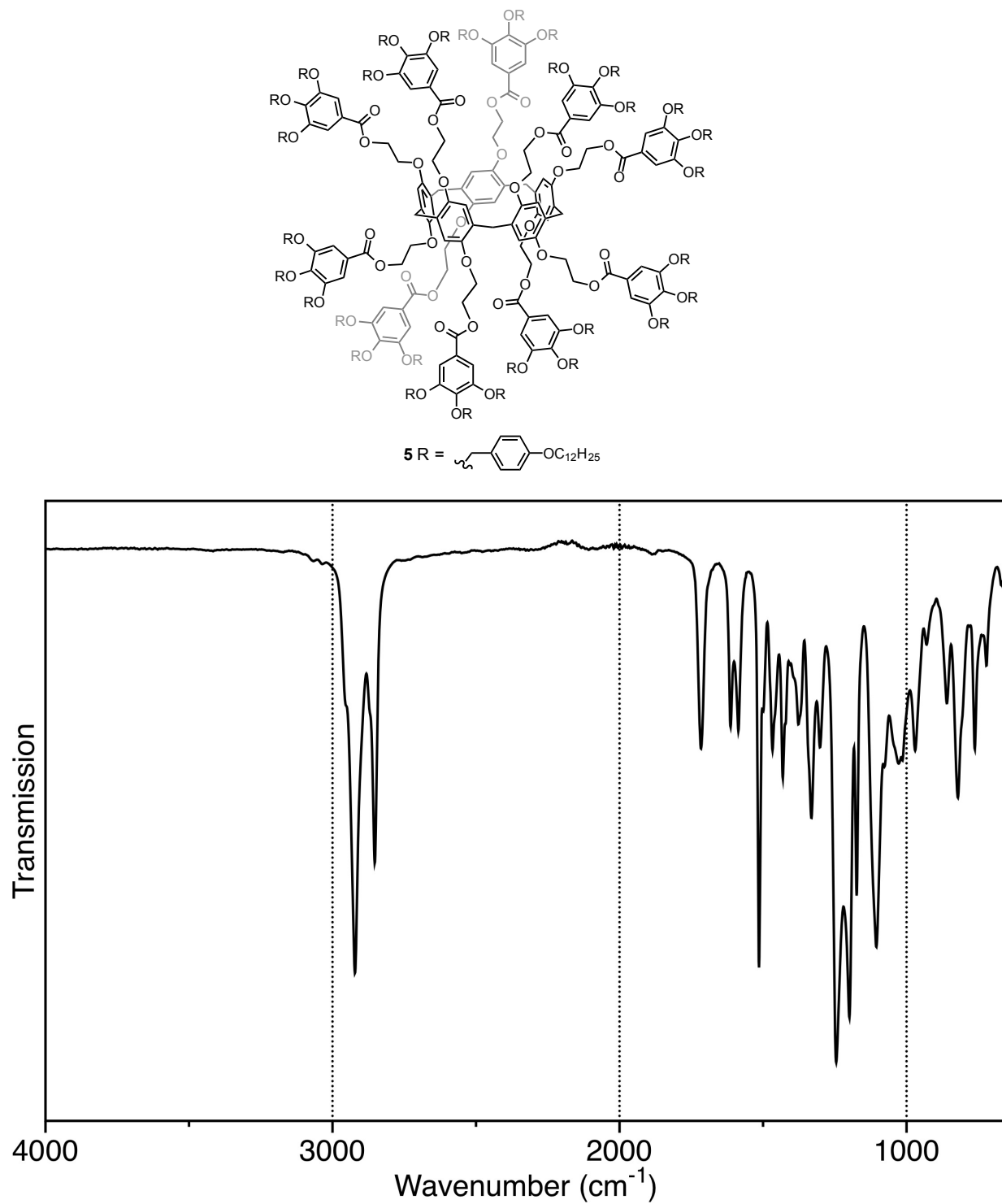


Figure S2d. IR spectrum of compound **5**.

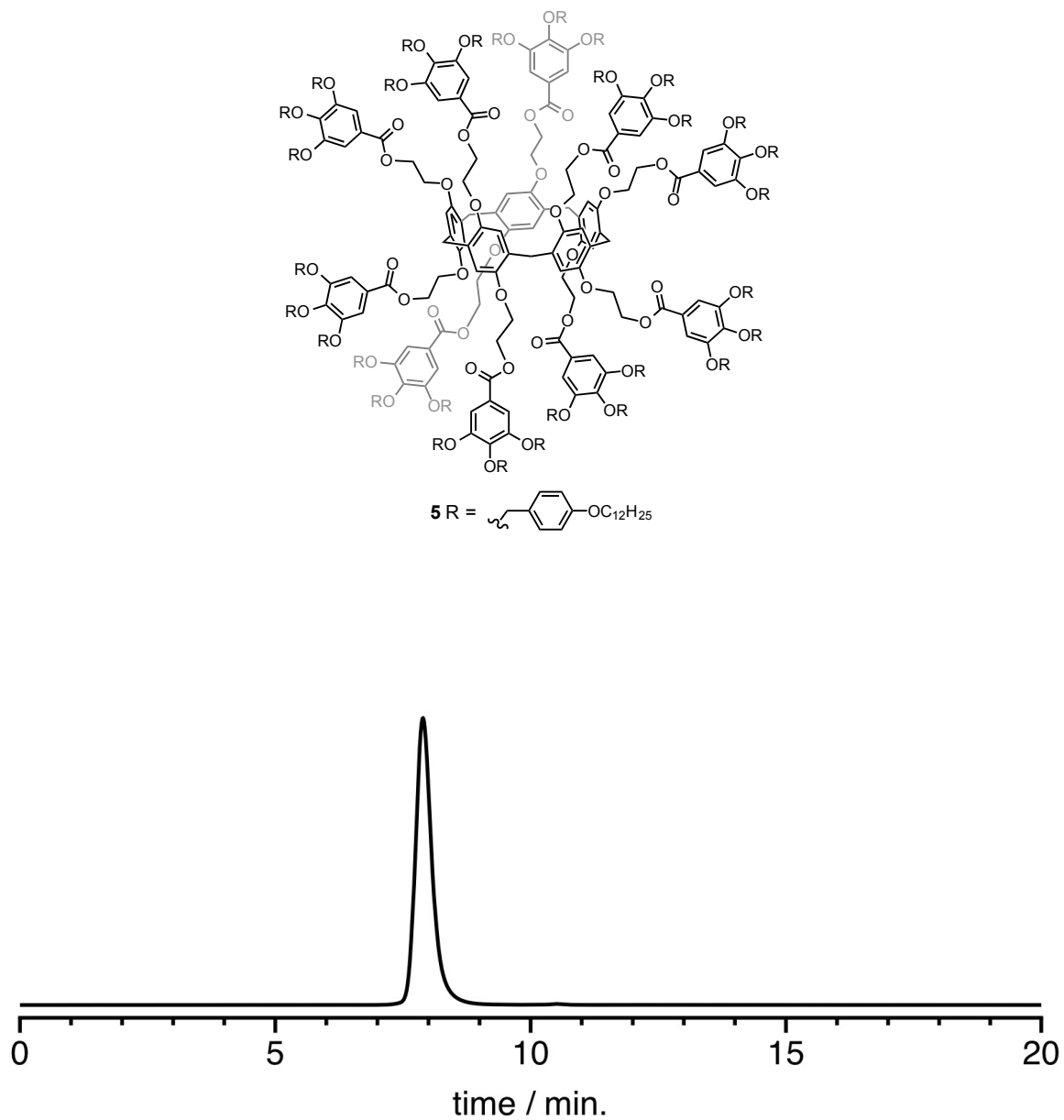


Figure S2e. HPLC trace on a size exclusion column (PLgel, CH₂Cl₂, UV detector at $\lambda = 254$ nm) obtained for compound **5**.

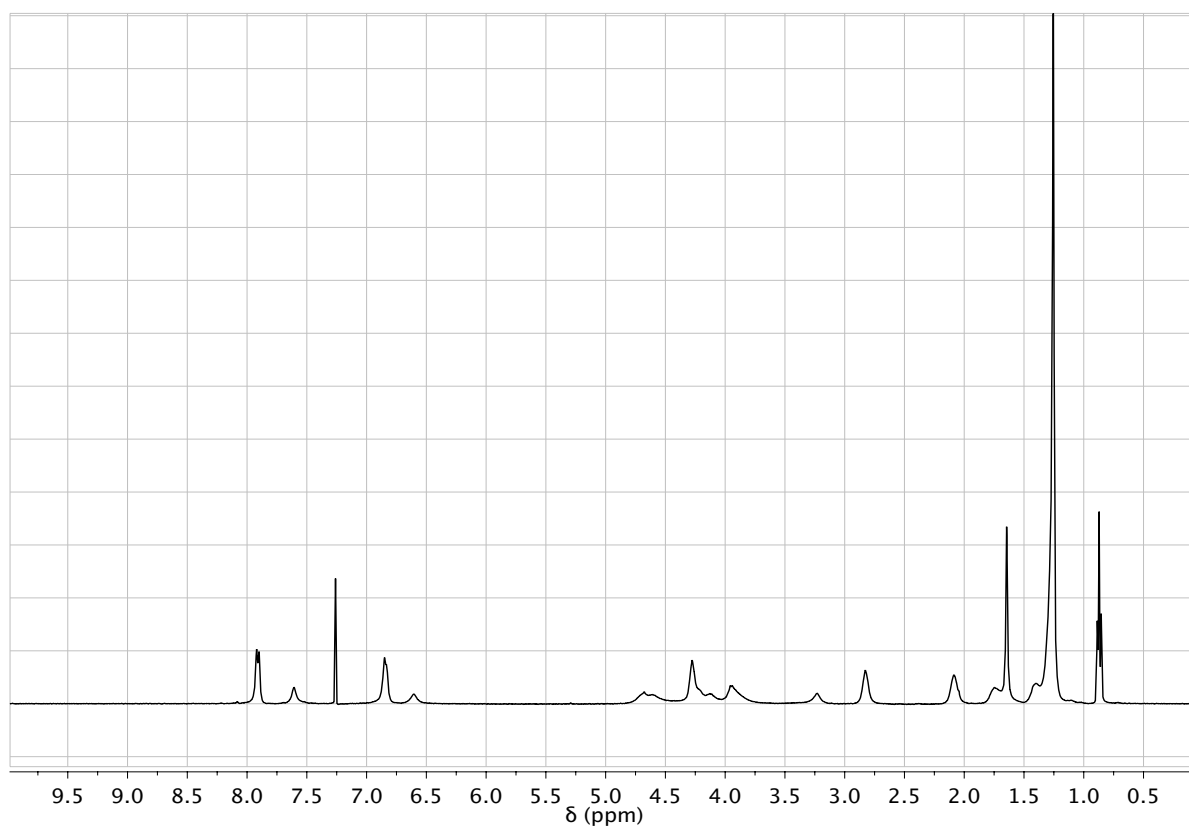
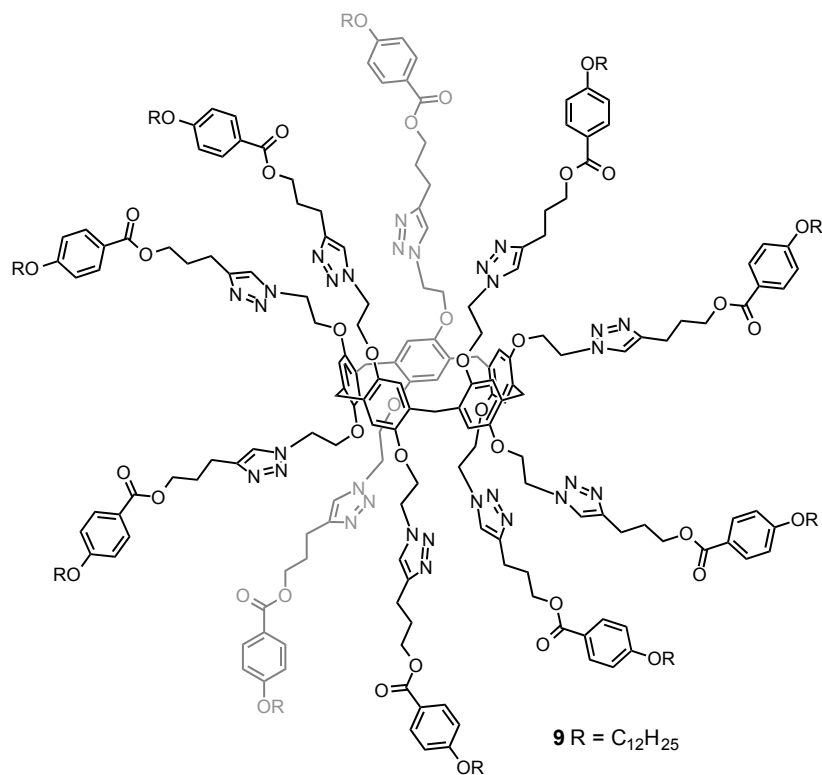


Figure S3a. ^1H NMR spectrum of compound **9** (CDCl_3 , 400 MHz).

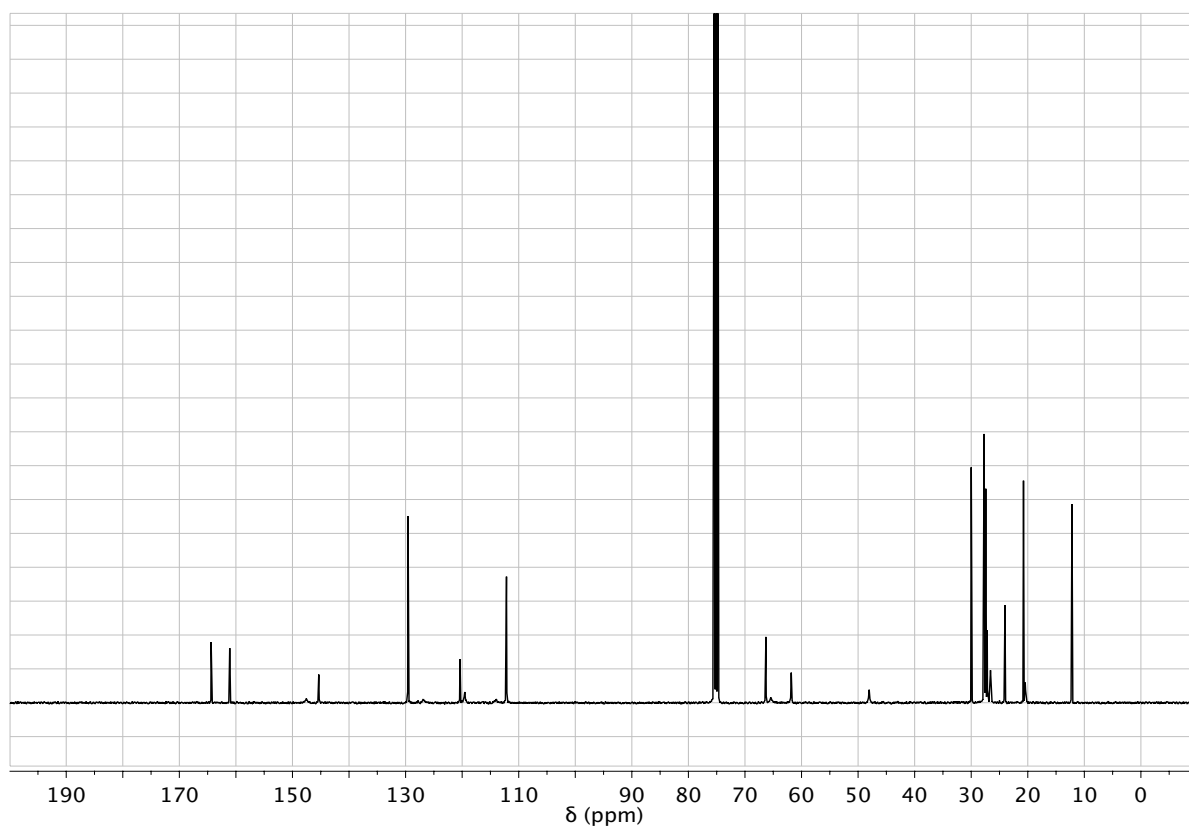
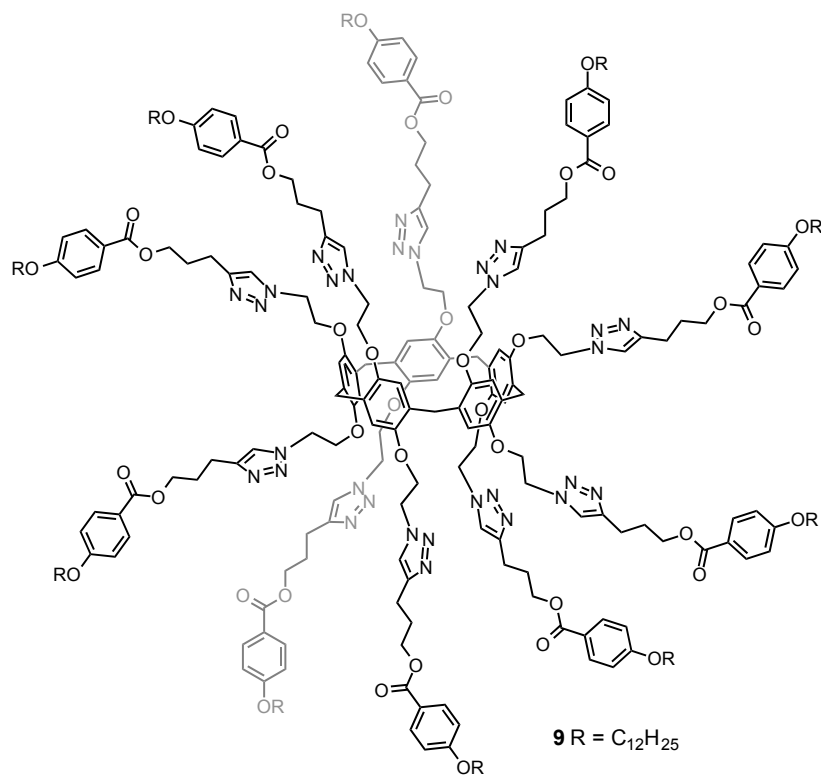


Figure S3b. ¹³C NMR spectrum of compound **9** (CDCl₃, 100 MHz).

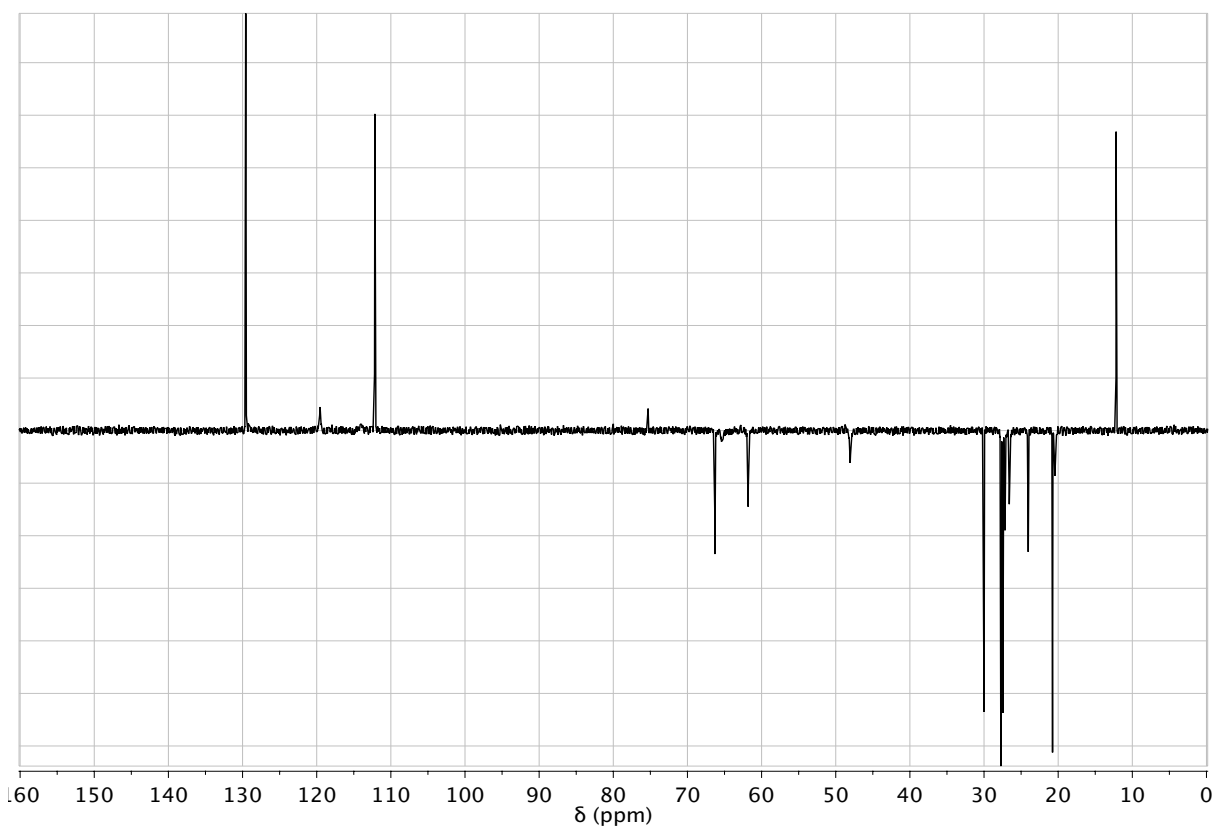
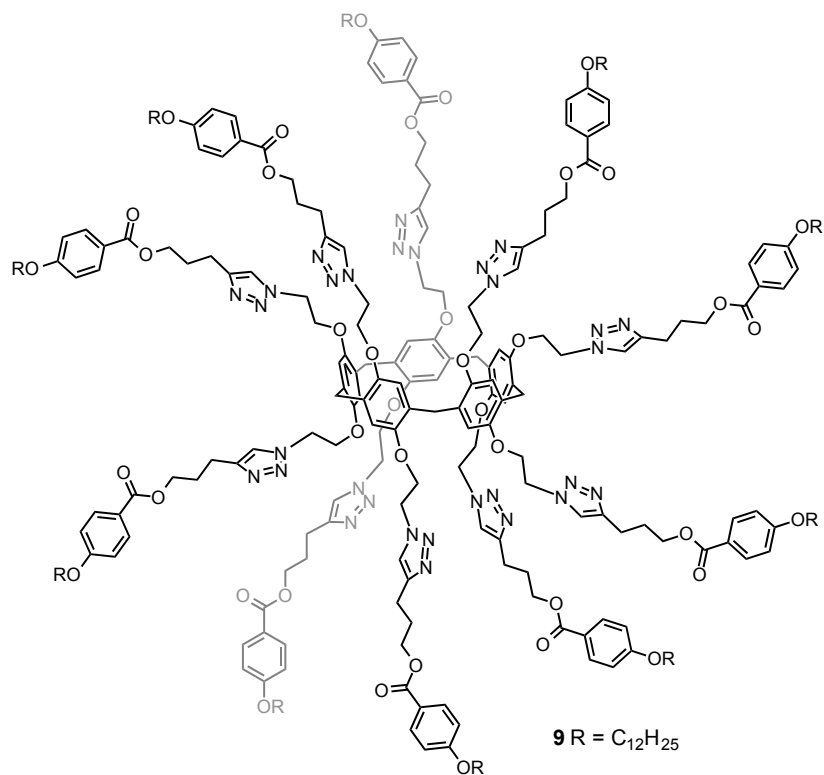
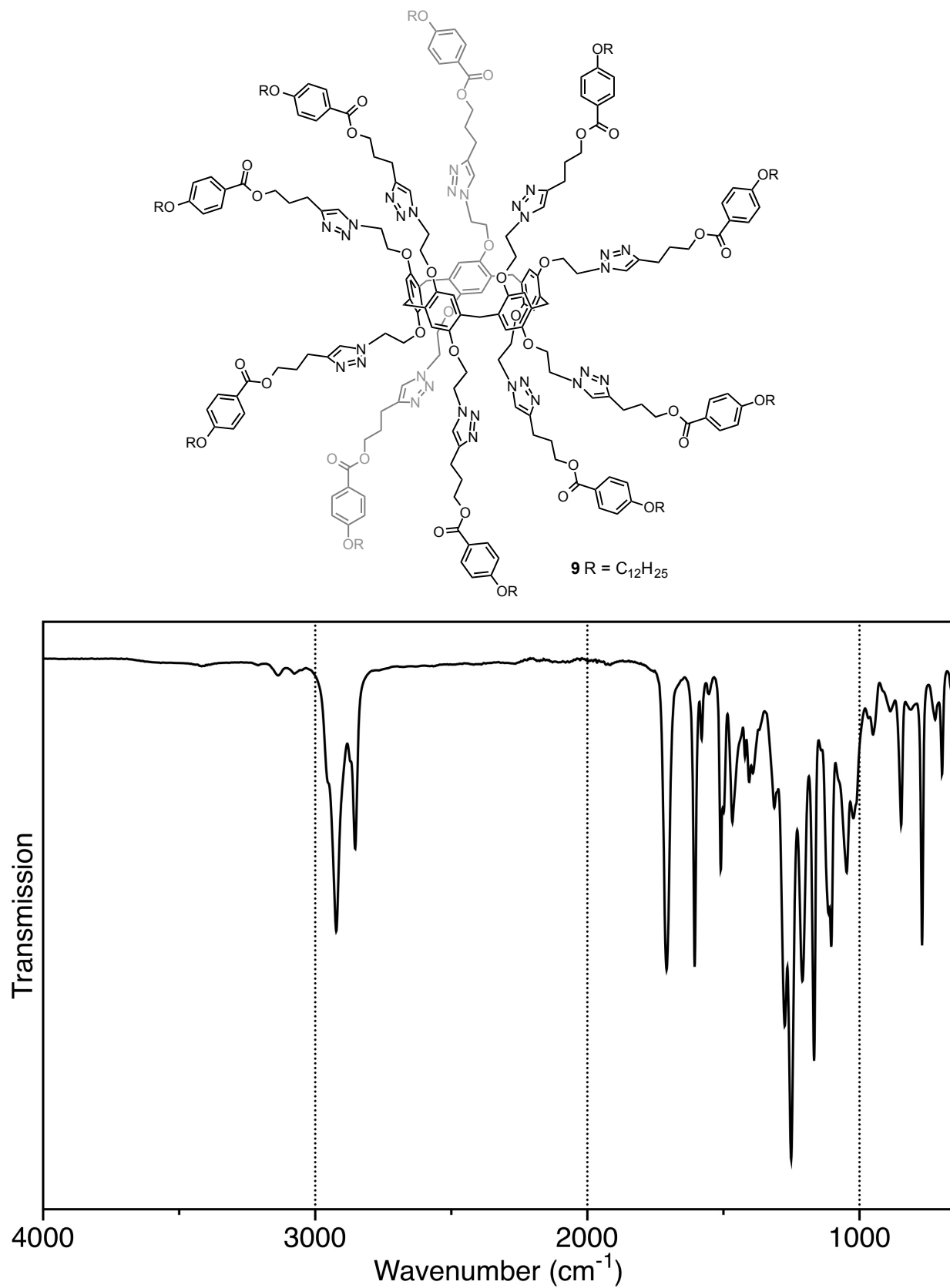


Figure S3c. DEPT spectrum of compound **9** (CDCl₃, 100 MHz).

**Figure S3d.** IR spectrum of compound **9**.

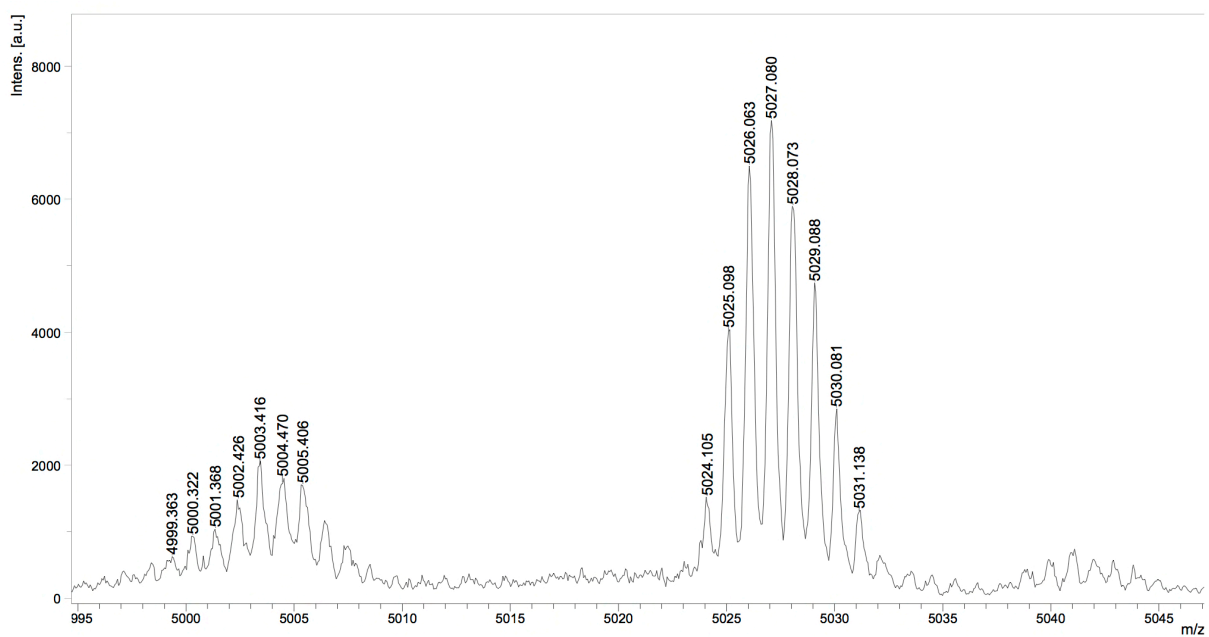
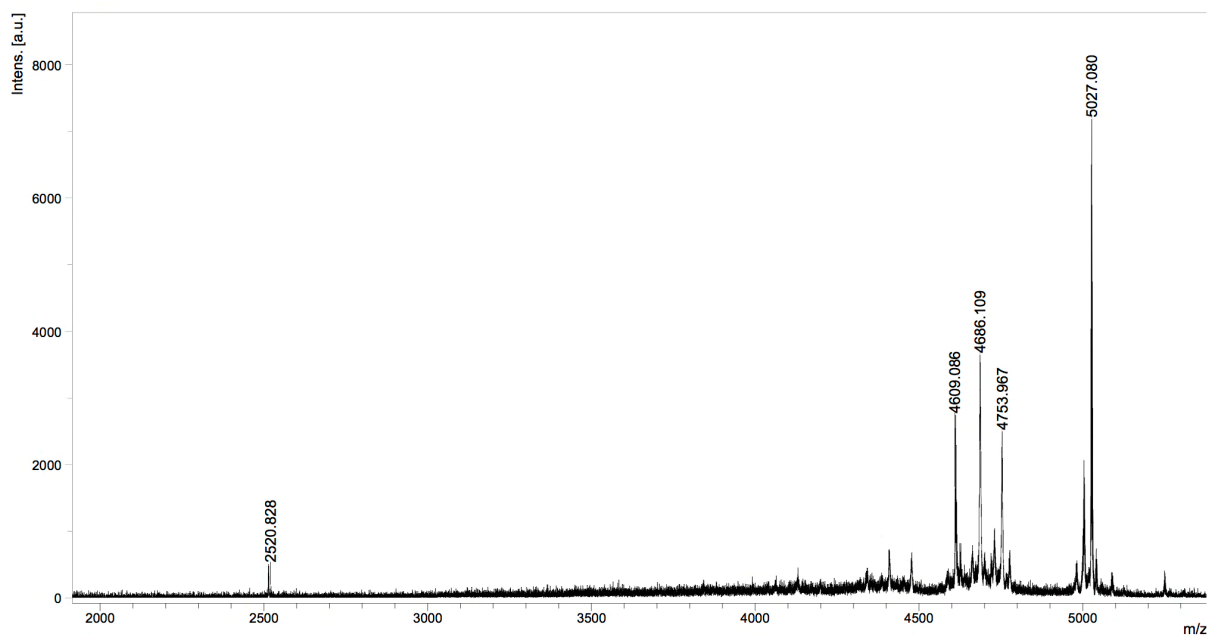


Figure S3e. MALDI-TOF mass spectrum of compound 9.

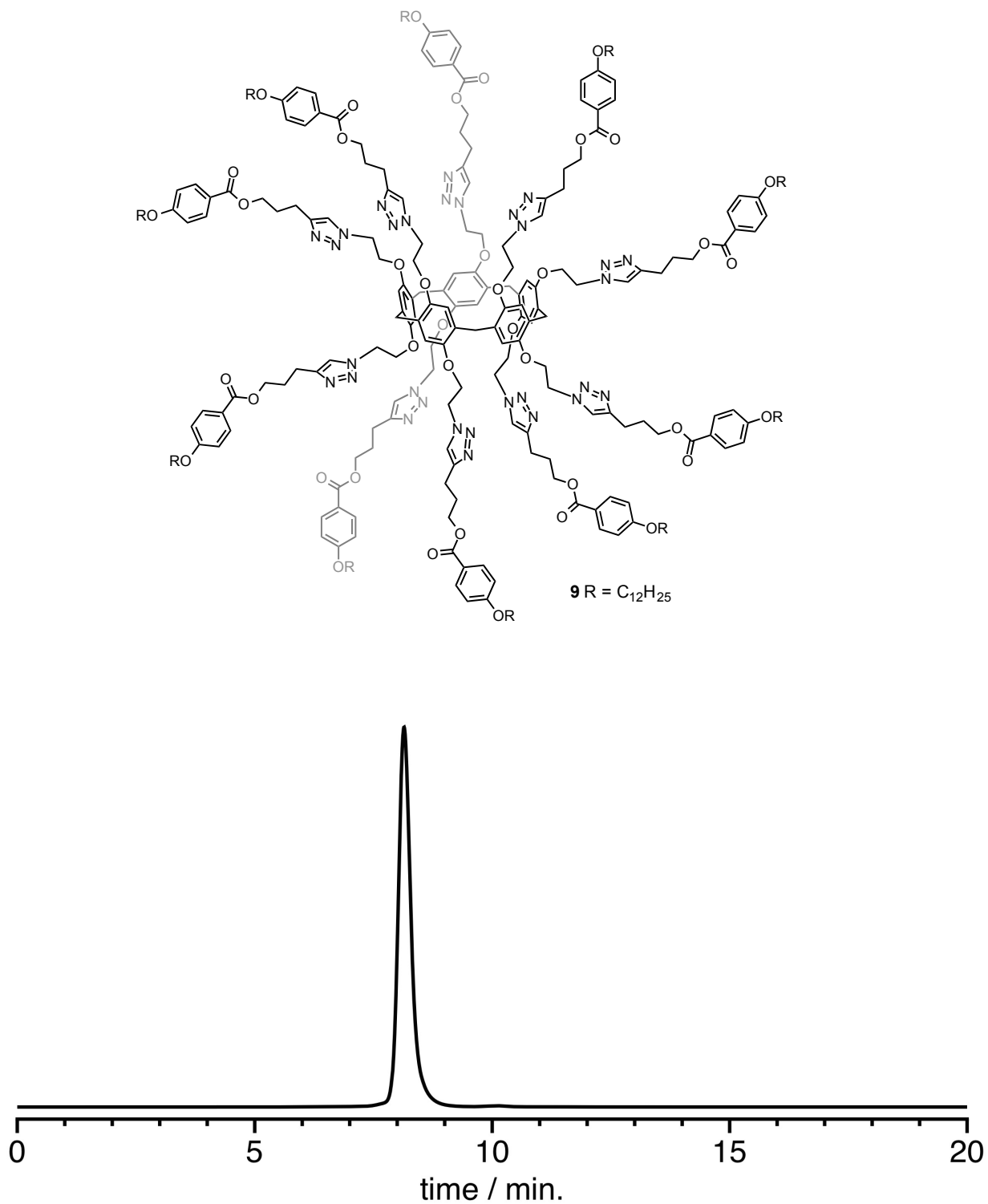


Figure S3f. HPLC trace on a size exclusion column (PLgel, CH₂Cl₂, UV detector at $\lambda = 254$ nm) obtained for compound **9**.

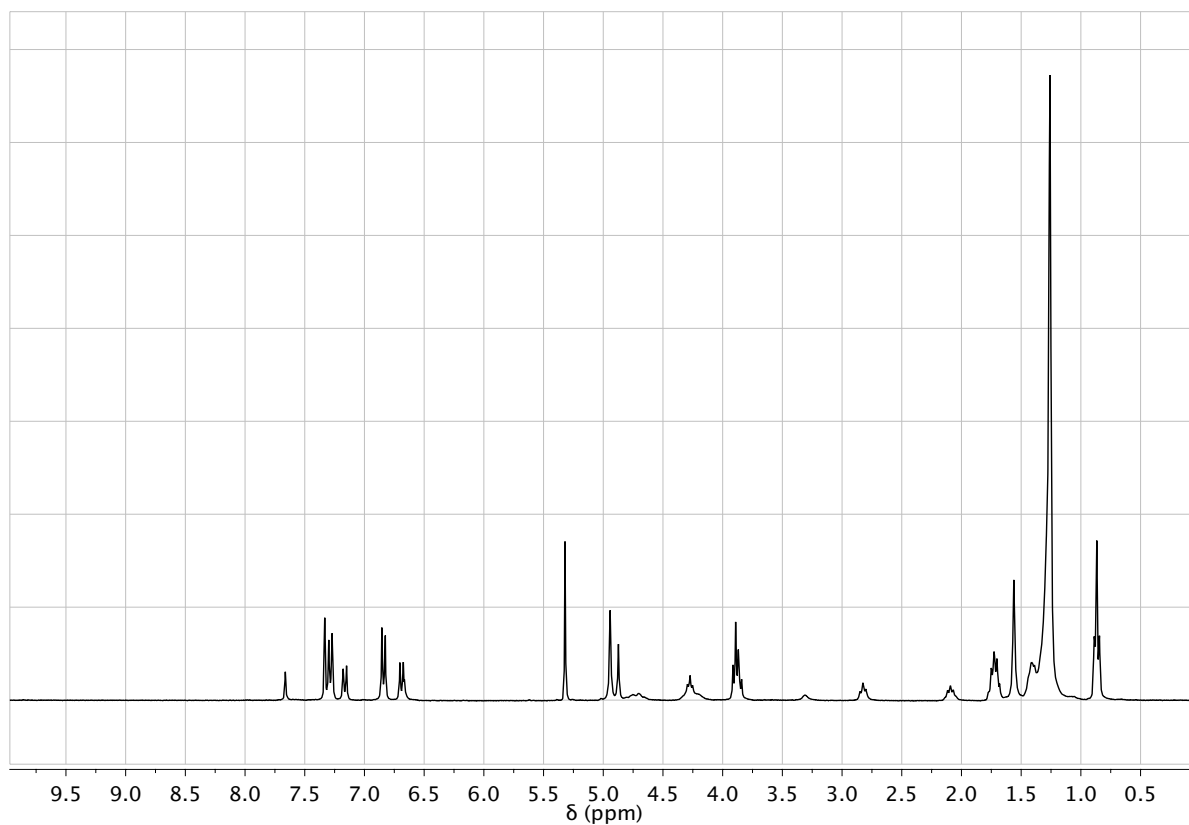
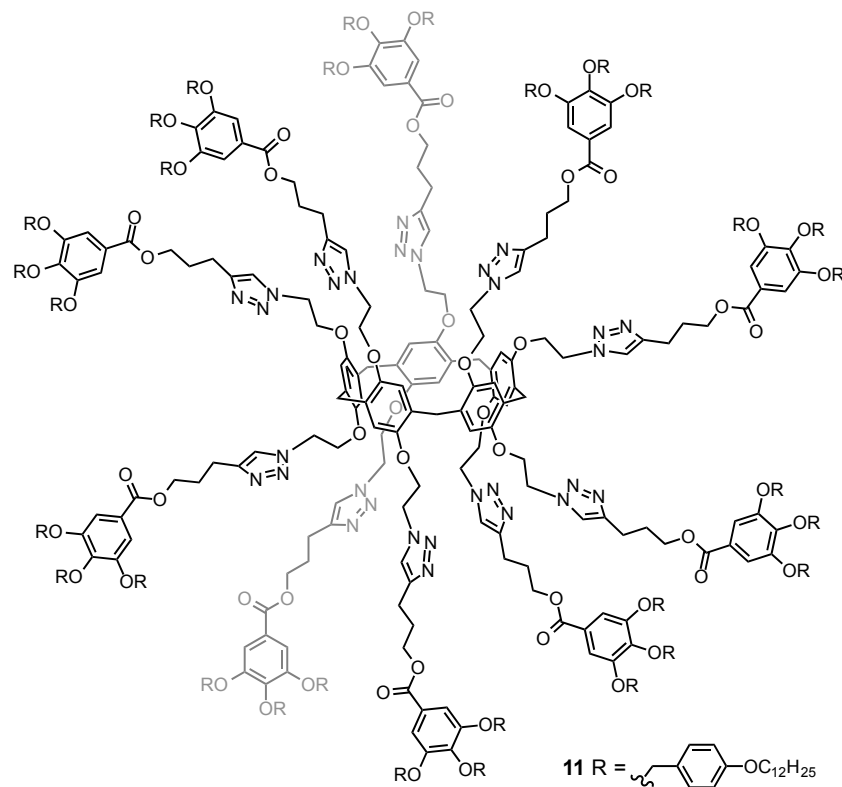


Figure S4a. ^1H NMR spectrum of compound **11** (CD_2Cl_2 , 300 MHz).

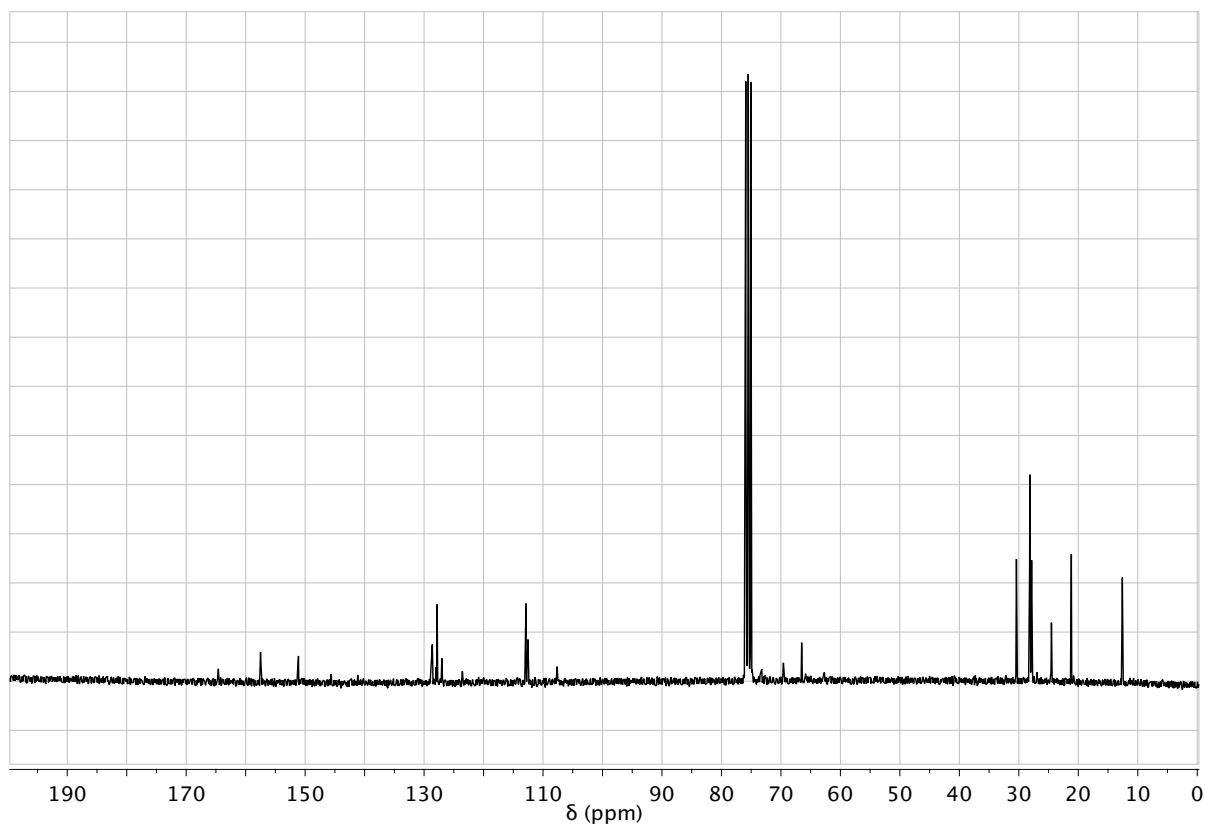
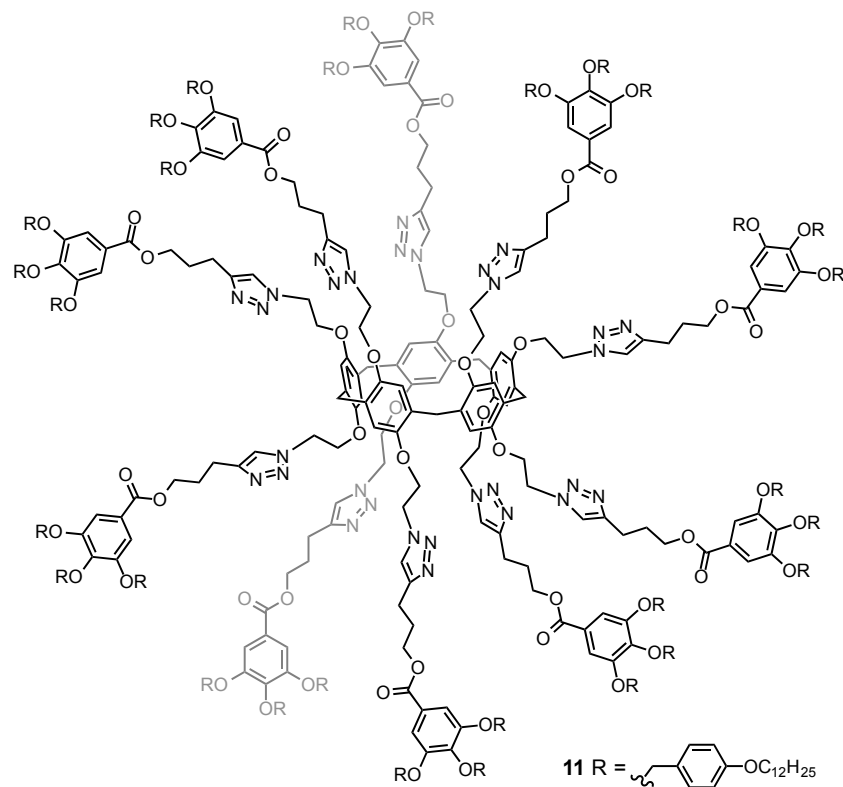


Figure S4b. ¹³C NMR spectrum of compound **11** (CD₂Cl₂, 75 MHz).

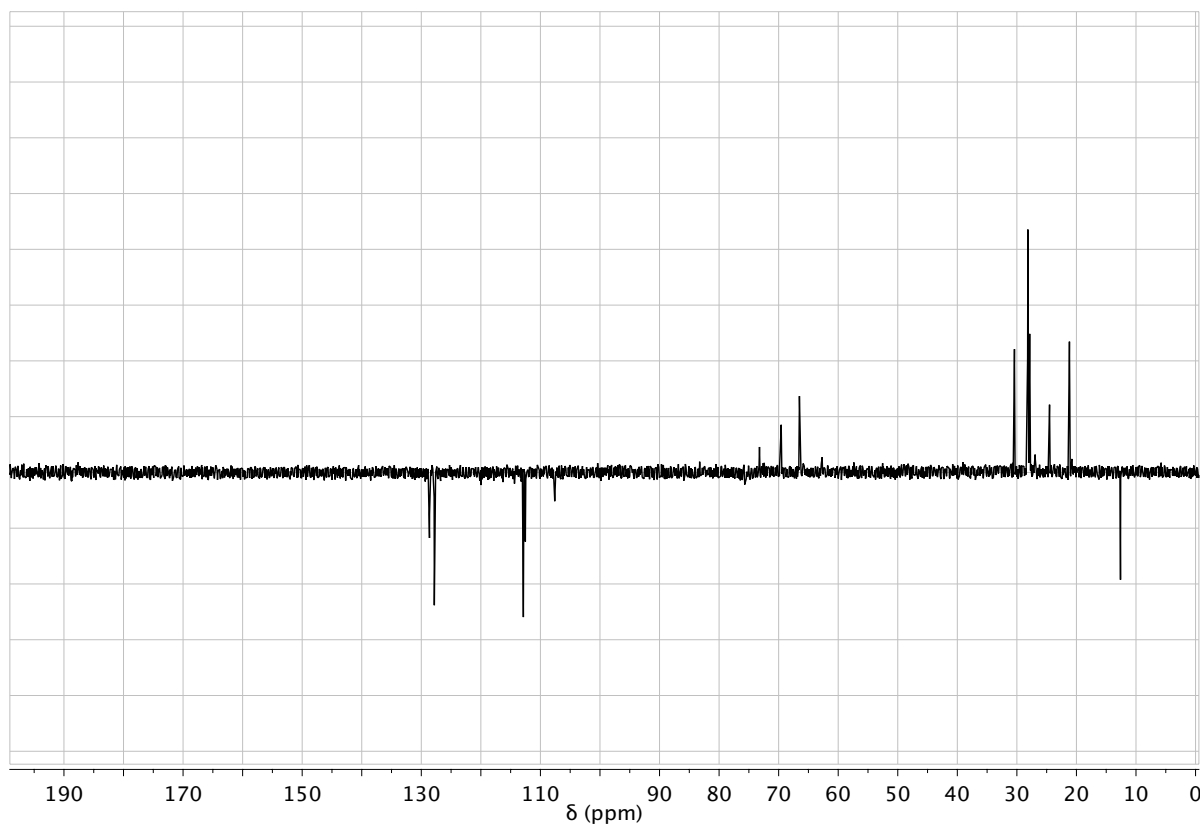
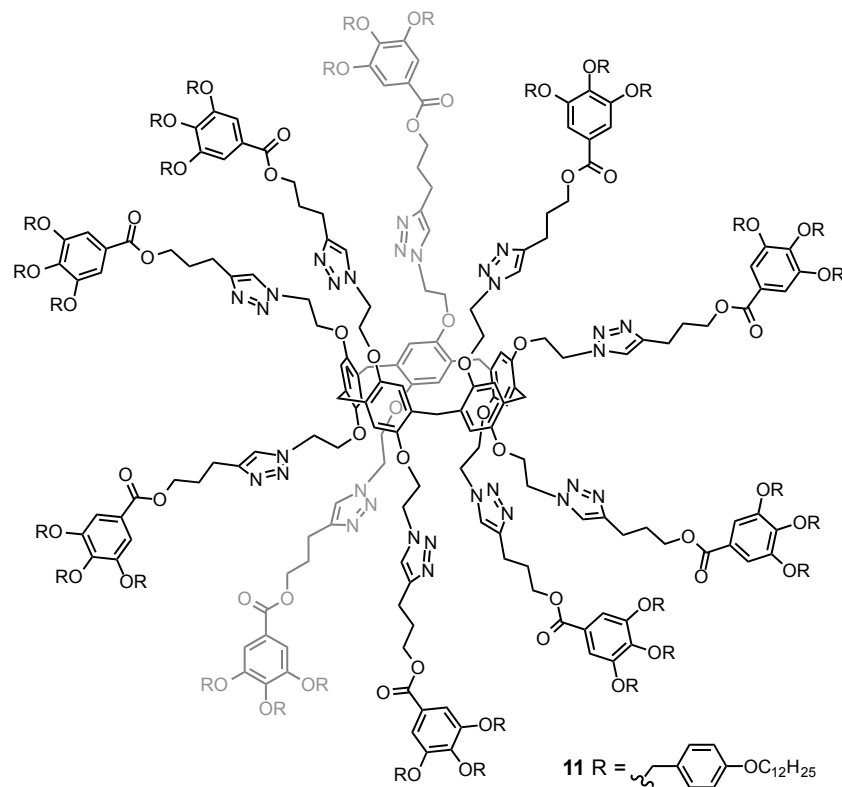


Figure S4c. DEPT of compound **11** (CD_2Cl_2 , 75 MHz).

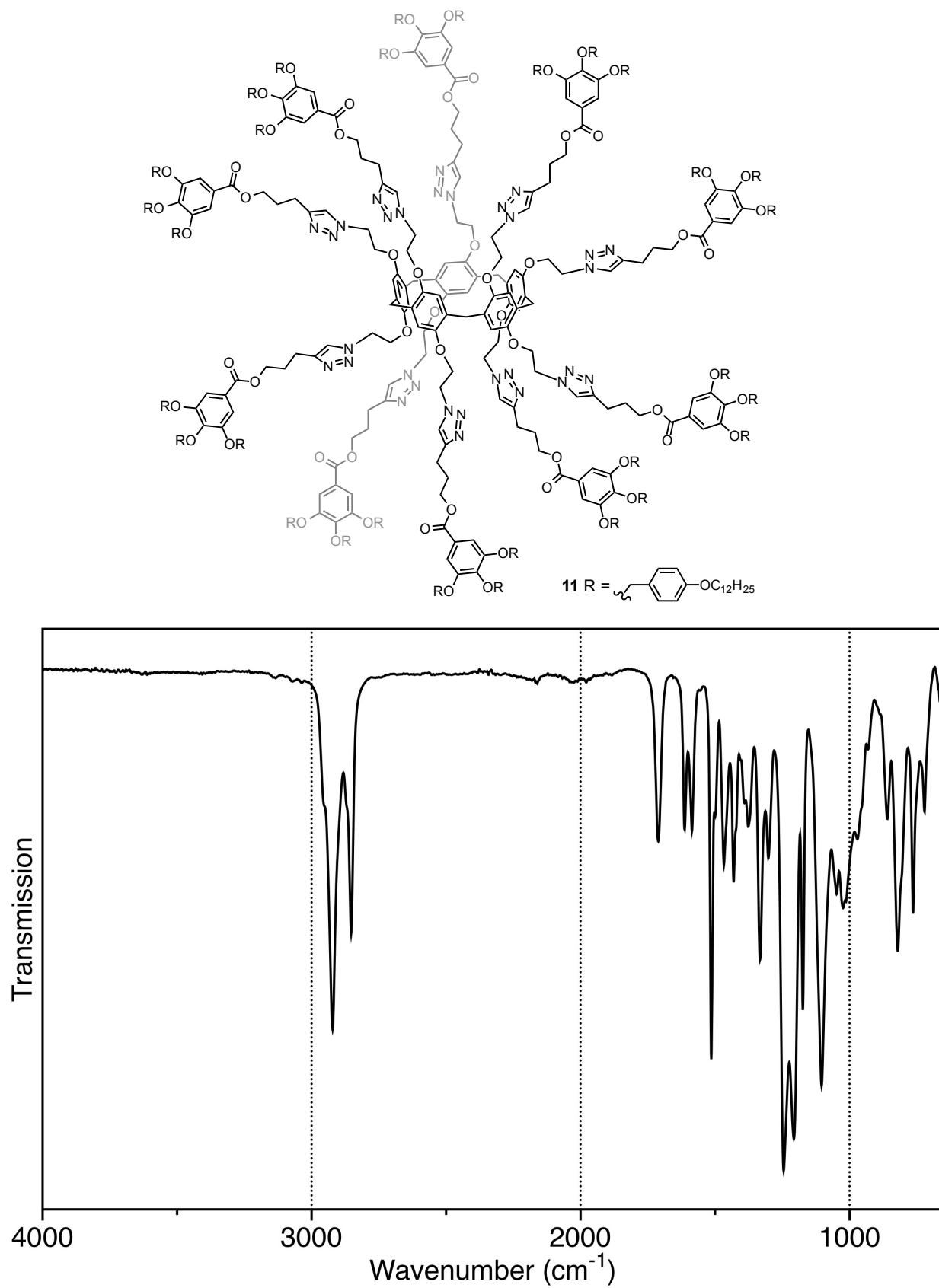


Figure S4d. IR spectrum of compound 11.

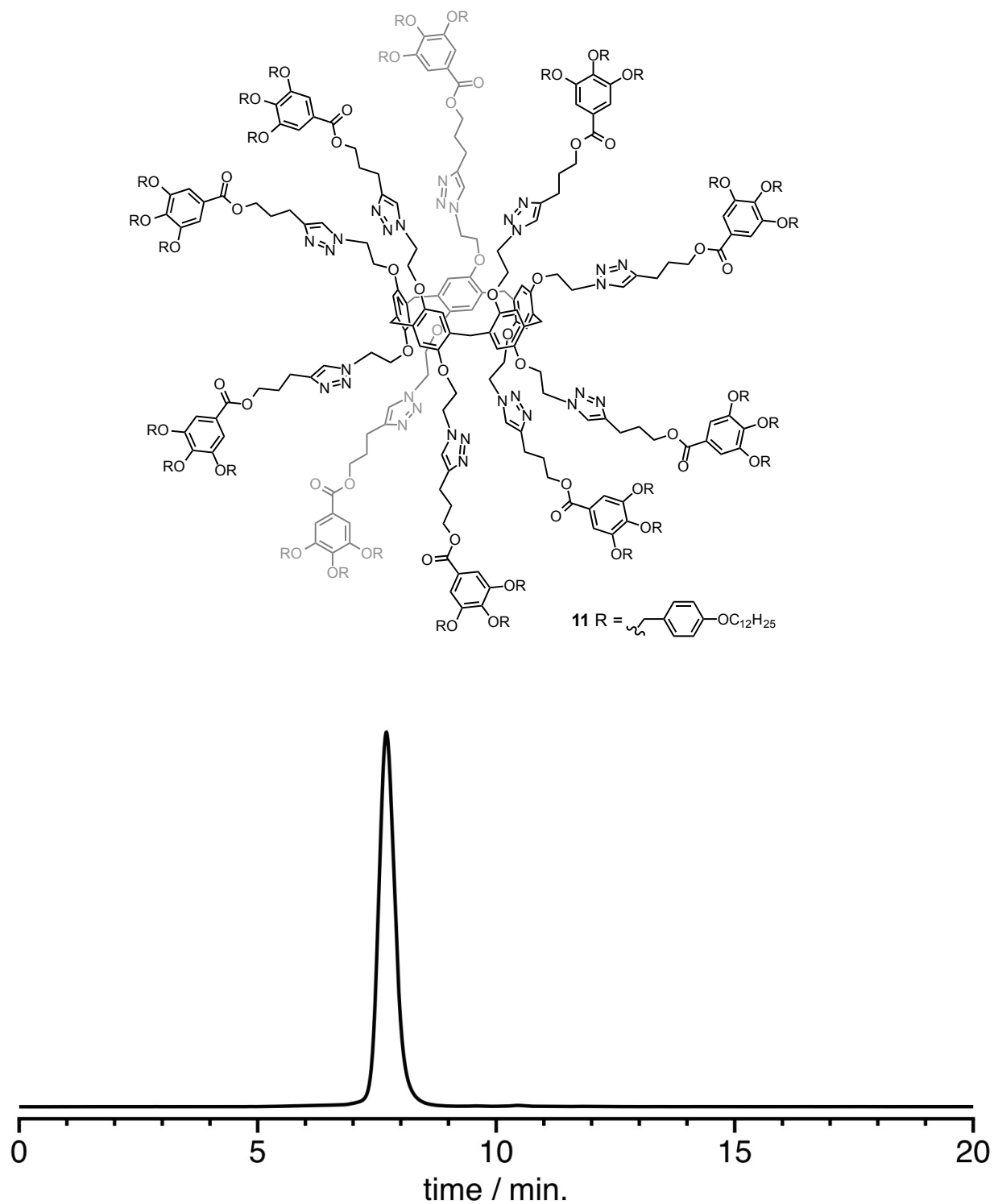


Figure S4e. HPLC trace on a size exclusion column (PLgel, CH_2Cl_2 , UV detector at $\lambda = 254$ nm) obtained for compound **11**.

S2. Supporting information (Chapter 3)

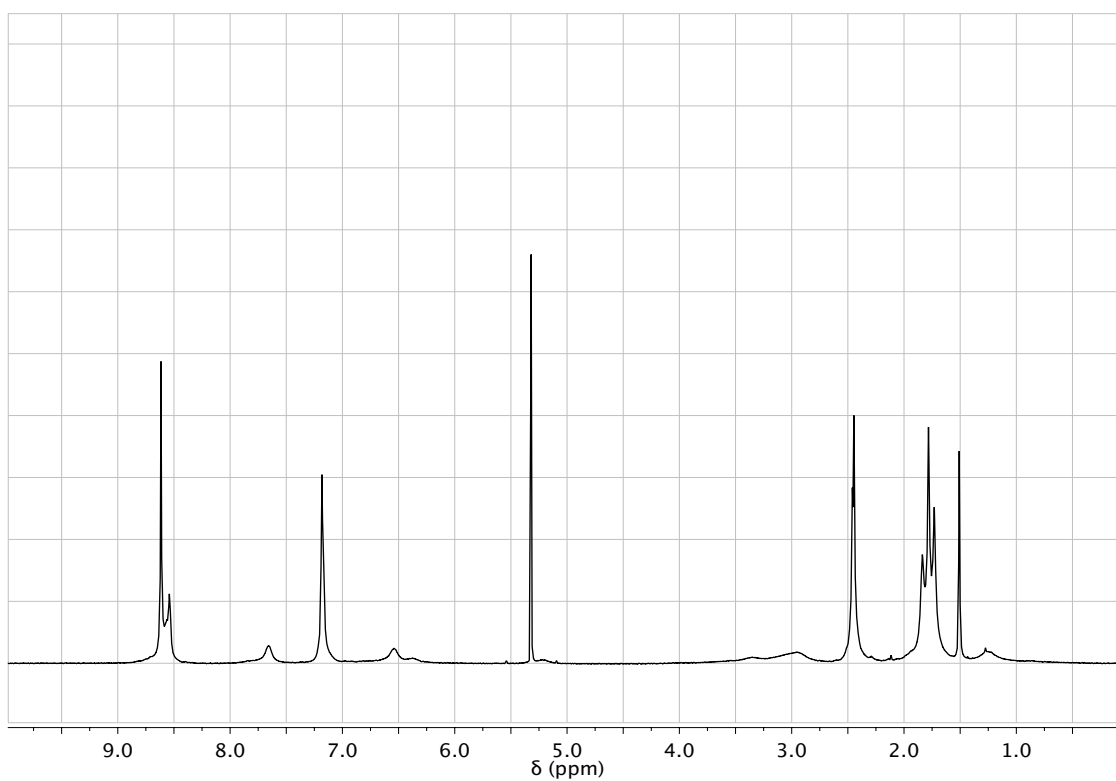
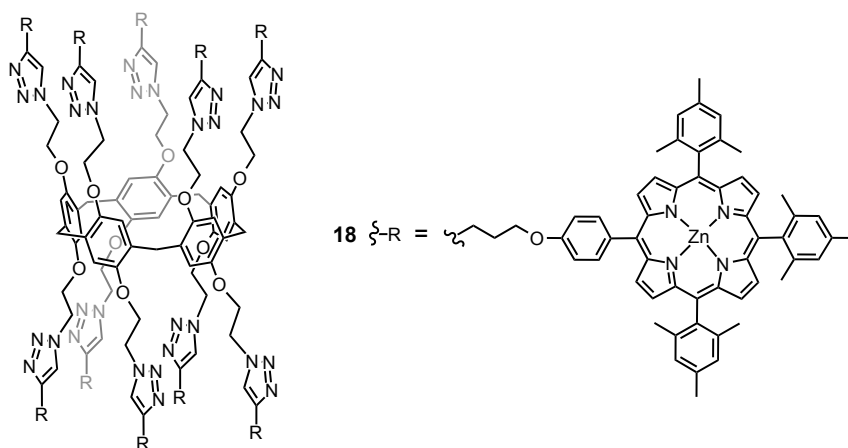


Figure S1a. ^1H NMR spectrum of compound **18** (CD_2Cl_2 , 400 MHz) at 25°C.

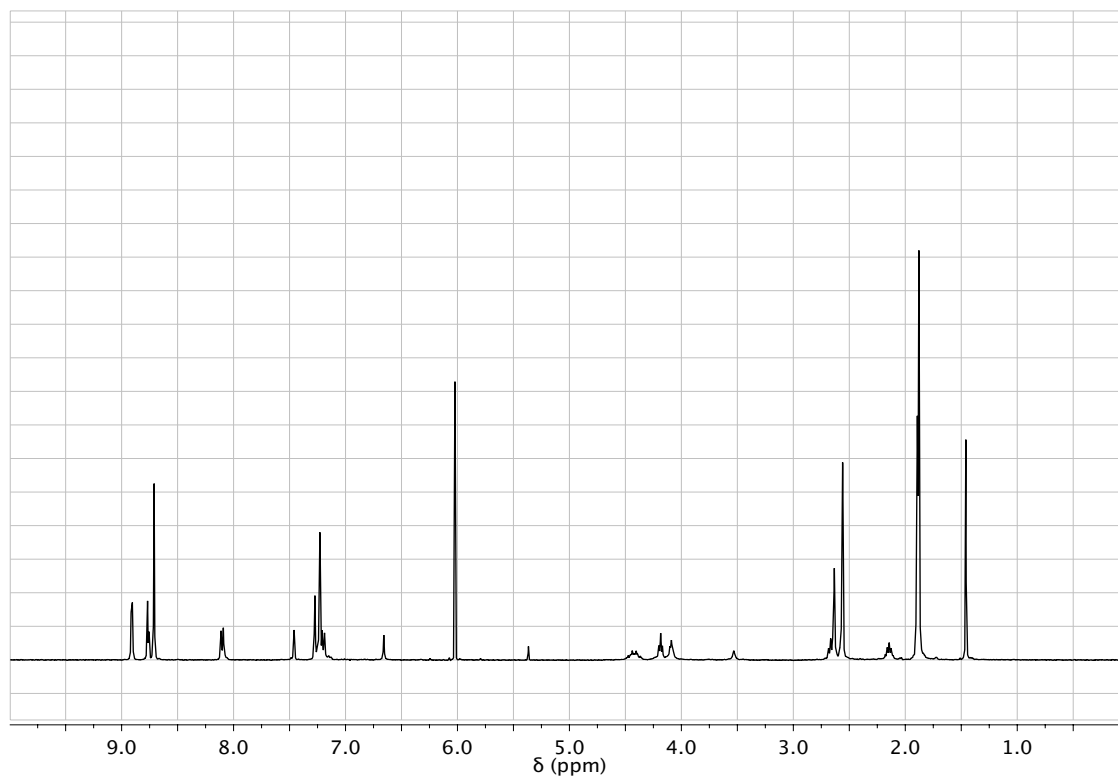
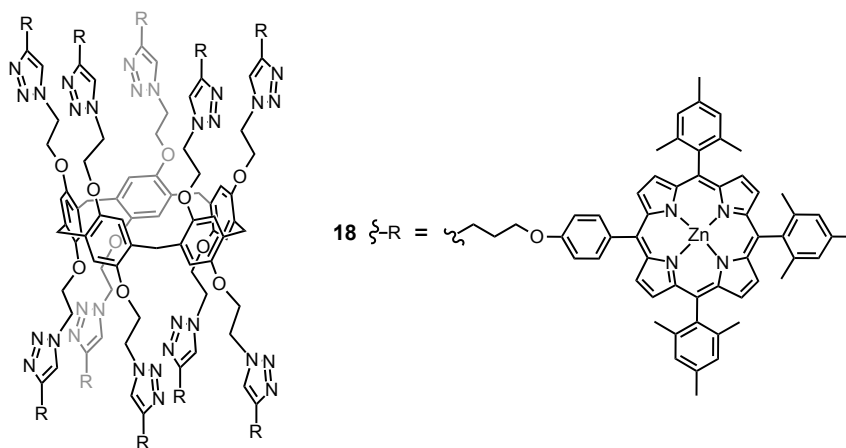


Figure S1b. ^1H NMR spectrum of compound **18** ($\text{C}_2\text{D}_2\text{Cl}_4$, 400 MHz) at 105°C.

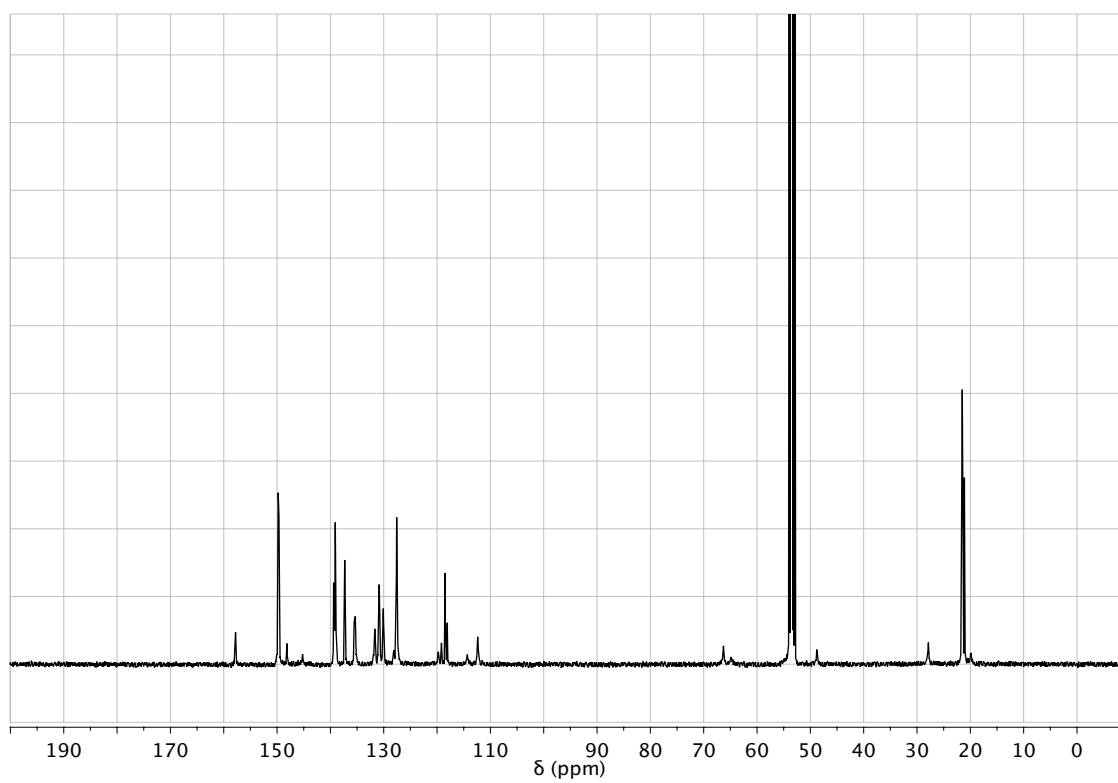
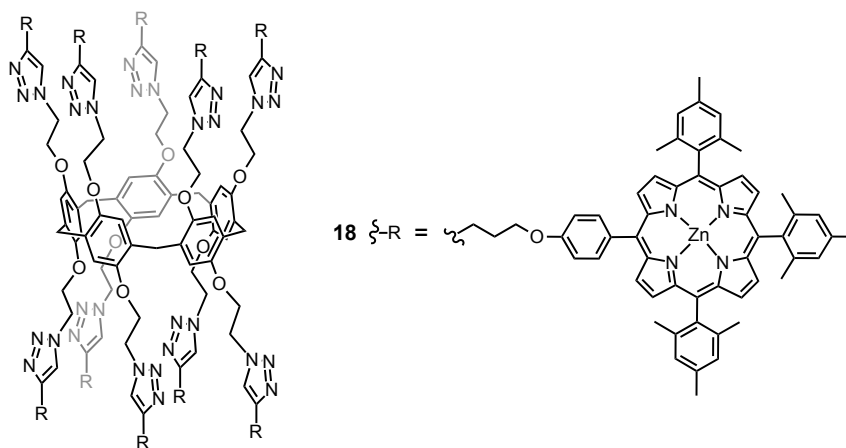


Figure S1c. ^{13}C NMR spectrum of compound **18** (CD_2Cl_2 , 100 MHz).

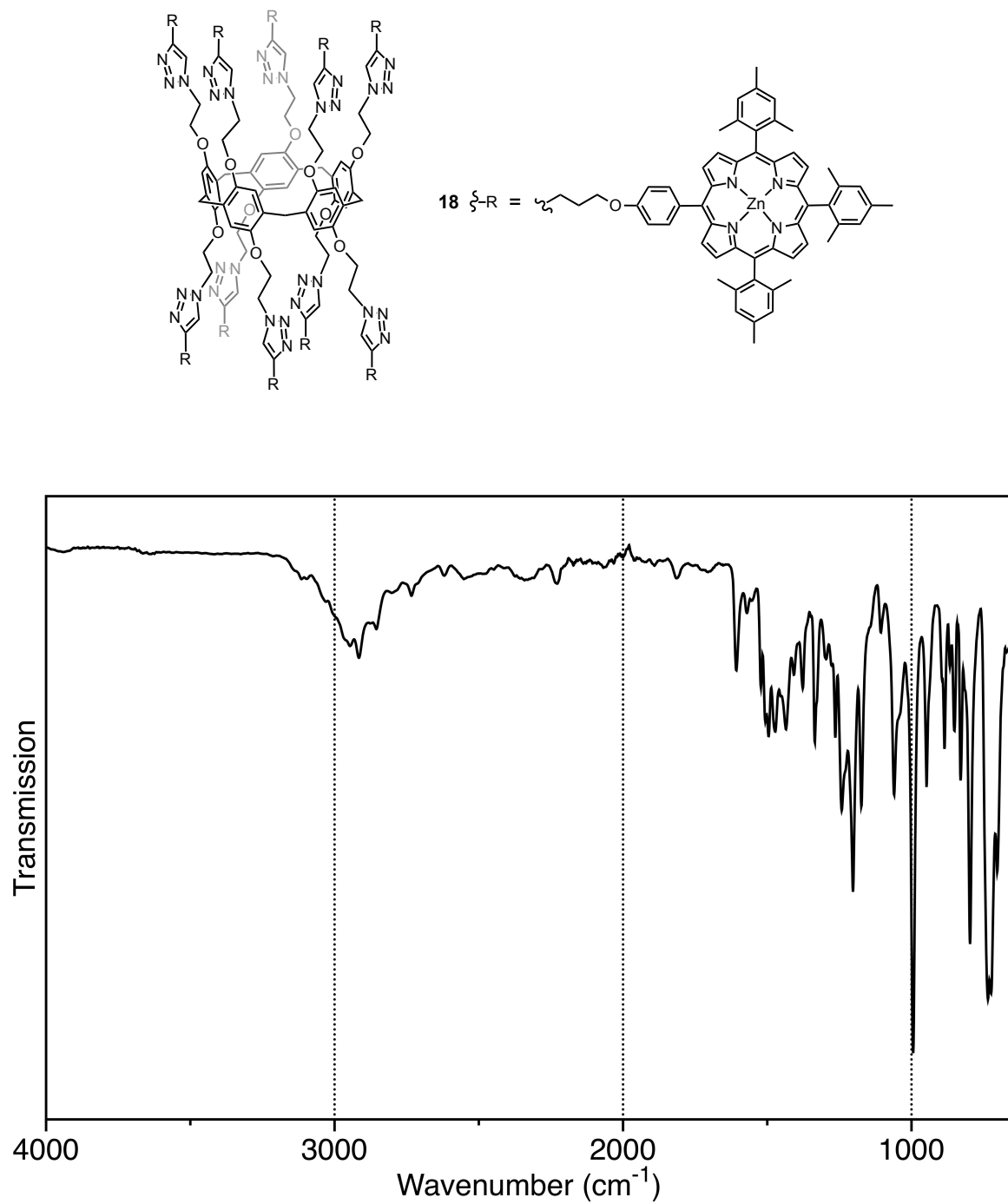


Figure S1d. IR spectrum of compound **18**.

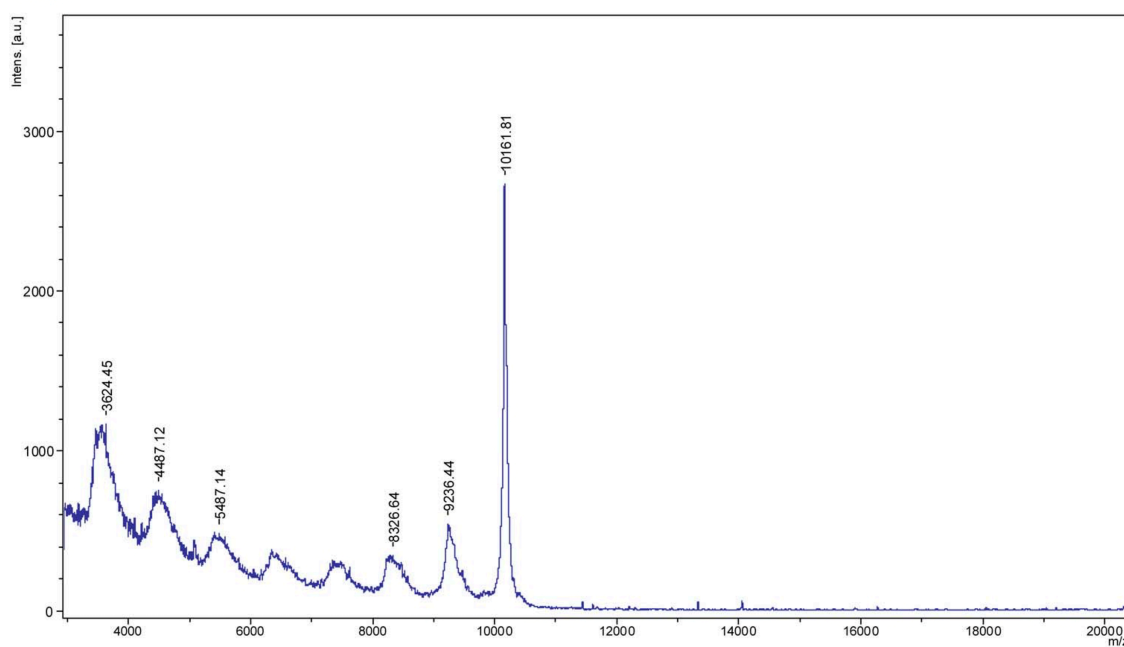
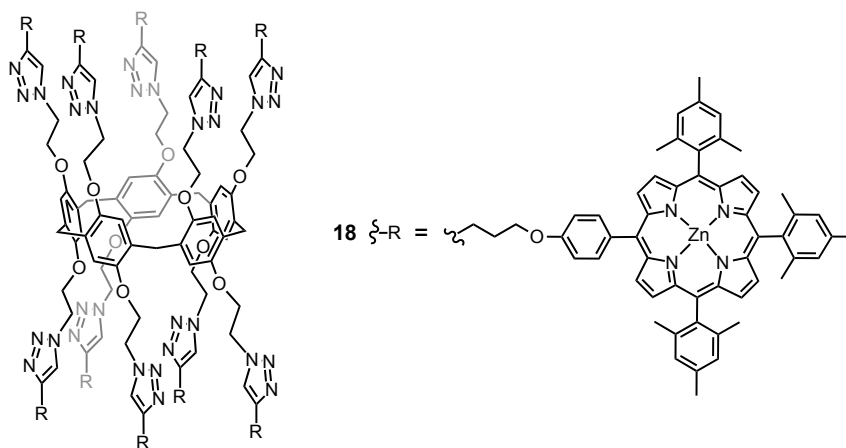


Figure S1e. MALDI-TOF mass spectrum of compound **18**.

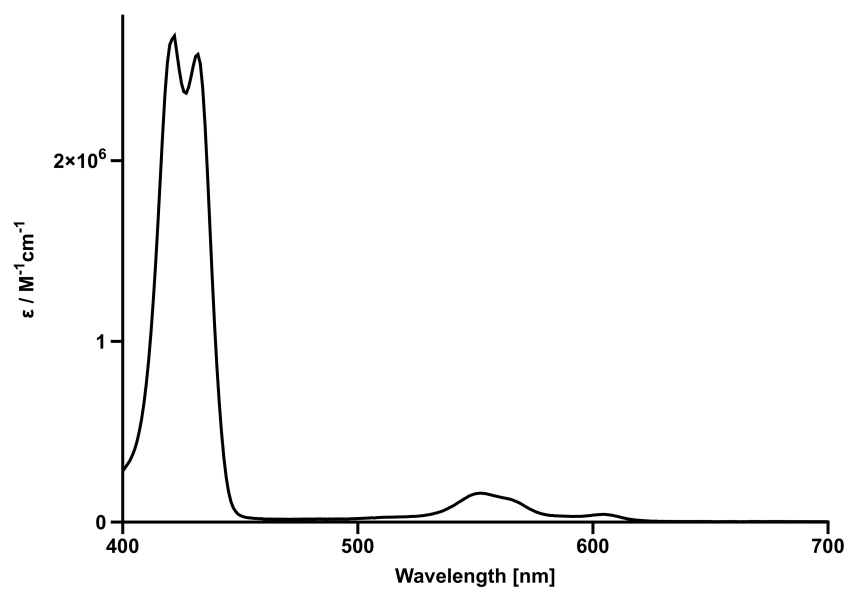
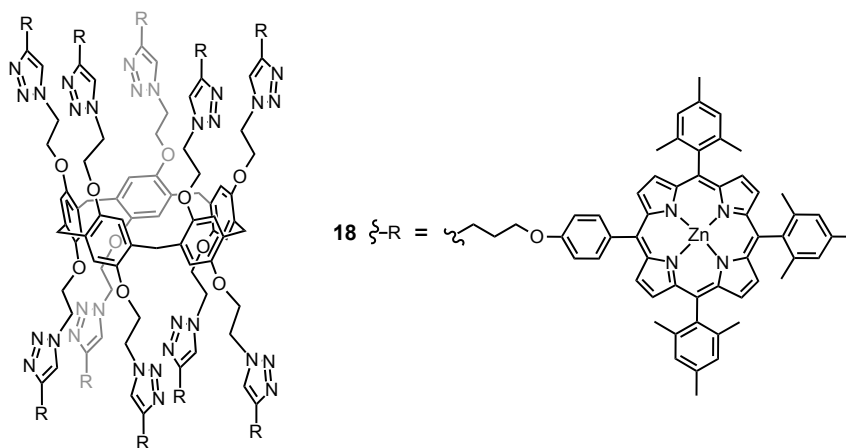


Figure S1f. UV/vis spectrum of compound **18** (CH_2Cl_2).

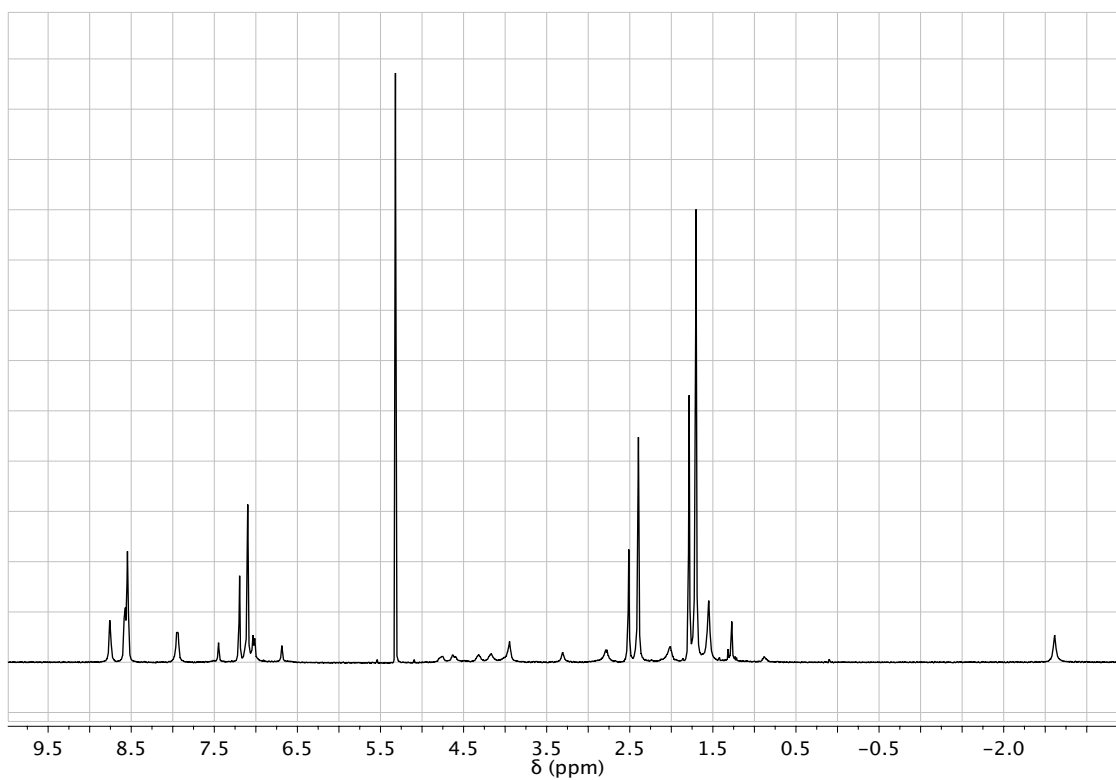
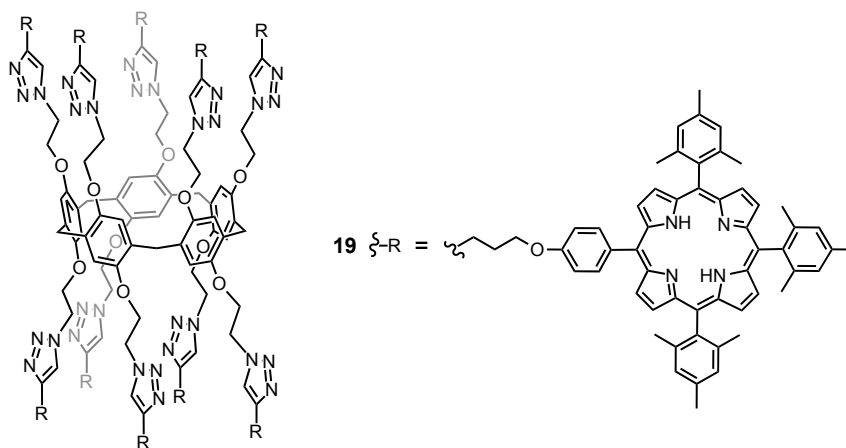


Figure S2a. ^1H NMR spectrum of compound **19** (CD_2Cl_2 , 400 MHz) at 25°C.

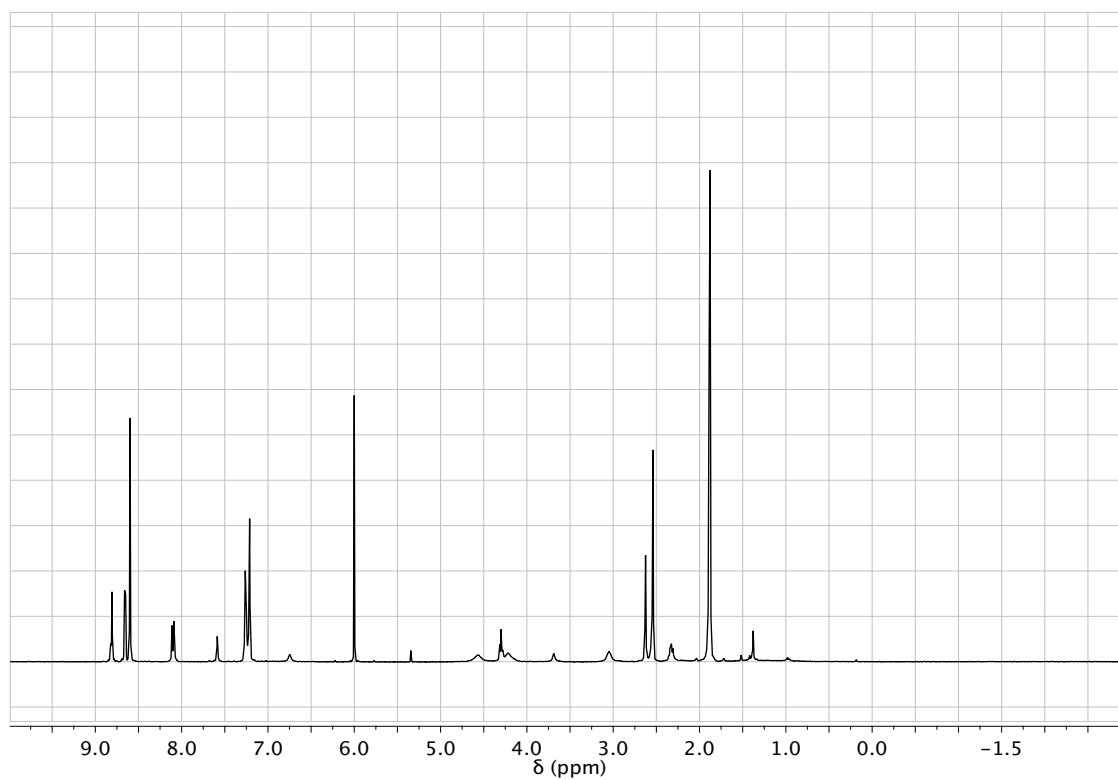
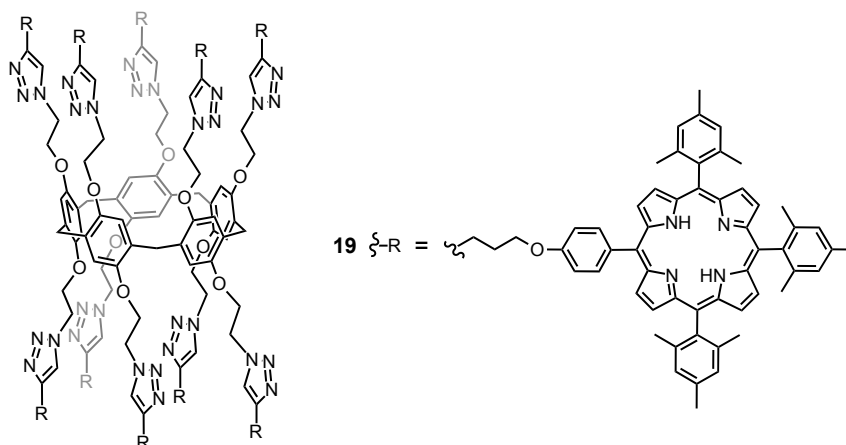


Figure S2b. ^1H NMR spectrum of compound **19** ($\text{C}_2\text{D}_2\text{Cl}_4$, 400 MHz) at 105°C.

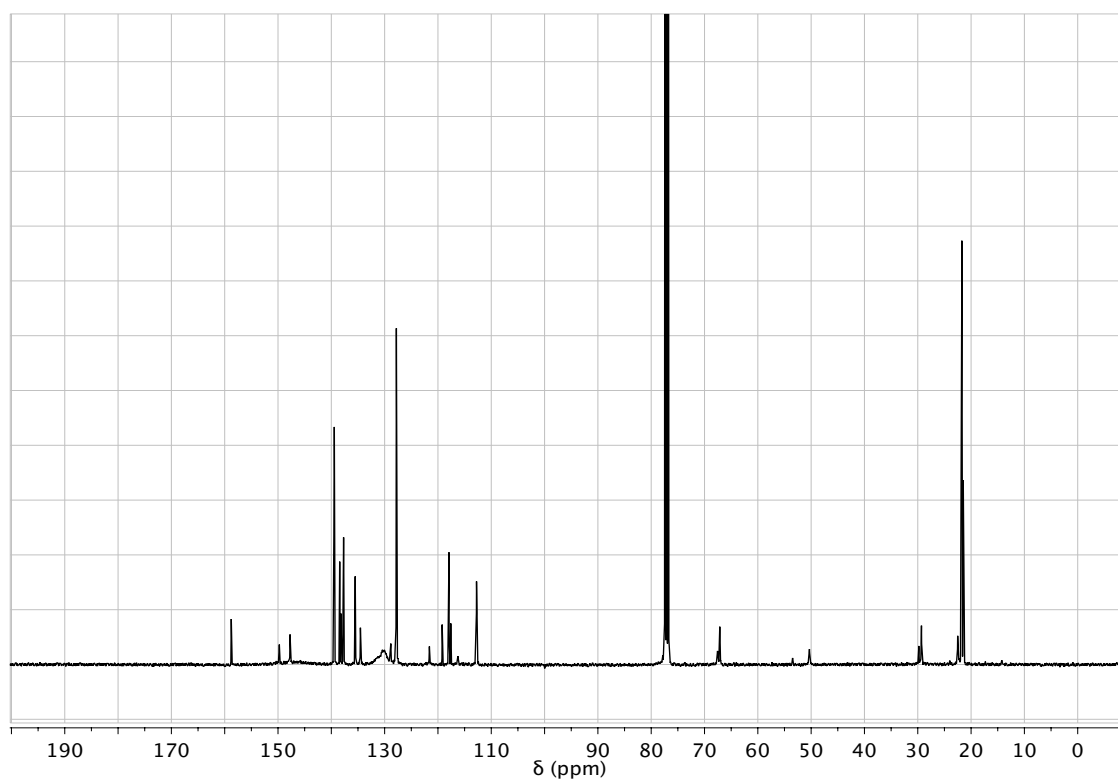
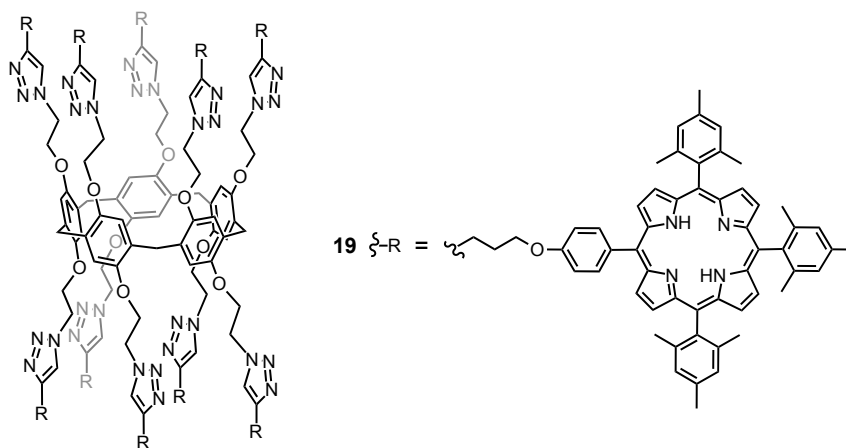


Figure S2c. ^{13}C NMR spectrum of compound **19** (CDCl_3 , 100 MHz).

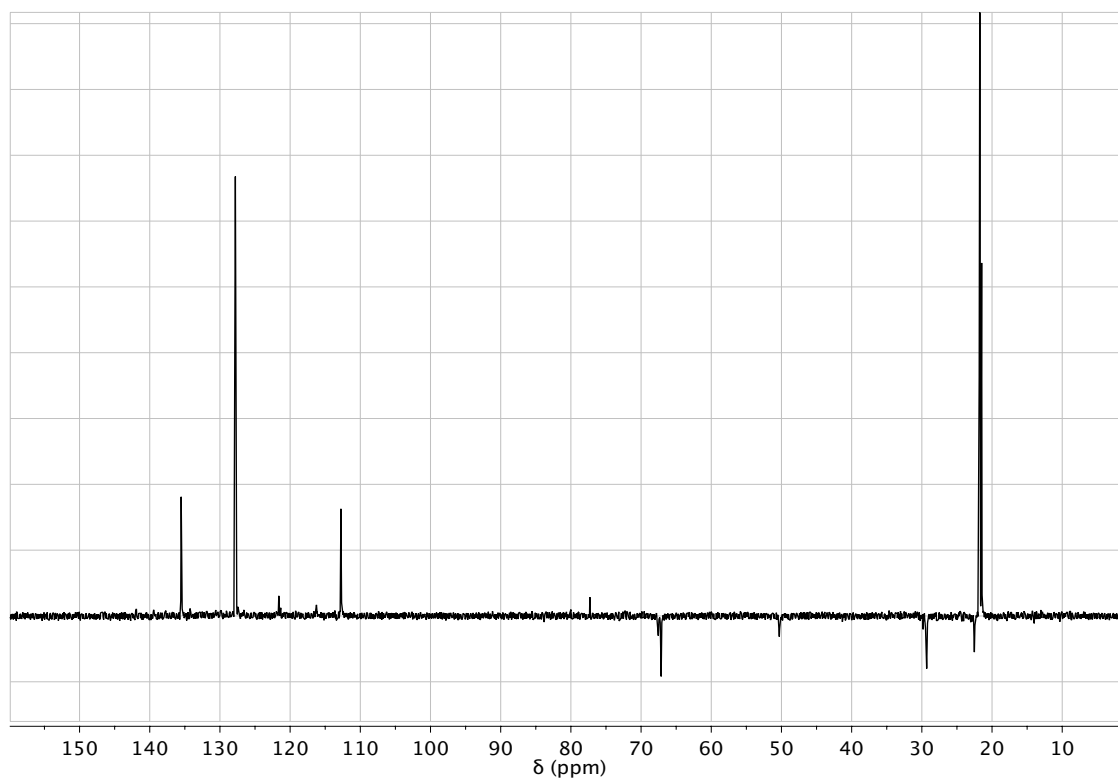
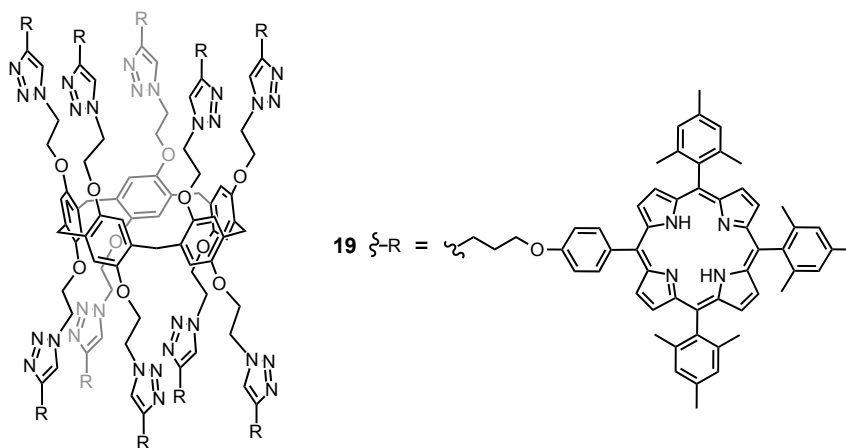


Figure S2d. DEPT spectrum of compound **19** (CDCl_3 , 100 MHz).

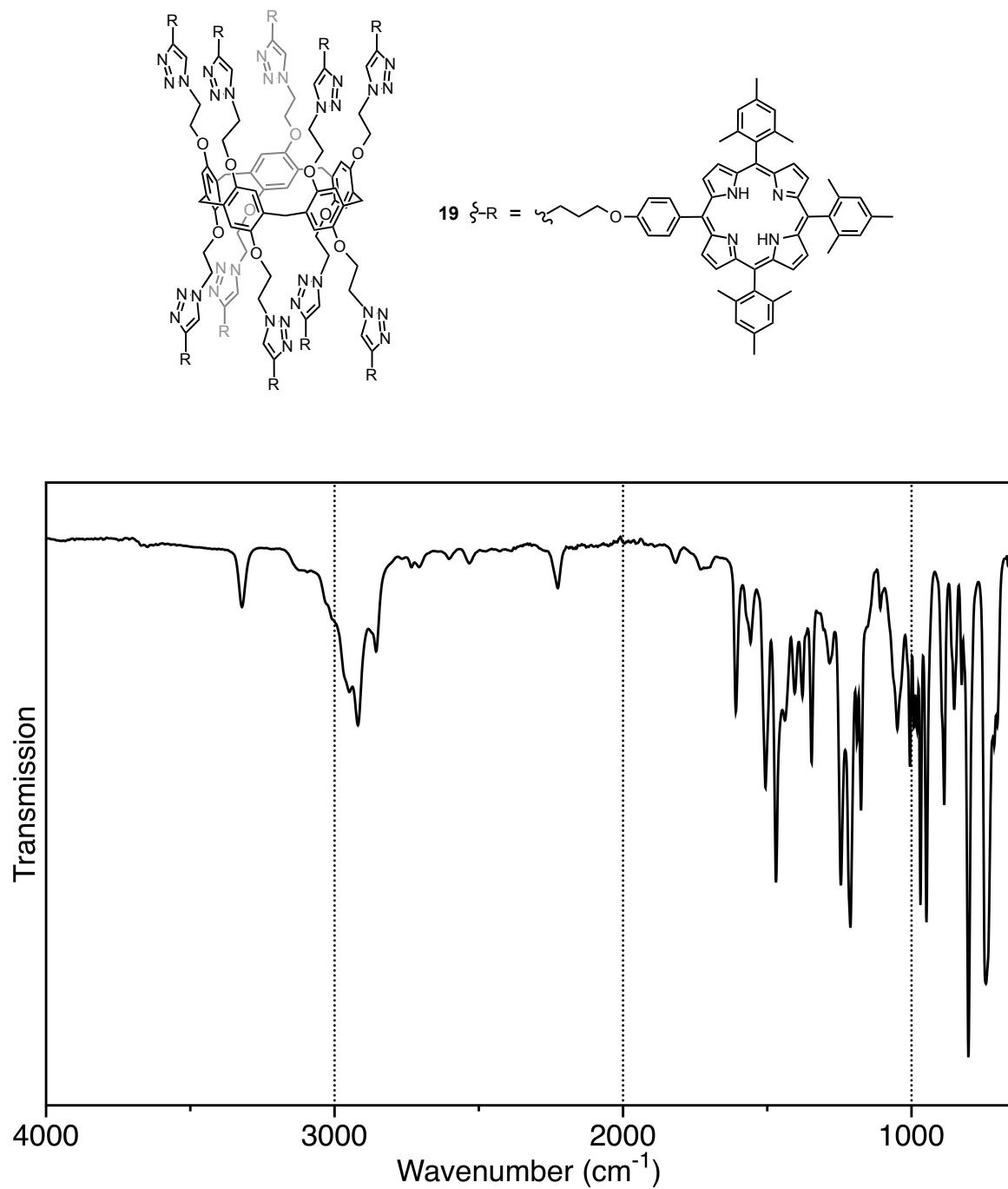


Figure S2e. IR spectrum of compound **19**.

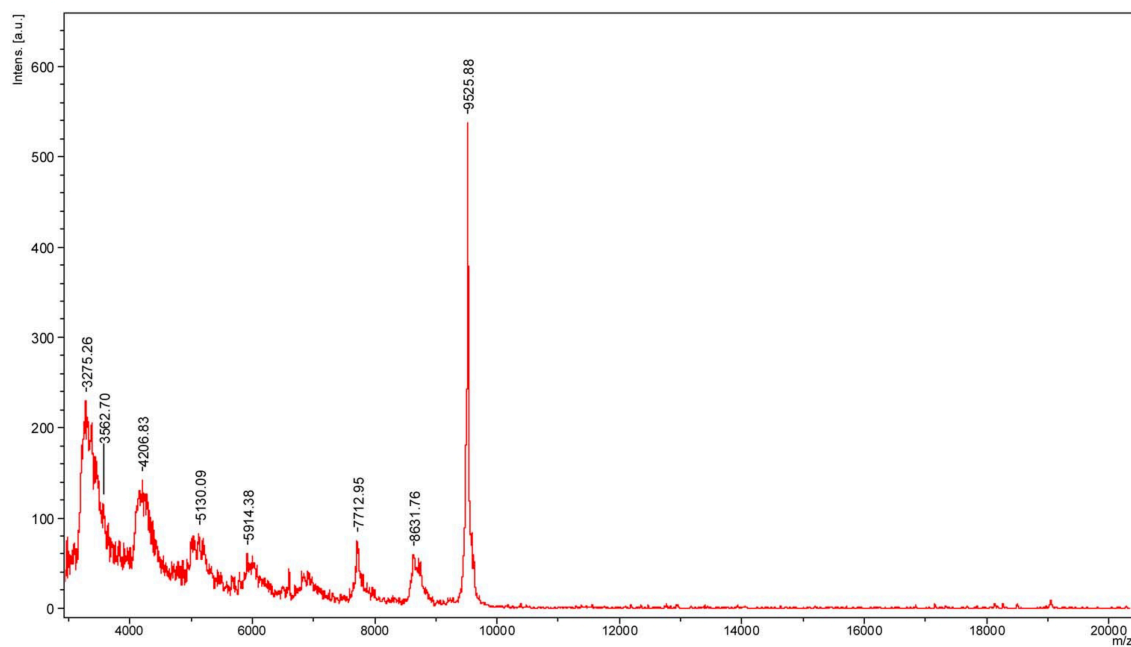
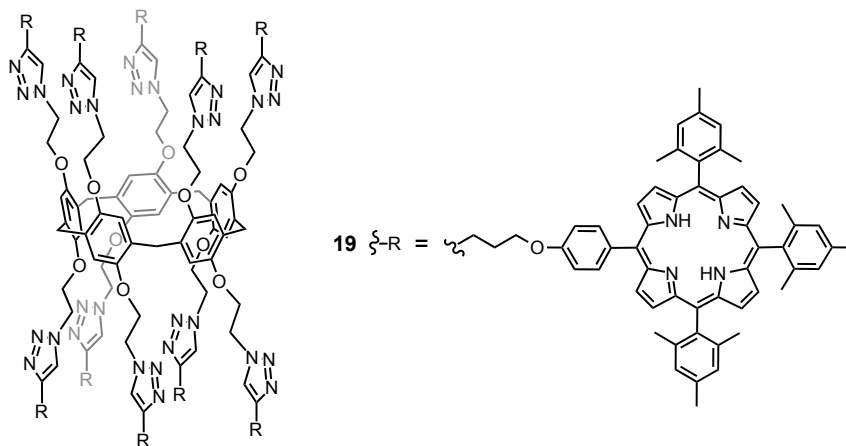


Figure S2f. MALDI-TOF mass spectrum of compound **19**.

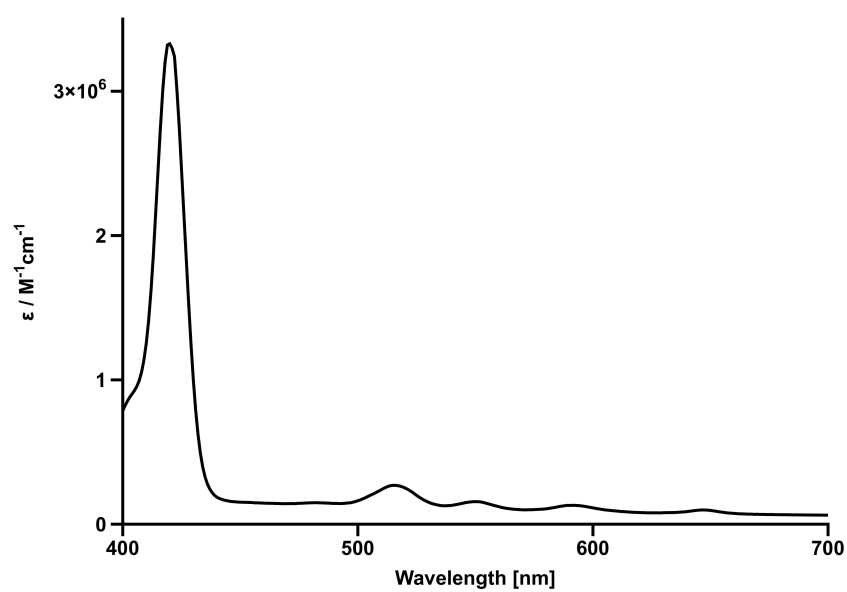
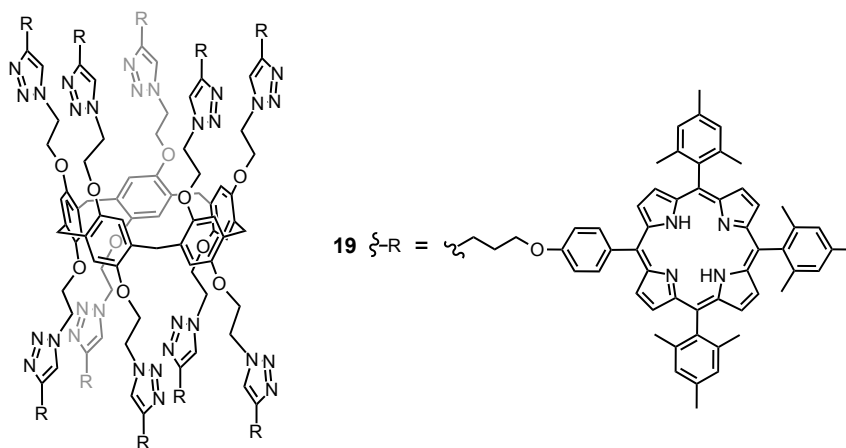


Figure S2g. UV/vis spectrum of compound **19** (CH_2Cl_2).

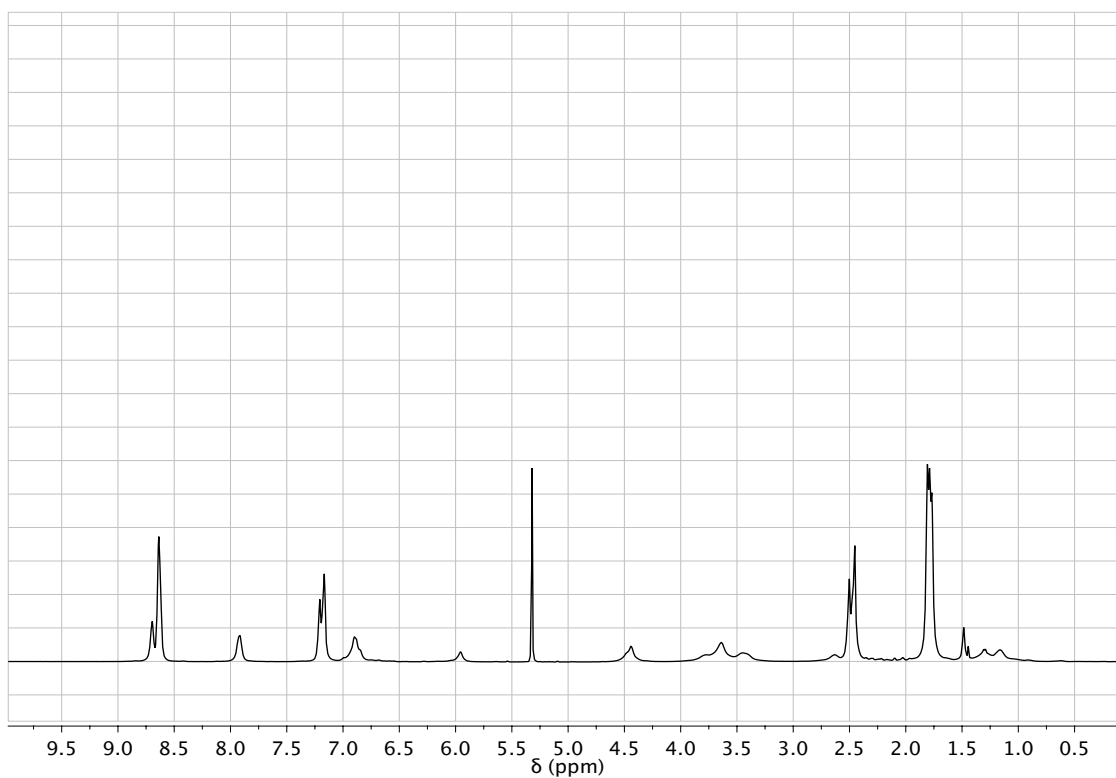
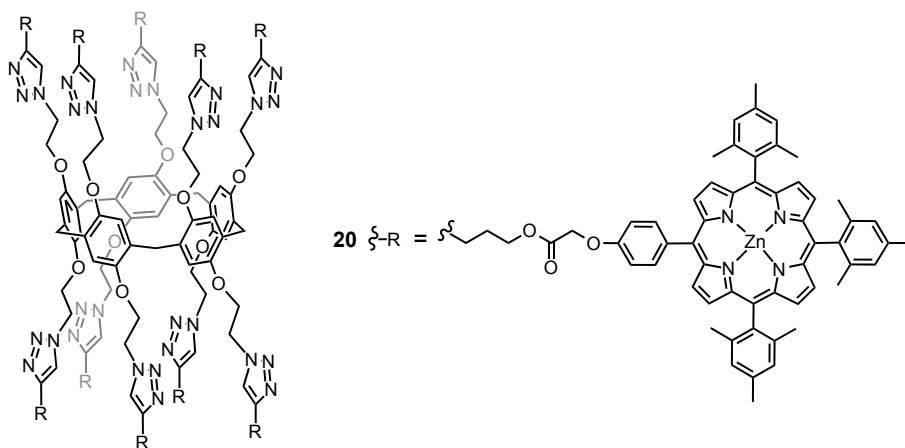


Figure S3a. ^1H NMR spectrum of compound **20** (CD_2Cl_2 , 400 MHz) at 25°C.

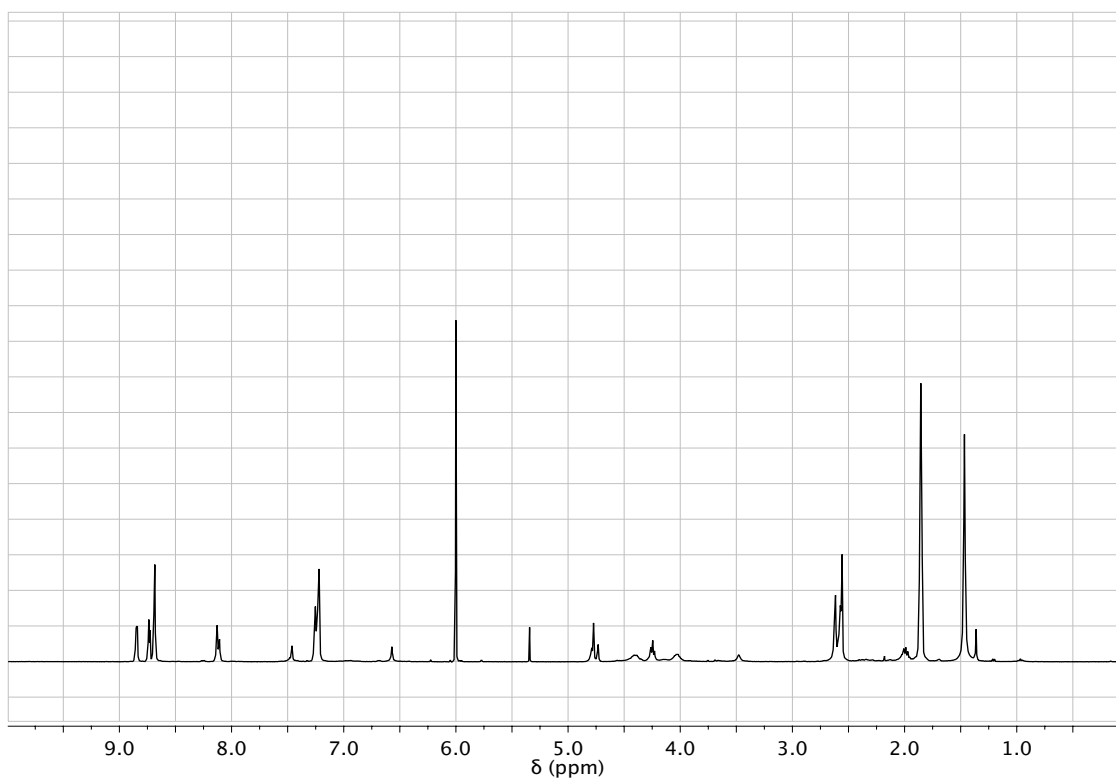
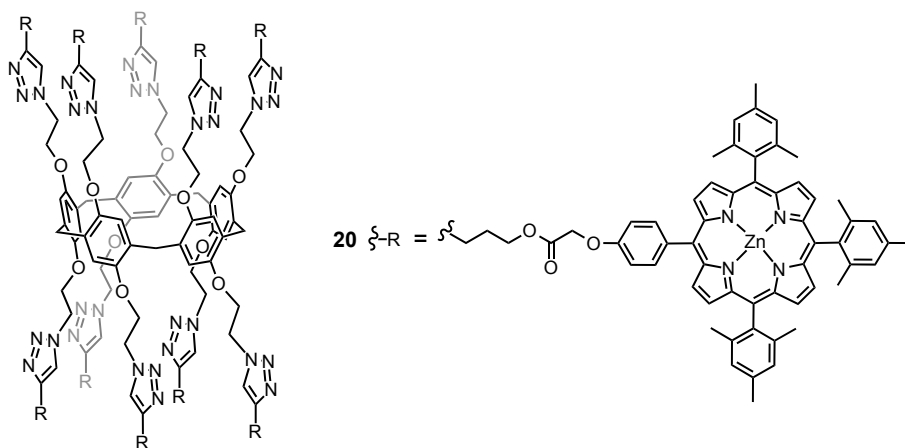


Figure S3b. ¹H NMR spectrum of compound **20** (C₂D₂Cl₄, 400 MHz) at 100°C.

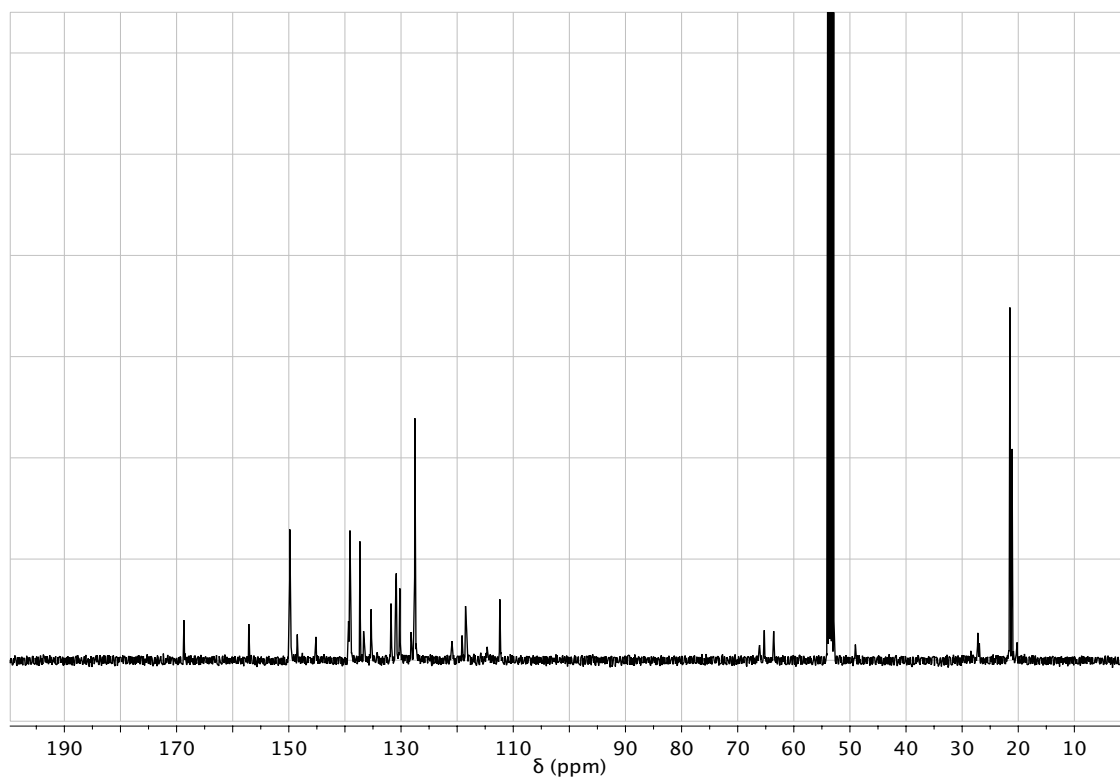
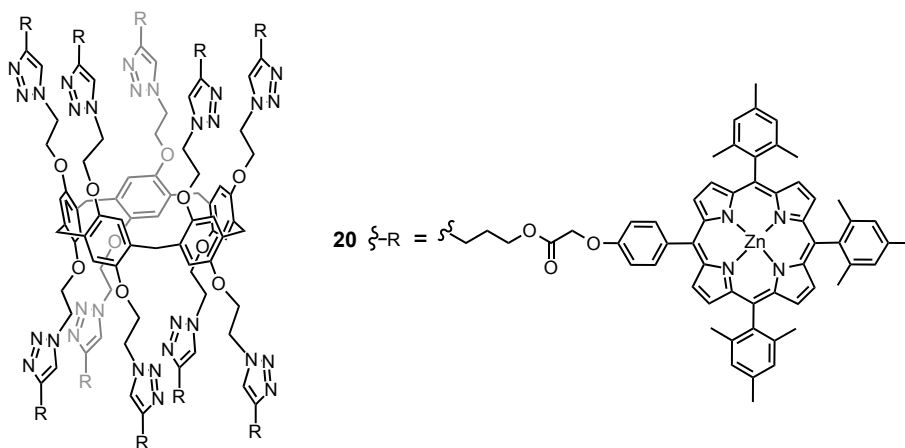


Figure S3c. ^{13}C NMR spectrum of compound **20** (CD_2Cl_2 , 100 MHz).

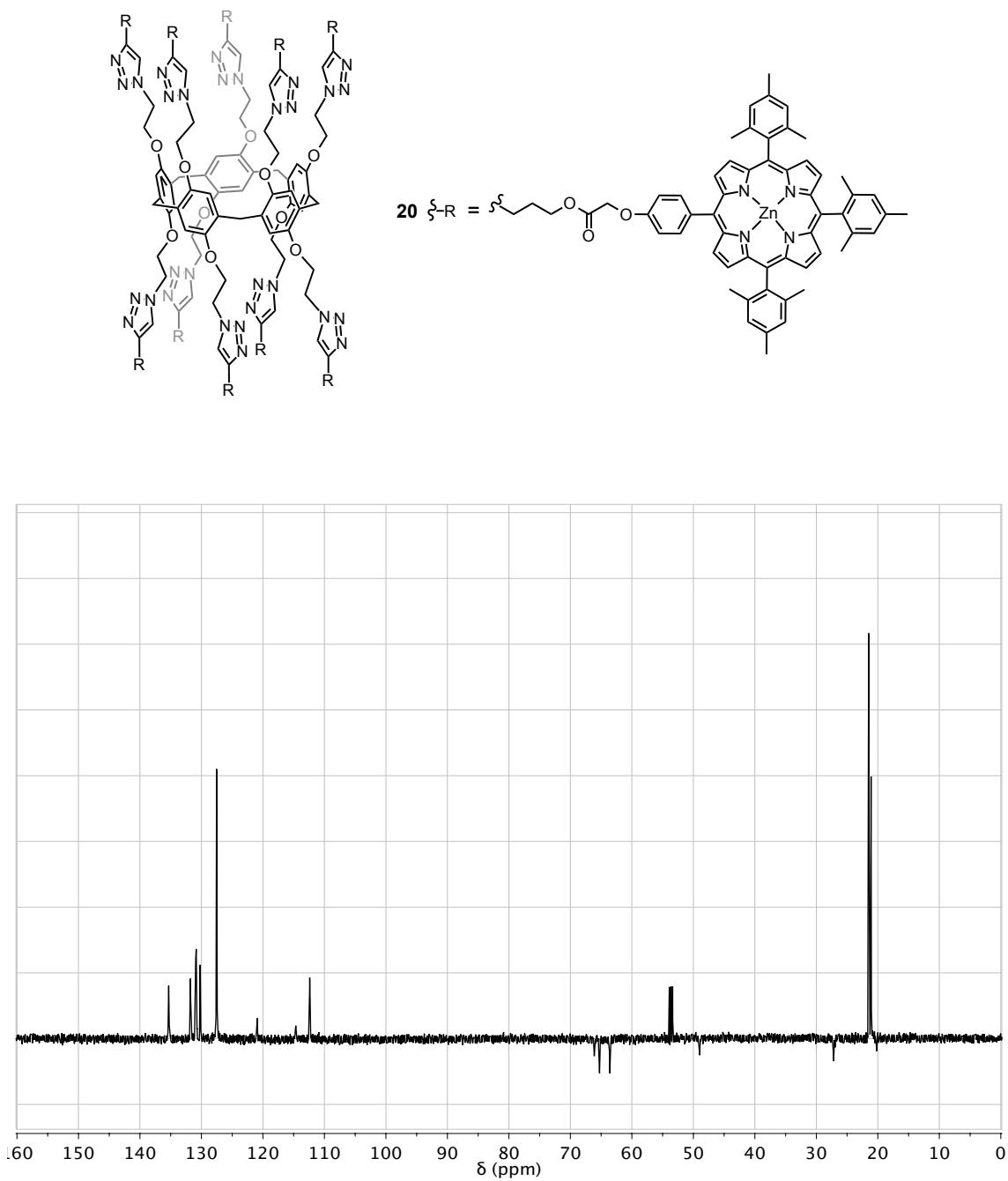
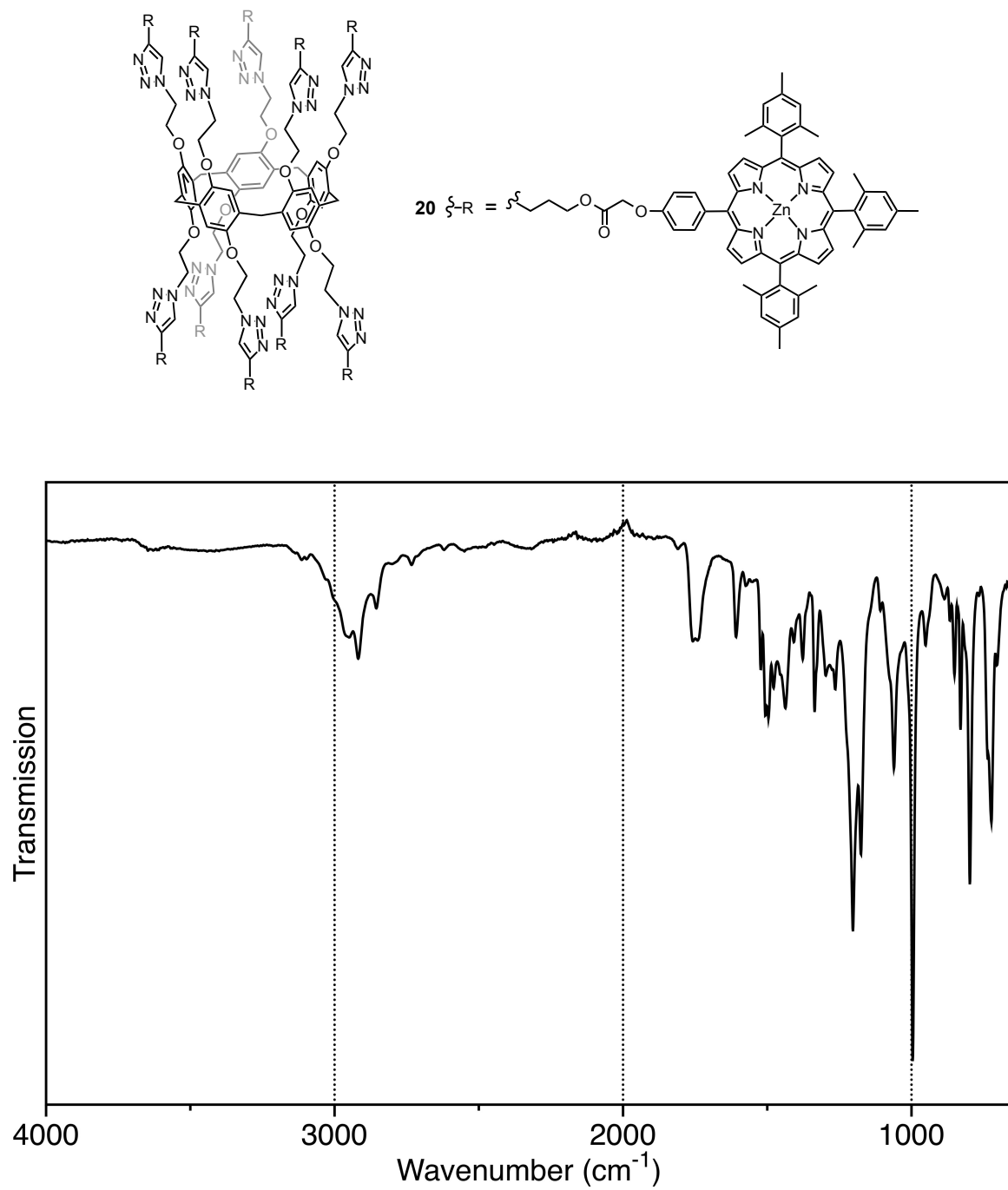


Figure S3d. DEPT spectrum of compound **20** (CD_2Cl_2 , 100 MHz).

**Figure S3e.** IR spectrum of compound **20**.

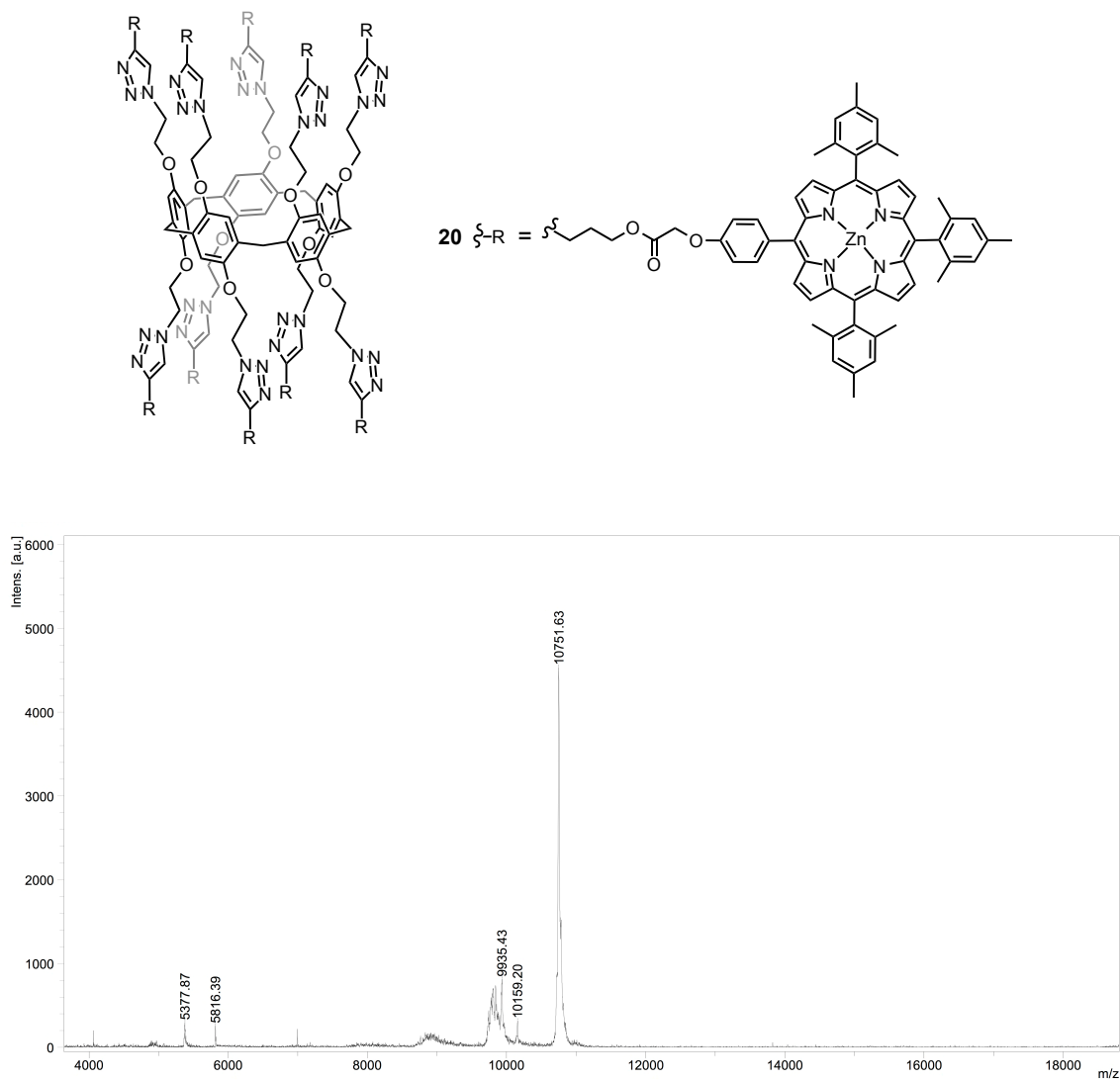


Figure S3f. MALDI-TOF mass spectrum of compound **20**.

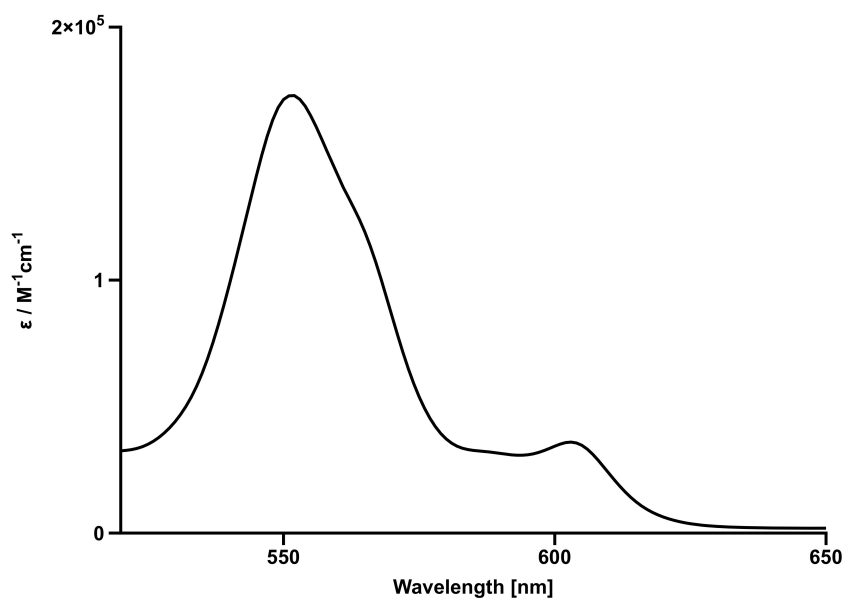
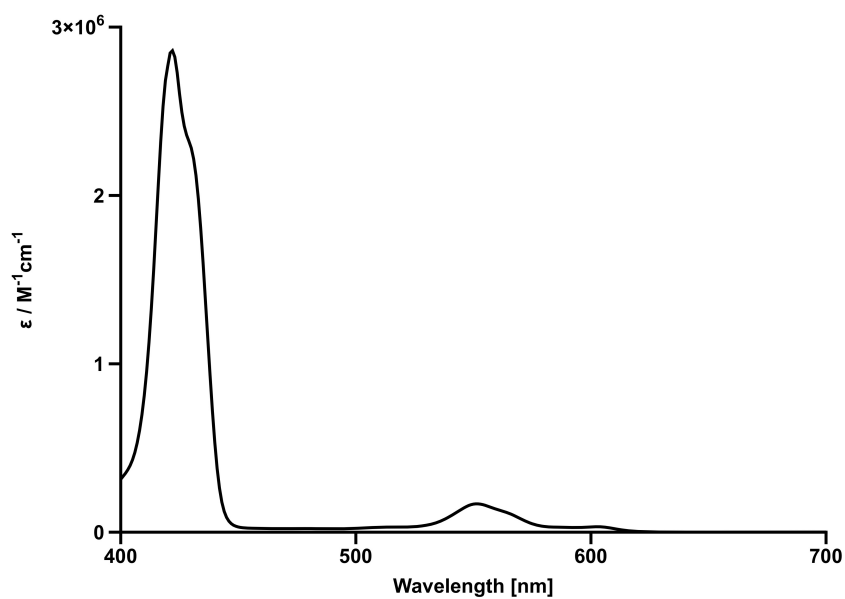
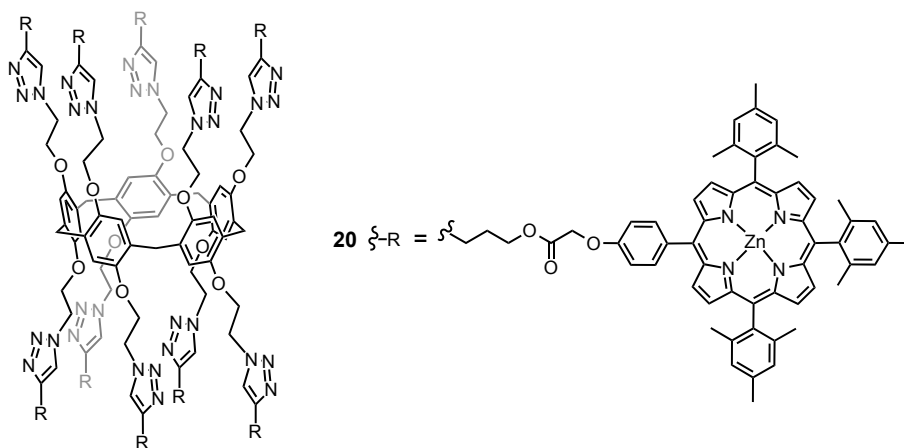


Figure S3g. UV/vis spectrum of compound **20** (CH_2Cl_2).

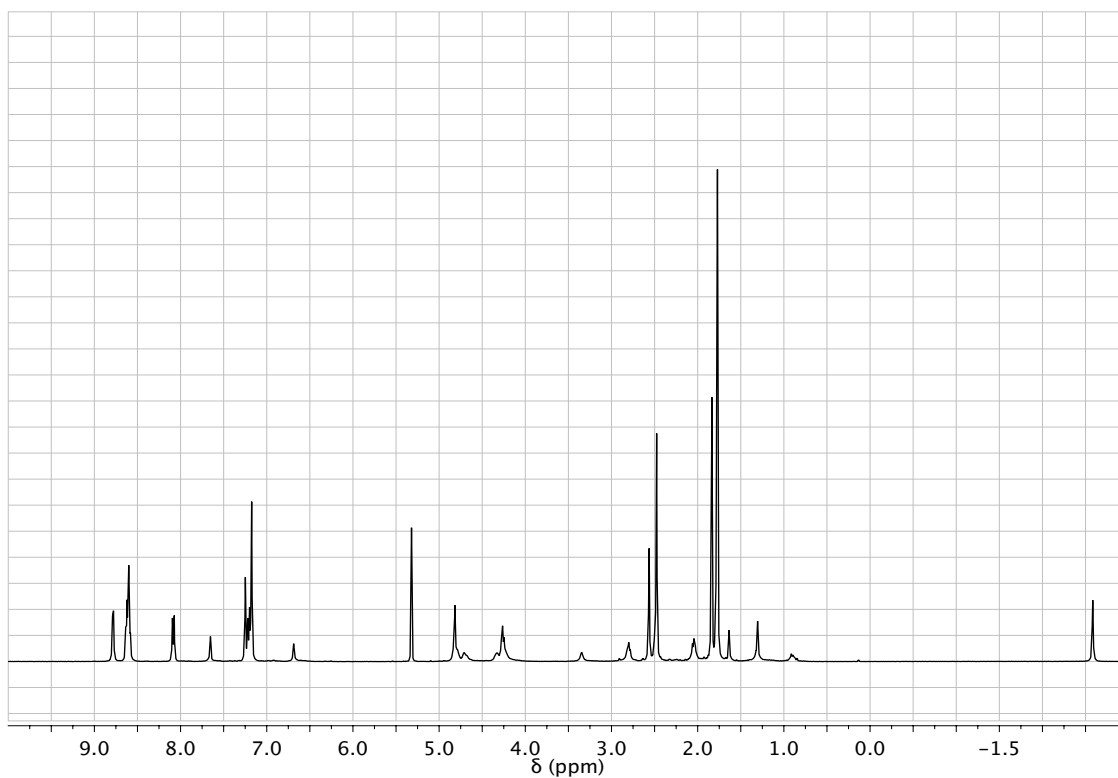
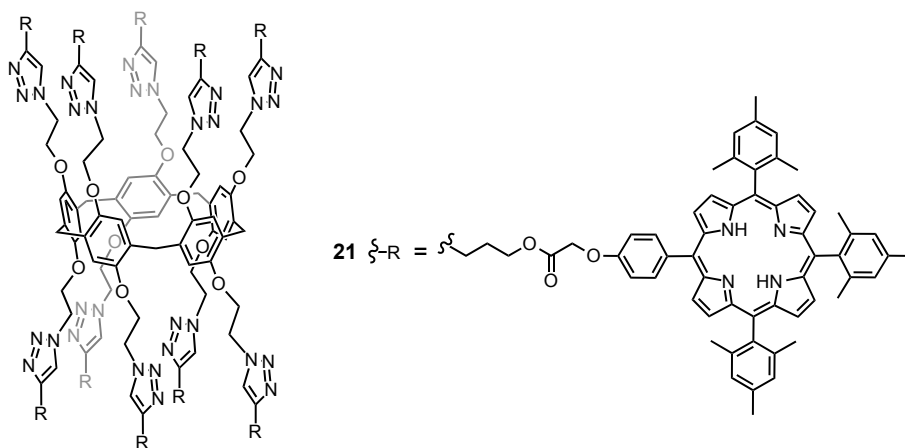


Figure S4a. ^1H NMR spectrum of compound **21** (CD_2Cl_2 , 400 MHz).

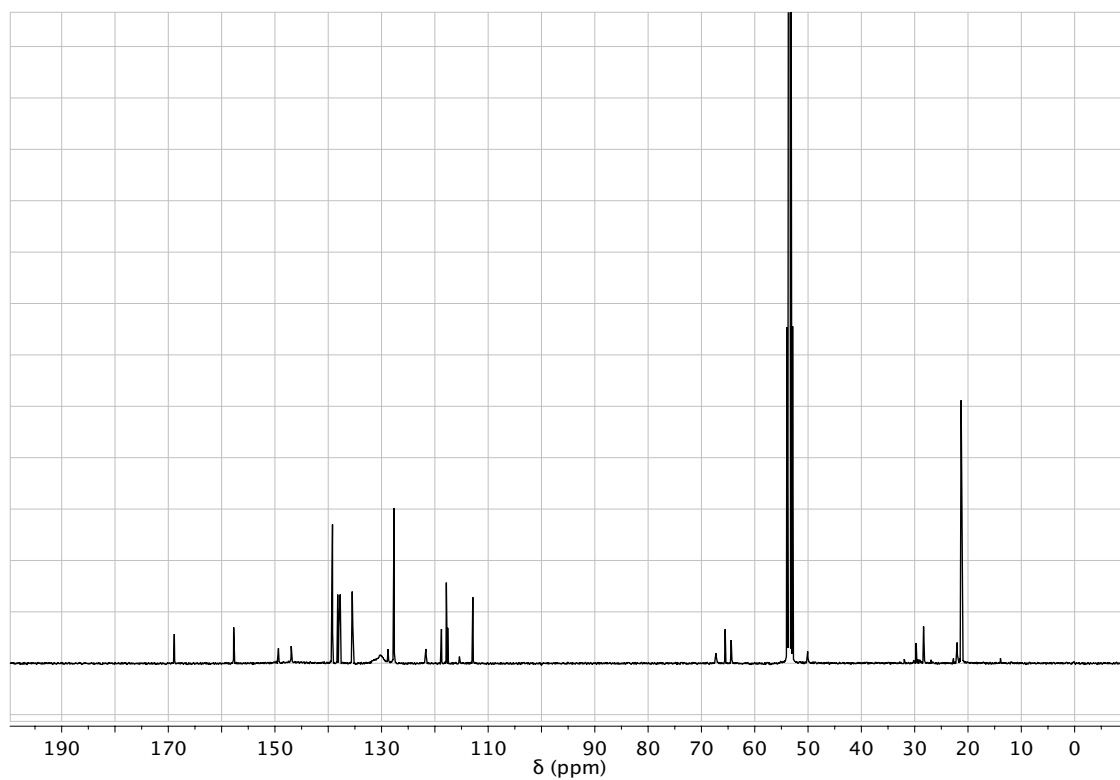
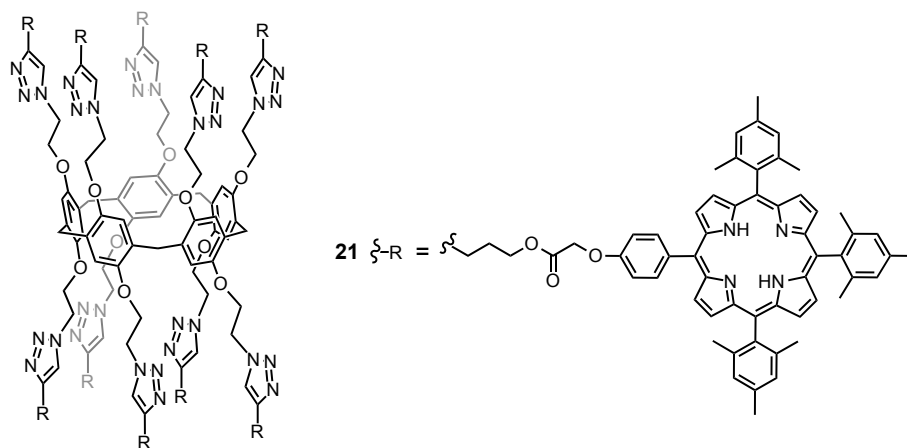


Figure S4b. ^{13}C NMR spectrum of compound **21** (CD_2Cl_2 , 100 MHz).

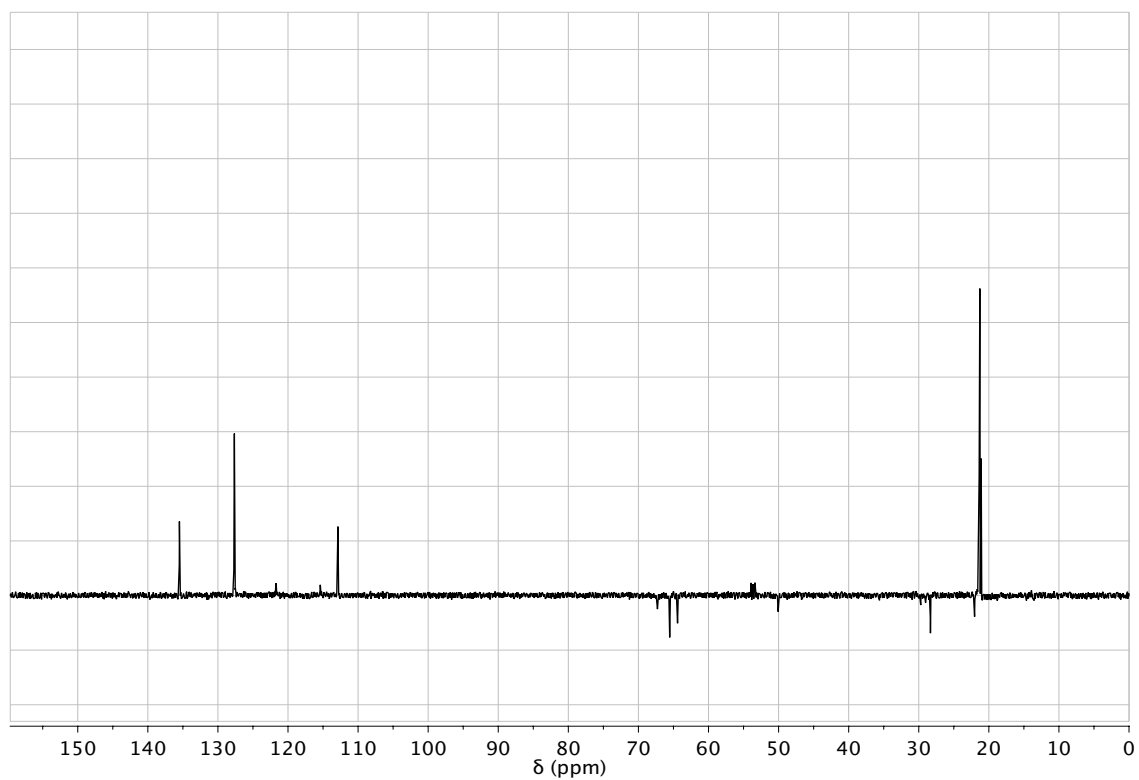
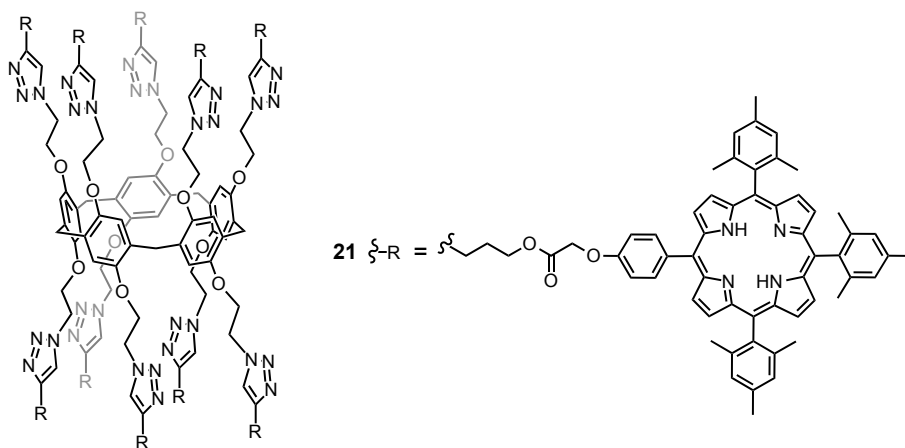


Figure S4c. DEPT of compound **21** (CD_2Cl_2 , 100 MHz).

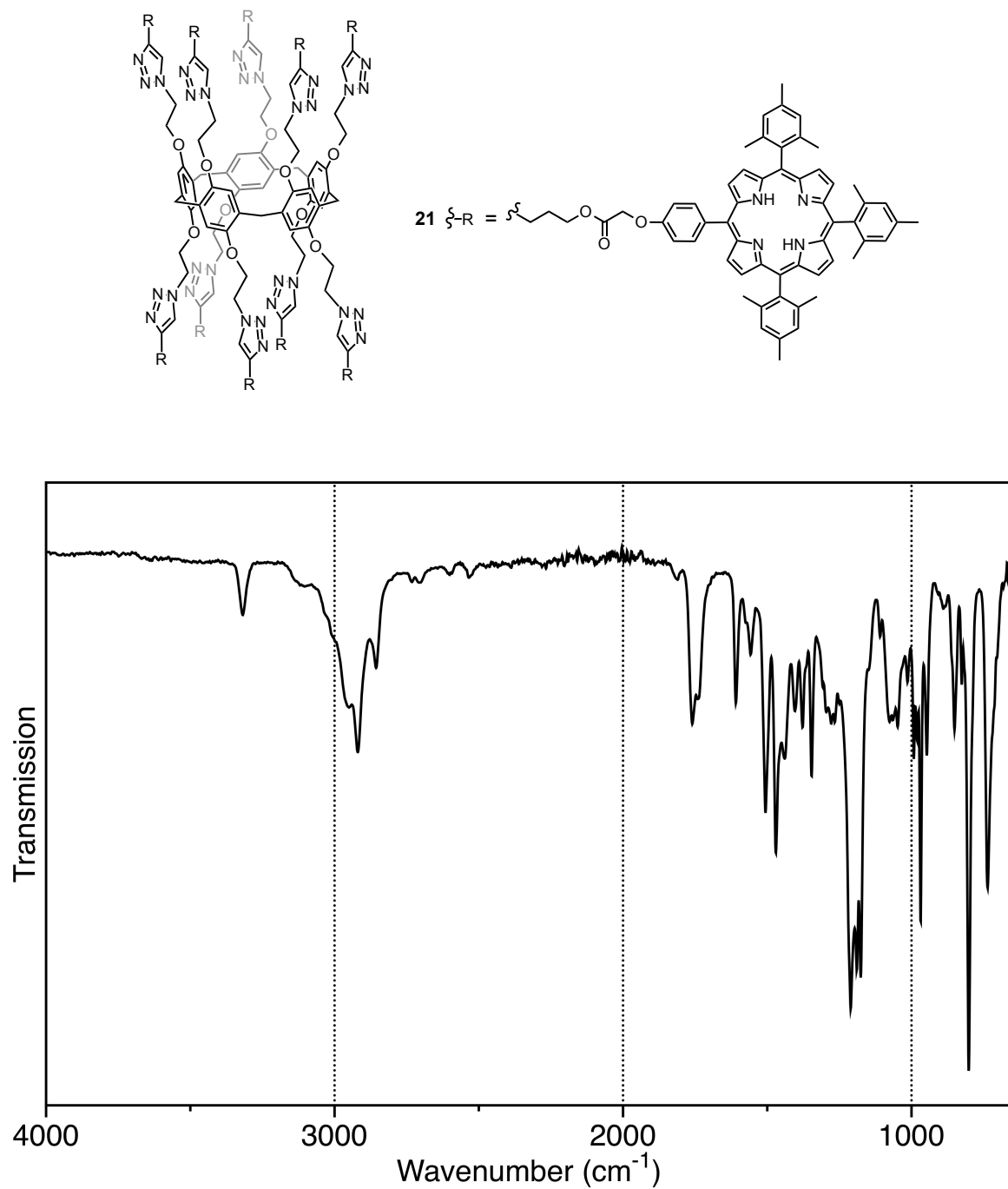


Figure S4d. IR spectrum of compound **21**.

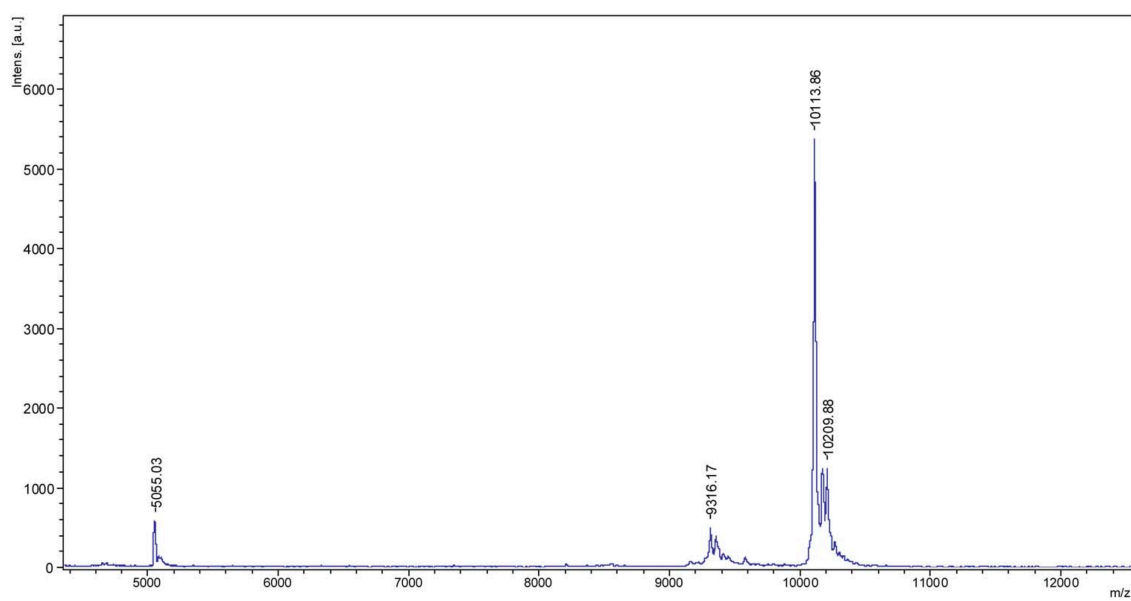
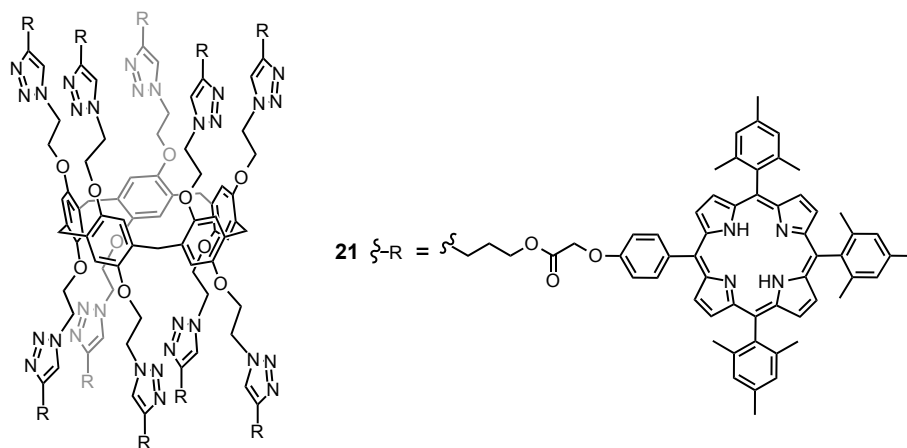


Figure S4e. MALDI-TOF mass spectrum of compound **21**.

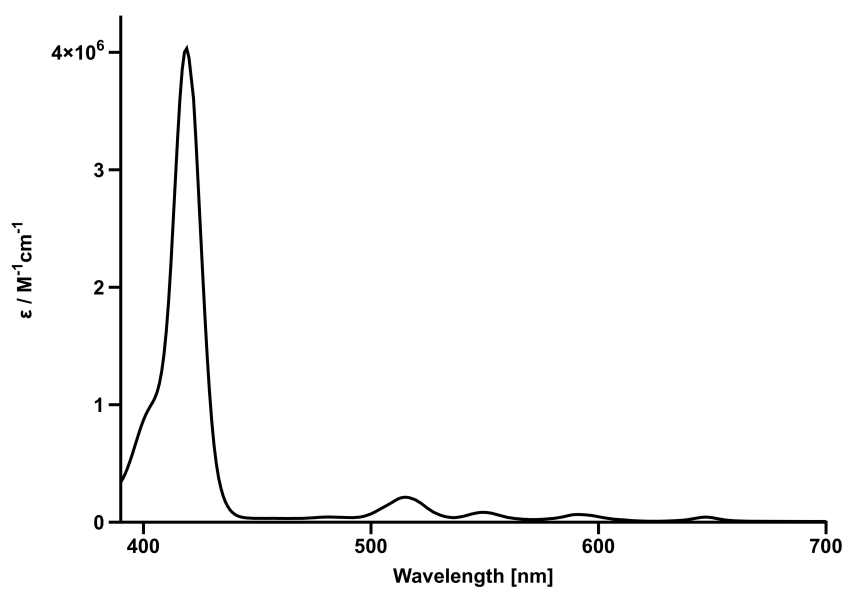
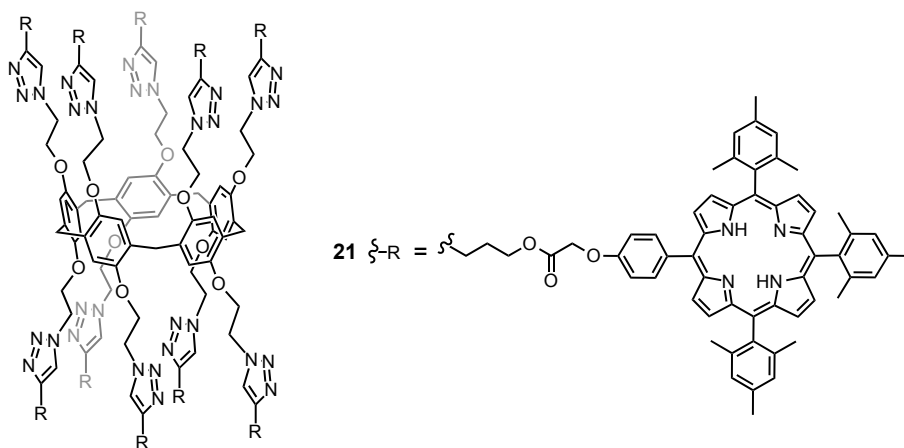


Figure S4f. UV/vis spectrum of compound **21** (CH_2Cl_2).

S3. Supporting information (Chapter 4)

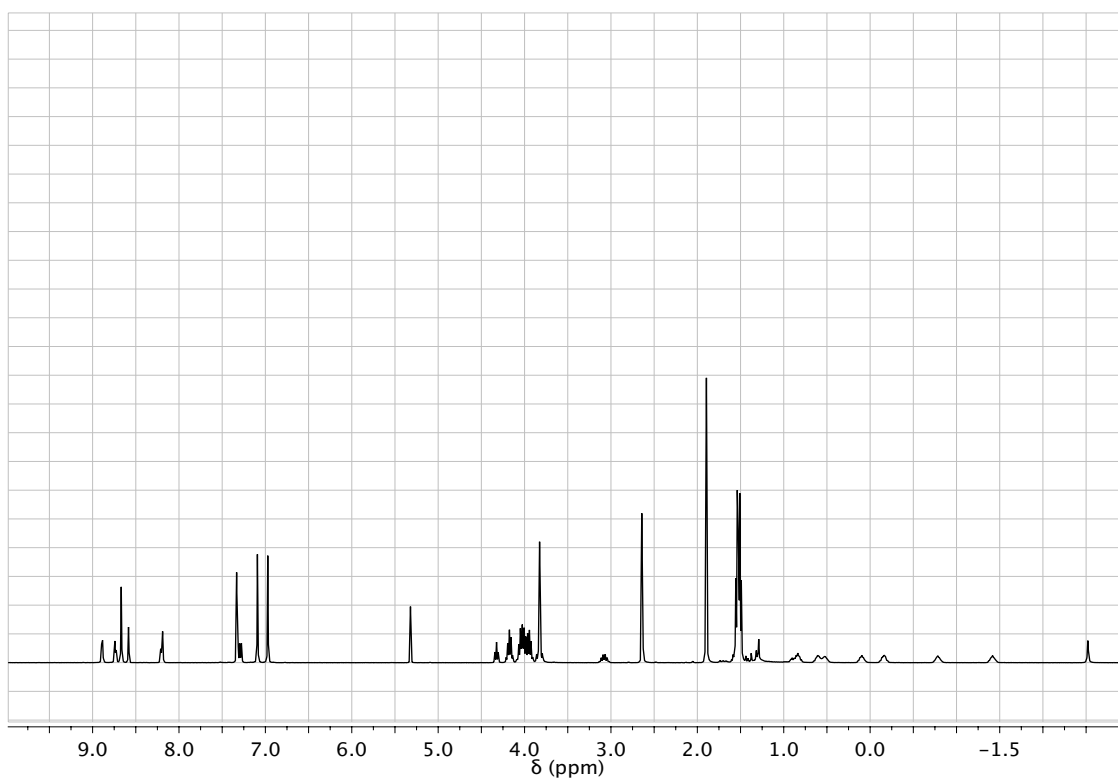
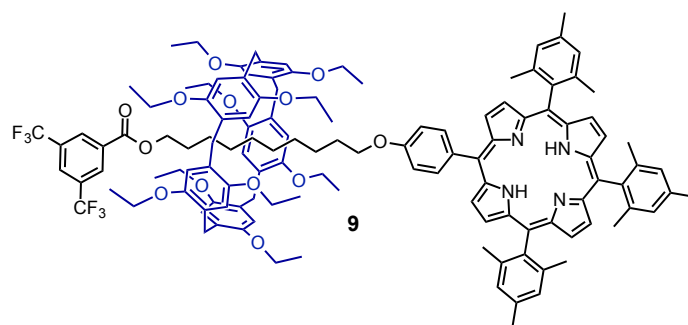


Figure S1a. ¹H NMR spectrum of compound **9** (CD₂Cl₂, 400 MHz).

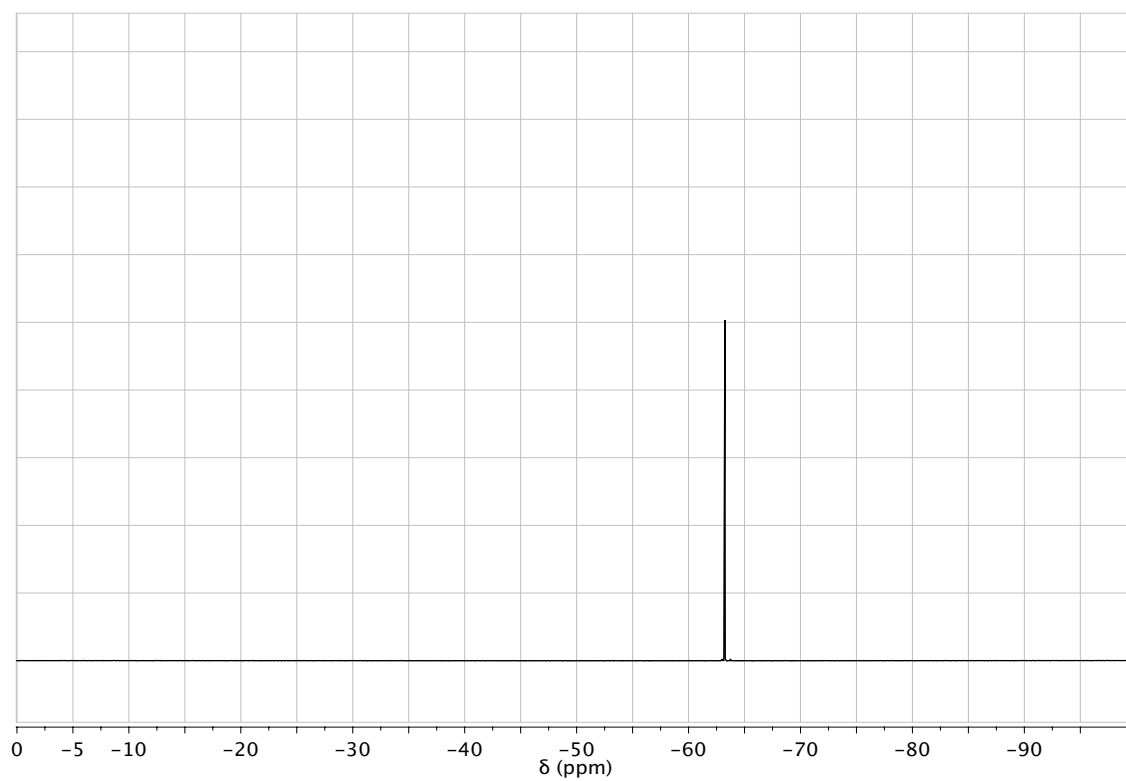
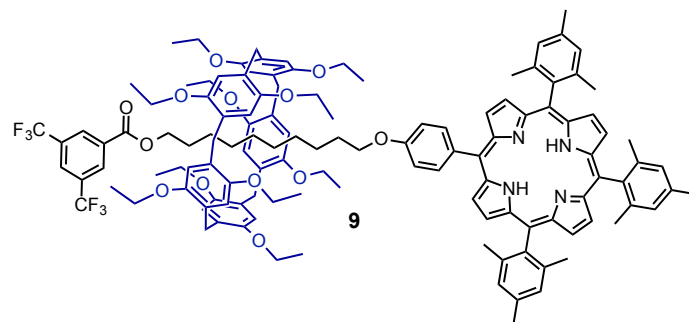


Figure S1b. ^{19}F NMR spectrum of compound **9** (CD_2Cl_2 , 376 MHz).

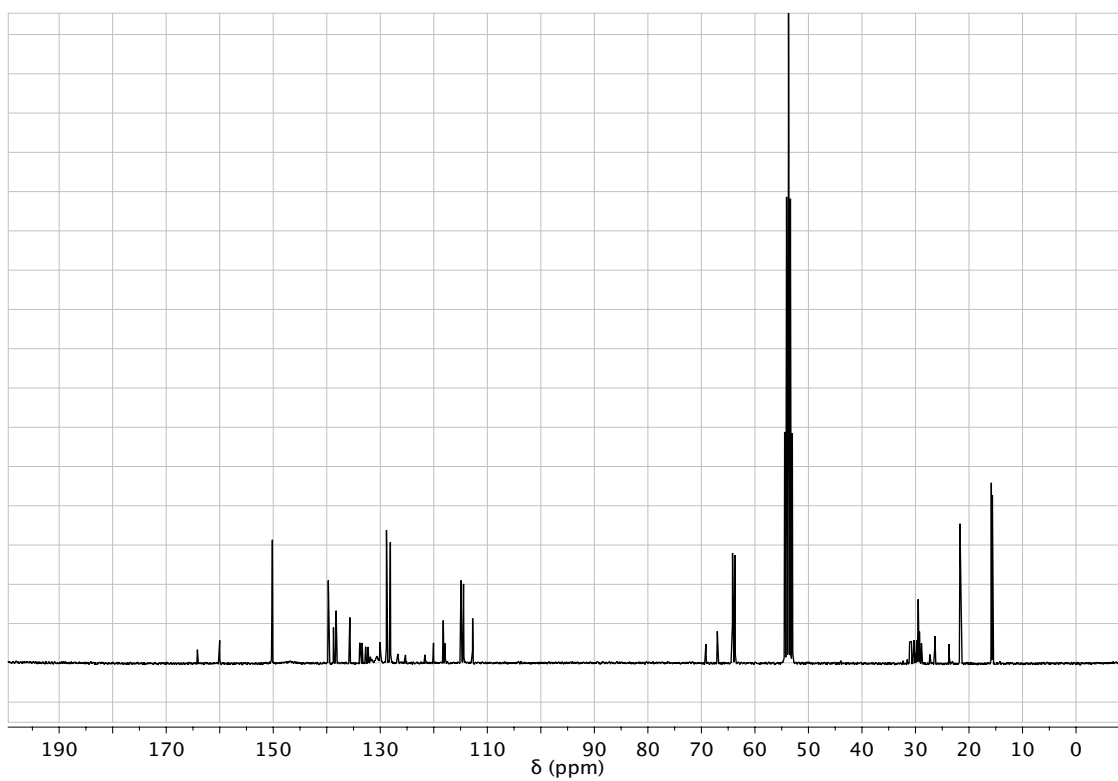
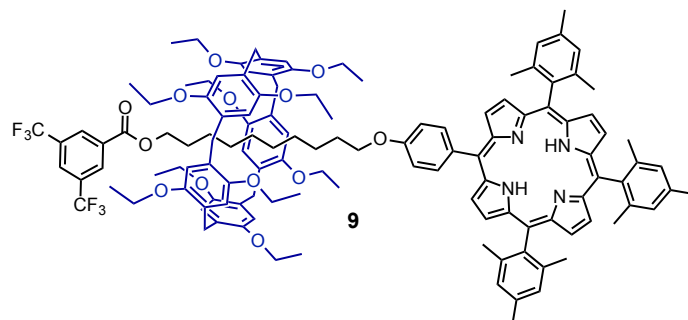


Figure S1c. ¹³C NMR spectrum of compound **9** (CDCl₃, 75 MHz).

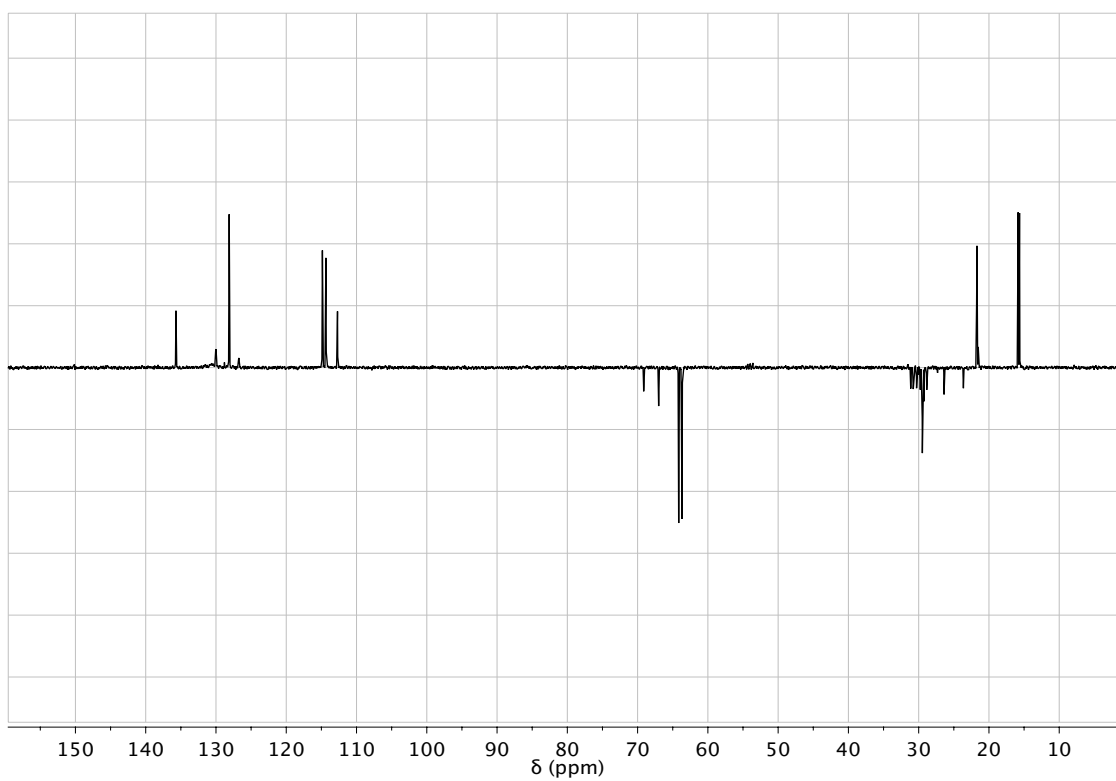
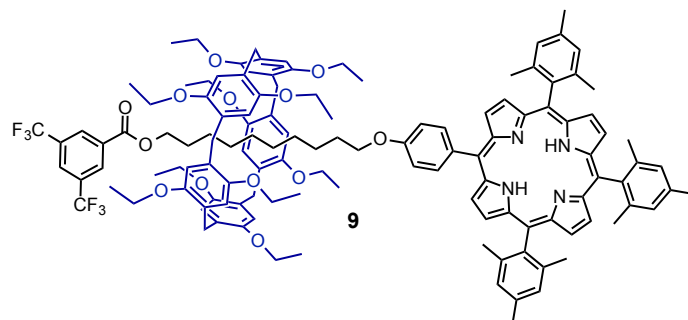


Figure S1d. DEPT spectrum of compound **9** (CDCl_3 , 75 MHz).

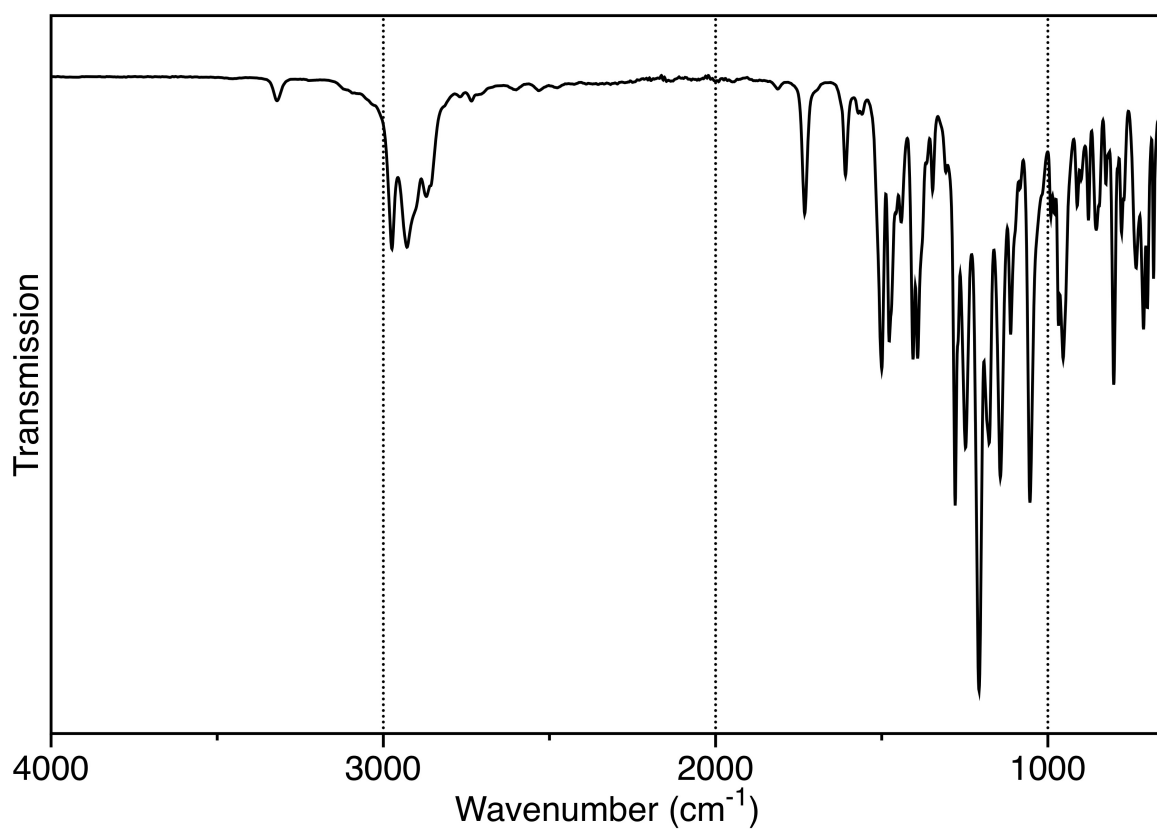
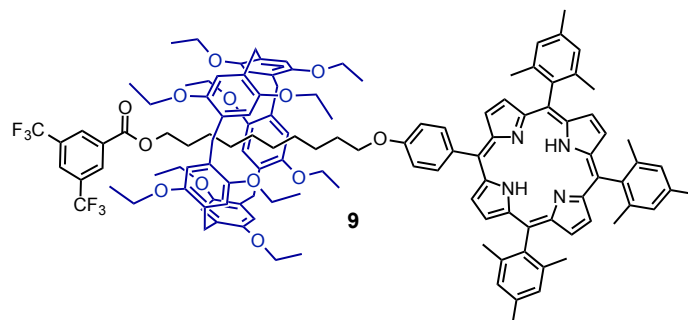


Figure S1e. IR spectrum of compound **9**.

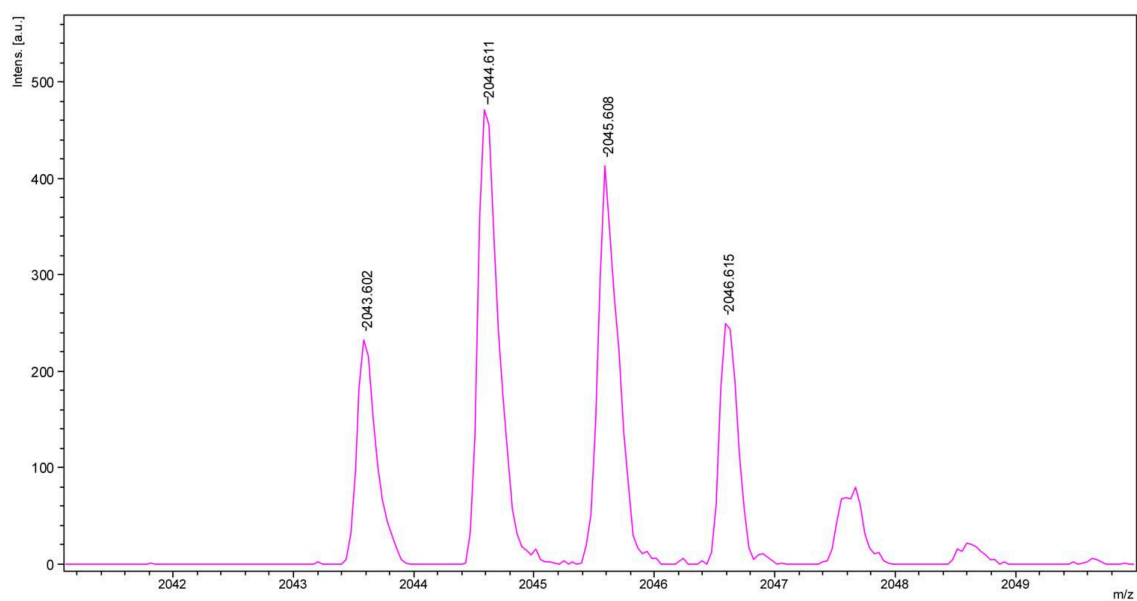
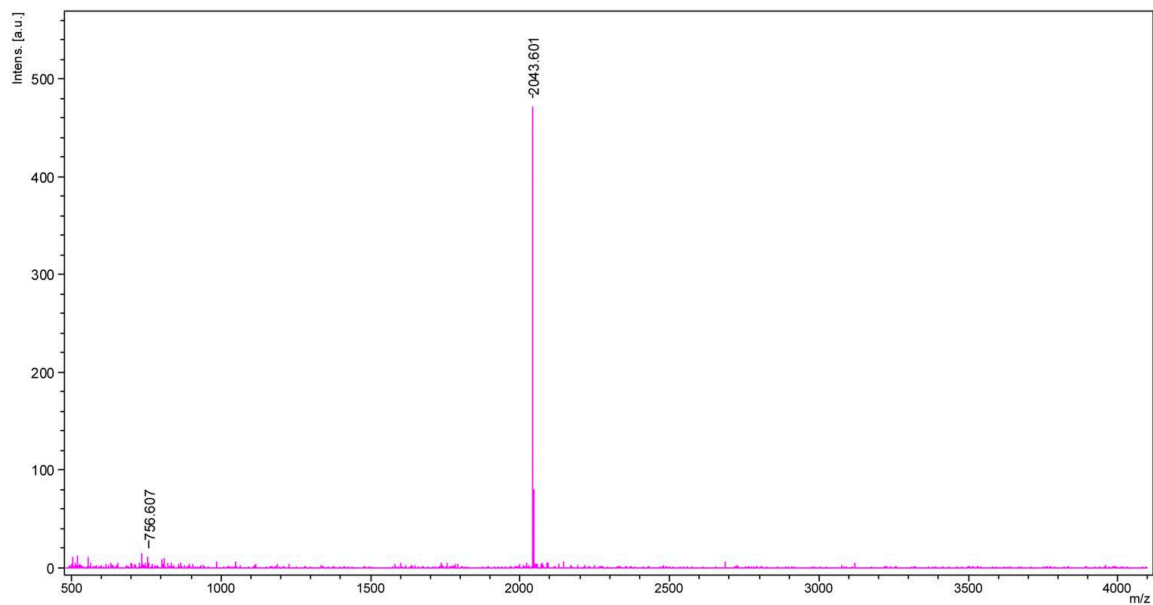
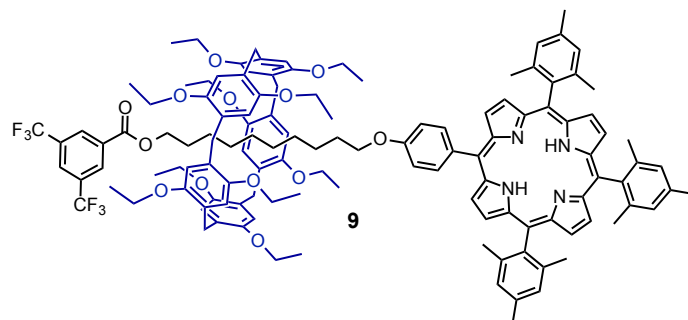


Figure S1f. MALDI-TOF mass spectrum of compound **9**.

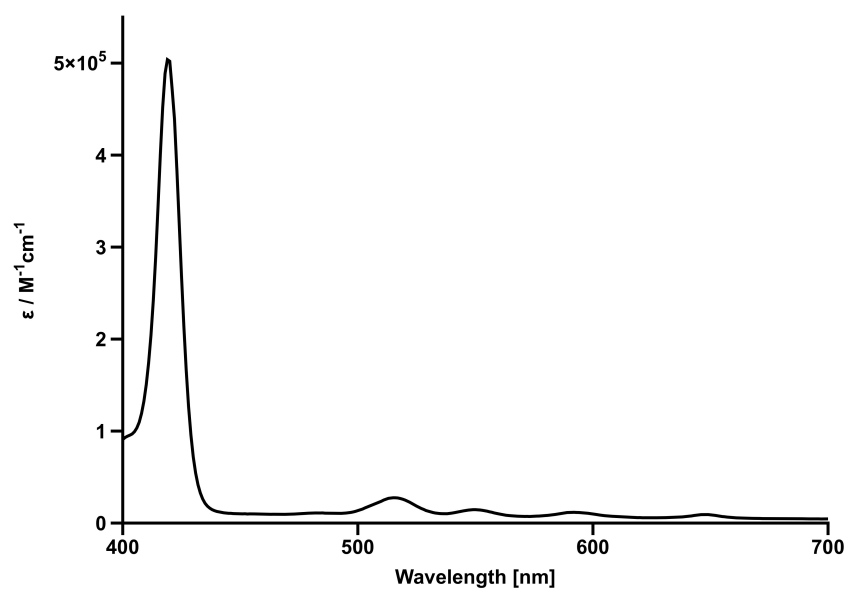
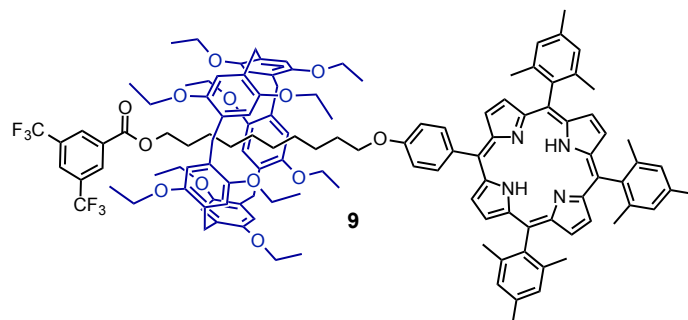


Figure S1g. UV/vis spectrum of compound **9** (CH_2Cl_2).

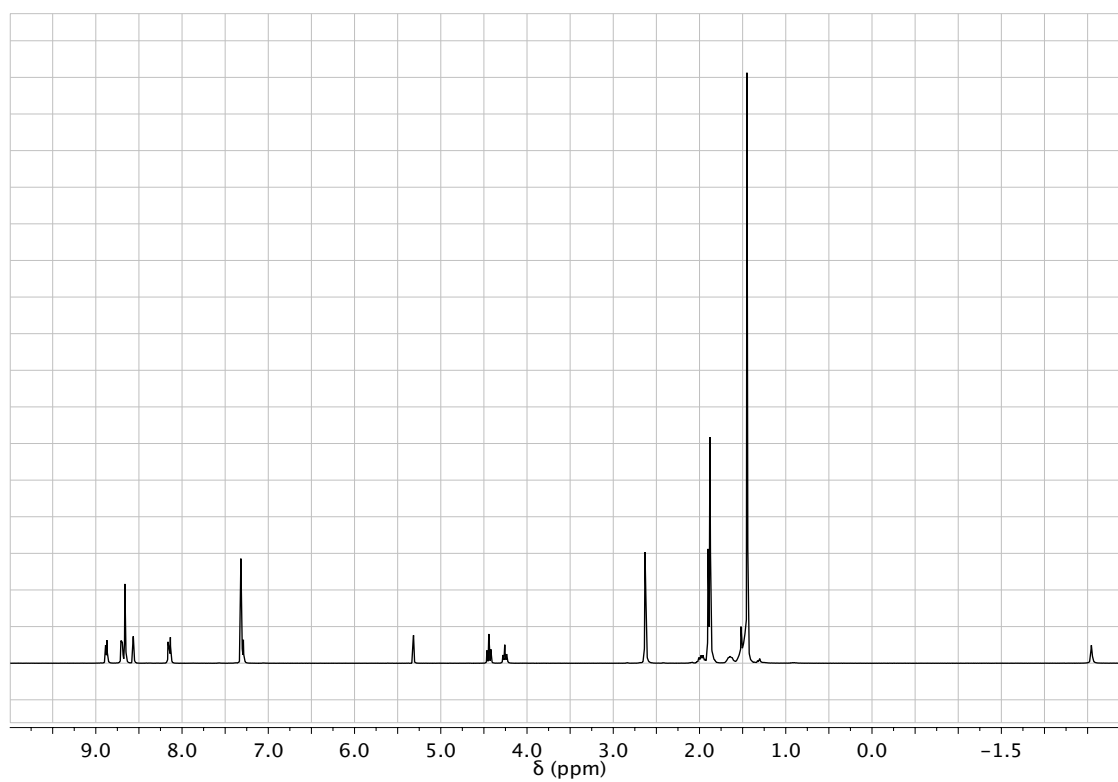
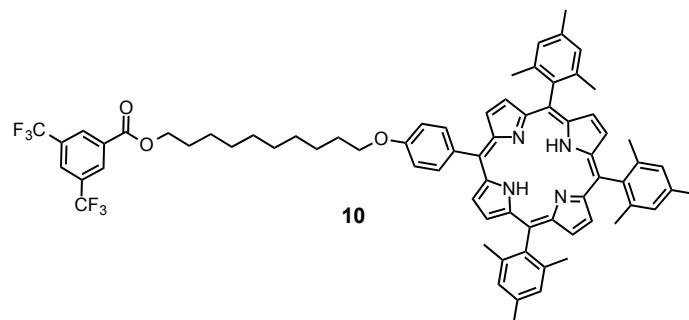


Figure S2a. ^1H NMR spectrum of compound **10** (CD_2Cl_2 , 300 MHz).

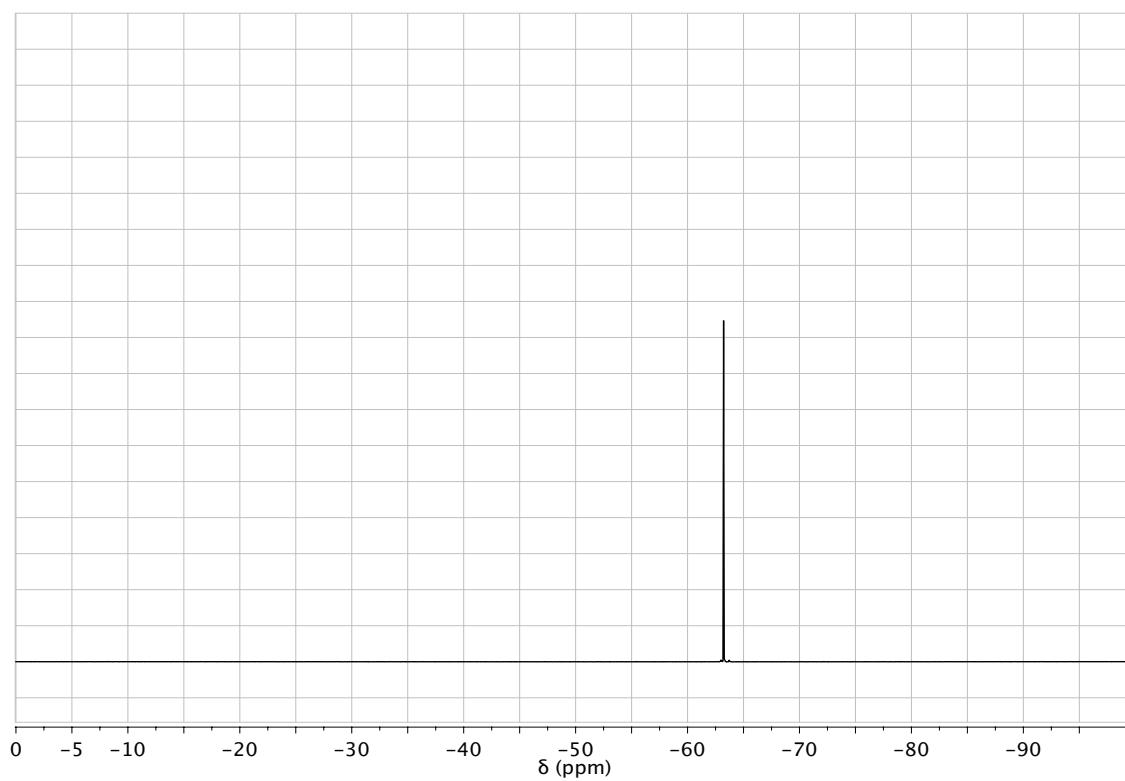
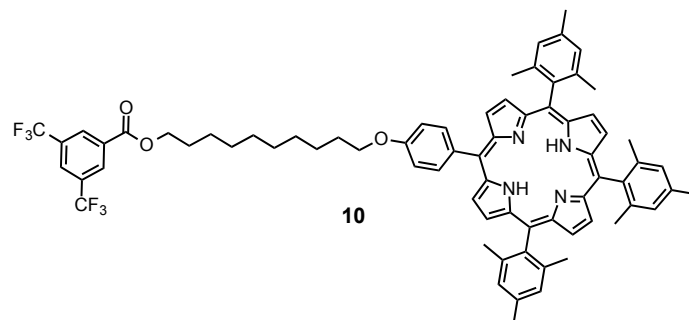


Figure S2b. ¹⁹F NMR spectrum of compound **10** (CD₂Cl₂, 376 MHz).

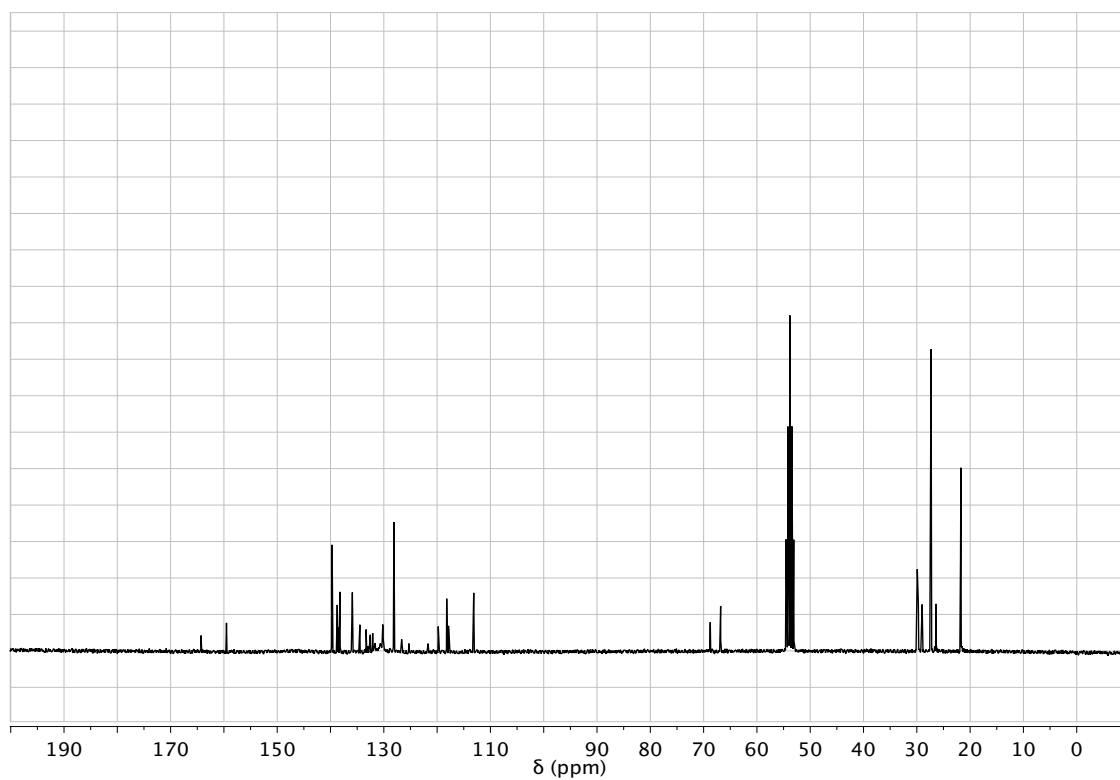
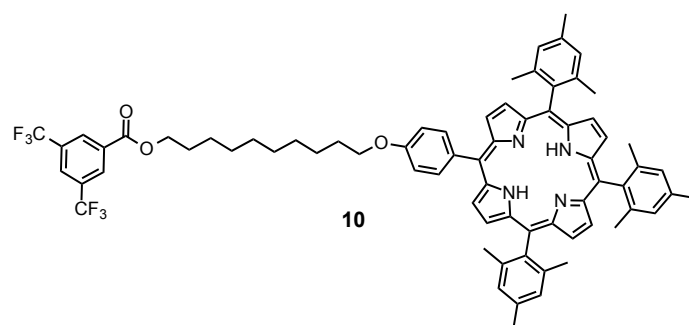


Figure S2c. ^{13}C NMR spectrum of compound **10** (CD_2Cl_2 , 75 MHz).

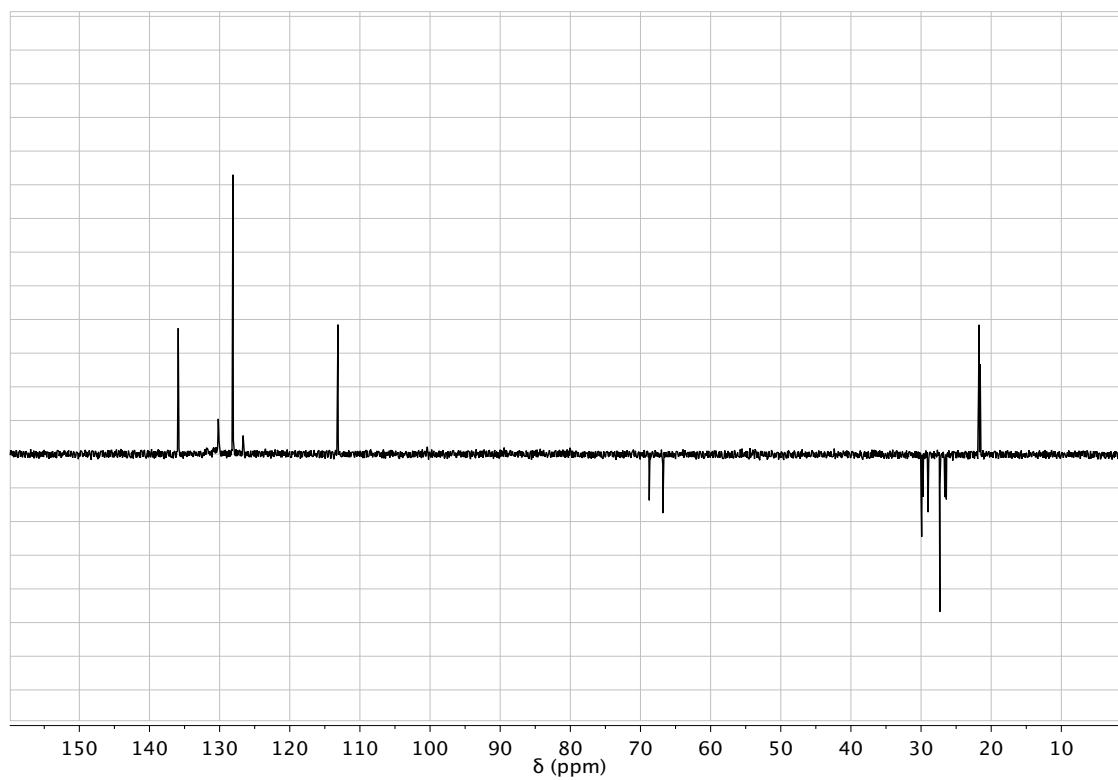
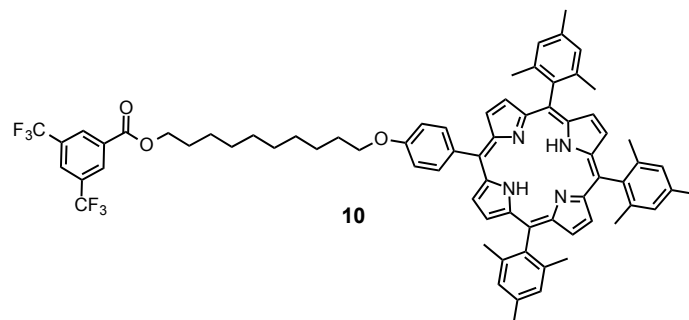


Figure S2d. DEPT spectrum of compound **10** (CD₂Cl₂, 75 MHz).

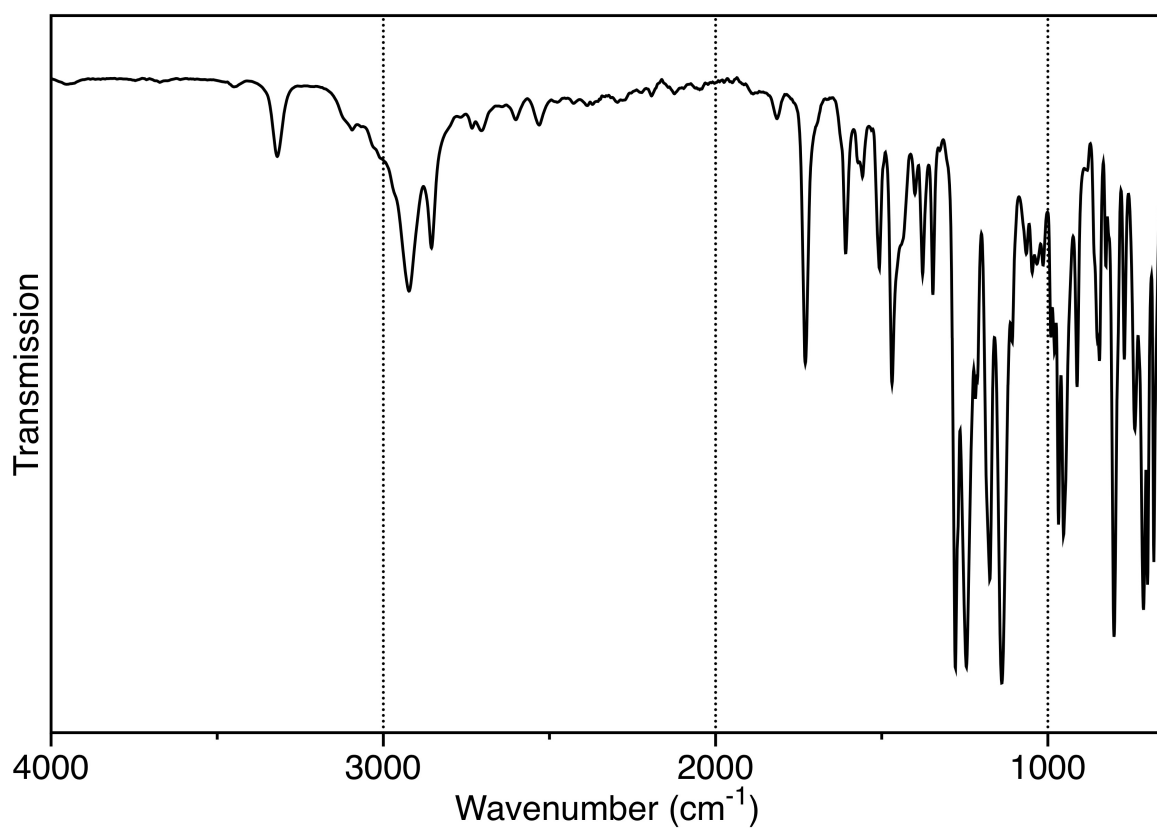
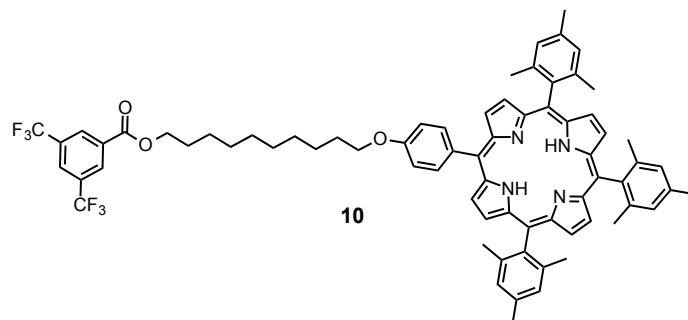


Figure S2e. IR spectrum of compound **10**.

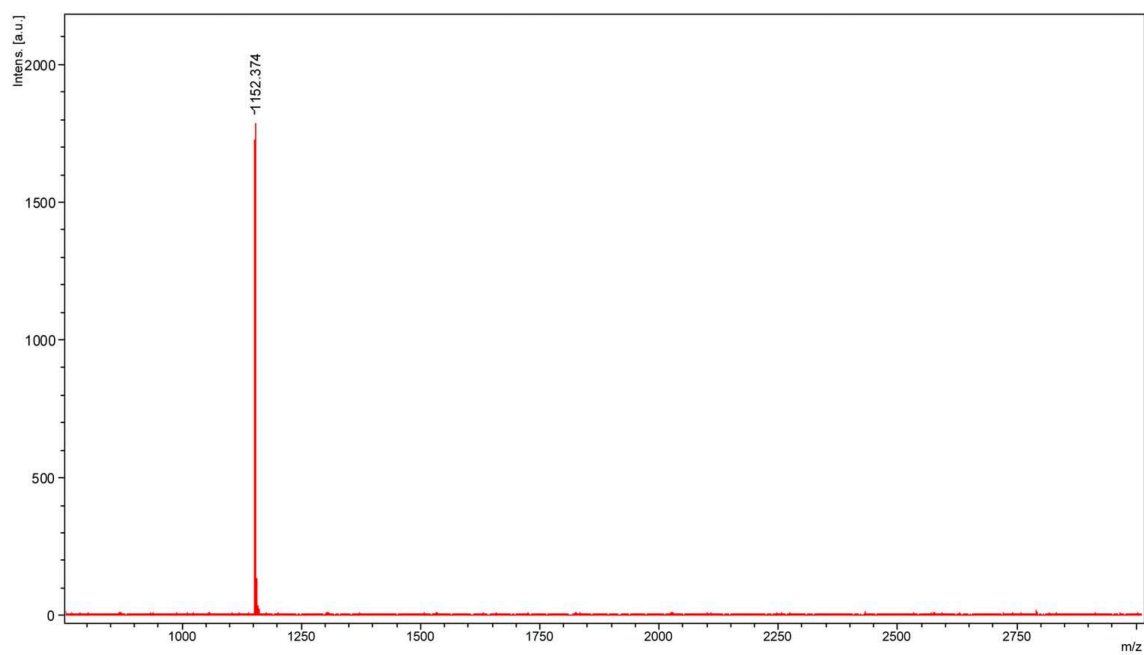
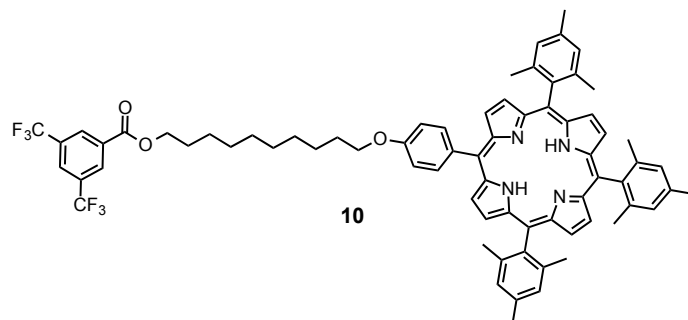


Figure S2f. MALDI-TOF mass spectrum of compound **10**.

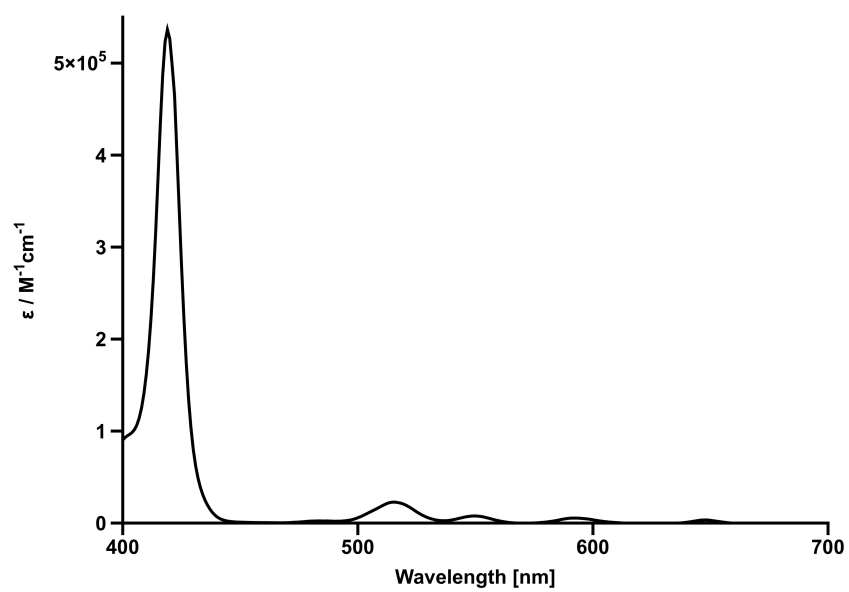
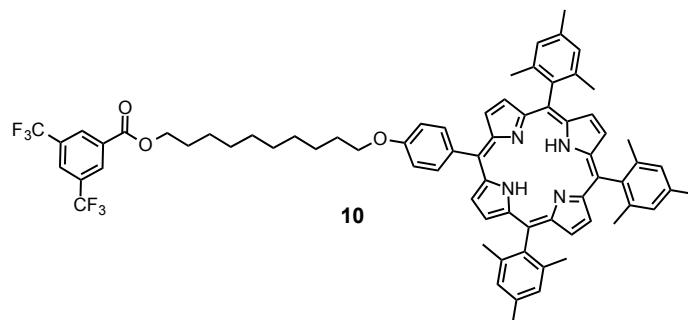


Figure S2g. UV/vis spectrum of compound **10** (CH_2Cl_2).

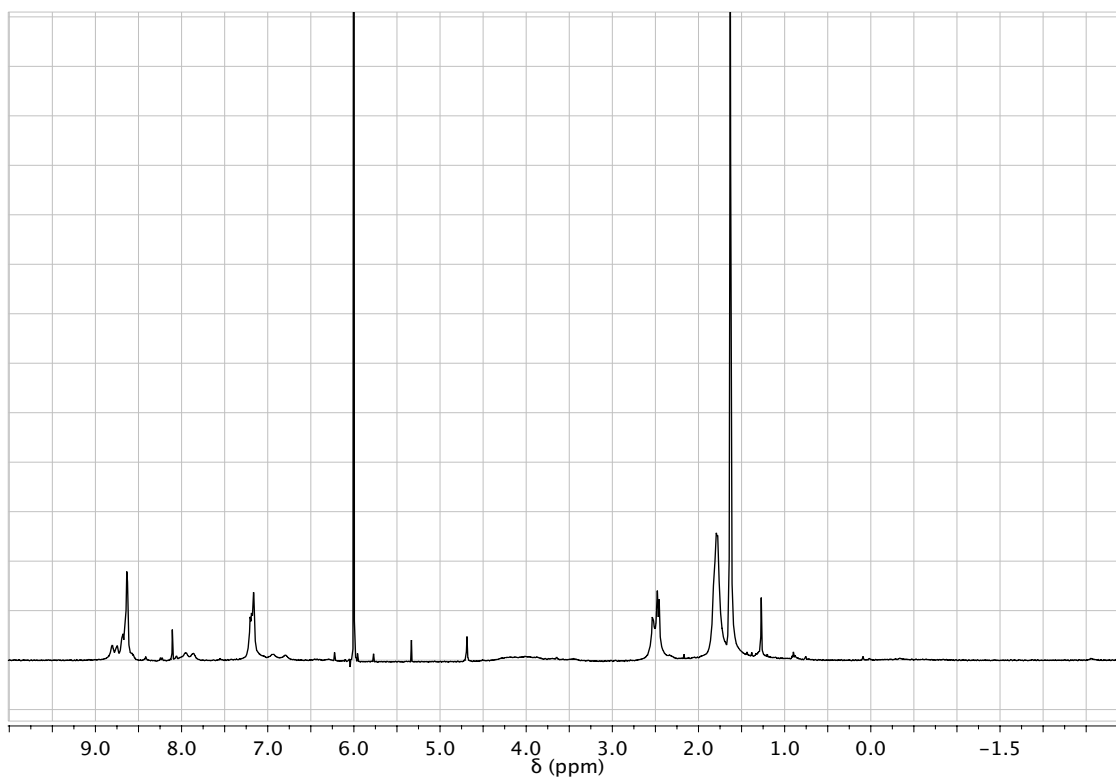
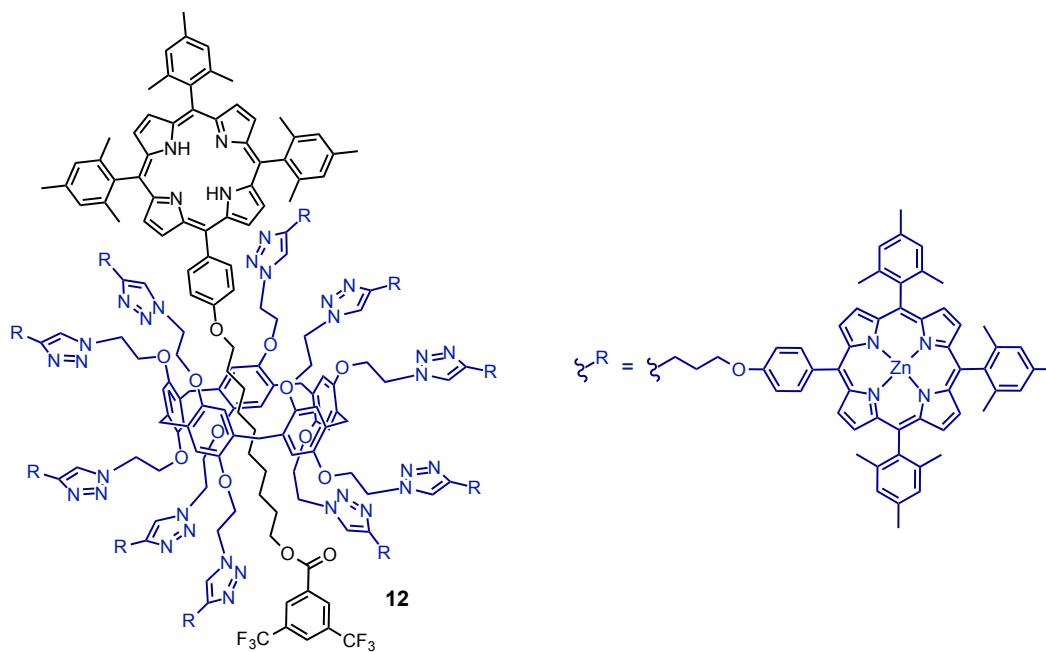


Figure S3a. ¹H NMR spectrum of compound **12** (C₂D₂Cl₄, 400 MHz).

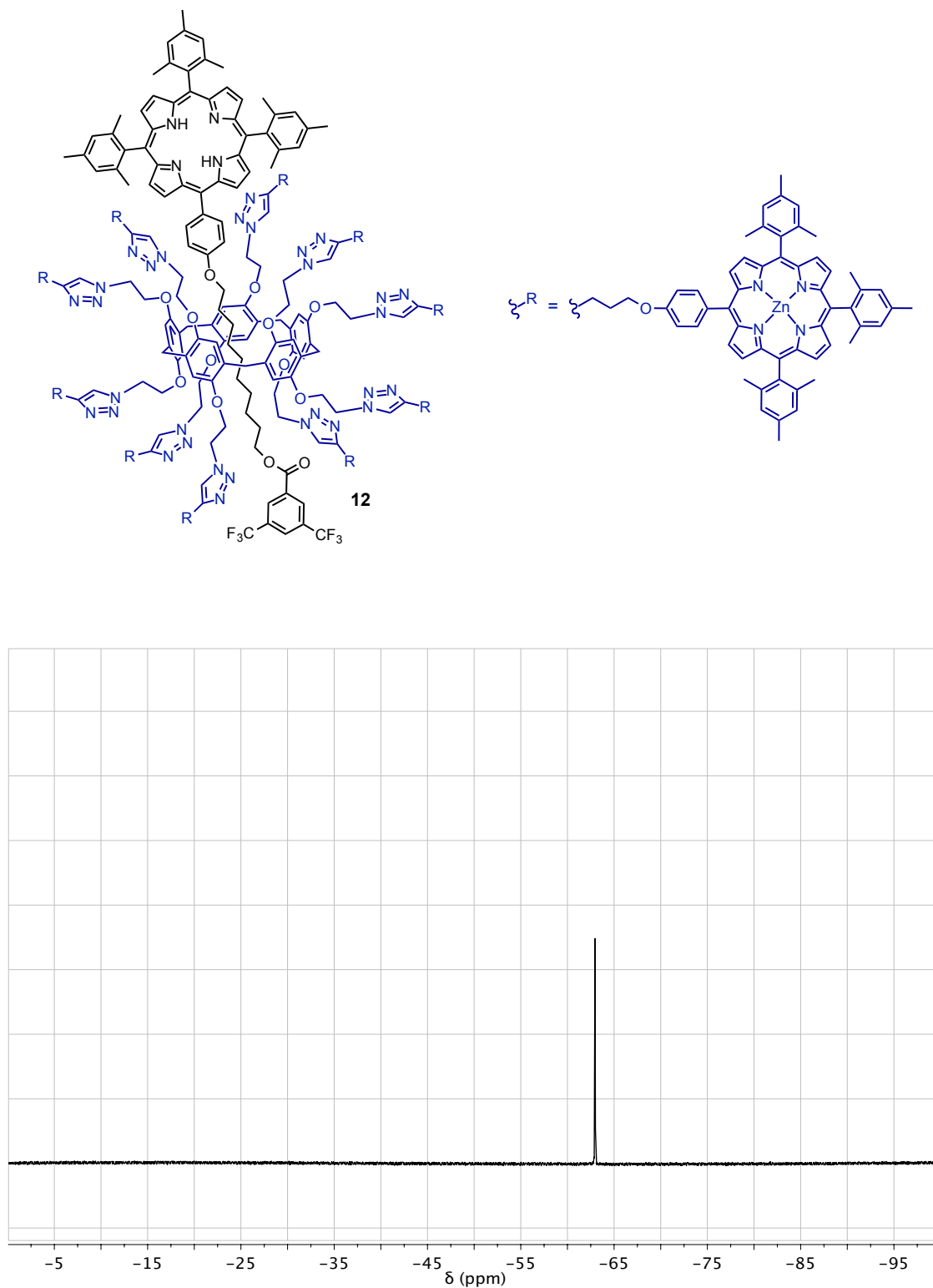


Figure S3b. ^{19}F NMR spectrum of compound **12** (CD_2Cl_2 , 376 MHz).

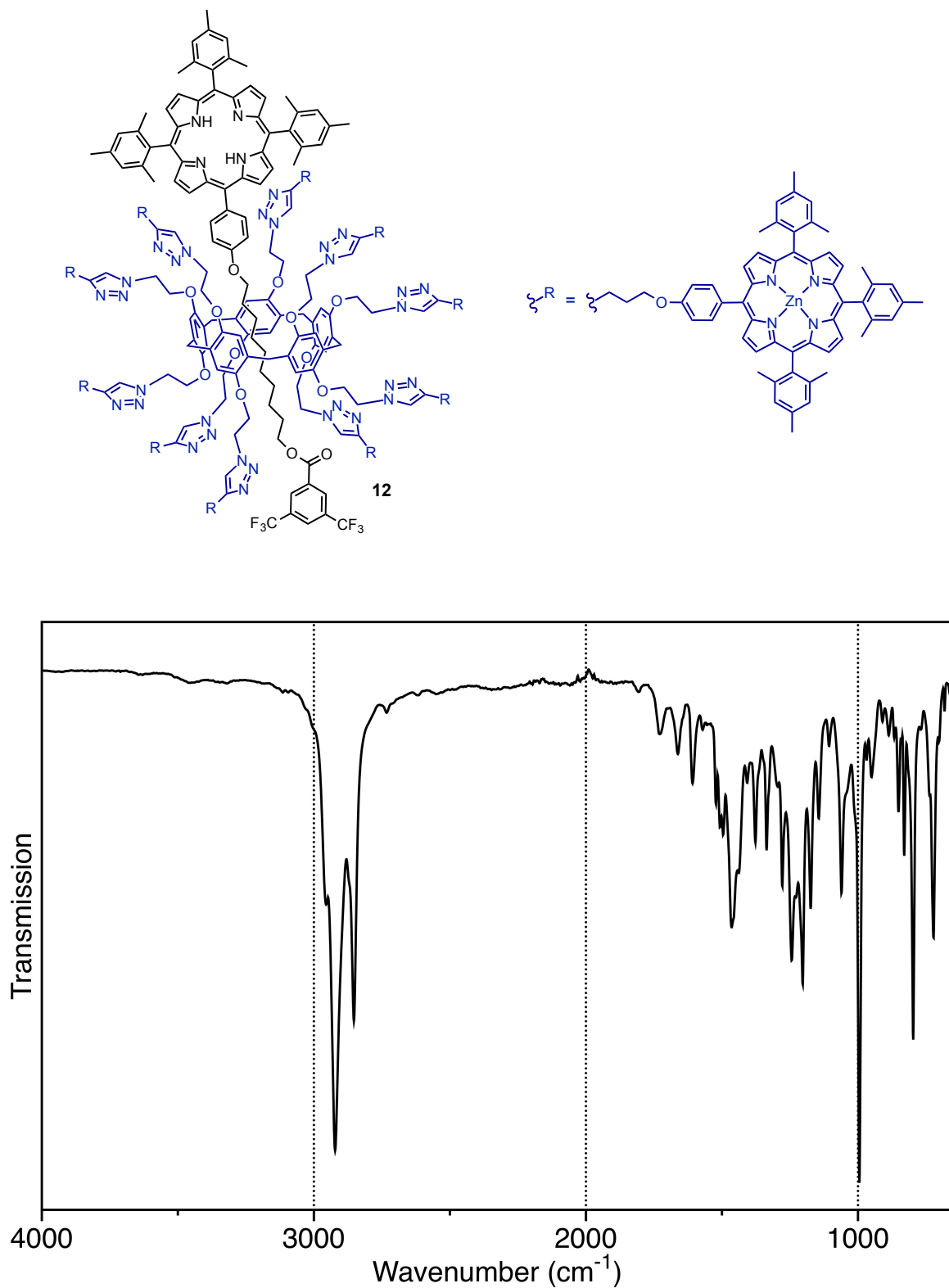


Figure S3e. IR spectrum of compound **12**.

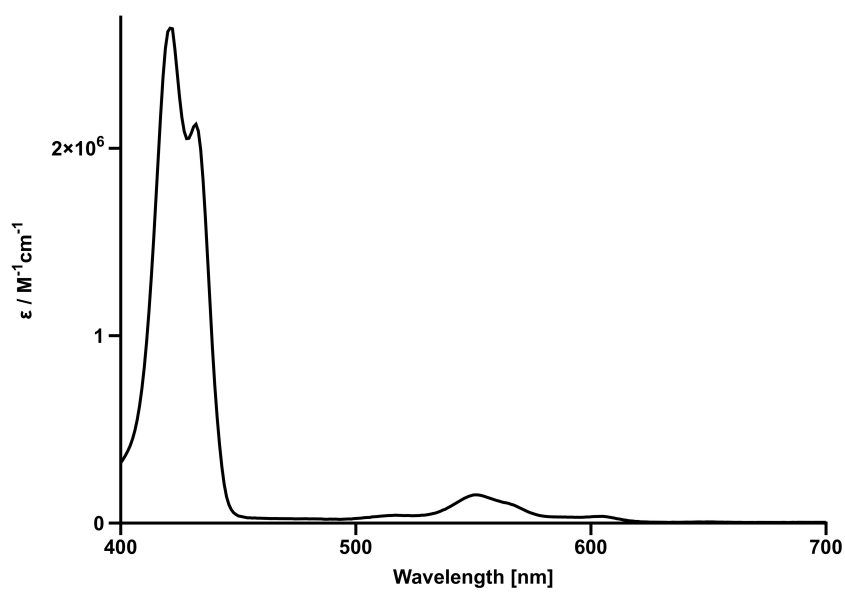
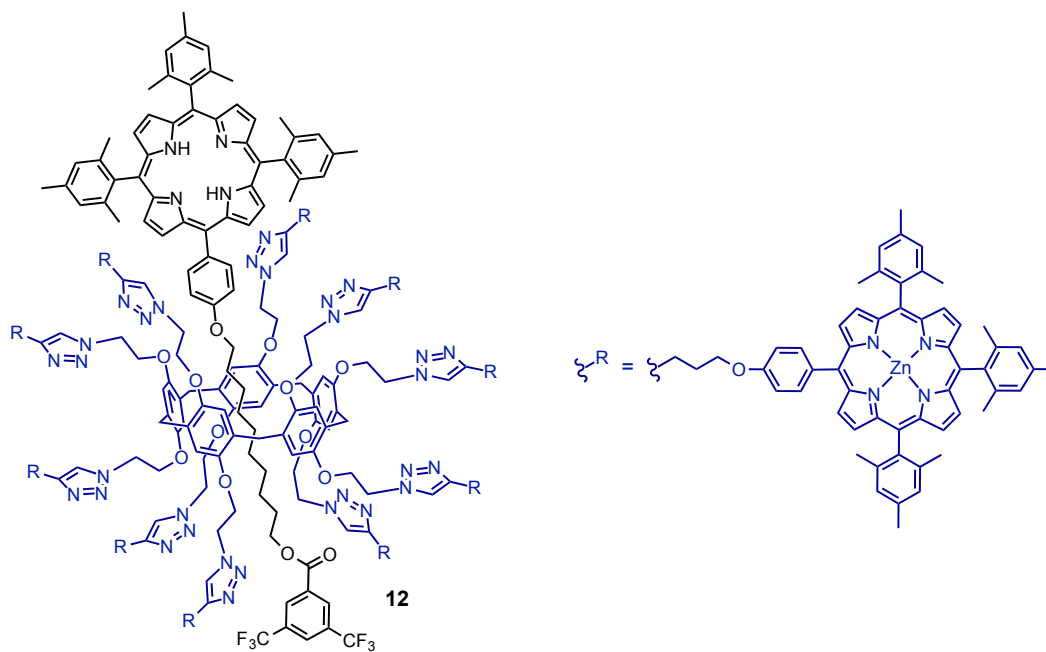


Figure S3g. UV/vis spectrum of compound **12** (CH_2Cl_2).

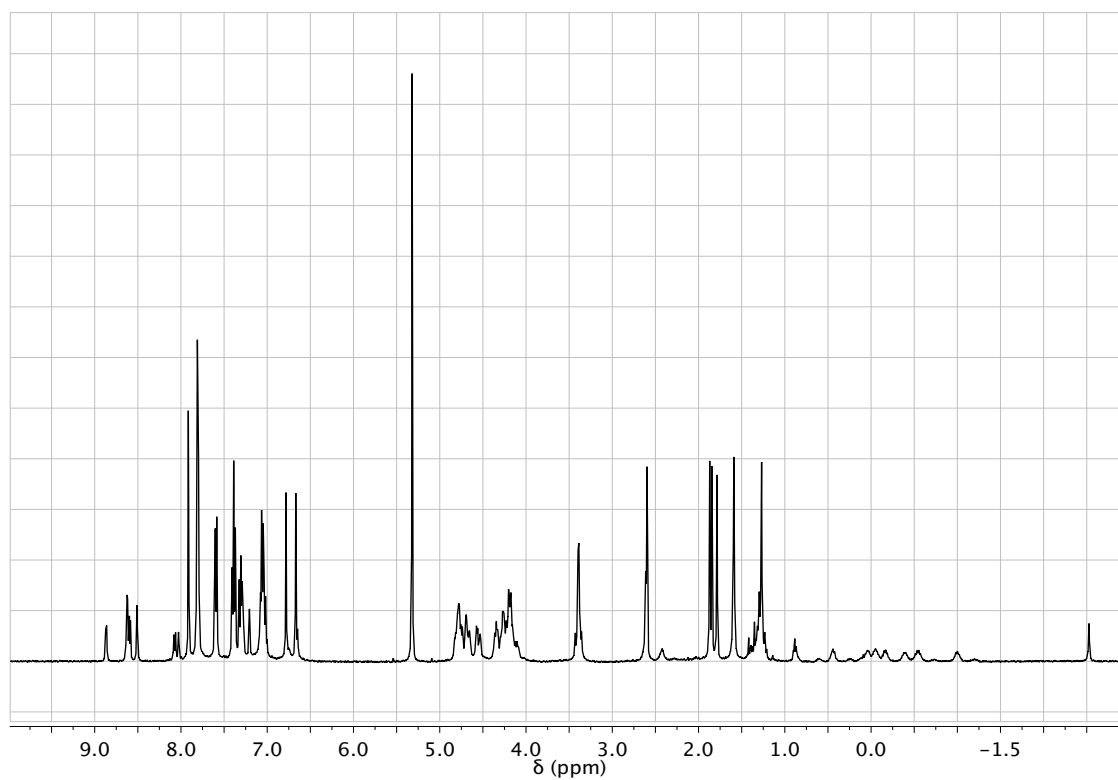
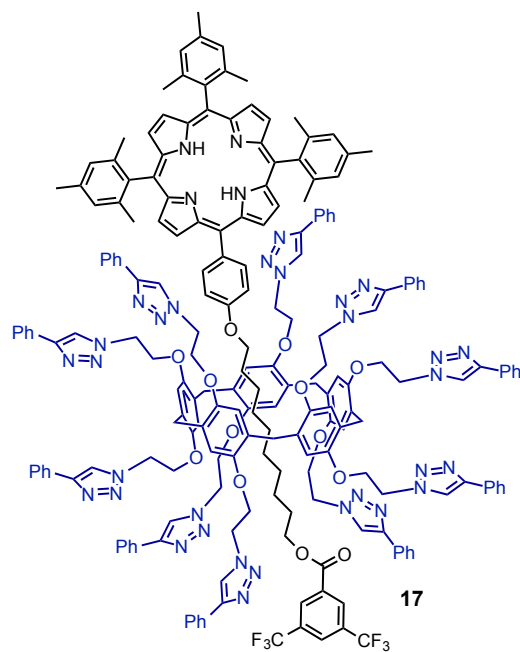


Figure S4a. ¹H NMR spectrum of compound **17** (CD₂Cl₂, 400 MHz).

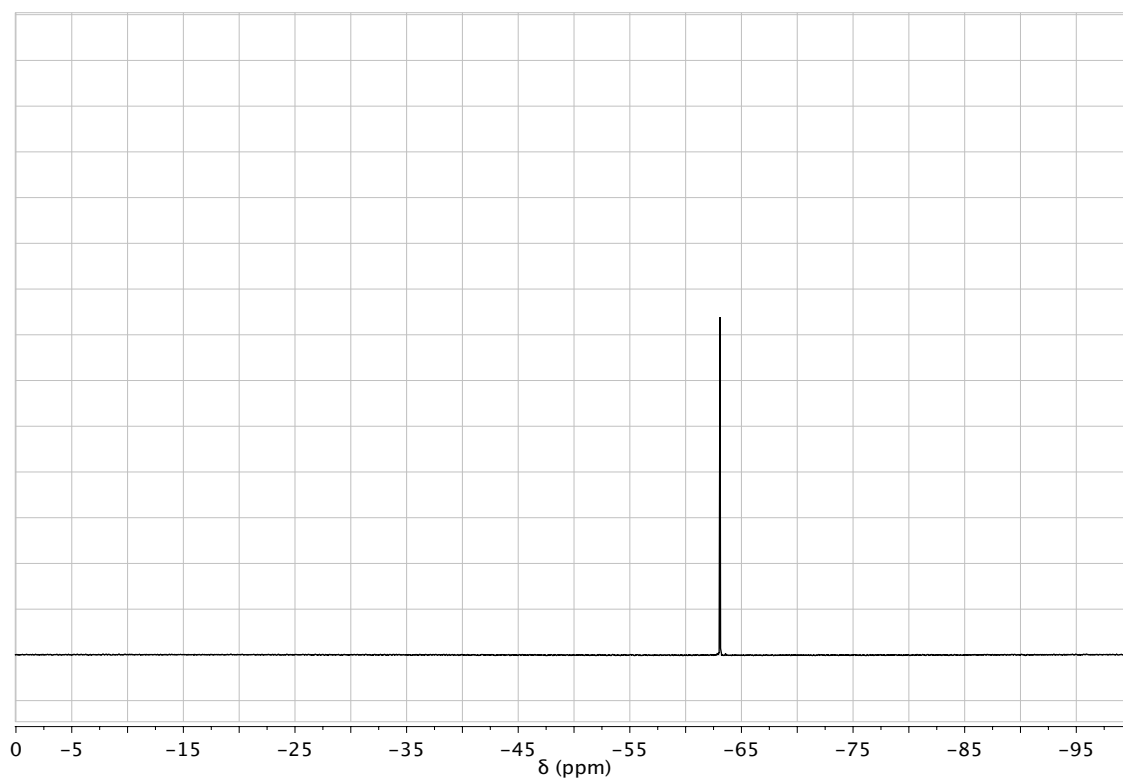
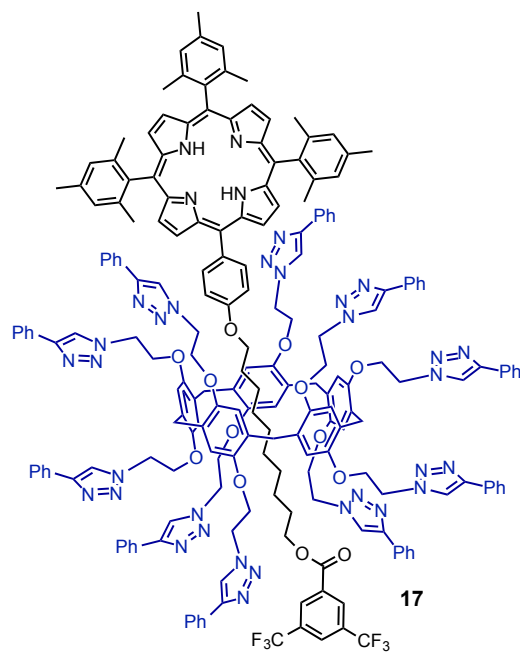


Figure S4b. ¹⁹F NMR spectrum of compound **17** (CD₂Cl₂, 376 MHz).

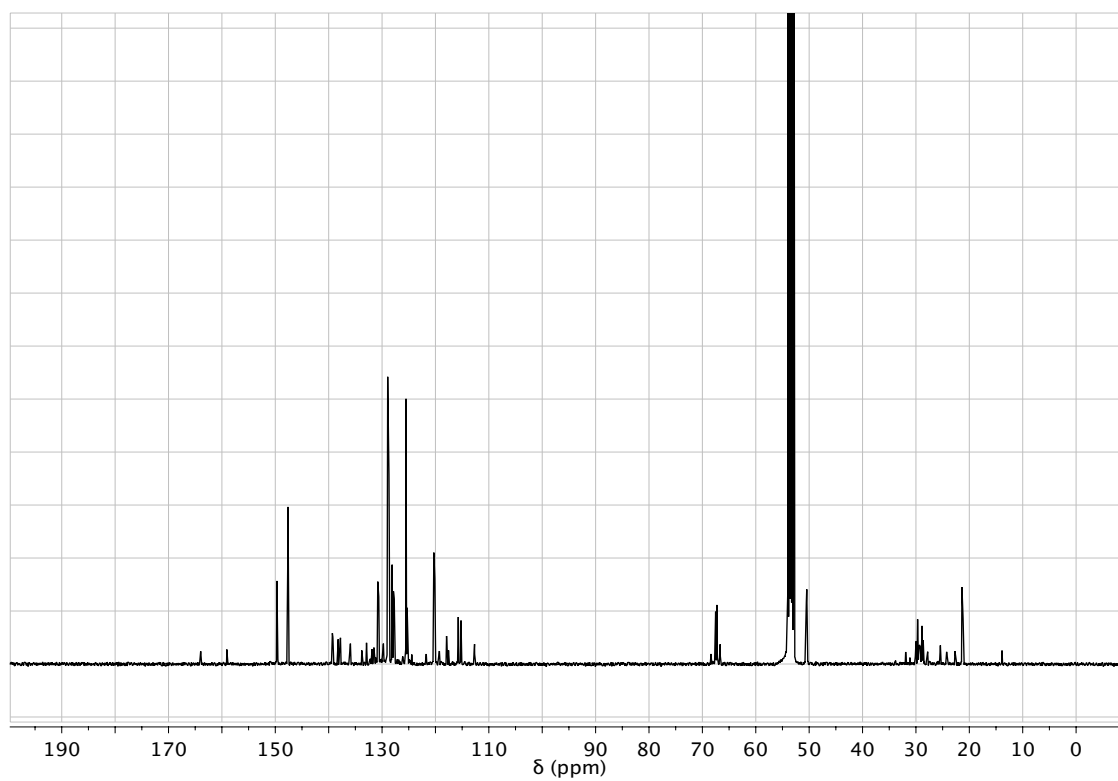
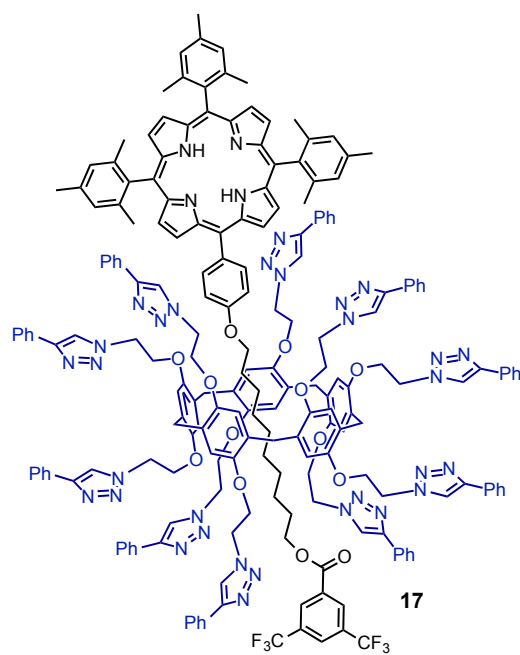


Figure S4c. ¹³C NMR spectrum of compound **17** (CD₂Cl₂, 100 MHz).

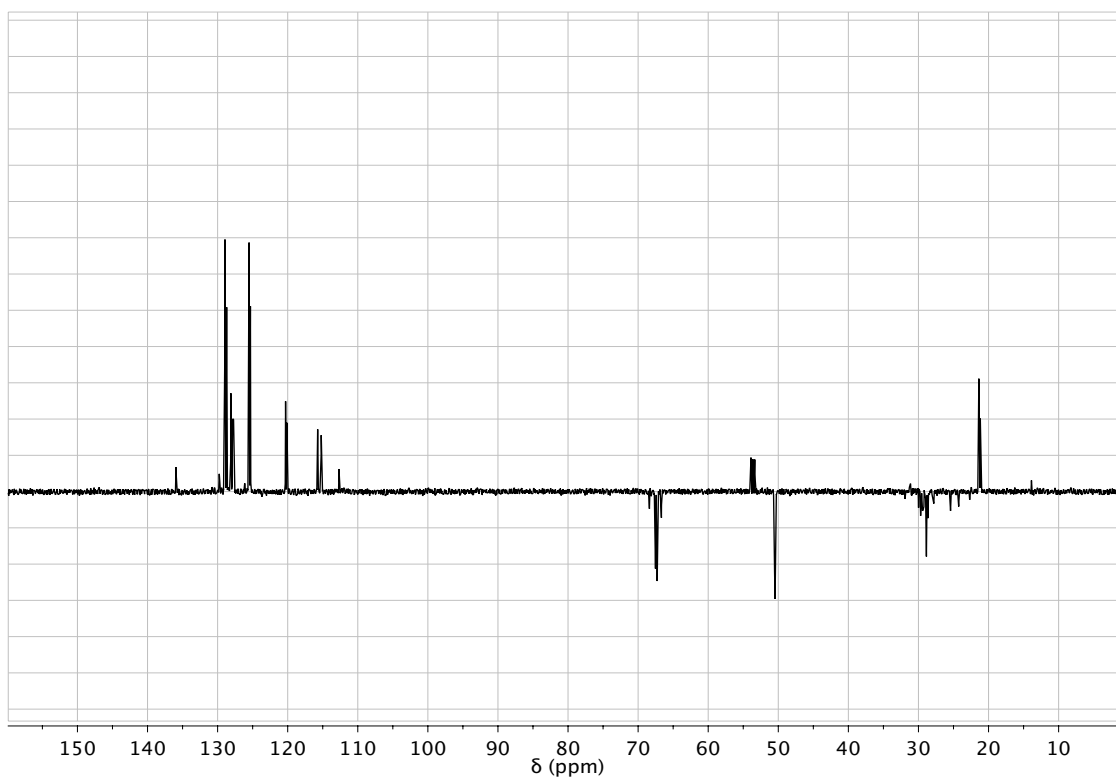
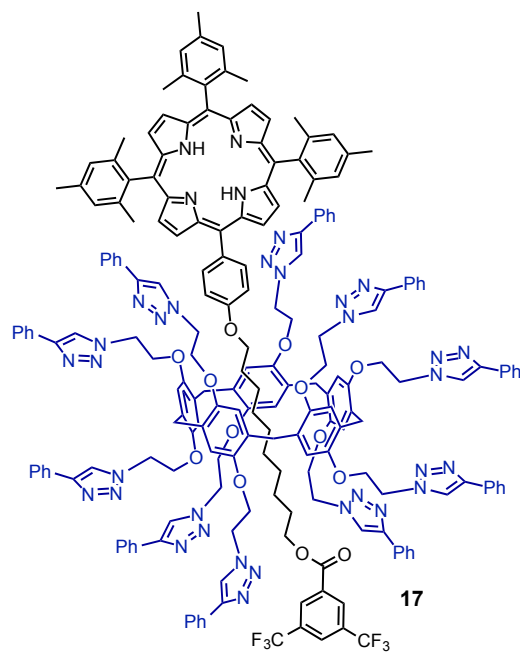


Figure S4d. DEPT of compound **17** (CD_2Cl_2 , 100 MHz).

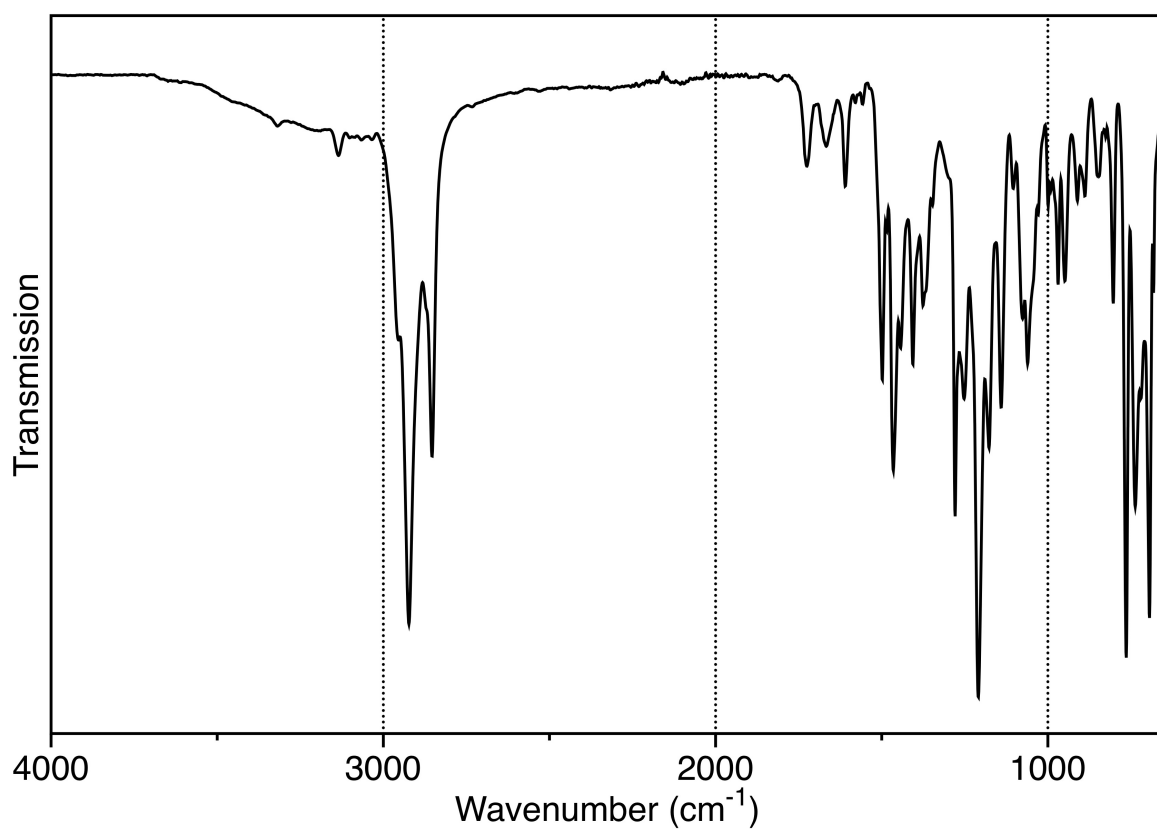
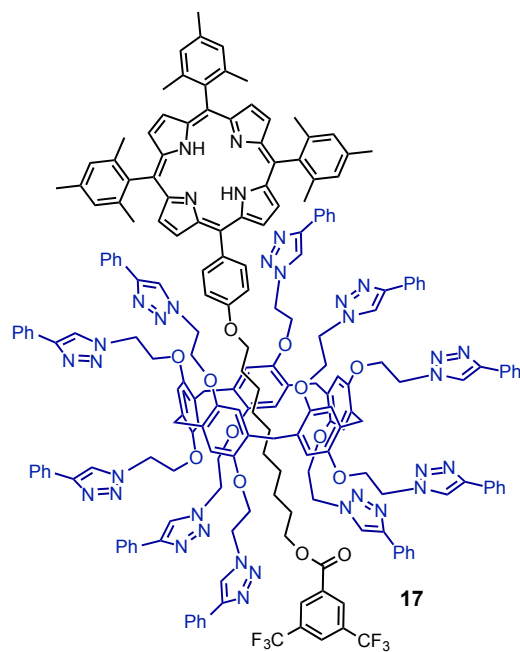


Figure S4e. IR spectrum of compound **17**.

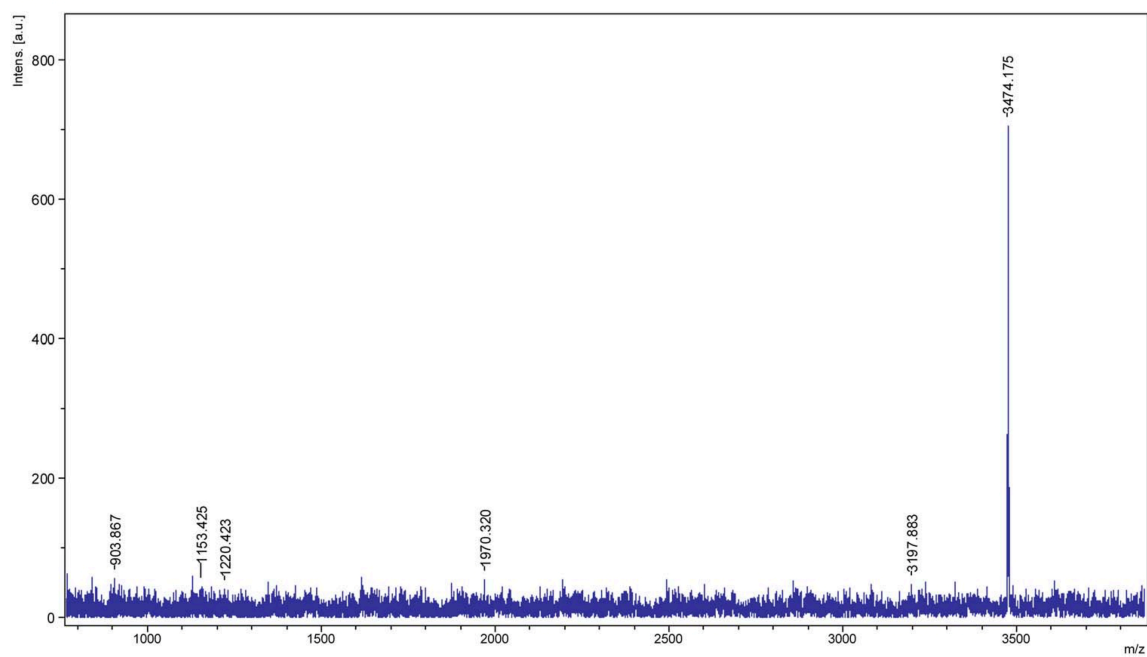
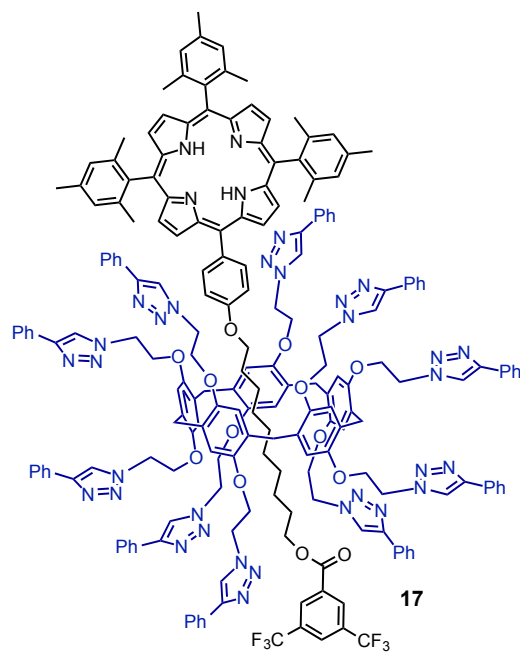


Figure S4f. MALDI-TOF mass spectrum of compound **17**.

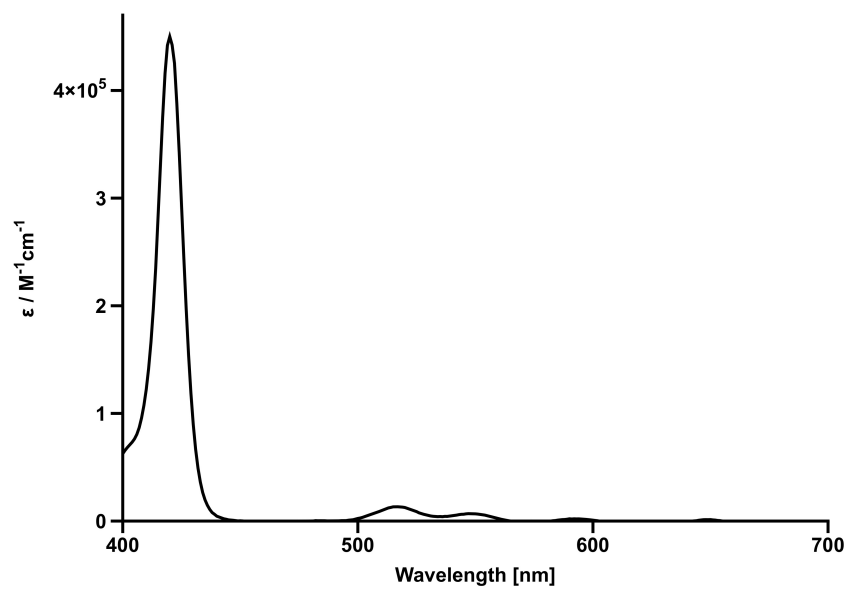
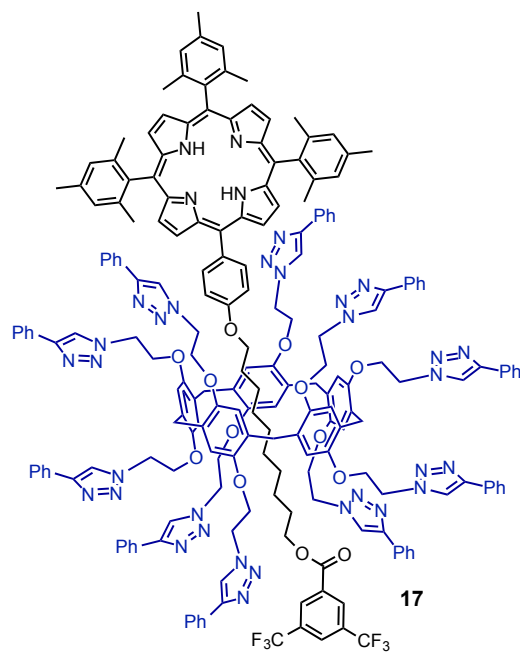


Figure S4g. UV/vis spectrum of compound 17 (CH_2Cl_2).

Le pillar[5]arène comme cœur polyfonctionnel pour l'élaboration de matériaux moléculaires

Résumé

La préparation de briques élémentaires de pillar[5]arènes « clickables » nous ont permis de construire des édifices moléculaires complexes, en greffant différents groupements fonctionnels autour du cœur macrocyclique. Dans ce contexte, des nouveaux dérivés du pillar[5]arène présentant des propriétés cristaux-liquides ont été synthétisés en greffant du p-dodecyloxybenzoate ou encore des dendrons de type percec. D'autres part, des dérivés pillaréniques portant des unités de porphyrines ont été préparés à partir du squelette « clickable » pillar[5]arène et de porphyrines de Zinc portant des fonctions alcynes vrai. Les études de ce système par RMN du proton à des températures variables ont permis de mettre en évidence un équilibre conformationnel dynamique conduisant au repliement des molécules. Ceci a été expliqué par une complexation intramoléculaire des porphyrines de Zinc par les groupements 1,2,3-triazole. Finalement un support « clickable » de type [2]rotaxane comportant une porphyrine base libre comme bouchon, a été préparé et ensuite fonctionnalisé par dix porphyrines de Zinc permettant l'obtention d'un dispositif supramoléculaire photoactif.

Mots Clés: chimie click, cristal liquide, pillar[5]arène, rotaxane, porphyrine, chimie supramoléculaire.

Abstract

Clickable pillar[5]arene building blocks have been used for the efficient grafting of peripheral subunits onto the macrocyclic core. New liquid-crystalline pillar[5]arene derivatives have been prepared by grafting either p-dodecyloxybenzoate groups or percec-type dendrons on the macrocyclic scaffold. On the other hand, pillar[5]arene derivatives bearing peripheral porphyrin subunits have been efficiently prepared from the clickable pillar[5]arene building block and Zn(II)-porphyrin derivatives bearing a terminal alkyne function. Owing to an intramolecular complexation of the peripheral Zn(II)-porphyrin moieties by 1,2,3-triazole subunits, an original dynamic conformational equilibrium leading to a folding of the molecules has been evidenced by variable temperature ^1H NMR studies. Finally, a clickable [2]rotaxane scaffold incorporating a free-base porphyrin stopper has been prepared and functionalized with ten peripheral Zn(II)-porphyrin moieties to afford a sophisticated photoactive supramolecular device.

Keywords: click chemistry, liquid crystal, pillar[5]arene, rotaxane, porphyrin, supramolecular chemistry.